MATHEMATICAL MODELING OF

HIGH TEMPERATURE FUEL CELLS

by

PABLO G. DEBENEDETTI

Ingeniero Químico, Universidad Nacional de Buenos Aires,
Facultad de Ingenieria
(1978)

SUBMITTED TO THE DEPARTMENT OF
CHEMICAL ENGINEERING
IN PARTIAL FULFILLMENT OF THE
REQUIREMENTS FOR THE
DEGREE OF

MASTER OF SCIENCE IN CHEMICAL ENGINEERING

at the

MASSACHUSETTS INSTITUTE OF TECHNOLOGY

August 1981

Signature of Author Signature redacted
Department of Chemical Engineering
August 7, 1981

Certified by Signature redacted
Costas G. Vayenas
Thesis Supervisor

Accepted by Signature redacted
Glenn C. Williams
Chairman, Department Committee

MATHEMATICAL MODELING OF HIGH TEMPERATURE FUEL CELLS

by

Pablo Gastón Debenedetti

Submitted to the Department of Chemical Engineering on August 7, 1981, in partial fulfillment of the requirements for the Degree of Master of Science in Chemical Engineering at the Massachusetts Institute of Technology

ABSTRACT

This work concerns the mathematical modeling of the steady state behaviour of high temperature fuel cells. Electrolyte (yttria-doped zirconia), electrolyte thickness (200 μm) and electrolyte resistivity temperature dependence considered here, correspond to cells built at MIT (3). H_2 and CO oxidation were the two reactions investigated. Polarization was taken as purely ohmic, design procedures for attaining mass transfer limitation-free operation at high conversions being given in this work. Activation overpotential-free operation for H_2 on Pt electrodes in high temperature fuel cells represents actual, experimentally verified behaviour (15,16), while results for CO oxidation represent a limiting behaviour which can at present be approached by the introduction of small (<5%) quantities of H_2, and which could be attained with an appropriate electrocatalyst (16).

The first part of the present work concerns the steady state modeling of the self-ignited, well mixed fuel cell. Power output, current output, conversion, thermodynamic efficiency, heat generation, heat removal and steady state multiplicity were analyzed, and the influence of process and cell design parameters upon these variables was discussed in detail. Scale-up criteria and practical limits of scale-up were presented. Cell output variables which cannot be simultaneously maximized were identified and the resulting trade-offs discussed. Conditions whereby ignited operation at high conversion (>97%), power density (0.1 W/cm^2) and current density (0.2 A/cm^2) can be attained by a parallel-fed stack were discussed. Preliminary design of a stacked assembly was presented.

A one dimensional model for a cross flow monolith fuel cell was developed in the second part of this work. Steady state multiplicity was found. Power output ($\sim$5 W per monolith) and conversion (>98%) corresponding to ignited operation suggest interesting possiblities for this new type of fuel cell.

Thesis Supervisor: Dr. Costas G. Vayenas

Title: J.R. Mares Associate Professor of Chemical Engineering

ACKNOWLEDGEMENTS

I would like to express my sincerest thanks to Professor Costas Vayenas for his enthusiasm, receptiveness, insight and human qualities, which have helped so much in turning this project into a fascinating personal and intellectual experience.

Extensive use was made of the Chemical Engineering Department's computer facilities, and I am grateful to Calvin Chew, Hisham Ettouney and Howard Bernstein for their help with many an "undebuggable" program. I am also grateful to all the members of Professor Vayenas' research group for the ideas that originated from our interaction. I owe special thanks to Cathy Teague for the many ways in which she helped, providing all necessary information on the NH_3 fuel cell which served as a starting point for the mathematical modeling. I enjoyed several illuminating discussions with Selim Edde, whose approach to chemical engineering problems from a non chemical engineering viewpoint proved to be invariably fruitful. Thanks for the typing of the manuscript are due to Larry Johnson.

The research was supported through N.S.F. grant CPE 8009436.

I am, foremost, indebted to my father for the moral and material support he provided throughout my education.

To the memory of my Mother

To my family (on both sides of the Atlantic)

TABLE OF CONTENTS

LIST OF FIGURES

LIST OF TABLES

1. INTRODUCTION

1.1 Definitions; thermodynamic constraints

Electrochemical energy conversion, as understood in the context of the present work, refers to processes which directly transform the heat released in a chemical reaction (i.e., with no intervention of moving parts) into electrical energy, thereby presenting the fundamental feature of avoiding energy losses due to intrinsic limitations imposed by the second law of thermodynamics. It is useful before getting involved with the subtleties and complexities which characterize mathematical modeling, which are almost always related to numerical rather than fundamental problems, to clearly define a few important thermodynamic parameters, and analyze the consequences of these definations, for these very simple quantities possess all the information needed in order to understand the potentialities, limitations and actual performance of electrochemical energy converters.

Consider the reversible, isothermal, isobaric transformation shown in figure 1.1.a, where reversiblity imposes the condition of an infinitely slow process, both an a macro and on a microscopic scale. The discussion applies to a continuous process, the "black box" being therefore an open system. The limitation to an open system is by no means a restrictive one, since the arguments that follow could easily be extended, with minor formal changes in the development, to a closed system, to arrive at exactly the same conclusions. The constructive details of the energy converter being irrelevant at the present

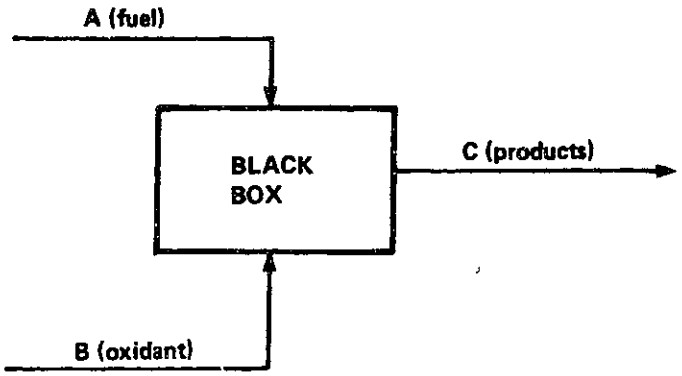

1.1.a

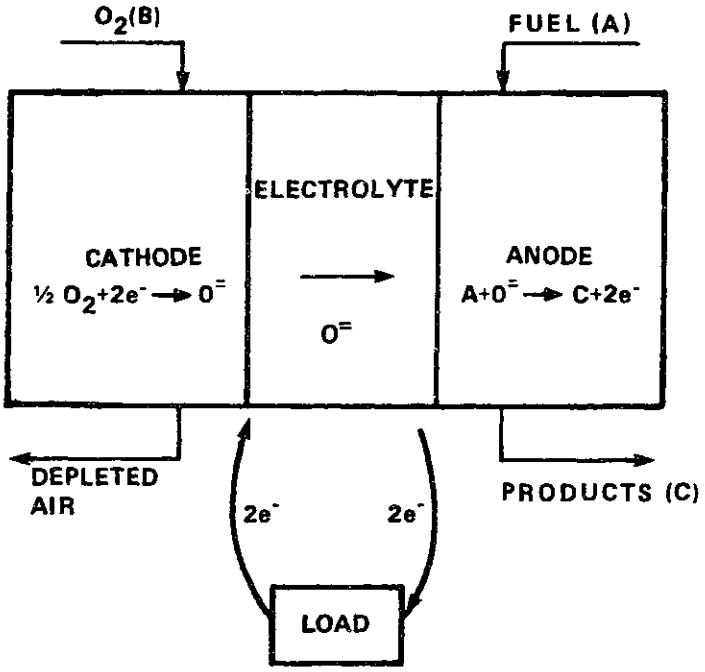

1.1.b

"BLACK BOX" AND FUEL CELL THERMODYNAMIC PROCESSES
FIGURE 1.1

stage, we are interested in the energy changes involved in the reaction

$$aA + bB \rightarrow cC \tag{1.1}$$

For isothermal operation, the net energy change (in minus out) per mole of A, associated with the flowing streams, is the enthalpy change for the reaction, $-\Delta H$. For a continuous, reversible, isothermal process, the maximum work obtainable is $-\Delta G$. It is only natural, therefore, to define a limiting, maximum achievable efficiency as the ratio of maximum obtainable work to net (in minus out) energy change associated with the flowing streams,

$$\eta_{max} = \frac{\Delta G}{\Delta H} \tag{1.2}$$

Equation (1.2) is not only a definition, but contains essentially all that is needed to analyze the thermodynamic feasibility of any proposed energy converter. In fact, as all thermodynamic relations involving the concept of reversibility, it sets a standard (unattainable in real life) to which one can compare the performance of an actual or prospective process. One cannot, of course, attain η_{max}; however, it is the goal towards which each improvement in design must tend. Note that equation (1.2), an arbitrary definition, should not be confused with the usual concept of efficiency, i.e., work obtained relative to <u>input</u>, which is always less than (or equal to) unity; η_{max}, as defined in equation (1.2), on the other hand, can be greater than unity, since it is the ratio of work obtained to net energy <u>change</u> associated with the flowing streams (but excluding the useful work

itself). The fundamental information contained in the defining expression for η_{max}, however, can easily be grasped if we view the denominator as a fixed value associated with the chemical system under consideration, and direct our efforts towards the design of an energy converter which approaches our goal as close as possible (the limiting value of the obtainable output being $-\Delta G$ also a property of the reacting system). The second law of thermodynamics naturally leads us to reject any machine which, in transforming the chemical energy of reactants into useful work, involves an indirect process in which heat is involved, since, even under conditions of reversibility, it cannot be completely transformed into work.

Consider, however, the <u>real</u> electrochemical energy converter depicted in figure 1.1.b, to which all of the present modeling work applies (see section 1.2). There are two very important characteristics associated with such a machine, namely

(i) the elementary processes whereby chemical energy is transformed into useful work, in the form of electricity, involve electron transfer between species (for H_2 as a fuel in an $O^{=}$ -conducting fuel cell, the elementary steps are $\frac{1}{2} O_2 + 2e^- \rightarrow O^{=}$ and $H_2 + O^{=} \rightarrow H_2O + 2e^-$) as opposed to molecular collisions; therefore, although an overall heat effect is associated with the reaction, it is not involved in any intermediate energy conversion, thus, the limitations imposed by the second law have been circumvected.

(ii) if we perform a thought experiment whereby the essentially irreversible process described above is imagined to take place under conditions approaching reversibility, then the work

produced by this electrochemical reactor tends, in the limit of reversible operation, to a maximum value. There being no other form of work (expansion, if and when it exists, is contained in the enthalpy terms), we conclude, by what is only apparently a circular argument, that such an asymptotic maximum work is, in effect, $-\Delta G$.

Consideration of equation (1.2) as the ideal limit which any energy-efficient converter should aim at approaching, has led us to conclude that a system such as the one schematized in figure 1.1.b is indeed thermodynamically "sound." Selection of an adequate chemical system and operating temperature univocally define η_{max}, the designer's ingenuity being then responsible for the attainment of as close an approximation to η_{max} as is economically feasible.

The various trade-offs involved are discussed in detail in section 2.1. It suffices here to mention, for example, that designing a fuel cell as a power source is completely different from designing a chemical reactor to produce useful chemicals and cogenerate electricity. Focusing briefly upon the variables related only to the chemical system under consideration, we can write

$$\Delta G = \Delta H - T\Delta S \tag{1.3}$$

Therefore,

$$\eta_{max} = 1 - \frac{T\Delta S}{\Delta H} \tag{1.4}$$

Neglecting variations in ΔH and ΔS with temperature, equation (1.4) explicity shows the importance of the entropy change as-

sociated with reaction (1.1) in determining the efficiency of the process. In fact, for an exothermic reaction, we can clearly divide chemical systems into two broad catagories, according to the sign of ΔS. Table 1.1 summarizes the most important features of such a classification.

For a system such as the one illustrated in figure 1.1.b, involving stoichiometric feed of pure reactants and products, and, therefore, no mixing effects upon ΔS, the results of table 1.1 are graphically displayed in figure 1.2 (ΔH and ΔS assumed to be independent of temperature). Table 1.2 gives values for standard (pure specie, 1 bar, gaseous state, system temperature) energy and entropy changes for various systems of practical interest, at 298 K.

Therefore, from a strictly thermodynamic point of view, we conclude that H_2, CO and C_2H_4 fuel cells should be operated at relatively low temperatures, the opposite being ture for NH_3, H_2/Cl_2 and CH_3OH systems. However, this approach considers exclusively those factors which depend only on the chemical system analyzed, and neglects the other fundamental factor, namely, the reactor. On the other hand, in considering the alternatives for a possible electrochemical energy converter, once a chemical system has been chosen, an adequate electrolyte material must be found such that the desired reaction does indeed take place. Thus, in figure 1.1.b, such an electrolyte would be entirely suitable for the CO fuel cell, as well as, for example, the H_2/H_2O fuel cell. The latter, however, could also be materialized with a proton-conducting electrolyte, which would thus lead to the same overall process through a different elementary mechanism. The operating

TABLE 1.1: Negative and Positive ΔS Reacting Systems

	$\Delta S < 0$	$\Delta S > 0$
η_{max}	<1	>1
effect of T	η_{max} decreases with T	η_{max} increases with T
physical consequence	effective exothermicity increases with T	endothermicity increases with T

TABLE 1.2: Some Possible Fuel Cell Systems, and Assoicated Thermodynamic Parameters

Reaction	ΔH_o (KJ/mole fuel)	ΔG_o (KJ/mole fuel)	ΔS_o (KJ/mole K)	η_{max} @ 298 K %
$H_2 + \frac{1}{2}O_2 \rightarrow H_2O(g)$	-241.99	-228.75	-0.044	94.5
$CO + \frac{1}{2}O_2 \rightarrow CO_2$	-283.18	-257.29	-0.087	91
$NH_3 + \frac{5}{4}O_2 \rightarrow NO + \frac{3}{2}H_2O(g)$	-226.66	-240.03	+0.044	105.90
$C_2H_4 + 3O_2 \rightarrow 2CO_2 + 2H_2O(g)$	-1323.85	-1314.96	-0.030	99.32
$H_2 + Cl_2 \rightarrow 2HCl(g)$	-184.75	-190.73	+0.020	103.2
$CH_3OH(g) + \frac{3}{2}O_2 \rightarrow CO_2 + 2H_2O(g)$	-676.45	-690.45	+0.047	102.1

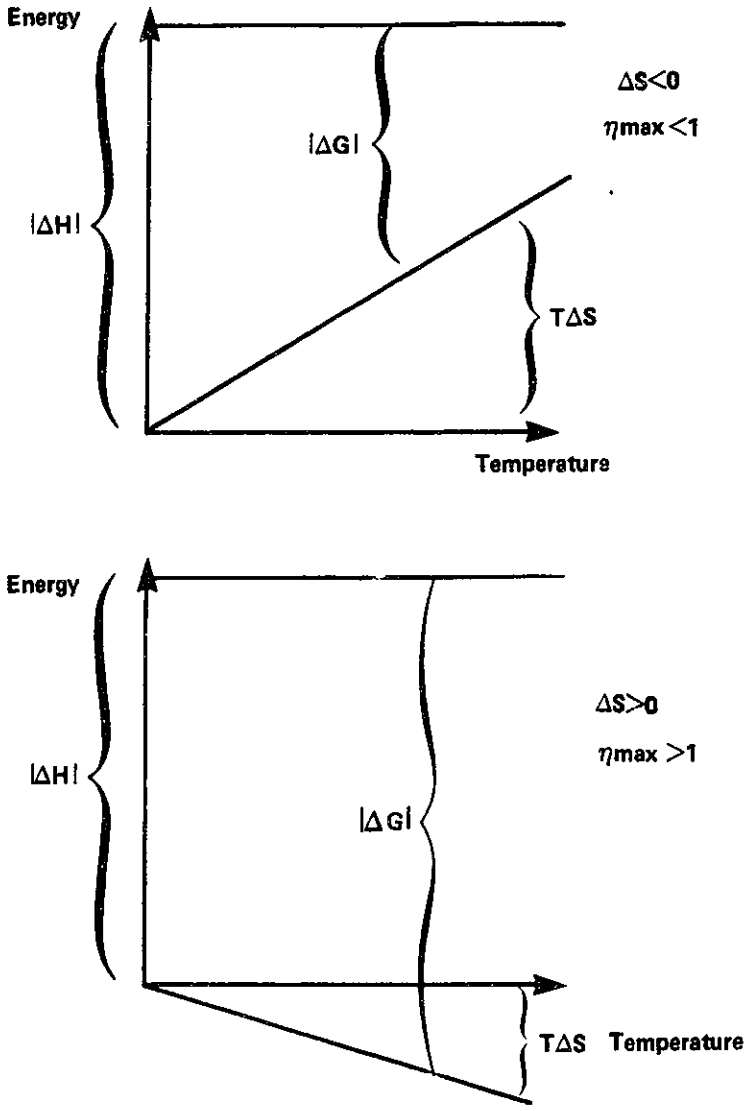

EFFECT OF ENTROPY CHANGE ON FUEL CELL THERMODYNAMIC PERFORMANCE
FIGURE 1.2

temperature of the fuel cell, therefore, is determined not through a thermodynamic criterion such as the one outlined above, but is set by the characteristics of the electrolyte, which can be liquid (low temperature fuel cells), molten (medium) or solid (high-temperature fuel cells).

The present work refers to the mathematical modeling of high temperature solid electrolyte fuel cells whose elementary current-conduction properties are such that the conducted specie is $0^{=}$. For the electrolyte and thickness-to-area ratios tested in previous work at MIT (1,2,3), the onset of conduction is 350°C (see section 1.2). In this context it is apparent, therefore that, if other process considerations don't dictate a different choice (such a process condition would be, for example, the availability of a high temperature mixed H_2-CO stream to be used as a fuel), a H_2/H_2O fuel cell should ideally be a low temperature cell (this is indeed the case with the aqueous KOH electrolyte cell). The object of the present work being the modeling of high temperature cells rather than actual design, however, the H_2/H_2O cell has been chosen for many of the examples, since, contrary to the CO/CO_2 system, where activation overpotential with current electrode materials does indeed exist, this is not the case for the hydrogen system, which provides the attractive feature of easily verifiable results, while the CO/CO_2 examples, on the other hand, correspond to the limiting behaviour which a system would show if the currently very active area of research in low activation polarization electrodes for hydrocarbon and fuel gases yields fruitful results (see Appendices I and II).

Restricting our attention to $0^{=}$ - conducting high temper-

ature cells, it is seen that electrolyte properties and thermodynamics do in fact point towards the same direction for systems with positive ΔS (NH_3, CH_3OH, for example), but the opposite is true for negative ΔS systems (H_2, CO, C_2H_4, for example). However, as can be graphically seen from figure 1.2, an increasing efficiency means that ΔG is an increasing fraction of ΔH, the desirable goal of maximizing useful work being approached at the expense of the system's effective exothermicity. This results in the following set of opposing trends (table 1.3), which constitute the frame within which the designer must operate when dealing with high temperature fuel cells. It is evident from table 1.3 that any real design will inevitably involve a compromise between these opposing tendencies. Thus, although Carnot limitations are still avoided with a high temperature fuel cell, our ability to approach η_{max} is limited by the properties of the electrolyte for negative ΔS systems,while it is our ability to achieve self sustained operation (and, therfore, overall plant energy efficiency) that is limited by electrolyte characteristics in positive ΔS systems.

Again, as was stated above, and will be explained in section 2.1, the final choice of operating parameters depends primarily on the two possible uses of a fuel cell: power generation vs. chemical conversion (with power co-generation). Also, although it may seem from table 1.3 that a high-temperature CO fuel cell is inherently (i.e., thermodynamically) inefficient, this is only true when compared with the intrinsic possiblities of the system, but even with the limitations imposed by high-temperature

TABLE 1.3: Trade-offs which characterize High Temperature Fuel Cells

	$\Delta S > 0$	$\Delta S < 0$
To increase η_{max}	operate @ high T	operate @ low T
Therefore, high T fuel cell is	thermodynamically correct	thermodynamically incorrect
However, to acheive ignited operation	more external heating is needed as T increases	increasing easiness as T increases

operation, the overall efficiency is still greater than thermal-mechanical-electrical indirect energy conversion.

Finally, it must be added that the efficiency considered up to now is only a limiting value, corresponding to ideal, reversible operation. As soon as the cell starts producing current at a finite rate, the voltage drops to some value smaller than the reservsible voltage, the latter being a unique function of temperature and activities of reactants and products, so that, for reaction (1.1.), which involves the passage of n electrons for each elementary event characterized by that particular stoichiometry

$$E_{rev}(T) = E^{\circ}(T) + \frac{RT}{n\mathcal{F}} \ln \frac{[a_B]^b [a_A]^a}{[a_C]^c} \qquad (1.5)$$

where $E^{\circ}(T)$ is the voltage that would result if all activities were unity. Grouping all forms of polarization together, we can relate E to E_{rev}, as follows

$$E = E_{rev} - \sum_i \phi_i \qquad (1.6)$$

The actual, irreversible power output of the fuel cell being EI, we can define an actual (as opposed to maximum) efficiency,

$$\eta = \frac{EI}{(-\Delta H)(\frac{I}{n\mathcal{F}})} = \frac{n\mathcal{F}E}{-\Delta H} = \eta_{max} \frac{E}{E_{rev}} \qquad (1.7)$$

Substitution of equation (1.6) into equation (1.7) leads to

$$\eta = \eta_{max} \left(1 - \frac{\sum_i \phi_i}{E_{rev}}\right) \qquad (1.8)$$

Equation (1.8) clearly shows that a good design should aim at the reduction of the polarization terms. Of these, ohmic overpotential is unavoidable, and design efforts oriented towards its reduction are mostly related to the attainment of as thin

an electrolyte-electrode assembly as possible within limits largely set by mechanical strength considerations, once the proper materials have been chosen. Concentration overpotential, arising when the rate at which reactants are supplied to the electrode becomes slow relative to anion conduction across the electrolyte, is an entirely fluid-mechancial problem, its solution depending primarily upon electrode design and fluid flow within the anodic and cathodic compartments (see Appendix I). Activation overpotential, on the other hand, is determined by the joint interaction of electrode material and temperature. It originates due to the finite, non-equilibrium rate at which electrodic reactions take place, as opposed to the equilibrium state implied in Nernst's equation. The exponential temperature dependence of the exchange current density (4), however, makes this overpotential of relatively minor importance in high temperature fuel cells (this is true for H_2/H_2O and Pt electrodes, but activation overpotential is observed with CO/CO_2 on Pt electrodes, see discussion in section 2.1.1.2 and Appendix II). As with non-electrochemical reactions, an adequate catalyst reduces the reaction's activation energy.

Detailed mathematical treatment of polarization is to be found in Bockris and Reddy (4). See discussions in Appendices I and II.

1.2 Previous work

The present work originated as an extension of research done at MIT by various investigators working with Professor Vayenas in the area of solid electrolyte fuel cells. Farr (2) worked on the high temperature NH_3 fuel cell, more recent

research in that area having been done by Teague (3). The cell used by the latter was in fact the starting point for the CSTR model (section 2.1). Figre 1.3 illustrates such a reactor, and figure 1.4 gives the basic dimensions. Figure 1.5 shows an adaptation of the reactor illustrated in figure 1.3 with provisions for an independent air feed, and figures 1.6a and 1.6b show a schematic exploded view of a single module, which could either be operated individually or in a stacked arrangement such as the one shown in figure 2.23. The first part of the present work, then, originating from a design such as the one shown in figure 1.3, applies both to figure 1.5 and, more realistically, to figures 1.6a or 1.6b (see Appendix III for stacked arrangements).

The alternative shown in exploded view in figure 1.6b has the advantage of having roughly twice as much active area per unit volume, when compared with figure 1.6a. However, cells are now separated only by the thin electrolyte layer, which is designed according to energy output, as opposed to structural, criteria, and, therefore, calls for more careful mechanical design. Also, note the fuel and air feed system. The equations to be presented, therefore, apply equally well to the elementary cell illustrated in figure 1.6b, provided, of course, the corrected quantities per cell are used. The results and equations apply directly, with no allowance to flows "per cell", to the unit shown in figure 1.6a (see schematic assembly, figure 2.23 and Appendix III for discussion on stack design).

The classic problem of CSTR multiplicity and stability has been treated by so many investigators that a complete literature

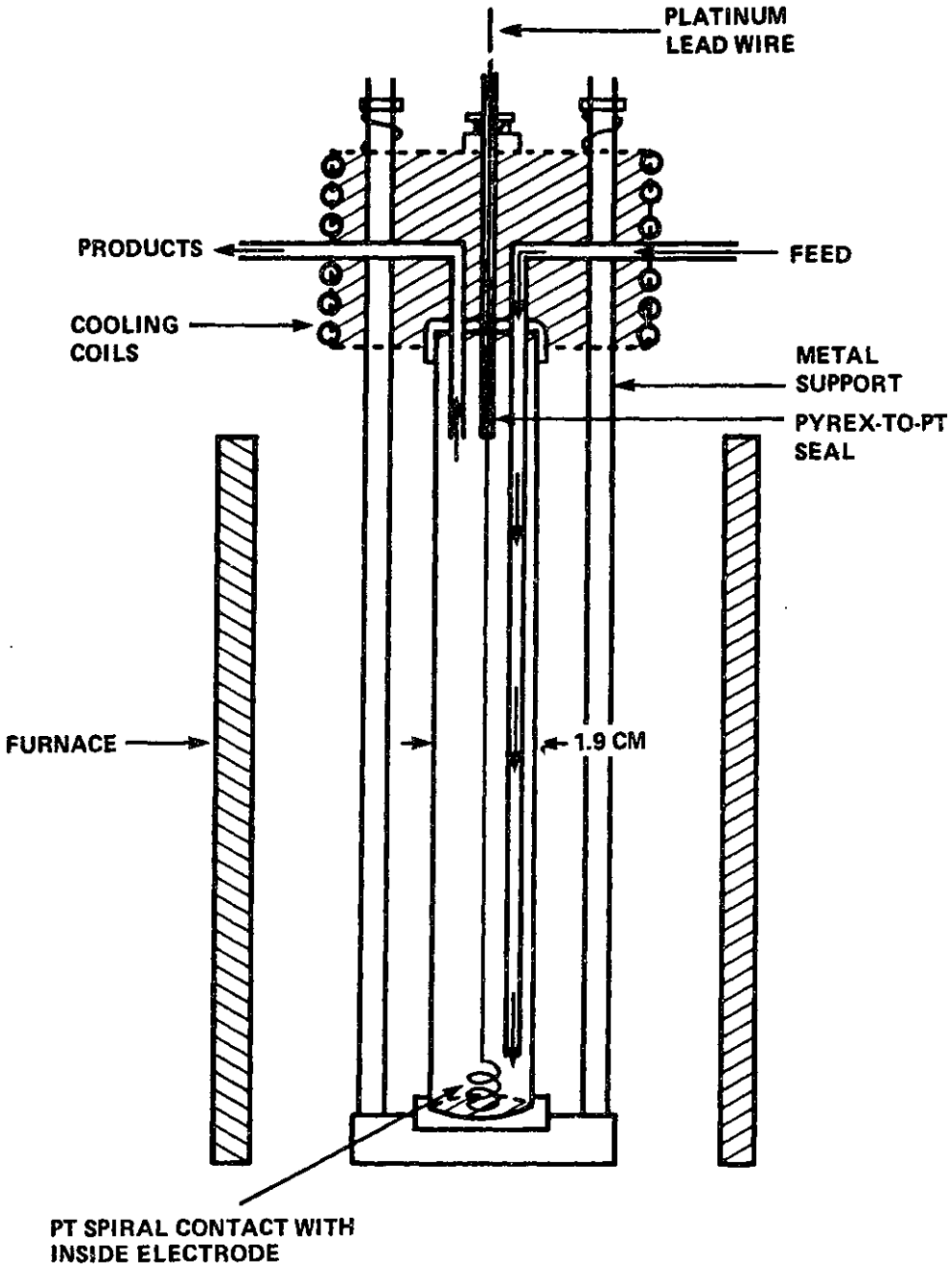

THE HIGH TEMPERATURE EXPERIMENTAL NH_3 FUEL CELL
FIGURE 1.3

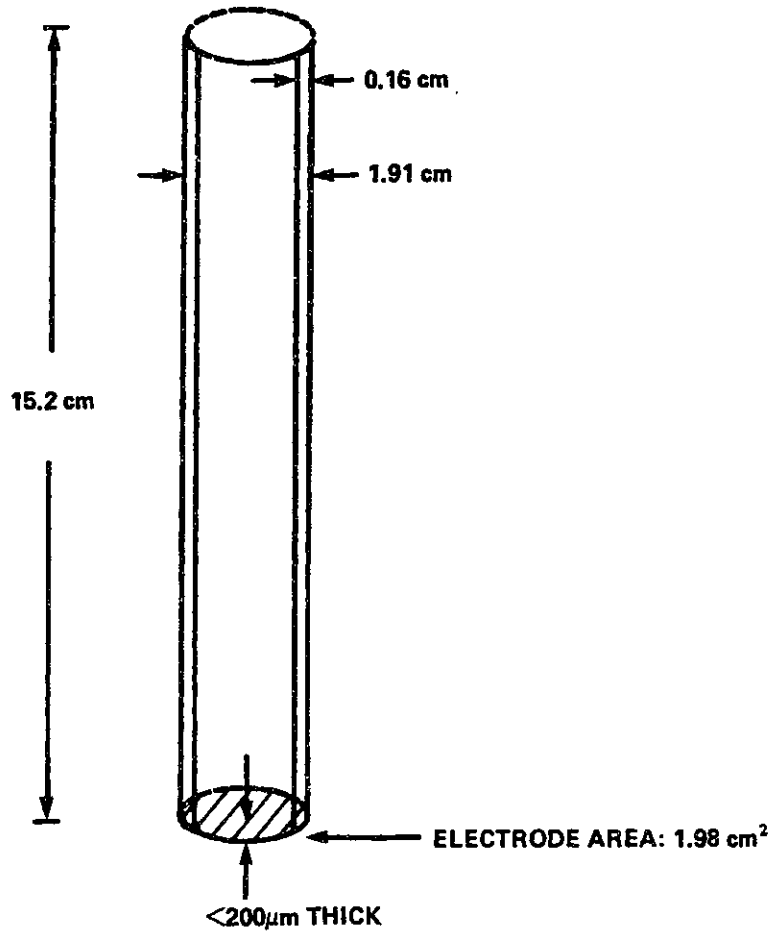

DIMENSIONS OF NH_3 FUEL CELL
FIGURE 1.4

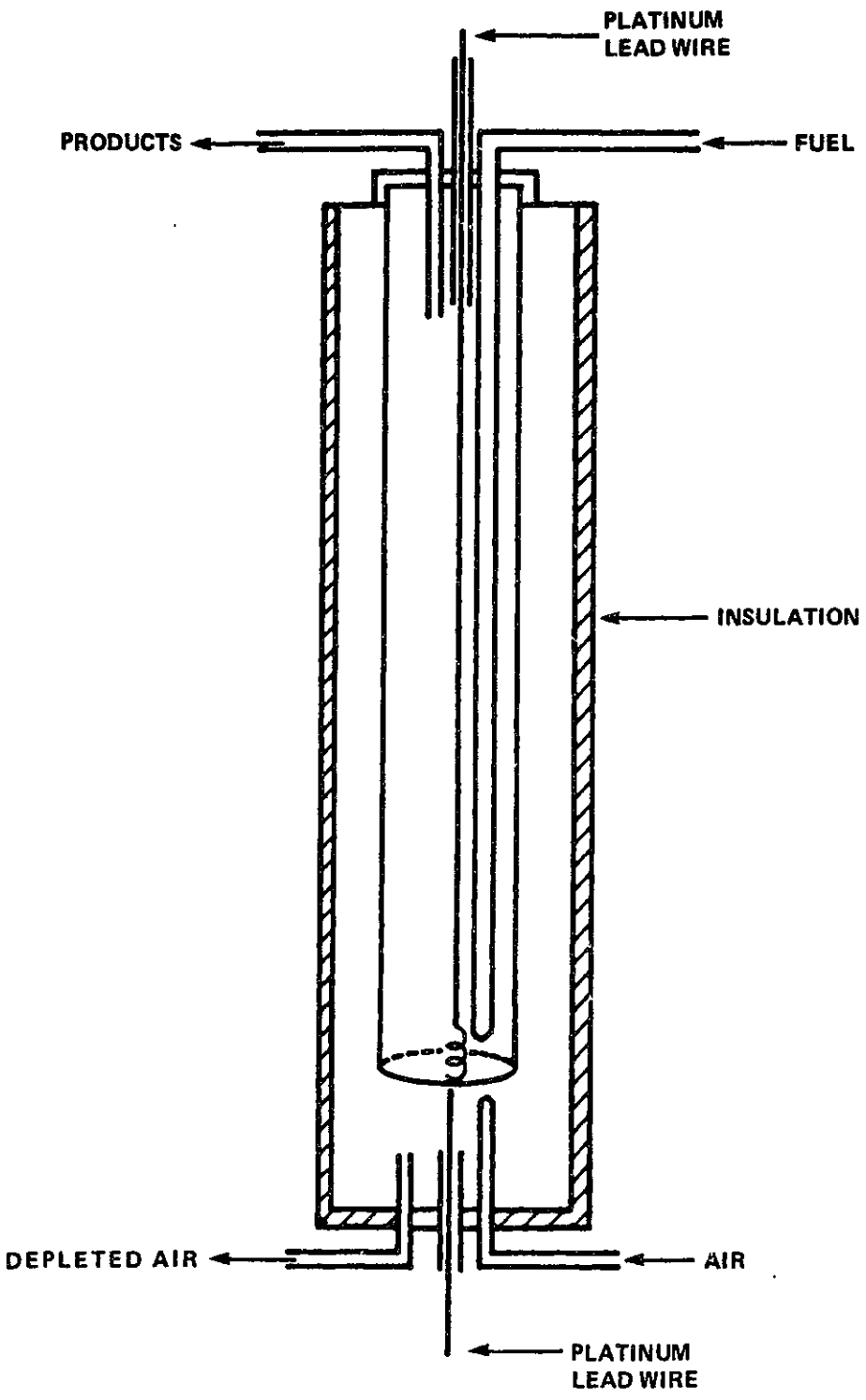

SKETCH OF AUTOTHERMAL EXPERIMENTAL FUEL CELL
FIGURE 1.5

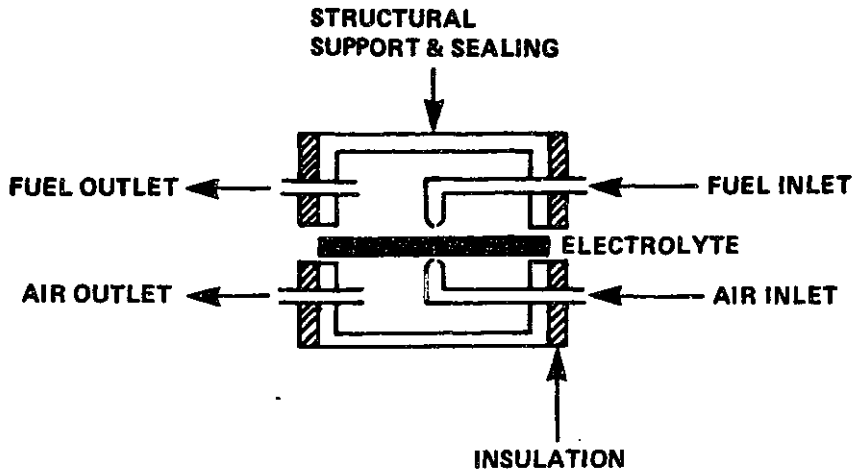

1.6a

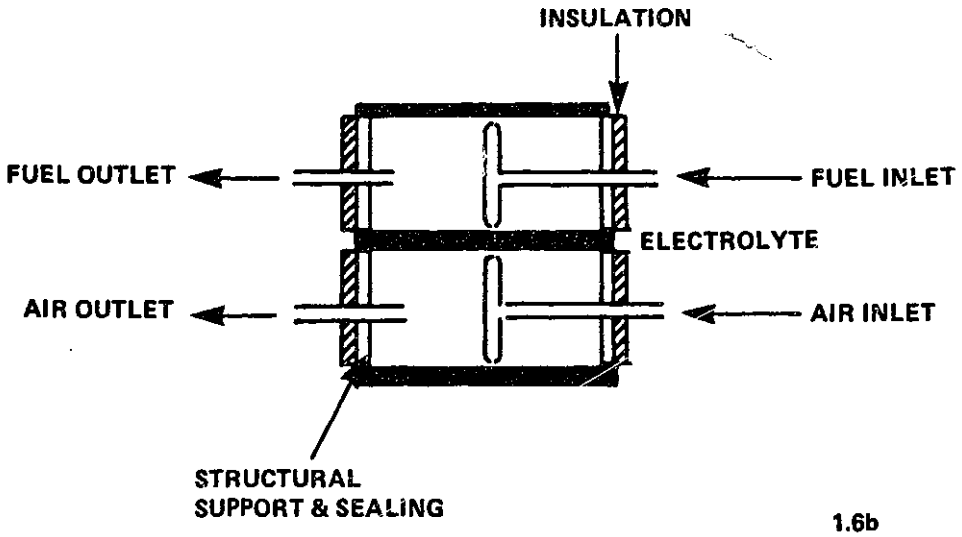

1.6b

ELEMENTARY COMPONENTS OF STACKED ASSEMBLY
FIGURE 1.6

review would exceed the scope of the present section. It is, however, appropriate to mention the pioneering contributions of Van Heerden (5,6), Aris and Amundson (7), and Biolus and Amundson (8). A thorough review of the field is provided by Schmitz (9).

Mathematical modeling of fuel cells from a reactor engineering viewpoint has been done by Sakellaropoulos and Francis (10), for liquid phase, low temperature fuel cells. High temperature fuel cells have been extensively investigated, and much research is currently being conducted in the area. Design criteria for power output maximization resulting from detailed modeling of the current flow in a bell and spigot-type reactor has been presented by Sverdrup, Warde and Eback (11). A brief summary of the current fuel cell technology, where the main trends, technologies and future outlook are presented is given by Adlhart (12), while Bockris and Reddy (4) lucidly cover the field of electrochemical energy conversion, explaining with telling clarity and synthetic power what are the main ideas, current problems, and desirable future trends which should be followed in further developments. Solid electrolytes and their applications are covered by Subbarao (13).

1.3 Scope of the present work

The scope of the present work is to apply the methods of chemical reactor analysis to the modeling of high temperature fuel cells. Although the qualitative features are independent of the actual electrolyte used, the resistance and activation energy values used correspond to ZrO_2 doped with 8% Y_2O_3, which

has been used in previous work at MIT (1,2,3). When necessary (see Appendix I) detailed consideration is given to electrodics, but, otherwise, the approach is that of reactor engineering. In this way, useful conclusions can be reached regarding scale up, steady state multiplicity, power output maximization, etc. It is hoped that the equations, graphs and discussions presented in the first part (CSTR model) will provide an analytical framework suitable for the design and analysis of electrochemical reactors. In this respect, it must be stressed that, although discussion and design suggestions are occasionally presented, the object of the present work is modeling rather than design, which would represent the logical extension and application of the model.

In the last part, a mathematical model is presented for a new type of electrochemical reactor, whose many interesting features range from its promising potential for commercial application to the theoretical curiosity of steady state multiplicity in a tubular reactor.

2. MATHEMATICAL MODELS

2.1 THE CSTR MODEL

2.1.1 Assumptions

Three main hypotheses were considered as starting points in the development of the CSTR model:

- the reactor behaves as a CSTR (continuous stirred tank reactor). This implies perfect mixing, and consequently, uniformity of all properties at any given instant throughout the reactor.
- the rate of the process (electrochemical reaction) is controlled by oxygen anion transport through the solid electrolyte.
- polarization is due exclusively to ohmic losses (i.e., activation and concentration overpotentials are not considered).

2.1.1.1 The CSTR assumption

Farr (1) and Farr and Vayenas (2) present results of reactor behaviour when subject to a step-function change in fuel feed concentration, and compare experimental results with the theoretical CSTR response curve, and the agreement is very good, all the more so if consideration is given to the reactor geometry used in those experiments, which would suggest a behaviour at least intermediate between perfect mixing and plug-flow. Since the present model considers similar flows but different geometries (see figures 1.3, 1.4, 1.5, 1.6) even farther removed from plug-flow characteristics, the CSTR assumption is an appropriate modeling hypothesis. The characterization of reactor flow behaviour from stimulus-response techniques is thoroughly discussed in

a number of reactor engineering standard texts, the classic reference being, of course, Levenspiel (14).

Teague (3) provides experimental evidence of the CSTR behaviour of the reactor used as a starting point in the present modeling. It must be noted that the peculiarities of the reacting system under consideration are such that, contrary to common CSTR applications, where reaction (and, therefore, heat generation) occur throughout the volume of the reacting phase, it is a surface phenomenon that must be considered here. Nevertheless, temperature uniformity is plausible in the light of the following arguments:

- although the converse is not necessarily true, a reactor showing CSTR behaviour from stimulus-response techniques implies a uniform temperature throughout its volume (since it is not possible to mix matter without achieving thermal uniformity).

- the experiments performed by Farr (1) were done under essentially isothermal conditions, acheived by placing the reactor in a furnace. In the present work, however, self ignited operation is investigated, and, as will be discussed later, heat losses to the surroundings are the realistic conditions under which the reactor operates. Nevertheless, in order to achieve self ignited operation, the reactor must either be thermally insulated, or an appropriate stacked arrangement must be devised (these points are analyzed in Appendix III); both solutions or their combinations, of course, lead to a condition whereby the controlling resistance to heat transfer is progressively displaced towards the outside of the reactor. In the limiting case, a com-

pletely adiabatic reactor is, by definition, free of radial temperature gradients. Figures 2.23 and III-2, in addition, are possible designs which respond to the energy equations presented in this work. Insulation of the outside surface (see section 2.1.3.5.2), comparison with figure 1.3 for which CSTR behaviour has been proved, and the combined effects of thermal backmixing between the various elements and well mixed air chamber, all point towards an operating regime that, for modeling purposes, can be considered as isothermal within the insulated cell.

2.1.1.2 The rate limiting step-ohmic polarization assumption

The possible sources of overpotential, namely, ohmic, activation and concentration are fundamentally different, not only in their mechanistic nature, but also when viewed as sources of inefficiency (see section 1.1). Ohmic losses are inevitable; one can, at most, reduce them through good engineering design and choice of materials, but they cannot be eliminated. Activation and concentration overpotentials, on the other hand, can and should be elminated, or, at least, limited. A thorough discussion of these sources of inefficiency, as well as many illuminating insights into electrochemical energy conversion are to be found in Bockris and Reddy (4).

Concentration overpotential arises when the rate of ionic transport across the electrolyte is fast relative to the rate of mass transfer from the bulk gas phase to the electrode-electrolyte interface. It therefore follows that, when operating at high current densities compatible with conversion and power outputs, engineering design should focus upon the gas feed system. Appendix I provides

an example of such an approach which must be applied to both fuel and air feed systems for a cell similar to the one shown in figure 1.6, whereby such a cell can operate essentially free of mass transfer constraints up to conversions of 98 to 99% for H_2/H_2O, and 96-97% for CO/CO_2.

Notice, furthermore, that with the low flows considered, pressure drop is negligible, and the mass transfer coefficient is thus limited by constructive (i.e., restriction orifice's size) factors. Coherently with the discussion in point 1.1, where it was shown that any deviation from the reversible voltage represents a drop in the cell's thermodynamic efficiency, and the calculations shown in Appendix I (similar calculations can, of course, be made for each particular cell design) which demonstrate the feasibility of increasing the mass transfer coefficient with no significant energy (i.e., pressure drop) expenditure, the model developed in the present work assumes mass transfer-limitation free operation. An engineering balance should be made in each case to determine the practical limit after which mass transfer enhancement becomes uneconomical, but, in any case, it is an error to accept concentration overpotential as a fact of life, which, contrary to ohmic losses, it is not, since it is not an inherent property of the materials, but a consequence of the cell's fluid mechanics.

Teague (3) treats the issue of mass transfer limitations for a fuel cell similar to the one shown in figure 1.3, for the NH_3 oxidation reaction, and presents experimental evidence to support the assumption of an essentially mass transfer limitation-free operation. However, current densities, in that work, were

roughly one order of magnitude lower than the maximum value considered in Appendix I, and the cell was operated at higher flows and lower conversions than the ones taken into account to calculate table I.2, hence the difference between the gas feed geometry used in that case (no restriction orifice, feed tube diamter $\sim$3 mm, tube to electrode distance $\sim$25 mm) and the values calculated in Appendix I.

Activation overpotential originates as a consequence of the non-equilibrium nature of actual electrodic processes, which results in deviations from the reversible (equilibrium) voltages predicted by Nernst's equation. Detailed mathematical treatment is to be found in standard electrochemical texts; again, Bockris and Reddy (4) provide an in-depth and lucid approach. A brief discussion of the subject and its relevance to high temperature fuel cells is presented in Appendix II of the present work.

To essentially eliminate this source of thermodynamic inefficiency, exchange current densities as high as possible should be acheived (see Appendix II), the latter being a measure of the equal and apposite rates at which the elementary processes under consideration take place under equilibrium conditions. This can be acheived through a combination of process conditions (high temperature, since electrode reactions are activated processes) and catalyst selection (the effect being sought in this case being the lowering of the activation barrier for the reaction considered). The latter is often the bottleneck, and such a combination of temperature and catalyst

has not yet been found for many reactions of potential application. Etsell and Flengas (15) discuss the overpotential behaviour of stabilized zirconia fuel cells with porous Pt electrodes, and, within the temperature range investigated (700°C to 1100°C) found essentially no activation overpotential for H_2/H_2O cells, but a relatively important overpotential for the CO/CO_2 system. Again, as shown in section 1.1, the field of research associated with hydrocarbon and CO oxidation electrodes is a very active one, the goal being the reduction or elimination of activation losses. In this respect, it is evident that any large scale electrochemical energy converter processing CO or hydrocarbons would have to be essentially free of activation losses if efficiency is of any concern. Thus, the activation-polarized-free results presented correspond to actual H_2 fuel cell behaviour, and, in the case of CO, to a limiting behaviour whose attainment is one of the goals of current research (see Appendix II). Note that activation overpotential could be included in a more general model, but the resulting cell would be operating with a built-in thermodynamic inefficiency. The discussions that follow therefore apply, it is hoped, to an energy-wise technically sound system, where all inefficiencies that the engineer can reduce or eliminate have been adequately dealt with, either through the cell's fluid mechanics (concentration) or materials (polarization).

The situation presently considered for modeling is therefore such that the reactor has been successfully engineered both through its fluid mechanics (mass transfer, concentration overpotential) and its components and operating conditions

(electrodic reaction rates, activation overpotential) and the rate of the overall process is not limited by either one of these factors. Thus, irrespective of the fact that the electrolyte or (at higher temperatures) the electrode resistance is predominant, it is an ohmic step that controls the rate of the overall process, reactants being transferred to reaction sites and electrodic reactions occuring at rates which are always equal to the overall process rate, but which, under the conditions considered, are always potentially faster.

Experimental evidence of this type of behaviour, apart from voltage measurements, can easily be obtained through anodic oxygen concentration monitoring. A process not controlled by diffusive or activation barriers would result in an O_2-free anode. This was indeed observed by Farr (1) and Teague (2). The Westinghouse fuel cell (16), operating with $CO-H_2$ mixtures, showed similar behaviour.

Finally, note that although all of the useful operating points and ignited steady states considered correspond to temperatures where activation effects can be neglected, a more general model would be more appropriate for the 600K-900K range (0.9 to 1.3 dimensionless temperature, for a feed temperature of 673K considered in most examples), though the general feature of the curves would be unaltered. The low temperature region (T<600K) is characterized, in all cases (see figures 2.4 to 2.29) by virtually zero values for all of the parameters (conversion, power output, efficiency, etc.) which is, of course, due to the fact that conduction is virtually nonexistent due to the exponential nature of the electrolyte resistance.

2.1.2 Governing equations

2.1.2.1 Material balance

For the general reaction

$$A + \frac{1}{2} O_2 \rightarrow B$$

the following elementary steps take place:

$$\frac{1}{2} O_2 + 2e \rightarrow O^{=} \qquad (2.1.1)$$

$$O^{=} + A \rightarrow B + 2e \qquad (2.1.2)$$

As explained in point 2.1.1.2, it is here assumed that the rate-limiting step is $O^{=}$ transport across the solid electrolyte. Under these conditions, a steady-state molar balance for species A can be written as follows:

$$F_i [A]_i = F[A] + \frac{I}{2\mathcal{F}} \qquad (2.1.3)$$

The CSTR assumption is implicit in the use of unsubscripted outlet parameters (i.e., outlet conditions identical to reactor conditions).

In order to calculate I, we can write, for the electric circuit schematically shown in figure 2.1, and considering ohmic overpotential exclusively,

$$E = E_{rev} - I(R_{el} + R_i) \qquad (2.1.4)$$

$$E = I R_{ex} \qquad (2.1.5)$$

Combining equations (2.1.4) and (2.1.5), we obtain an expression for I in terms parameters and variables which are either arbitrary (R_{ex}), fixed by design (R_{el}) or functions of temperature and/or

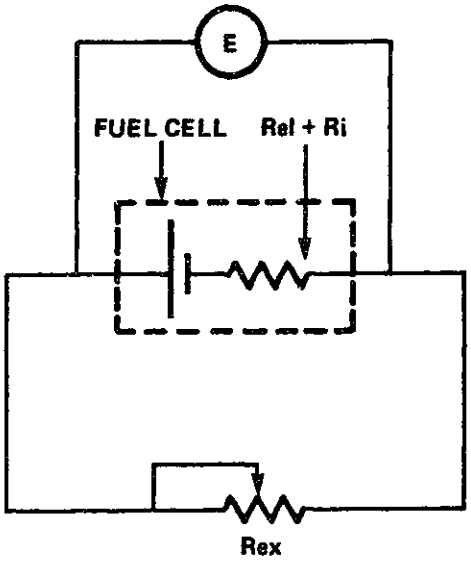

E = Voltage produced by fuel cell
Rel = Electrode resistance
Ri = Electrolyte resistance
Rex = External load (variable)

CIRCUIT FOR CSTR FUEL CELL
FIGURE 2.1

conversion only,

$$I = \frac{E_{rev}}{R_{ex} + R_{el} + R_i} \tag{2.1.6}$$

Therefore,

$$E = \frac{(E_{rev})R_{ex}}{R_{ex} + R_{el} + R_i} \tag{2.1.7}$$

Equation (2.1.7) clearly shows that the voltage will approach open circuit voltage as the external load is progressively increased. Equation (2.1.3) can now be written as follows:

$$F_i[A]_i = F[A] + \frac{E_{rev}}{2\mathcal{F}(R_{ex} + R_{el} + R_i)} \tag{2.1.8}$$

The electrode resistance, R_{el}, is a relatively temperature-independent component of cell resistance, and consists of:

i. electrode-electrolyte contact resistance

ii. electrode film resistance

iii. electrode film-current collector contact resistance

Previous work done at MIT (2) with fuel cell geometries similar to the one serving as the basis for the present CSTR model show that R_{el} is usually around 0.5 ohm. In the present work, R_{el} is one of the parameters whose effect upon cell performance is investigated.

The electrolyte resistance, R_i, is exponentially dependent upon temperature. It is, in fact, interesting to note that the last term on the right hand side of equation (2.1.8) is equivalent to the global reaction rate term in in the corresponding material balance equation for the "standard" (i.e. non-electrochemical) CSTR. Thus, if either R_{ex}, R_{el}, or both, are much bigger than

R_i, the temperature dependence of the reaction rate is limited to the relatively weak (when compared to an Arrhenius type behavior) temperature dependence of E_{rev}.

On the other hand, when R_i becomes important relative to R_{ex} and R_{el}, Arrhenius-type behaviour is observed. We thus encounter another important peculiarity of the fuel cell when viewed as a chemical reactor: the rate of chemical reaction (and, therefore, of heat generation) are very easily controlled through R_{ex}. Contrary to the considerable transients involved in the cooling of a liquid-phase reactor, the gas-phase high temperature fuel cell can be instantaneously "freezed" (provided, of course, that there is no oxygen in the reactor, which is coherent with the assumption that anion transport across the electrolyte is the rate-determining step) by increasing R_{ex}.

R_i can be calculated from the following expressions, of which equation (2.1.10) is only valid for 8% Y_2O_3-doped ZrO_2:

$$R_i = \frac{rd}{S} \tag{2.1.9}$$

$$r = r_* \exp\left(\frac{9700}{T}\right) = 4.1666 \times 10^{-3} \exp\left(\frac{9700}{T}\right) \ (\Omega\text{-cm}) \tag{2.1.10}$$

d and S are also parameters in the present model, although, for most of the calculations, they were kept at the values indicated in figure 1.4.

E_{rev} can be calculated from Nernst's equation:

$$E_{rev} = E^0 + \frac{RT}{2\mathcal{F}} \ln \frac{a_{O_2}^{0.5} a_A}{a_B} \tag{2.1.11}$$

Assuming ideal behaviour, which is justified in view of the fact that the operating pressure is atmospheric and the oper-

ating temperatures are relatively high, and, further, noting that the standard state considered is that of gaseous pure specie at 1 atm and system temperature, we can, with negligible error, write

$$E_{rev} = E^\circ + \frac{RT}{2\mathcal{F}} \ln \frac{P_{O_2}^{0.5} P_A}{P_B} \qquad (2.1.12)$$

Since we operate at unit pressure, equation (2.1.12) can be further written as:

$$E_{rev} = E^\circ + \frac{RT}{2\mathcal{F}} \ln \frac{y_{O_2}^{0.5} y_A}{y_B} \qquad (2.1.13)$$

Here, of course, y_{O_2} refers to oxygen activity on the cathodic side of the fuel cell (if sufficient excess air is provided, y_{O_2} will approach the limiting value of 21%; the trade-offs involved in selecting the appropriate air feed rate are discussed in section 2.1.3).

Since, by hypothesis, there is no oxygen present in the anode compartment, there is no change in mole number as a result of the chemical reaction, so that we can finally express equation (2.1.13) in terms of temperature and A-specie conversion x:

$$E_{rev} = E^\circ + \frac{RT}{2\mathcal{F}} \ln \frac{y_{O_2}^{0.5} (1-x)}{x} \qquad (2.1.14)$$

Substituting equation (2.1.14) into equation (2.1.8), and dividing through by $F_i [A]_i$, we finally have the dimensionless steady-state material balance for the ohmic-polarized fuel cell in which the reaction $A + 0.5\ O_2 \rightarrow B$ takes place

$$x = \frac{E^\circ + \frac{RT}{2\mathcal{F}} \ln \frac{y_{O_2}^{0.5}(1-x)}{x}}{(2\mathcal{F}) F_i [A]_i \left(R_{ex} + R_{el} + R_i^\circ \exp \frac{9700}{T}\right)} \qquad (2.1.15)$$

where (see equations (2.1.9) and (2.1.10)) R_i° replaces the 4.1666×10^{-3} d/S term.

As can be seen, equation (2.1.15) contains two unknowns (x

and T), the additional relation needed being provided by the energy balance. Since the first step involved in analyzing the steady state beaviour of the fuel cell is to solve equation (2.1.15) (i.e., for a given T, solve for x and then calculate any desired term, such as heat generation, heat removal, etc., from the energy balance), it is appropriate to briefly discuss the general features of equation (2.1.15), which can be rewritten as follows:

$$x = \alpha + \beta \ln \frac{1-x}{x} \tag{2.1.16}$$

$$\alpha = \frac{E^\circ + \frac{RT}{2\mathcal{F}} \ln y_{O_2}^{0.5}}{2\mathcal{F} F_i [A]_i (R_{ex} + R_{el} + R_i^\circ \exp \frac{9700}{T})} \tag{2.1.17}$$

$$\beta = \frac{RT}{(2\mathcal{F})^2 F_i [A]_i (R_{ex} + R_{el} + R_i^\circ \exp \frac{9700}{T})} \tag{2.1.18}$$

α and β are functions of T, exclusively; furthermore, α can be positive, negative, or zero, but β can only be positive. To satisfy the material balance, we must have

$$\phi = (x-\alpha-\beta \ln \frac{1-x}{x}) = 0 \tag{2.1.19}$$

The general qualitative behaviour of the ϕ vs. x relationship is seen in figure 2.2.

Figure 2.2.a shows the behaviour of the last term $(-\beta \ln \frac{1-x}{x})$ as a function of x, and the arrows indicate the influence of β (i.e., as T increases, so does β and the function becomes steeper). In figure 2.2.b. $x-\beta \ln \frac{1-x}{x}$ is plotted as a function of x. Since the logarithmic term becomes 0 at x = 0.5, all of the curves pass through the 0.5, 0.5 point. It can be seen that, as T (and therefore β) increases, the curve intersects the x axis at progressively

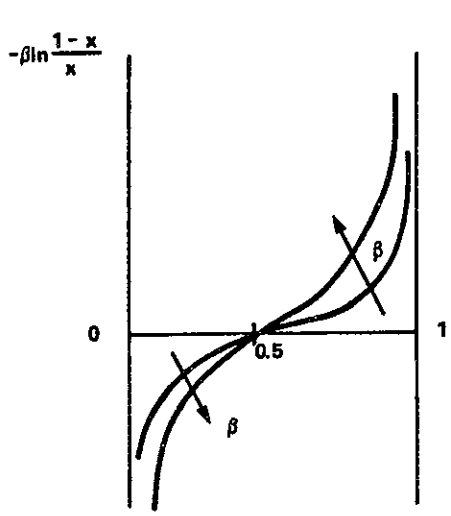

2.2.a

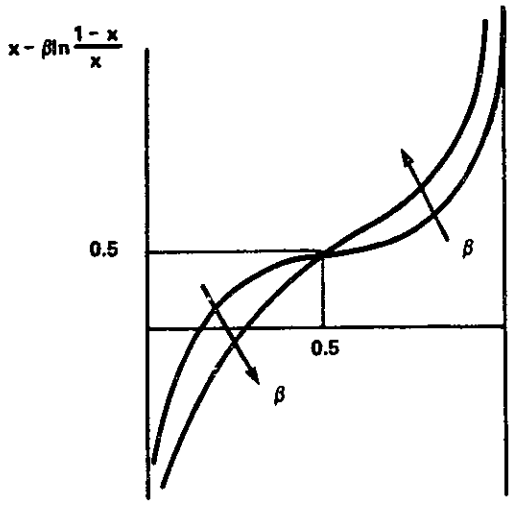

2.2.b

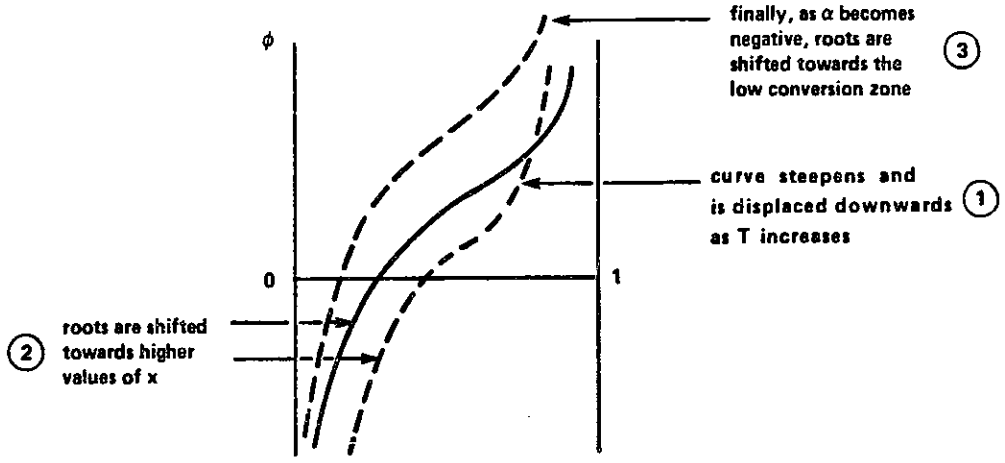

2.2.c

BEHAVIOUR OF MATERIAL BALANCE FUNCTION
FIGURE 2.2

higher values of conversion. It is therefore the temperature dependence of α that determines the behaviour of the material balance equation.

Since $y_{O_2} < 1$, the logarithmic term in α (see equation (2.1.17)) is negative and decreases with temperature (increasing in absolute value). $E°$, on the other hand, is positive (the fuel cell produces current), but can increase or decrease with temperature, according to the entropy vs. temperature characteristics of the system. In the H_2/H_2O and CO/CO_2 systems, $E°$ decreases with temperature (negative entropy change), so that, unless a very low air feed causes y_{O_2} to become small (and consequently the logarithmic term becomes sufficiently large in absolute value so that α is always negative), α is positive at low temperatures and negative at high temperatures. Consequently, the curves in figure 2.2.b are shifted downwards at low values of T, but at sufficiently high values of T, they are shifted upwards, with the consequence that roots of the ϕ vs. x equation, which without the presence of α would occur at progressively higher values of conversion as T increases, can, given the above conditions, occur at decreasing values of conversion at sufficiently high temperatures (in other words, the material balance curve for the system exhibits a maximum). This is indeed what is observed in figures 2.4 and 2.5.

Since the material balance (x vs. T) curve is, except for a scale factor, the heat generation vs. T curve (in the case of a fuel cell this is not exactly true, except as a limiting case, as will be shown in the discussion of the energy balance, but

the qualitative arguement still holds true), another interesting feature of fuel cells is therefore the existence of heat generation vs. temperature functions which exhibit not asymptotic behaviour but can show a maximum, and, moreover, the characteristics of this curve depend upon the air feed and the entropy change associated with the system under consideration. Figure 2.2.c qualitatively illustrates the behaviour of the ϕ vs. x function that leads to a maximum in the material balance (x vs. T) curve.

So far, in discussing the material balance curve, it has been assumed that the reaction under consideration is irreversible. The limit of applicability of this hypothesis can readily be calculated, as follows (although the treatment is general, the specific cases of CO and H_2 oxidation systems are considered here):

$$K = \frac{P_{CO_2}}{P_{CO}\, P_{O_2}^{1/2}} = \exp\left(\frac{-\Delta G_1^\circ}{RT}\right) \qquad (2.1.20)$$

$$K = \frac{P_{H_2O}}{P_{H_2} P_{O_2}^{1/2}} = \exp\left(\frac{-\Delta G_2^\circ}{RT}\right) \qquad (2.1.21)$$

Subscripts 1 and 2 refer to the CO and H_2 oxidation reactions, respectively. From Perry and Chilton (17), the following data are available for the reactions under consideration:

$$CO + \frac{1}{2} O_2 \rightarrow CO_2 \begin{cases} \Delta G^\circ = -61.452 \text{ Kcal/mole @ 298 K} \\ \Delta H^\circ = -67.636 \text{ Kcal/mole @ 298 K} \end{cases}$$

$$H_2 + \frac{1}{2} O_2 \rightarrow H_2O(g) \begin{cases} \Delta G^\circ = -54.6351 \text{ Kcal/mole @ 298 K} \\ \Delta H^\circ = -57.7979 \text{ Kcal/mole @ 298 K} \end{cases}$$

From these figures, we can calculate $\Delta S°$ @ 298·K, and we obtain

$$\Delta S_1^\circ = -0.02075 \frac{\text{Kcal}}{\text{mole K}} \tag{2.1.22}$$

$$\Delta S_2^\circ = -0.0106 \frac{\text{Kcal}}{\text{mole K}} \tag{2.1.23}$$

Since the present calculation is only good for estimation purposes, we can write

$$\Delta G°(T) \sim \Delta H^\circ_{298} - T\Delta S°_{298} \tag{2.1.24}$$

Therefore, expressing energy in joules, we have

$$\Delta G_1^\circ \sim -283178{\cdot}4 + 86.876T \tag{2.1.25}$$

$$\Delta G_2^\circ \sim -241988{\cdot}2 + 44{\cdot}38T \tag{2.1.26}$$

From equations (2.1.20) and (2.1.21), when O_2 formation is negligible,

$$p_{O_2}^{1/2} = \frac{p_{CO_2}}{K_1 p_{CO}} = \frac{x_1}{K_1(1-x_1)} \tag{2.1.27}$$

$$p_{O_2}^{1/2} = \frac{p_{H_2O}}{K_2 P_{H_2}} = \frac{x_2}{K_2(1-x_2)} \tag{2.1.28}$$

Solving for x,

$$x = \frac{1}{1 + \dfrac{1}{K\, p_{O_2}^{1/2}}} \tag{2.1.29}$$

Equations (2.1.27) and (2.1.28) give the amount of oxygen to be found in equilibrium with the reacting species, as a function of the conversion acheived through the electrochemical process. Conversely, equation (2.1.29) can be used to calculate the maximum conversion that can be acheived in the fuel cell before a <u>specified</u> amount of oxygen is detected assuming chemical equilibrium is attained. Combining equations (2.1.29), (2.1.25), (2.1.20),(2.1.21), and setting $P_{O_2} = 10^{-3}$, we obtain the results shown in Table 2.1.

TABLE 2.1:

Temperature and conversion limits within which $p_{O_2} < 10^{-3}$ atm

T (°K)	x_1	x_2
500	1	1
1000	0.999999998	0.999999998
1500	0.99985	0.999975
2000	0.95798	0.996859
2500	0.43064	0.945295

The reverse reaction can therefore be neglected within the limits specified by table 2.1

Before proceeding on to discuss the energy balance, it is worthwhile to note that multiplying equations (2.1.6) and (2.1.7), an expression for the power output of the fuel cell is obtained in terms of T, x and independently variable system parameters:

$$EI = \text{Power output} = \frac{E_{rev}^2 R_{ex}}{(R_{ex}+R_{el}+R_i)^2} \qquad (2.1.30)$$

2.1.2.2 Energy balance

Throughout the following discussion, ideal gas and ideal solution behaviour are assumed, and, therefore, pure component, rather than partial molal enthalpies, are used. Given the range of temperatures and pressure (atmospheric) in which the model is subsequently applied, these assumptions involve negligible error. Again, consider the general reaction:

$$A + \frac{1}{2} O_2 \rightarrow B$$

Fuel, A is fed either pure, or, more generally, a diluent gas, C(N_2 or He, for example) is added to the feed. Though the treatment is identical, the results presented here consider N_2 as diluent gas. Figure 2.3 schematically illustrates the control volume for the energy balance calculation. The enthalpy flux associated with the fuel feed can be written as:

$$\underline{\text{Fuel enthalpy flux}} = \dot{N}_{Ai}[H_{Ao} + \hat{C}p_{Ai}(T_i-T_o)]+\dot{N}_C[H_{Co}+\hat{C}p_{Ci}(T_i-T_o)] \qquad (2.1.31)$$

The subscripted heat capacity has the following meaning:

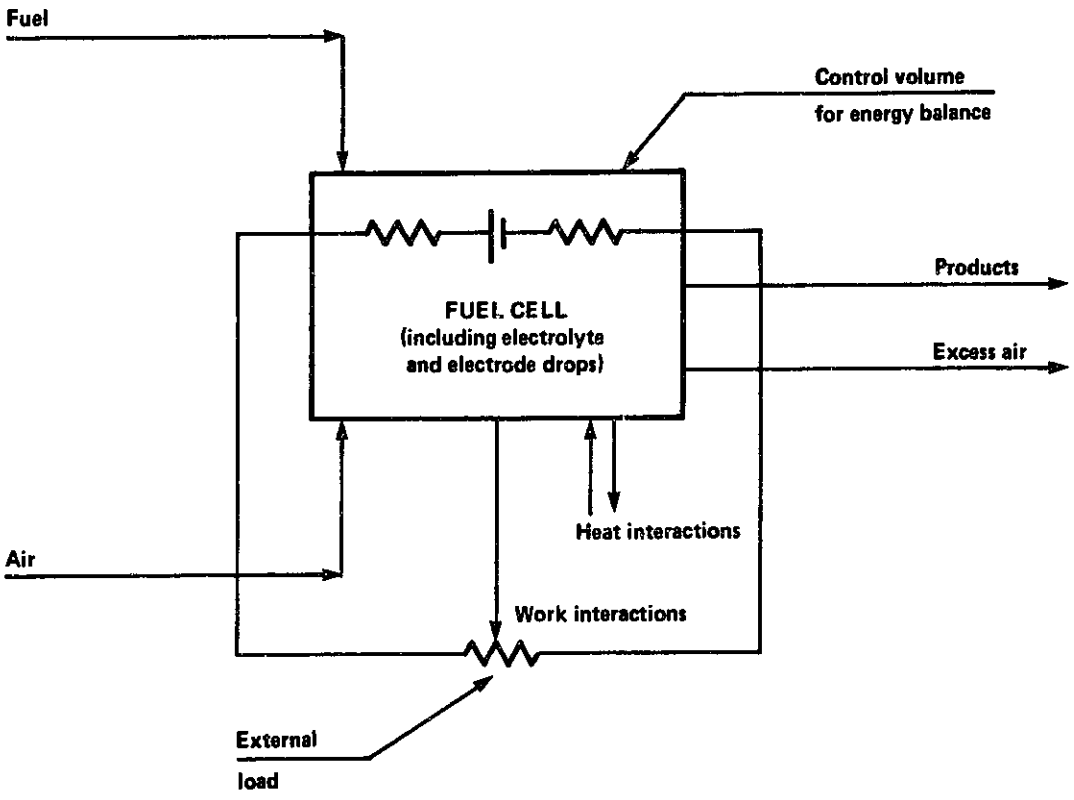

CONTROL VOLUME FOR ENERGY BALANCE
FIGURE 2.3

$$\hat{Cp}_i = \frac{\int_{T_o}^{T_i} Cp\,dT}{T_i - T_o} \qquad (2.1.32)$$

The notation convention is therefore:

^ = indicates an averaged property

i = indicates upper limit of integration

Since the diluent is an element, its pure component enthalpy can be set to o. Equation (2.1.31) can be rewritten as follows:

Fuel enthalpy flux:

$$\dot{N}_{Ai}\ H_{Ao} + (\dot{N}_{Ai}+\dot{N}_c)\,[y_{Ai}\hat{Cp}_{Ai} + (1-y_{Ai})\hat{Cp}_{Ci}]\,(T_i-T_o) \qquad (2.1.33)$$

The bracketed term is simply an averaged molar heat capacity. Denoting this term by $\hat{Cp}_{fi}$, where subscript f indicates fuel feed stream, the fuel enthalpy flux is:

Fuel enthalpy flux: $\dot{N}_{Ai}\ H_{Ao} + (\dot{N}_{Ai}+\dot{N}_c)\hat{Cp}_{fi}\,(T_i-T_o)$ (2.1.34)

The H_{Ao} term also disappears, of course, if the fuel is an element (H_2, for example). In considering the air enthalpy flux, it is convenient to "separate" the reacting oxygen from the rest of the air flow. As can be seen from equations (2.1.1) and (2.1.2), 0.5 moles of oxygen are consumed per mole of fuel reacted. Consequently, the molar flux of oxygen actually taking part in the electrochemical reaction is given by

Reacting oxygen molar flux: $\frac{0.5\ I}{2\mathcal{F}} = \dot{N}_{O_2} = \frac{I}{4\mathcal{F}}$ (2.1.35)

The associated enthalpy flux is thus

Reacting oxygen enthalpy flux: $\frac{I}{4\mathcal{F}}\hat{Cp}_{O_2 j}\,(T_j-T_o)$ (2.1.36)

Where j denotes air inlet conditions.

$$\hat{Cp}_i = \frac{\int_{T_o}^{T_i} Cp\,dT}{T_i - T_o} \qquad (2.1.32)$$

The notation convention is therefore:

$\hat{}$ = indicates an averaged property

i = indicates upper limit of integration

Since the diluent is an element, its pure component enthalpy can be set to o. Equation (2.1.31) can be rewritten as follows:

Fuel enthalpy flux:

$$\dot{N}_{Ai}\ H_{Ao} + (\dot{N}_{Ai}+\dot{N}_c)\left[y_{Ai}\hat{Cp}_{Ai} + (1-y_{Ai})\hat{Cp}_{Ci}\right](T_i-T_o) \qquad (2.1.33)$$

The bracketed term is simply an averaged molar heat capacity. Denoting this term by $\hat{Cp}_{fi}$, where subscript f indicates fuel feed stream, the fuel enthalpy flux is:

$$\text{Fuel enthalpy flux: } \dot{N}_{Ai}\ H_{Ao} + (\dot{N}_{Ai}+\dot{N}_c)\hat{Cp}_{fi}(T_i-T_o) \qquad (2.1.34)$$

The H_{Ao} term also disappears, of course, if the fuel is an element (H_2, for example). In considering the air enthalpy flux, it is convenient to "separate" the reacting oxygen from the rest of the air flow. As can be seen from equations (2.1.1) and (2.1.2), 0.5 moles of oxygen are consumed per mole of fuel reacted. Consequently, the molar flux of oxygen actually taking part in the electrochemical reaction is given by

$$\text{Reacting oxygen molar flux: } \frac{0.5\ I}{2\mathcal{F}} = \dot{N}_{O_2} = \frac{I}{4\mathcal{F}} \qquad (2.1.35)$$

The associated enthalpy flux is thus

$$\text{Reacting oxygen enthalpy flux: } \frac{I}{4\mathcal{F}}\hat{Cp}_{O_2 j}\ (T_j-T_o) \qquad (2.1.36)$$

Where j denotes air inlet conditions.

Air will, in general, be fed at a rate higher than stoichiometric (see section 2.1.3 for a discussion of air feed rate determination), so that, to make the equations as general as possible, the excess air will, for the moment, be arbitrary, although it is obvious that the air flow will be some multiple of the stoichiometric requirement. Therefore, calling $\dot{N}_{Air}$ the arbitrary air feed rate, and assuming the air composition to be 79% N_2 and 21% O_2 by volume, the N_2 and non-reacting O_2 fluxes are:

$$\underline{N_2 \text{ molar flux}}: \quad 0.79\ \dot{N}_{Air} \tag{2.1.37}$$

$$\underline{O_2 \text{ (non-reacting) molar flux}}: \quad 0.21\ \dot{N}_{Air} - \frac{I}{4\mathcal{F}} \tag{2.1.38}$$

The associated enthalpy fluxes are therefore:

$$\underline{N_2 \text{ enthalpy flux:}} \quad 0.79\ \dot{N}_{Air}\ \hat{Cp}_{N_2 j}\ (T_j - T_o) \tag{2.1.39}$$

$$\underline{O_2 \text{ (non-reacting) enthalpy flux:}}$$

$$(0.21\ \dot{N}_{Air} - \frac{I}{4\mathcal{F}})\ \hat{Cp}_{O_2 j}\ (T_j - T_o) \tag{2.1.40}$$

The total non-reacting air enthalpy flux is therefore

$$\underline{\text{Non-reacting air enthalpy flux:}}$$

$$(\dot{N}_{Air}\ \hat{Cp}_{Air j} - \frac{I}{4\mathcal{F}}\ \hat{Cp}_{O_2 j})\ (T_j - T_o) \tag{2.1.41}$$

Adding (2.1.34), (2.1.36) and (2.1.41) we obtain the total enthalpy input rate to the control volume:

$$\underline{\text{Enthalpy input:}}$$

$$\dot{N}_{Ai} H_{Ao} + (\dot{N}_{Ai} + \dot{N}_c)\hat{Cp}_{fi}(T_i - T_o) + \dot{N}_{Air}\hat{Cp}_{Air j}(T_j - T_o) \tag{2.1.42}$$

The products consist, in the more general case, of diluent gas, C, unreacted fuel, A, and combustion product, B. No O_2 is present in this stream, as a consequence of the fundamental hypothesis (see 2.1.1.2) whereby oxygen electrolyte transport is the rate-

limiting step for the whole process.

The enthalpy output associated with the products is, therefore

$$\underline{\text{Enthalpy output:}}\ \dot{N}_{Ai}\ (1-x)\,[H_{Ao} + \hat{C}p_A(T-T_o)] + \dot{N}_C\hat{C}p_C(T-T_o) + \\ + \dot{N}_{Ai}\ x\ [H_{BO} + \hat{C}p_B(T-T_o)] \qquad (2.1.43)$$

Unsubscripted quantities (specific heats and temperatures) refer to reactor conditions (equal to outlet conditions, in view of the CSTR hypothesis).

Equation (2.1.43) can be conveniently rearranged to read

$$\underline{\text{Enthalpy output:}}\ \dot{N}_{Ai}\ [(1-x)H_{Ao} + x\ H_{Bo}] + (\dot{N}_{Ai}+\dot{N}_C)\hat{C}p_p(T-T_o) \qquad (2.1.44)$$

Here, $\hat{C}p_p$ denotes a molar average product heat capacity, i.e.

$$\hat{C}p_p = (1-y_{Ai})\ \hat{C}p_C + y_{Ai}\ x\ \hat{C}p_B + y_{Ai}\ (1-x)\ \hat{C}p_A \qquad (2.1.45)$$

Note that there is no change in mole number associated with the reaction occuring in the anodic chamber, since the following mole balances apply:

$$\dot{N}_A = \dot{N}_{Ai}\ (1-x) \qquad (2.1.46)$$

$$\dot{N}_C = \dot{N}_C \qquad (2.1.47)$$

$$\dot{N}_B = \dot{N}_{Ai}\ x \qquad (2.1.48)$$

$$\dot{N}_{TOTAL} = \dot{N}_{Ai} + \dot{N}_C \ = \text{inlet flow to anode} \qquad (2.1.49)$$

The enthalpy output associated with the excess air is

$$\underline{\text{Excess air enthalpy output:}} \\ (\dot{N}_{Air}\hat{C}p_{Air} - \tfrac{I}{4\mathcal{F}}\hat{C}p_{O_2})\ (T-T_o) \qquad (2.1.50)$$

Finally, the system may undergo heat interactions with the environment, and produces a net energy output. The heat interaction may be expressed as

$$\underline{\text{Heat interaction:}} \quad UA(T-T_c) \qquad (2.1.51)$$

This form of the above expression requires some clarification: implicit in equation (2.1.51) is the assumption that the system's only temperature to be considered is T. This is true if the heat interaction involves cooling the anodic chamber by means of a cooling coil, for example. As it turns out, self ignited operation is a very desirable goal, for fuel cell operation at other than laboratory conditions, and, in fact, most of the results to be presented are concerned with the determination of process conditions whereby ignited operation can be achieved, and, in all cases, this involved some appropriate modification of cell geometry (stacking) in such a way that heat losses could be conveniently reduced. This being the case, the problem is then not how to cool the reactor, but, rather, how to keep it from losing heat. Therefore in all of the results presented the heat interaction involved consisted in heat losses to the environment, which, of course, are primarily dependent on system geometry. The U term, therefore, for a reactor geometry like the one shown in figure 1.5, suitable for experimental purposes, contains several resistances to heat transfer lumped together, and may involve any one of the following (appropriately combined):

heat transfer from gas to reactor walls

heat transfer across reactor walls

heat transfer from reactor walls to excess air

heat transfer from excess air to external walls

heat transfer across external walls

heat transfer from external walls to surroundings

The complexities of the first three mechanisms can be eliminated in the case of a well-mixed air-chamber (i.e., not only do we assume that air leaves at the same temperature as the products, but it is everywhere at this temperature). It is evident (see figure 1.5), that, as the controlling resistance to heat transfer is displaced towards the outside, isothermal conditions within the reactor tend to prevail (in the limit, a perfectly insulated reactor contains no radial gradients). Nevertheless, any series steady state heat transfer problem can be reduced to an expression such as equation (2.1.51)(assuming a well mixed air chamber), but the individual effects can only be evaluated once U is explicitly expressed in terms of the single resistances. On the other hand, it can be seen that cells such as the ones shown in figure 1.6 (which represent a more practical and realistic design) when properly insulated, and considering that anode and cathode are separated by the extremely thin electrolyte, can be modeled through equation (2.1.51) very adequately. In the limit, U represents the heat transfer coefficient of the insulation.

From the above brief considerations, it should be evident that a thorough study of possible cell configurations and their corresponding heat transfer characteristics is a logical extension of the present work when modeling an experimental reactor such as the one shown in figure 1.5; however, in considering a practical design (figures 1.6.a,1.6.b), a simple equation such as (2.1.51) is not only adequate, but extremely

useful also, providing, as it does, a means of estimating insulation thickness and stacking. Therefore, although the equations and results presented are completely general, the conclusions apply directly to a cell arrangement such as the one shown in figures 2.23, III-1 and III-2, composed of units such as the ones shown in figure 1.6, but verification of the implied isothermality and perfect mixing should precede any application of such relationships to a cell such as the one illustrated in figure 1.5, or, if designing such a reactor, chamber geometry (especially air chamber) and insulation should be so specified as to satisfy the above requirements, if the model is to apply. Returning to the energy balance, the work interaction can be simply expressed as

$$\underline{\text{Work interaction}}: \; EI \tag{2.1.52}$$

The complete steady-state energy balance can be written combining equations (2.1.34), (2.1.36), (2.1.41), (2.1.44), (2.1.50), (2.1.51) and (2.1.52),

$$\begin{aligned}&\dot{N}_{Ai}\, H_{AO} + (\dot{N}_{Ai} + \dot{N}_C)\hat{C}p_{fi}(T_i - T_o) + \frac{I}{4\mathcal{F}}\hat{C}p_{O_2 j}\,(T_j - T_o) + \\ &+ (\dot{N}_{Air}\hat{C}p_{Airj} - \frac{I}{4\mathcal{F}}\hat{C}p_{O_2 j})(T_j - T_o) = \dot{N}_{Ai}\,[(1-x)H_{Ao} + x\,H_{BO}] + \\ &+ (\dot{N}_{Ai}+\dot{N}_c)\,\hat{C}p_p(T-T_o) + (\dot{N}_{Air}\hat{C}p_{Air} - \frac{I}{4\mathcal{F}}\hat{C}p_{C_2})(T-T_o) + UA(T-T_c) + EI\end{aligned} \tag{2.1.53}$$

The various terms in this equation can be reordered as follows:

$$\begin{aligned}&\dot{N}_{Ai}\, x(H_{Ao}-H_{BO}) - EI + (\dot{N}_{Ai} + \dot{N}_c)\hat{C}p_{fi}(T_i - T_o) + \frac{I}{4\mathcal{F}}\hat{C}p_{O_2 j}\,(T_j - T_o) + \\ &+ (\dot{N}_{Air}\,\hat{C}p_{Airj} - \frac{I}{4\mathcal{F}}\hat{C}p_{O_2 j})(T_j - T_o) = (\dot{N}_{Ai}+\dot{N}_C)\hat{C}p_p(T-T_o) + \\ &+ (\dot{N}_{Air}\hat{C}p_{Air} - \frac{I}{4\mathcal{F}}\hat{C}p_{O_2})(T-T_o) + UA(T-T_c)\end{aligned} \tag{2.1.54}$$

The first two terms on the left-hand side can be simplified

considering the assumption (see 2.1.1.2) that oxygen anion transport is the rate-limiting step. When this is so, the following equation holds:

$$\dot{N}_{Ai}\, x = \frac{I}{2\mathcal{F}} \tag{2.1.55}$$

Equation (2.1.55), of course, is exactly equivalent to the final expression for the material balance, i.e., equation (2.1.15). If mass transfer becomes rate-controlling, fuel and oxygen can react at a rate not governed by current flow, and neither equation holds. The pure component enthalpy difference, moreover, is $-\Delta H^{\circ}_{0}$, where the superscript indicates unit activity, and the subscript, reference temperature. Therefore,

$$\dot{N}_{Ai} x (H_{AO}-H_{BO}) - EI = \frac{I}{2\mathcal{F}} [-\Delta H^{\circ}_{0} - 2\mathcal{F}E] = (-\Delta H^{\circ}_{0})\frac{I}{2\mathcal{F}} \left[1 - \frac{E}{(-\Delta H^{\circ}_{0}/2\mathcal{F})}\right] \tag{2.1.56}$$

Equation (2.1.56) is a very important one, since it expresses both the rate of heat generation, and the efficiency with which chemical energy is converted into electrical energy. In fact, the overall exothermal process generates heat at the rate given by

$$\underline{\text{Heat "generation" rate:}}\ (-\Delta H^{\circ}_{0})\ \frac{I}{2\mathcal{F}} \tag{2.1.57}$$

of which a fraction is converted into electrical energy

$$\underline{\text{Fraction converted to electrical work:}}\ \frac{E}{(-\Delta H^{\circ}_{0}/2\mathcal{F})} \tag{2.1.58}$$

It is therefore appropriate to identify this term with an efficiency, and we can therefore say

$$\eta = \frac{E}{(-\Delta H^{\circ}_{0}/2\mathcal{F})} \tag{2.1.59}$$

The term $(-\Delta H^{\circ})/2\mathcal{F}$ has units of voltage, and it will henceforth be called "thermoneutral" voltage (i.e., a system operating at a voltage equal to the thermoneutral would convert all of its chemical energy to electrical energy, with no exothermic effects associated with the overall process, assuming adiabatic operation, which means that reactants must be fed at operating temperature, acheiving, consequently, self-sustained isothermal operation, hence the illustrative, if slightly informal term "thermoneutral"). This brief discussion of equations (2.1.56) to (2.1.59) leads quite naturally to one of the main points to be understood with respect to fuel cell operation, namely, that the maximum efficiency attainable at any given temperature corresponds to zero power output ($I \to 0$, $E \to E_{rev}$, $R_{ex} \to \infty$), so that it is impossible to simultaneously maximize efficiency and power output. Furthermore, it is worthwhile to note that, even if heat effects are thermodynamically inefficient, a high-temperature solid electrolyte fuel cell operates only at high temperatures, and hence a compromise is again necessary if the system is to operate authothermally. Finally, bebefore proceeding further in the derivation of the energy balance, a final point is worthy of comment, namely, the influence of the entropy change associated with the reaction upon the thermodynamic efficiency and energy conversion characteristics.

From equation (2.1.7), it can be seen that the actual voltage is very simply related to the reversible (Nernst) voltage. Therefore we can write

$$E = \frac{R_{ex}\, E_{rev}}{R_{ex}+R_{el}+R_i} = \left(\frac{R_{ex}}{R_{ex}+R_{el}+R_i} \right) \left[E^{\circ} + \frac{RT}{2\mathcal{F}} \ln \frac{y_{O_2}^{0.5}(1-x)}{x} \right] \quad (2.1.60)$$

The first term in brackets is, of course, related to the Gibbs free energy,

$$E^\circ = \frac{-\Delta G^\circ}{2\mathcal{F}} \tag{2.1.61}$$

But

$$\Delta G^\circ = \Delta H^\circ - T\Delta S^\circ \tag{2.1.62}$$

ΔS° is, of course, a function of temperature but for the present purpose it suffices to put $\Delta H^\circ \sim \Delta H_0^\circ$, $\Delta S^\circ \sim \Delta S_0^\circ$, and therefore

$$\Delta G^\circ(T) \simeq \Delta H_0^\circ - T\Delta S_0^\circ \tag{2.1.63}$$

It can therefore be seen that, for systems where ΔS_0° is negative, ΔG° will decrease <u>in absolute value</u> with temperature, the converse being true for systems characterized by positive entropy changes. This means that the first (and most important, except at very high or very low convenrsions, in which case the logarithmic term becomes important) component of cell voltage decreases with temperature for negative entropy systems (H_2 and CO, for example), but increases with temperature for systems characterized by a positive entropy change (NH_3 fuel cell, for example). The qualitative conclusion to be drawn from this is that, at sufficiently high temperatures, and given an inherently small electrode resistance, the external load becomes the controlling resistance, E behaves as E_{rev}, and, unless extremely high or extremely low conversions make the logarithmic term important, the voltage behavior is mainly characterized by E°, in which case we can schematize the following trends as we increase the temperature for any given fixed conversion.

Negative entropy change → decreasing efficiency →

increasing effective exothermicity

Positive entropy change → increasing efficiency →

system tends to cool itself

Of course, high electrode resistances, extreme conversions, etc. contribute to alter or mask these qualitative features which, nevertheless should be borne in mind while analyzing possible fuel cell systems. Thus, one would expect a H_2 or a CO fuel cell to operate autothermally with increased easiness as the system temperature is increased, while the converse is true for the NH_3 fuel cell.

Dropping the superscript on the enthalpy of reaction term, since ideal solutions are assumed throughout, we have

$$(-\Delta H_o)\ \frac{I}{2\mathcal{F}}\left[1-\frac{E_{rev}R_{ex}}{\Sigma R(-\Delta H_o/2\mathcal{F})}\right]+(\dot{N}_{Ai}+\dot{N}_c)\hat{C}p_{fi}(T_i-T_o)+$$

$$+\dot{N}_{Air}\hat{C}p_{Airj}(T_j-T_o)\ =\ UA\ (T-T_c)+(\dot{N}_{Ai}+\dot{N}_c)\hat{C}p_p(T-T_o)+$$

$$+\left[\dot{N}_{Air}\hat{C}p_{Air}-\frac{I}{4\mathcal{F}}\hat{C}p_{O_2}\right](T-T_o) \qquad (2.1.64)$$

Where

$$\Sigma R = R_{ex} + R_{el} + R_i^\circ\ \exp\left(\frac{9700}{T}\right) \qquad (2.1.65)$$

The current can be related to temperature and conversion through equations (2.1.6) and (2.1.14), to obtain the following expression for the energy balance:

$$\left\{\frac{(-\Delta H_o)\ \{E^\circ+\frac{RT}{2\mathcal{F}}\ln\ [y_{O_2}^{0.5}(1-x)/x]\}}{2\mathcal{F}[R_{ex}+R_{el}+R_i^\circ\ \exp\frac{9700}{T}]}\right\}\left\{1-\frac{E^\circ+\frac{RT}{2\mathcal{F}}\ln[y_{O_2}^{0.5}(\frac{1-x}{x})]}{(1+\frac{R_{el}}{R_{ex}}+\frac{R_i^\circ}{R_{ex}}\exp\frac{9700}{T})(\frac{-\Delta H^\circ}{2\mathcal{F}})}\right\}+$$

$$+\ (\dot{N}_{Ai}+\dot{N}_c)\hat{C}p_{fi}(T_i-T_o)+\dot{N}_{Air}\hat{C}p_{Airj}(T_j-T_o)=\ UA(T-T_c)\ +$$

$$+\left\{(\dot{N}_{Ai}+\dot{N}_c)\hat{C}p_p+\dot{N}_{Air}\hat{C}p_{Air}-\left[\frac{E^\circ+\frac{RT}{2\mathcal{F}}\ln\frac{y_{O_2}^{0.5}(1-x)}{x}}{4\mathcal{F}(R_{ex}+R_{el}+R_i^\circ\exp\frac{9700}{T})}\right]\hat{C}p_{O_2}\right\}(T-T_o)$$

(2.1.66)

Care must be taken not to confuse E° with E_0, the former being a function of temperature, and the latter no.

Equation (2.1.66) is still not completely explicit in x, since the conversion is contained in the $\hat{C}p_p$ term. Furthermore, since the material and energy balance must be solved simultaneously, the molar fluxes must be related to the volumetric flow rate used in the material balance which is the quantity experimentally measured. Thus

$$F_i[A]_i = \dot{N}_{Ai} \tag{2.1.67}$$

$$\dot{N}_c = F_i[A]_i\left(\frac{1-y_{Ai}}{y_{Ai}}\right) \tag{2.1.68}$$

Therefore,

$$\dot{N}_{Ai}+\dot{N}_c = F_i[A]_i\left\{\frac{1-y_{Ai}}{y_{Ai}}+1\right\} = \frac{F_i[A]_i}{y_{Ai}} = \frac{F_i\pi_i}{RT_i} \tag{2.1.69}$$

But the experimentally measured quantity is the feed flow rate at some reference condition; for convenience let this reference conditions be T_o, as for datum enthalpies, and atmospheric pressure. Furthermore, allowing for pressure drop across the feed orifice, (see Appendix I), and assuming ideal gas behaviour,

$$F_i = \left(\frac{F_o T_i}{T_o}\right)\left(\frac{\pi_o}{\pi_i}\right) \tag{2.1.70}$$

Therefore,

$$\dot{N}_{Ai}+\dot{N}_c = \frac{F_o\pi_o}{R\,T_o} \tag{2.1.71}$$

Note, however, that even if fuel cell operation were not atmospheric, equation (2.1.71) would still be valid, since the molar flow rate is independent of pressure.

In addition, we note that y_{O_2} is not an independent variable, as equation (2.1.66) would seem to imply, but is determined by N_{Air} and I as follows:

$$\underline{\text{Total moles of air fed per unit time:}} \quad \dot{N}_{Air} \tag{2.1.72}$$

$$\underline{\text{Total moles of } O_2 \text{ fed per unit time:}} \quad 0.21\ \dot{N}_{Air} \tag{2.1.73}$$

$$\underline{\text{Moles of } O_2 \text{ reacted:}} \quad \frac{I}{4\mathcal{F}} \tag{2.1.74}$$

$$\underline{\text{Mole fraction of } O_2 \text{ in outlet air stream:}} \quad \frac{0.21\ \dot{N}_{AIR} - \frac{I}{4\mathcal{F}}}{\dot{N}_{AIR} - \frac{I}{4\mathcal{F}}} \tag{2.1.75}$$

There is still a further question concerning y_{O_2}. The flow characteristics of air within the exterior of the anodic chamber depend primarily upon the system goemetry and air flow rate. Thus, unless a specific geometry is considered, y_{O_2} cannot be properly defined. In the present model, the air chamber has been assumed well mixed, and, consequently, y_{O_2} can be calculated from equation (2.1.75), or, more correctly, equation (2.1.75) can be substituted back into equation (2.1.66) with the appropriate expressions, i.e., equations (2.1.6) and (2.1.14), used to calculate I. However, a further simplification can be introduced if we define a new parameter, the ratio of actual air feed rate to stoichiometric requirement.

Let, therefore,

$$Z = \frac{\text{Actual air feed rate}}{\text{Stoichiometric air feed rate}} \tag{2.1.76}$$

Under the assumption that air is always fed at a certain ratio with respect to its stoichiometric requirements, we have

$$\underline{O_2 \text{ stoichiometric requirement:}} \quad \frac{I}{4\mathcal{F}} \tag{2.1.74}$$

$$\underline{\text{Air stoichiometric requirement:}} \quad \frac{I}{0.21(4\mathcal{F})} \tag{2.1.77}$$

$$\underline{\text{Air actual feed rate:}} \quad \frac{Z\ I}{0.21(4\mathcal{F})} = \dot{N}_{Air} \tag{2.1.78}$$

Equation (2.1.75) then becomes

$$\underline{y_{O_2} \text{ at outlet}} = \frac{\frac{ZI}{4\mathcal{F}} - \frac{I}{4\mathcal{F}}}{\frac{ZI}{0.21(4\mathcal{F})} - \frac{I}{4\mathcal{F}}} = \frac{Z-1}{\frac{Z}{0.21}-1} = \frac{0.21(Z-1)}{Z-0.21} \tag{2.1.79}$$

Note that for a well mixed air chamber a stoichiometric air feed (Z=1) leads to an indertermination in equation (2.1.66), since the logarithmic term becomes infinite. Substituting equations (2.1.71), (2.1.78) and (2.1.79) into equation (2.1.66), we finally obtain, after some algebraic manipulation, and use of equation (2.1.45) (see section 2.1.2.6 for dimensionless equations)

$$\frac{(-\Delta H_o)\{E^\circ+(\frac{RT}{2\mathcal{F}})\ln\left[\sqrt{\frac{0.21(Z-1)}{Z-0.21}}\ (\frac{1-x}{x})\right]\}}{2\mathcal{F}[R_{ex}+R_{el}+R_i^\circ \exp\frac{9700}{T}]}\left\{1-\frac{E^\circ+(\frac{RT}{2\mathcal{F}})\ln\left[\sqrt{\frac{0.21(Z-1)}{Z-0.21}}(\frac{1-x}{x})\right]}{(1+\frac{R_{el}}{R_{ex}}+\frac{R_i^\circ}{R_{ex}}\exp\frac{9700}{T})(\frac{-\Delta H_o}{2\mathcal{F}})}\right\}+$$

$$+\frac{F_o\pi_o}{R\ T_o}\{[y_{Ai}\hat{C}p_{Ai}+(1-y_{Ai})\hat{C}p_{ci}](T_i-T_o)-[(1-y_{Ai})\hat{C}p_c+y_{Ai}x\hat{C}p_B+$$

$$+\ y_{Ai}(1-x)\hat{C}p_A](T-T_o)\}+$$

$$+\frac{E^\circ+(\frac{RT}{2\mathcal{F}})\ln\left[\sqrt{\frac{0.21(Z-1)}{Z-0.21}}\ (\frac{1-x}{x})\right]}{4\mathcal{F}(R_{ex}+R_{el}+R_i^\circ \exp\frac{9700}{T})}\left\{\frac{Z}{0.21}\ [\hat{C}p_{Airj}(T_j-T_o)-\hat{C}p_{Air}(T-T_o)]+\right.$$

$$\left.+\ \hat{C}p_{O_2}(T-T_o)\right\}-UA(T-T_c)=0 \tag{2.1.80}$$

The material balance can finally be expressed including the correct expression for y_{O_2}:

$$x = \frac{E^\circ + \left(\frac{RT}{2\mathcal{F}}\right) \ln\left[\sqrt{\frac{0.21(Z-1)}{Z-0.21}}\left(\frac{1-x}{x}\right)\right]}{2\mathcal{F}\left(R_{ex}+R_{el}+R_i^\circ \exp\frac{9700}{T}\right)\left(\frac{F_o y_{Ai} \pi_o}{RT_o}\right)} \qquad (2.1.81)$$

Equations (2.1.80) and (2.1.81), then, together with appropriate expressions for the heat capacities and E° as a function of temperature, are to be solved simultaneously for a variety of cases and conditions in order to arrive at a meaningful picture of the steady state characteristics of the high temperature fuel cell. The assumptions and restrictions involved in this derivation are now listed for completion:

(i) perfect mixing of fuel and air chambers

(ii) ohmic polarization

(iii) anion transport through electrolyte is the rate controlling step (equivalent to (ii))

(iv) air feed is a fixed multiple of the stoichiometric requirement throughout (i.e., Z and not $\dot{N}_{Air}$ is arbitrarily fixed)

(v) the overall process can be written as $A + \frac{1}{2} O_2 \rightarrow B$

(vi) electrolyte resistance can be expressed through equation (2.1.10)

(vii) the overall heat interaction can be expressed by means of equation (2.1.51)

(viii) atmospheric pressure within the cell

The high non-linearity of equations (2.1.80) and (2.1.81) mandates the use of a computer if, as in the present case, a systematic study of these equations, their meaning and consequences,

and their behaviour under differing external parameters, etc., is to be undertaken. If must be noted that assumption (iv) can be dropped and the equations can still be solved: this would involve replacing y_{O_2} by the corresponding expression (2.1.75), and I writeen in terms of conversion through equation (2.1.55). The resulting expression, involving the parameter $\dot{N}_{Air}$ instead of Z, can be similarly obtained and is not considered here. Furthermore, the assumption of perfect air mixing could presumably be dropped while still using a unique value for y_{O_2}; this would involve the choice of a suitable averaging of inlet and outlet oxygen concentrations.

2.1.3 Results

2.1.3.1 The steady state material balance

Equation (2.1.81) was solved by means of Newton-Raphson's method, which is particularly suitable in this case, in view of the function's behaviour (see figure 2.2). The approach was to use T as the independent variable and calculate the corresponding x-value. The fuel cell operating point, of course, is determed by simultaneously solving equations (2.1.80) and (2.1.81).

Figure 2.4 shows the effect of external load upon conversion for the CO/CO_2 system, and figure 2.5 the corresponding curves for the H_2/H_2O system. Note the maximum in the x vs. T curves for all values of R_{ex} as discussed in section 2.1.2.1 and figure 2.2. The effect of R_{ex} is evident, and, as explained in section 2.1.2.1, provides an excellent means of "freezing" the reactor if and when necessary.

Figure 2.6 illustrates the effect of air feed ratio (see

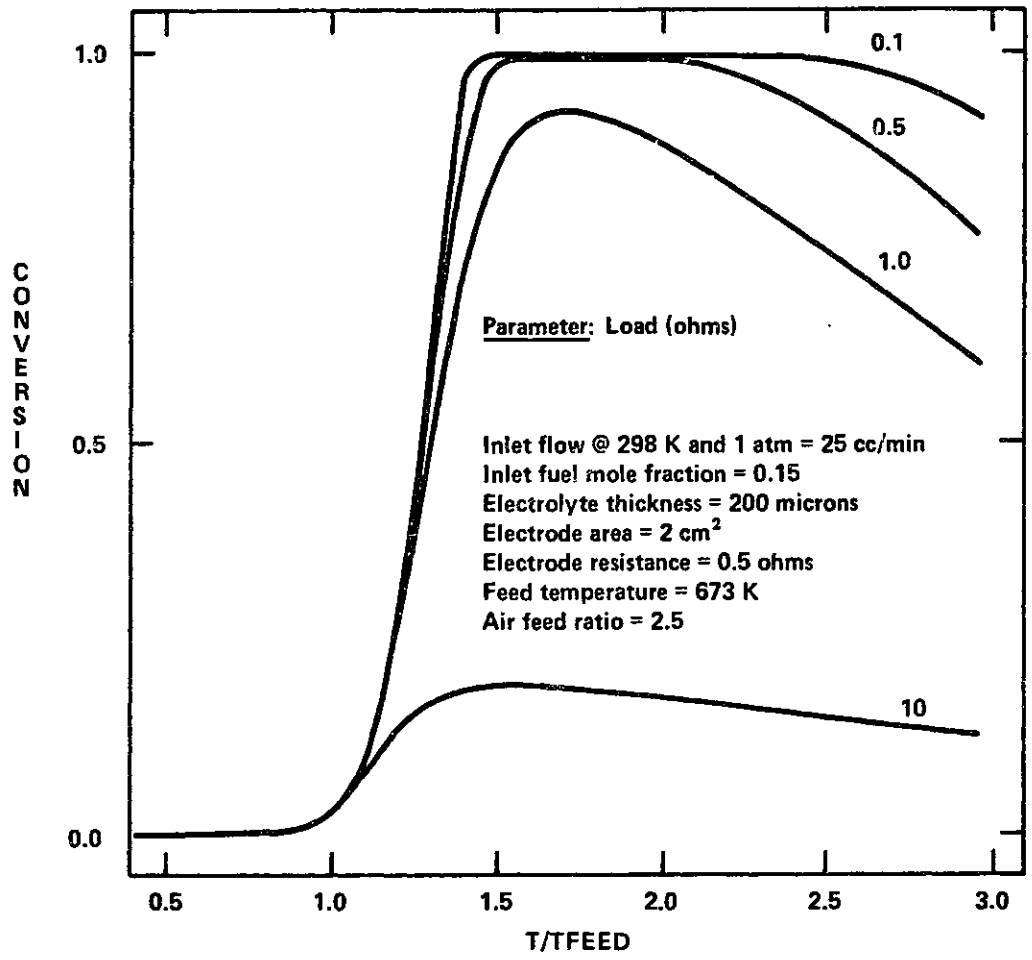

INFLUENCE OF LOAD UPON CONVERSION (CO/CO_2 CELL)
FIGURE 2.4

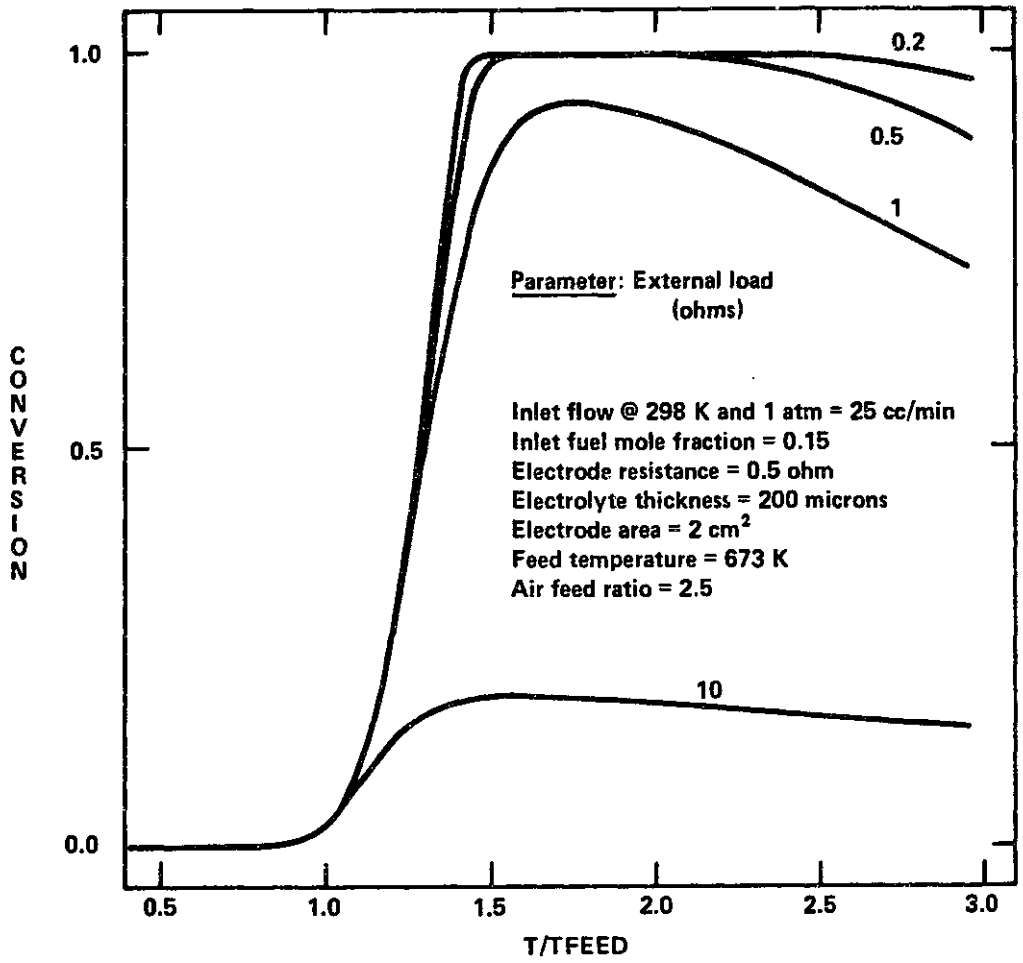

EFFECT OF LOAD UPON CONVERSION (H_2/H_2O CELL)
FIGURE 2.5

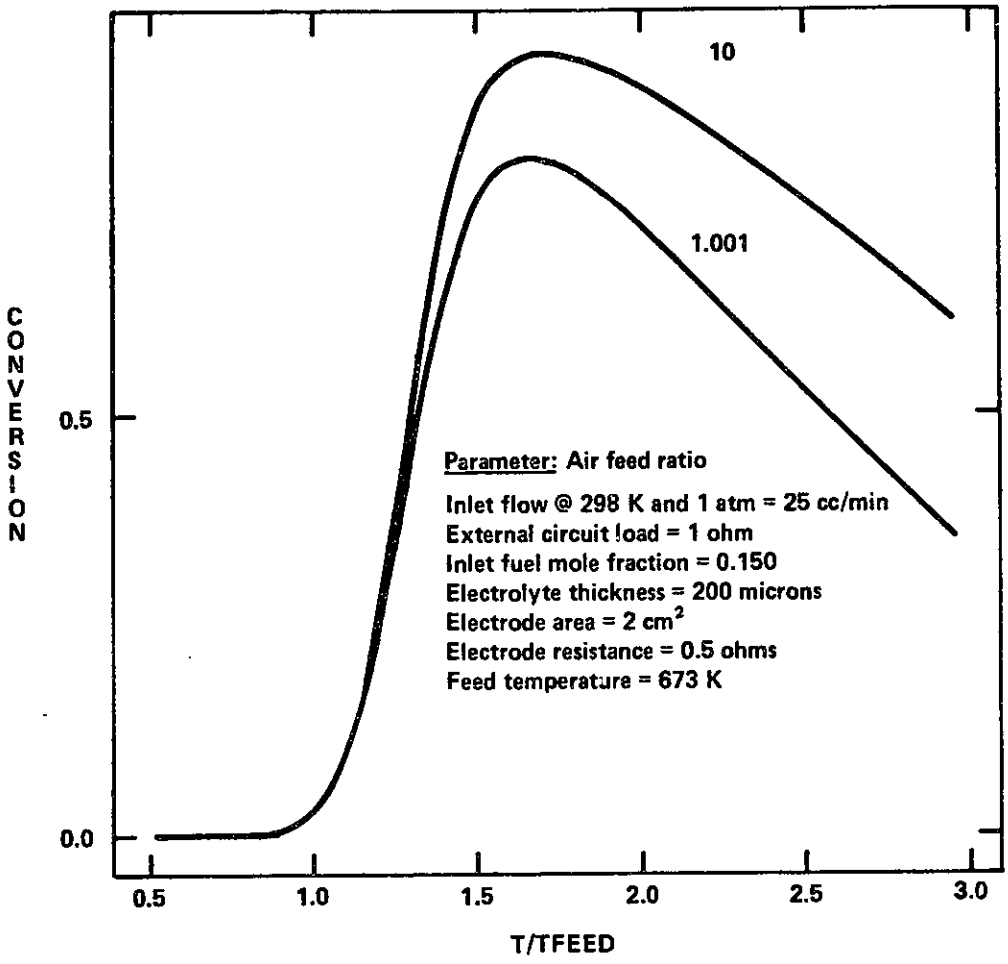

INFLUENCE OF AIR FEED RATIO UPON CONVERSION (CO/CO_2 CELL)
FIGURE 2.6

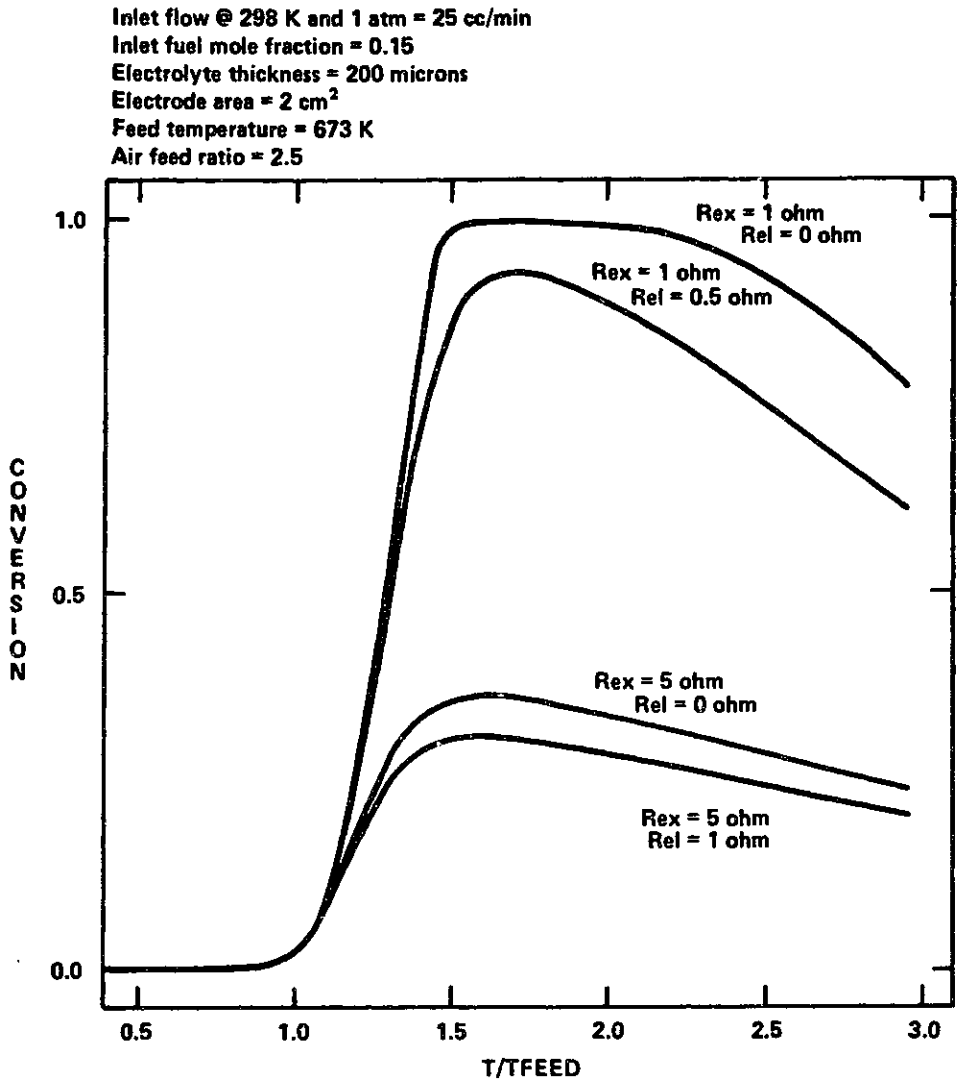

INFLUENCE OF ELECTRODE RESISTANCE UPON CONVERSION (CO/CO_2 CELL)
FIGURE 2.7

defining equation, 2.1.76) upon conversion, for the CO/CO_2 system. As can be seen from equation (2.1.79), y_{O_2} approaches the limiting value of 0.21 at high air feed rates, thus maximizing the driving force for oxygen transport. At extremely low air feed rates, on the other hand, y_{O_2} becomes small, and the logarithmic term associated with y_{O_2} correspondingly more negative. One would therefore expect Z to influence the steady state conversion, as shown in figure 2.6. As stated earlier, the assumption of a well mixed air chamber was made in obtaining figure 2.6. Although the effect would be gradually reduced as the flow pattern deviates from perfect backmixing, the qualitative argument is still valid. These results show the importance of determining an "optimum" air feed ratio. In fact, increasing air feed causes a desirable increase in conversion which must, however, be weighed against the increased pumping costs; moreover,as will be seen in the discussion of the energy balance, a high air feed rate tends to cool the fuel cell and may lead to unignited operation. Furthermore, precisely because air tends to cool the fuel cell, it must be preheated, as will be shown later. Obviously, a high air flow would also increase the preheat duty. Thus, the "optimum" air feed ratio cannot be determined solely from material balance considerations.

Figure 2.7 shows the corresponding effect of electrode resistance upon conversion. It can be seen that efforts towards eliminating electrode resistance depend very strongly upon the relative magnitude of this component of cell resistance compared to total (i.e., electrolyte + external + electrode) resistance.

In fact, as can be seen from figure 2.7 and the preceeding figures, at the values of external and electrode resistance considered, all curves essentially coincide up to values of T $\sim$ 800°K ($\sim$1.2 T_{feed}, with T_{feed} 673°K), indicating that the controlling resistance is the electrolyte resistance, with the external and electrode resistance becoming important for T > 870°K (approximately), a qualitative behaviour to be expected in view of the exponential dependence of R_{ex} on T. Thus, once the temperature-independent resistances control the flow of current through the fuel cell, an increase in R_{el} produces an effect which depends not only upon the magnitude of such an increase, but also upon the ratio of electrode to total resistance. In the particular case of figure 2.7, increasing R_{el} from 0 to 0.5 ohm has a more pronounced negative effect upon conversion when R_{ex} is 1 ohm than does a corresponding increase from 0 to 1 ohm with R_{ex} at 5 ohm, the reason being, of course, that, in the latter case, R_{ex} constitutes a much larger fraction of the total resistance.

2.1.3.2 Power output

From equation (2.1.5),

$$E = I\ R_{ex} \qquad (2.1.5)$$

Multiplying by I, we obtain the power output,

$$P = I^2 R_{ex} \qquad (2.1.82)$$

Since the current, I, is linearly related to the conversion through equation (2.1.55), equation (2.1.82) then simply states that the power output for any given temperature will be proportional

to the square of the corresponding conversion (for a fixed flow rate). Thus, for a fixed value of external load, the power generation vs. T curve will have the same qualitative features as the material balance (x vs. T) curve, though it will be distorted due to the 2nd power on I (i.e., if the conversion curve shows a maximum, so will the power curve). However, the proportionality coefficient between power and I^2, namely R_{ex}, has, as was seen in figures 2.4, 2.5 and 2.7, the effect of "freezing" the reactor, reducing conversion. Thus, there will be an external load that will yield the maximum power output. Note that differentiating equation (2.1.30) and solving for the value of R_{ex} that maximizes the function yields a relationship involving parameters which are functions of T and x (E_{rev}) or T (R_i). Thus, the concept of "optimum" R_{ex} is a loose one unless the operating temperature is defined and the material balance solved. Figure 2.8 shows, in fact, that a 10 ohm external load is best up to T/T feed $\sim$ 1.25, and a 1 ohm external load for T/T feed > 1.25. Figure 2.9 gives the corresponding values for H_2. The ordinate in figures 2.8 and 2.9 gives the power output per unit electrode sufrace (2 cm^2 in the case of the geometry considered).

Combining equations (2.1.82) and (2.1.55), we obtain

$$P = (2\mathcal{F}\dot{N}_{Ai})^2 \, x^2 \, R_{ex} \tag{2.1.83}$$

Furthermore, from equation (2.1.81),

$$x\,\dot{N}_{Ai} = \frac{E^\circ + \frac{RT}{2\mathcal{F}} \ln\left[\sqrt{\frac{0.21(Z-1)}{Z-0.21}}\left(\frac{1-x}{x}\right)\right]}{2\mathcal{F}\left(R_{ex} + R_{el} + R_i^\circ \exp\frac{9700}{T}\right)} \tag{2.1.84}$$

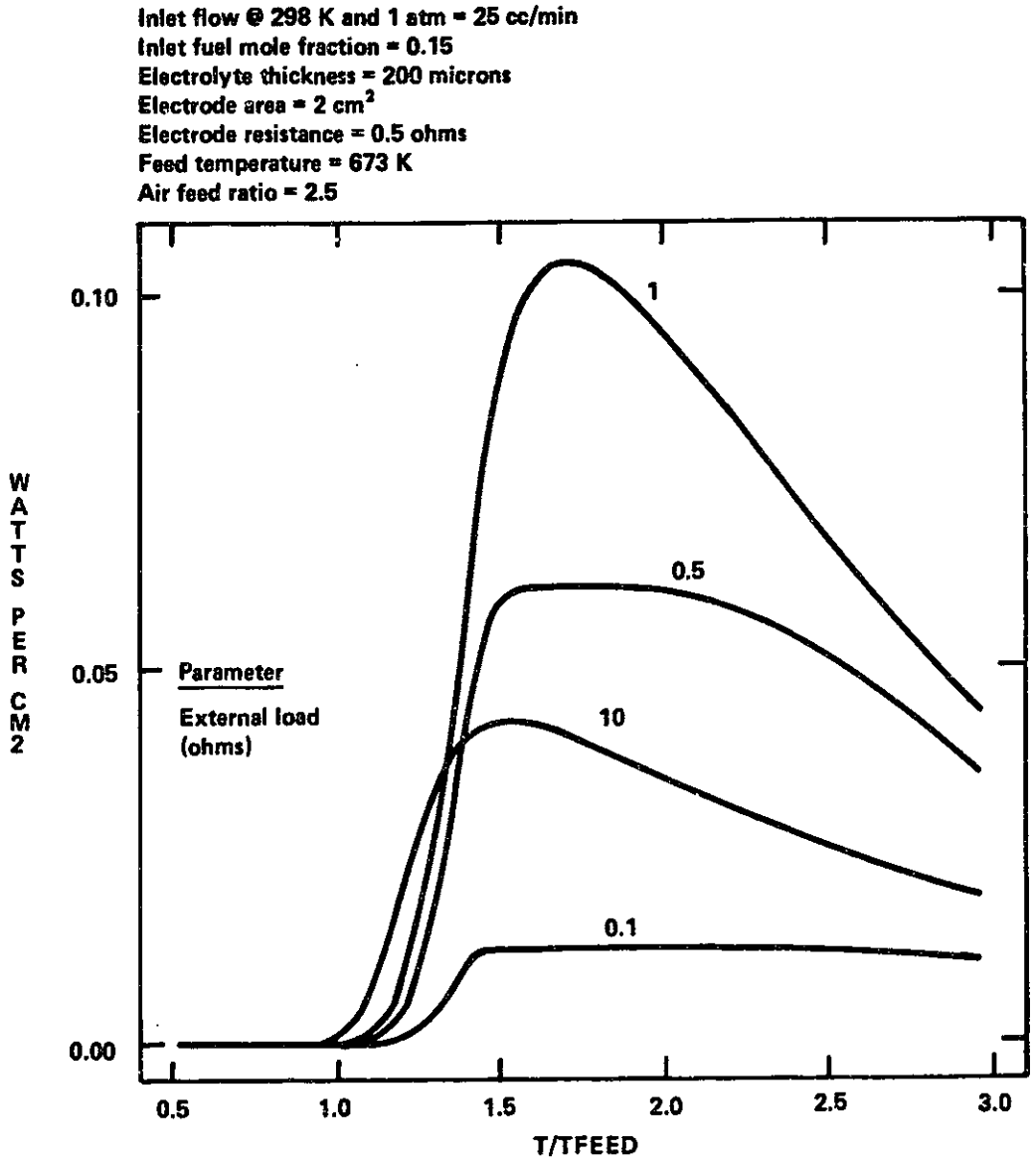

INFLUENCE OF LOAD UPON POWER OUTPUT (CO/CO_2 CELL)
FIGURE 2.8

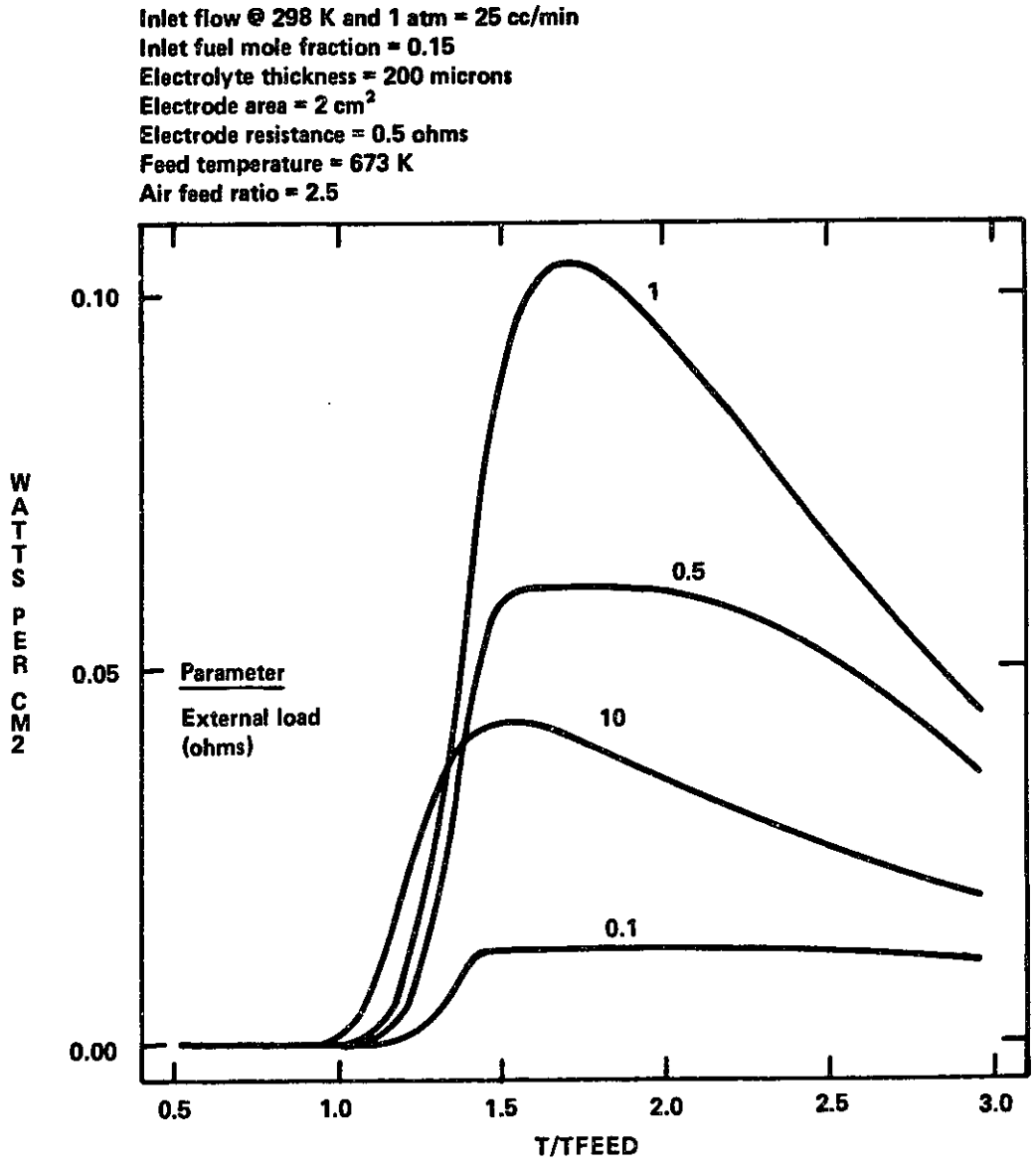

INFLUENCE OF LOAD UPON POWER OUTPUT (CO/CO_2 CELL)
FIGURE 2.8

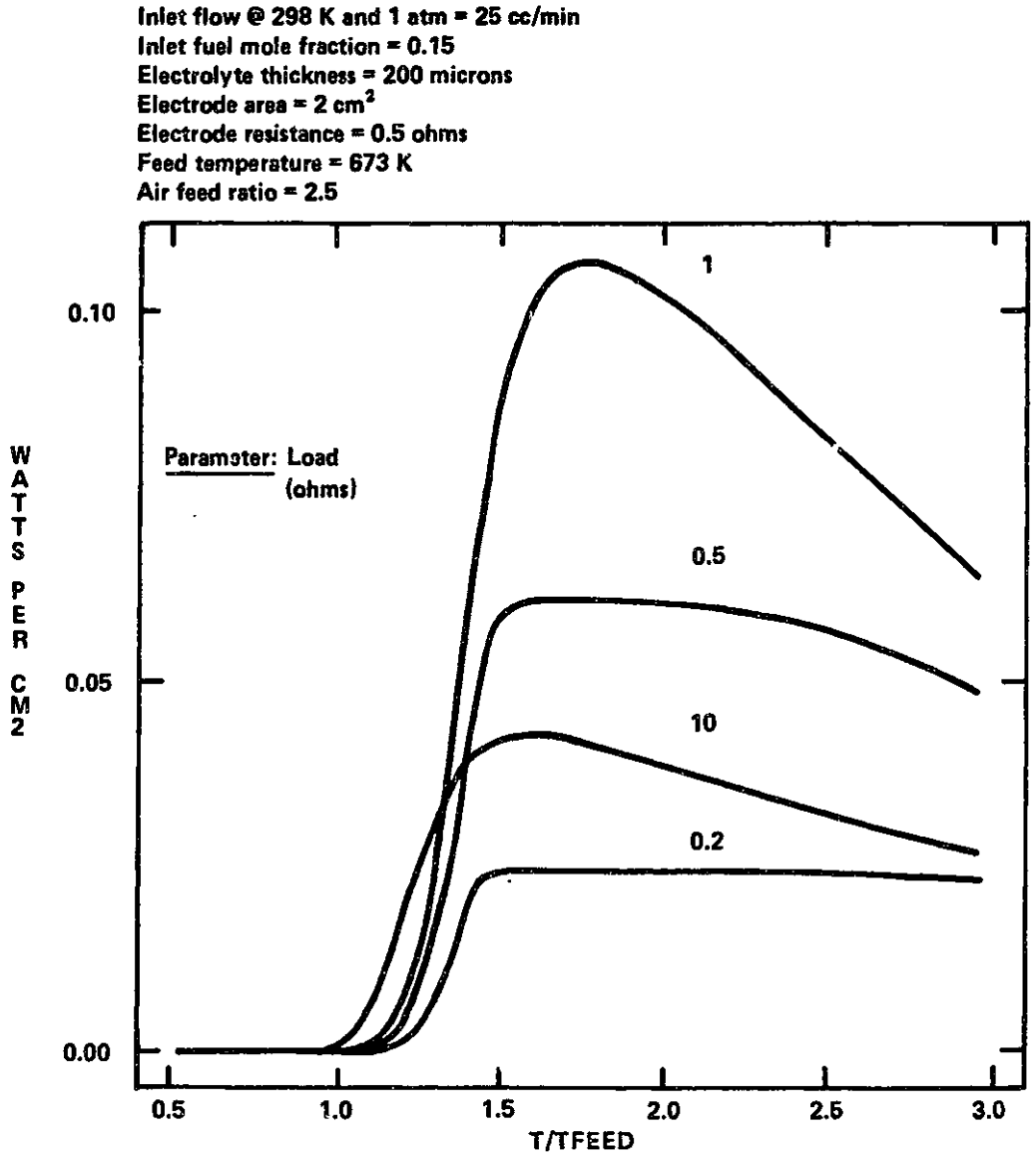

EFFECT OF LOAD UPON POWER OUTPUT (H_2/H_2O CELL)
FIGURE 2.9

At the operating temperatures of interest, the controlling resistances are the temperature-independent ones. Futhermore, except at extremely high or low values of the conversion, the voltage is primarily determined by E°. We can thus put, under the above limiting conditions,

$$x \dot{N}_{Ai} \sim \frac{E^\circ}{2\mathcal{F}(R_{ex}+R_{el})} \qquad (2.1.85)$$

Therefore, substituting into equation (2.1.83),

$$P \sim \frac{(E^\circ)^2 R_{ex}}{(R_{ex}+R_{el})^2}$$

This expression is to be compared with the equivalent rigorous equation, namely, equation (2.1.30). However, as the molar fuel feed is increased, the conversion becomes lower, and the logarithmic term becomes important, with a consequent <u>increase</u> in power output. Thus, we are confronted with another trade-off: power generation vs. reactant conversion. The choice depends of course upon the process in consideration, the reactants and products involved, etc. For example, if consideration is given to an NH_3 fuel cell, where the aim is to generate nitric oxide and <u>co</u>-generate electricity, a high conversion would be the natural choice. Note that, although equation (2.1.83) is specific to the stoichiometry under consideration, the argument is true regardless of reaction stoichiometry, since, although the expression in the logarithmic term will change, it will always increase as x tends to 0 and vice versa. Figure 2.10 illustrates the previous point, and the trade-offs involved. Note, especially, the opposing trends of power output and conversion. In figure 2.10b, the increase in efficiency is due to the lowered conversion's

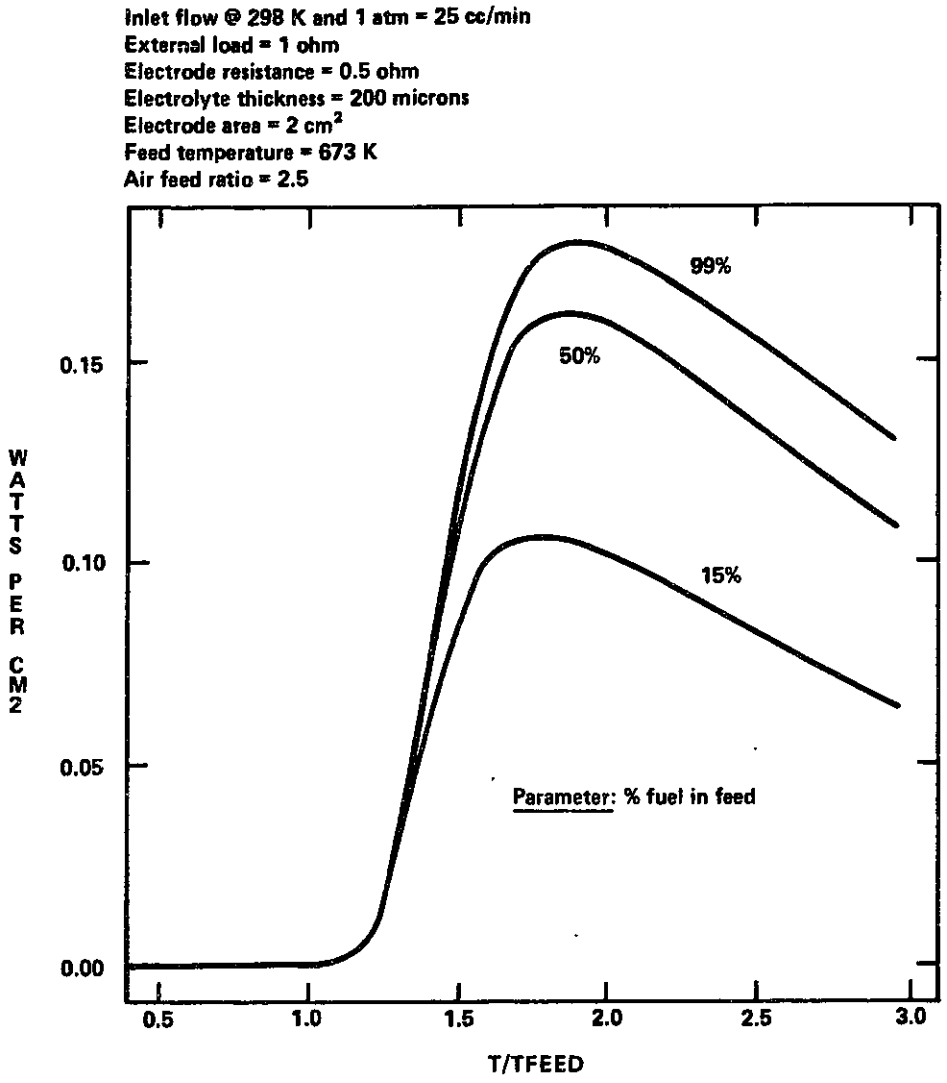

INFLUENCE OF FUEL CONCENTRATION UPON POWER OUTPUT (H_2/H_2O CELL)
FIGURE 2.10a

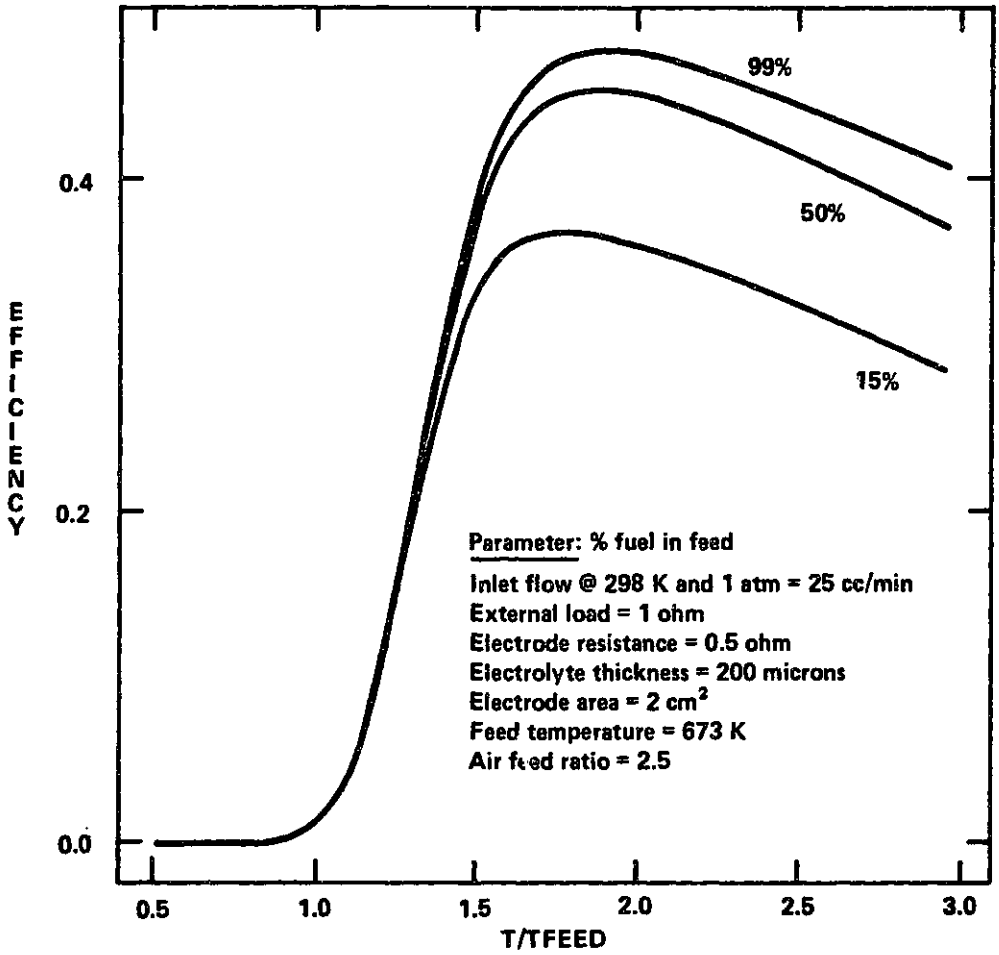

INFLUENCE OF FUEL CONCENTRATION UPON EFFICIENCY (H_2/H_2O CELL)
FIGURE 2.10b

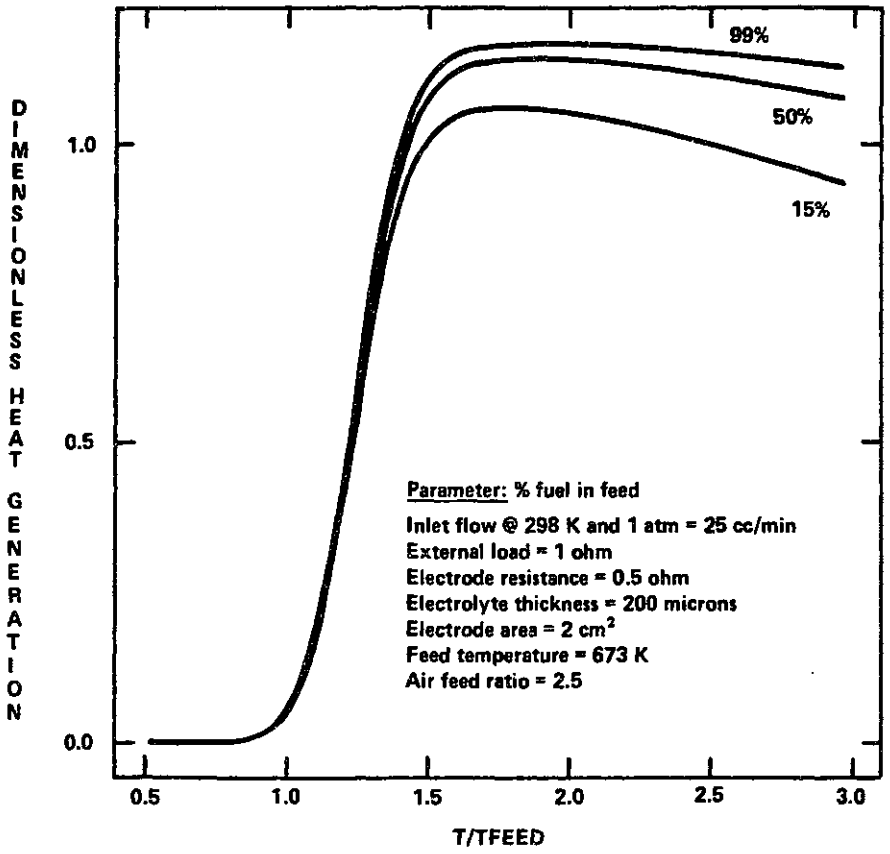

INFLUENCE OF FUEL CONCENTRATION UPON HEAT GENERATION (H_2/H_2O CELL)
FIGURE 2.10c

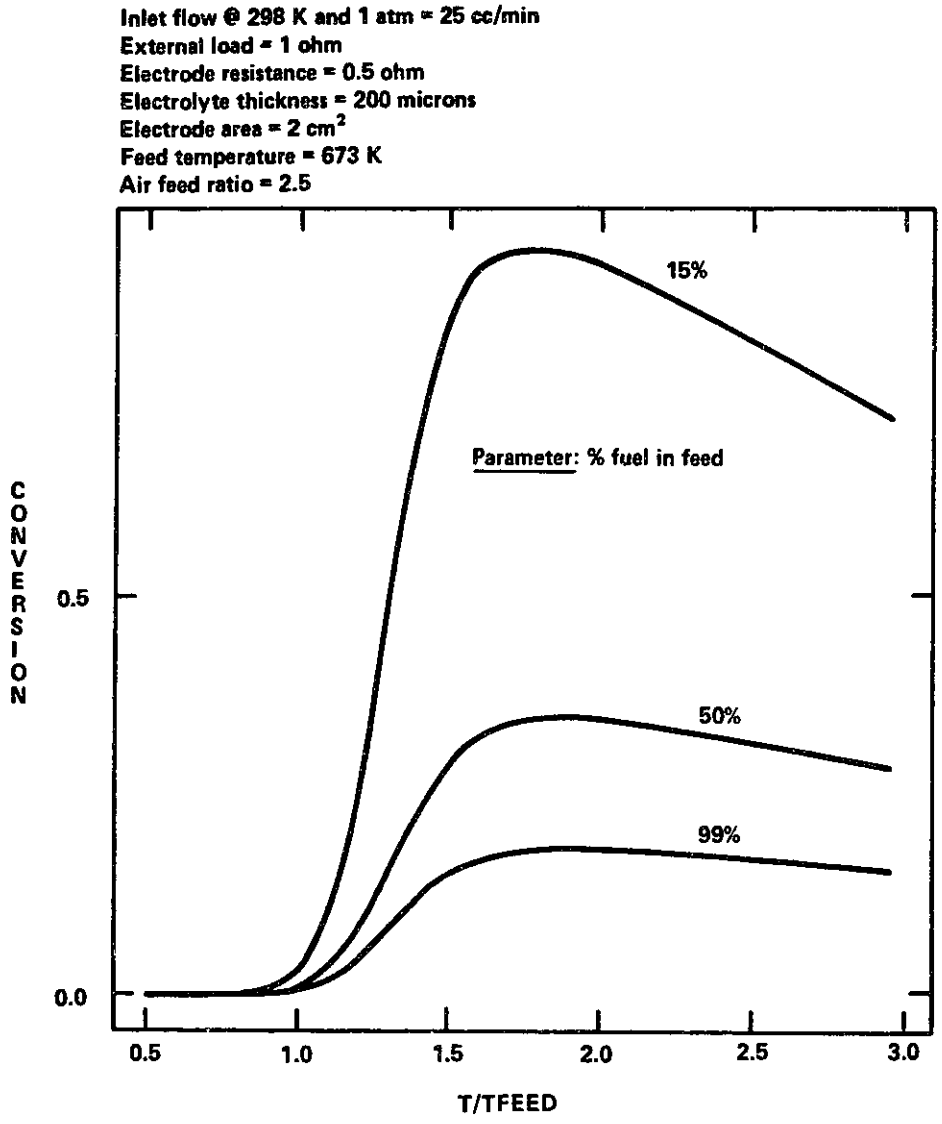

INFLUENCE OF FUEL CONCENTRATION UPON CONVERSION (H_2/H_2O CELL)
FIGURE 2.10d

effect upon the logarithmic voltage component (recall that E_{rev} and E are related by equation (2.1.7)).

2.1.3.3 Efficiency

Efficiency was defined in equation (2.1.54) as the ratio of actual to thermoneutral voltage,

$$\eta = \frac{E}{E_{TN}} \tag{2.1.86}$$

From equation (2.1.7),

$$\eta = \frac{E_{REV}}{[1+ \frac{R_{el}}{R_{ex}} + \frac{R_i^\circ}{R_{ex}} \exp \frac{9700}{T}] E_{TN}} \tag{2.1.87}$$

Again, for the geometry presently considered, and at the temperatures of interest for operation (see figure 2.33), we can write, with small error,

$$\eta \sim \frac{E_{REV}}{(1+ \frac{R_{el}}{R_{ex}}) E_{TN}} = \frac{E^\circ + \frac{RT}{2\mathcal{F}} \ln \left[\frac{\sqrt{0.21}(Z-1)}{Z-0.21} (\frac{1-x}{x}) \right]}{(1 + \frac{R_{el}}{R_{ex}}) E_{TN}} \tag{2.1.88}$$

At a given flow rate, increasing R_{ex} will cause both the denominator to decrease and the conversion to decrease (see figures (2.5) and (2.6)), with a consequent increase in the logarithmic term. Both effects point in the same way, and the efficiency is thus increased. Here, again, a compromise is to be sought. In fact, according to figures 2.11 and 2.12, the highest efficiency for the range of loads considered, corresponds to operation with a 10 ohm external resistance, which is clearly not suitable for power generation, let alone conversion (see figures (2.4),(2.5), (2.8) and (2.9)).

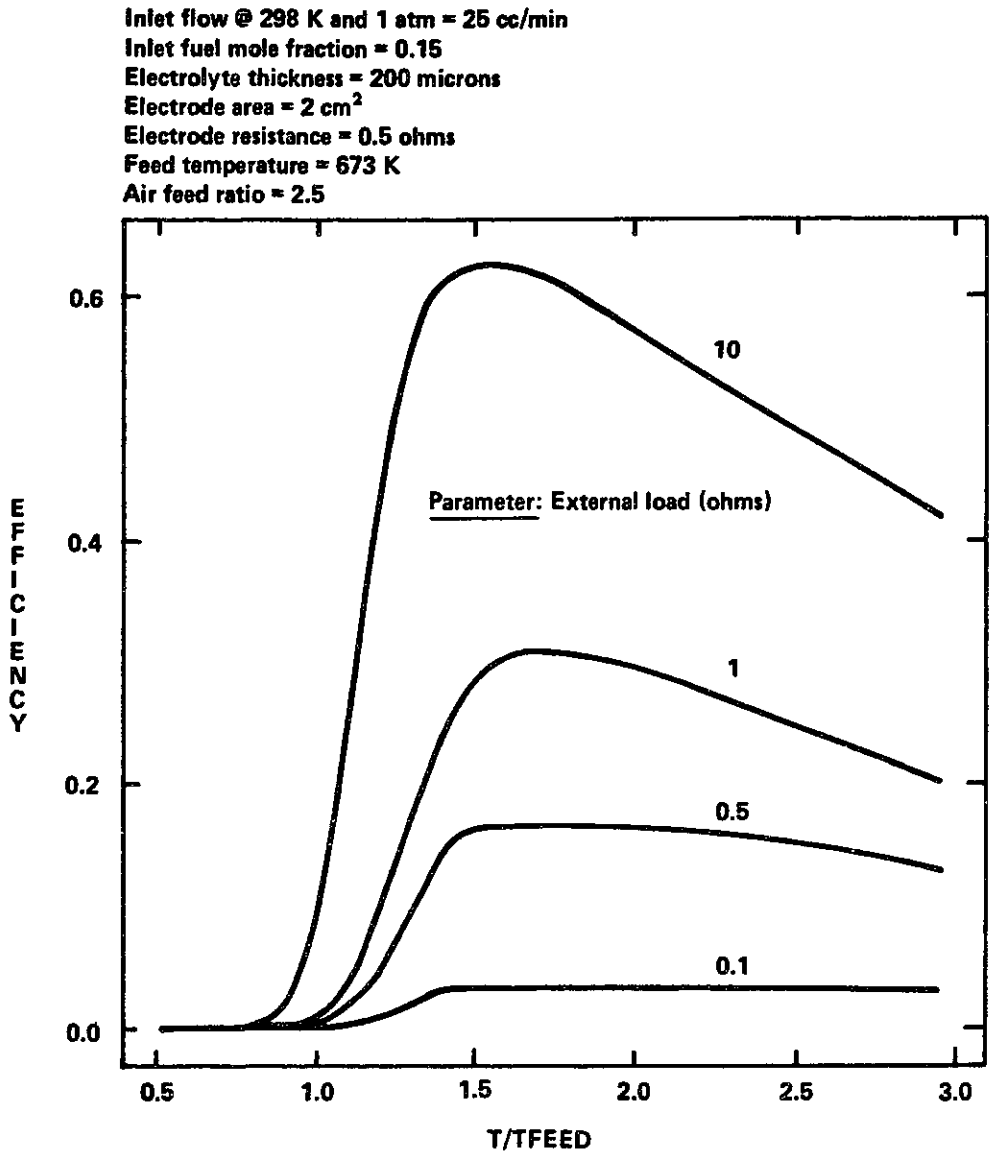

INFLUENCE OF LOAD UPON EFFICIENCY (CO/CO_2 CELL)
FIGURE 2.11

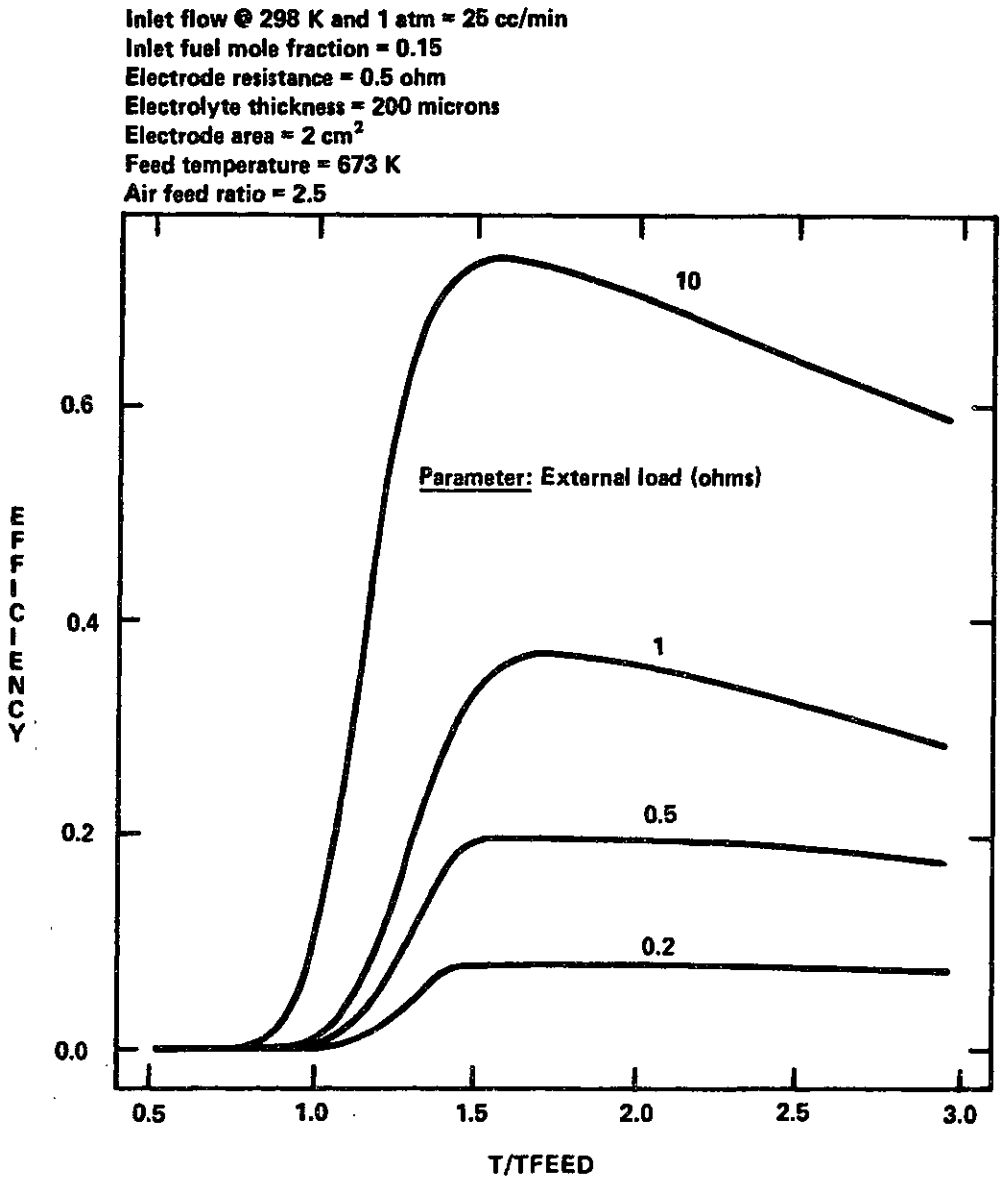

EFFECT OF LOAD UPON EFFICIENCY (H_2/H_2O CELL)
FIGURE 2.12

2.1.3.4 Heat generation

Heat generation is given by

$$\dot{Q} = (1 - \eta)\left(\frac{I}{2\mathcal{F}}\right)(-\Delta H_o) \qquad (2.1.89)$$

Since I is directly proportional to conversion, equation (2.1.89) shows that heat generation is closely related to conversion, a fact which is almost trivially obvious were it not for the $1-\eta$ term. In fact, only when $\eta \to o$ does the similarity between heat generation and conversion curves apply rigorously. Figures 2.13 and 2.14 illustrate this fact (the corresponding efficiency curves are figs. 2.11 and 2.12). The remarkable feature of figures 2.13 and 2.14 is, as was anticipated in the discussion of the material balance equation, the existence of a heat generation curve which shows a maximum, even though, as table 2.1 shows, the reaction is, for all practical purposes, irreversible within the limits which are specified there. The heat generation term was non-dimensionalized by dividing equation (2.1.89) through by $F_i[A_i]\hat{C}p_{fi}T_i$.

2.1.3.5 Steady state analysis

2.1.3.5.1 The dimensionless equations

Equation (2.1.80) can be rewritten as follows:

$$F_i\rho_i\hat{C}p_{fGi}(T_i-T_o)+W\frac{I}{2\mathcal{F}}\hat{C}p_{O_2Gj}(T_j-T_o)=\frac{WI}{2\mathcal{F}}\left(\frac{Z}{0.233}-1\right)\hat{C}p_{AirGm}(T-T_j)+$$

$$+ F\rho\hat{C}p_{pG}(T-T_o)+UA(T-T_c)-\left(1-\frac{E}{E_{TN}}\right)(-\Delta H_o)\frac{I}{2\mathcal{F}} \qquad (2.1.90)$$

In equation (2.1.90) a mass rather than a molar basis was adopted for the enthalpy flux terms, and the corresponding mass heat

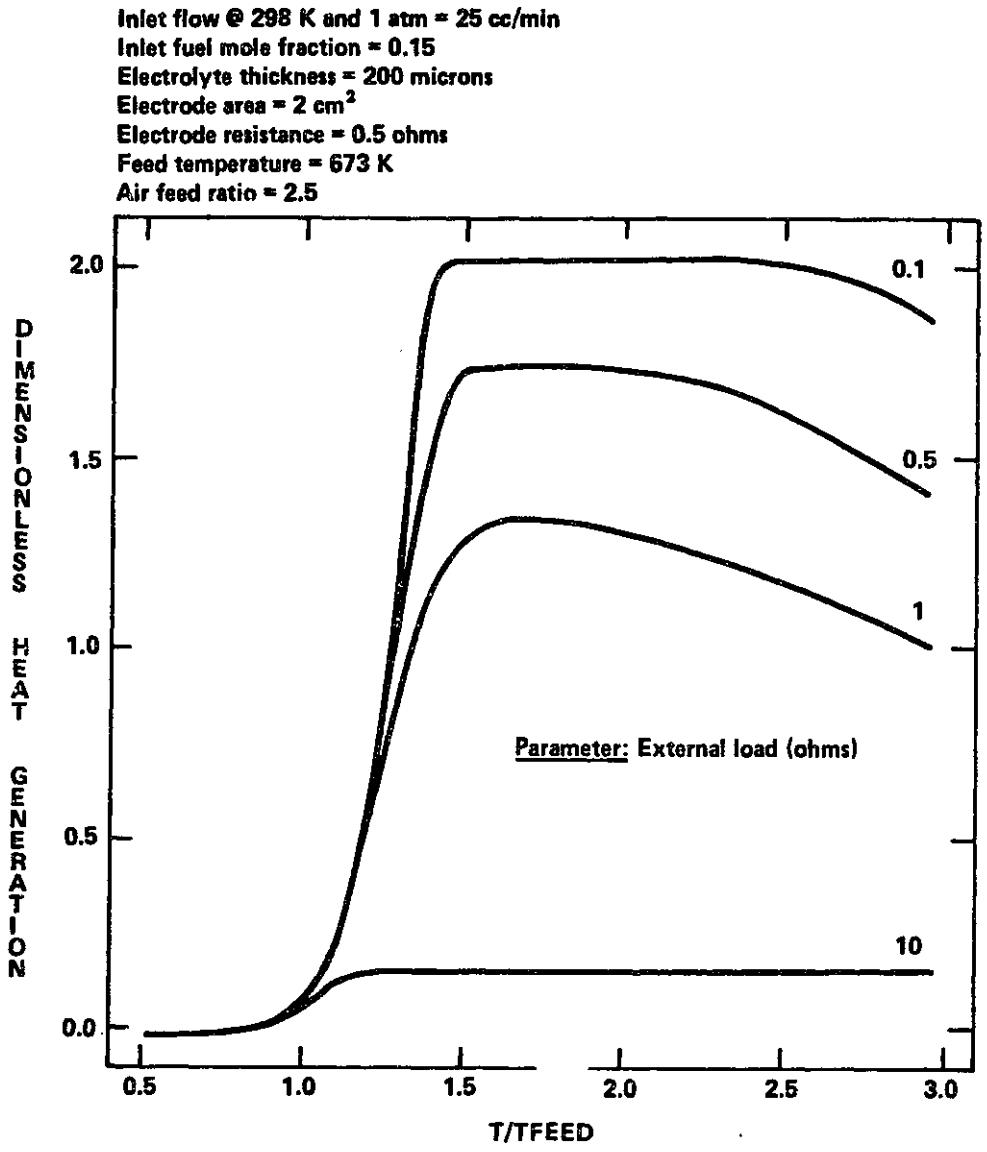

INFLUENCE OF LOAD UPON HEAT GENERATION (CO/CO_2 CELL)
FIGURE 2.13

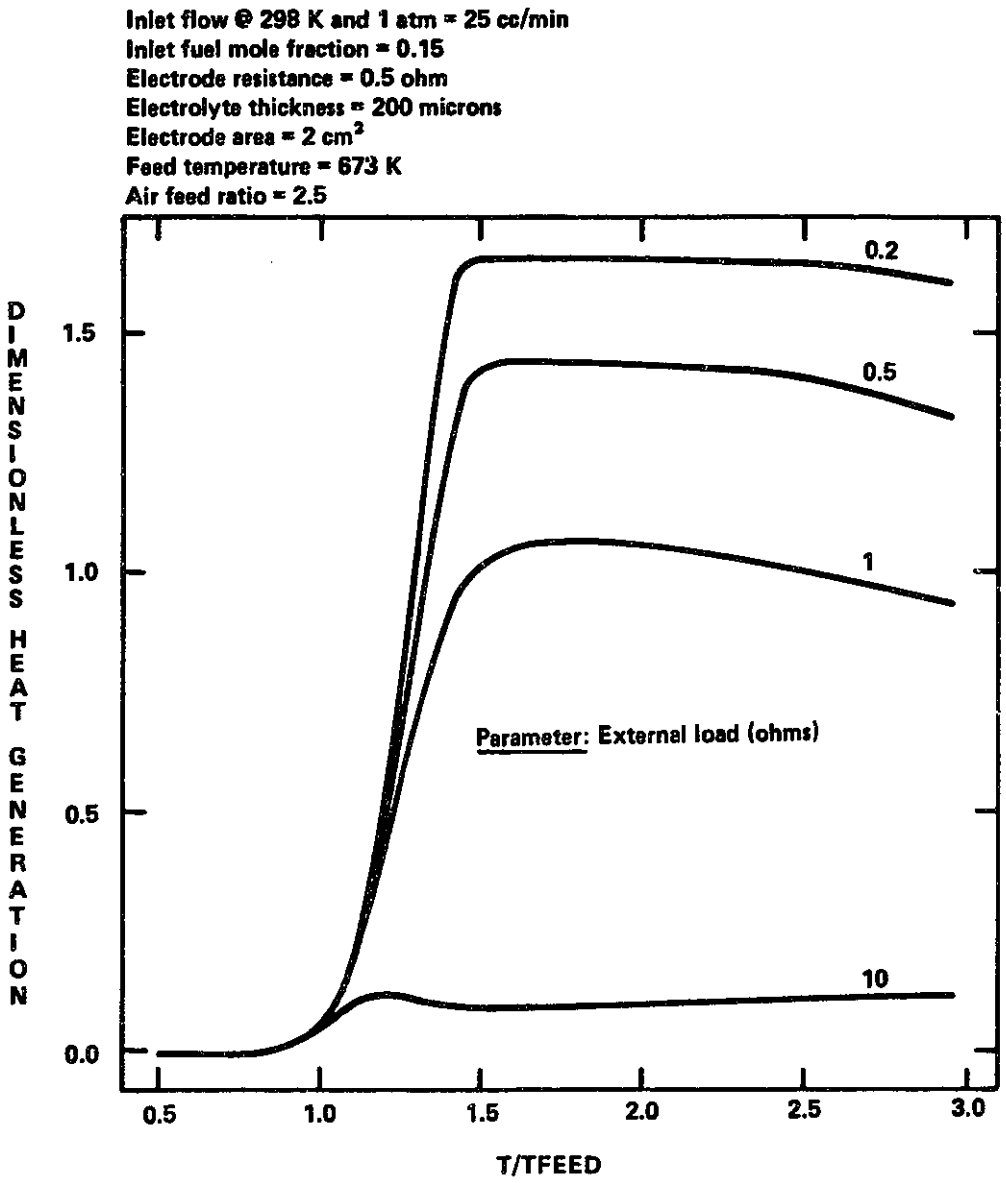

EFFECT OF LOAD UPON HEAT GENERATION (H_2/H_2O CELL)
FIGURE 2.14

capacities used. The $-\Delta H_o$ term is, of course, molar. The W coefficient corresponds to the mass of oxygen consumed per mole of fuel reacted; the air specific heat is calculated at an average temperature between inlet and outlet conditions, and contains the appropriately averaged oxygen and nitrogen heat capacities, according to air outlet composition. The 0.233 term corresponds to the weight fraction of oxygen in air, coherent with a 21% O_2 - 79% N_2 molar composition.

Dividing through by $F_i \rho_i \hat{C}p_{fGi} T_i$, the equation is rendered dimensionless. The following are the dimensionless parameters governing the fuel cell behaviour:

$$N_1 = \frac{WE_0^\circ}{2\mathcal{F} R_{ex} F_i \rho_i} \qquad (2.1.91)$$

$$N_2 = \frac{\hat{C}p_{O_2 Gj}}{\hat{C}p_{fGi}} \qquad (2.1.92)$$

$$N_3 = \frac{R_{el}}{R_{ex}} \qquad (2.1.93)$$

$$N_4 = \frac{E^*}{RT_i} \qquad (2.1.94)$$

$$N_5 = \frac{r^* d}{S R_{ex}} \qquad (2.1.95)$$

$$N_6 = \frac{E^\circ}{E_0^\circ} \qquad (2.1.96)$$

$$N_7 = \frac{RT_i}{2\mathcal{F} E_0^\circ} \qquad (2.1.97)$$

$$N_8 = \frac{\hat{C}p_{AirGm}}{\hat{C}p_{fGi}} \qquad (2.1.98)$$

$$N_9 = \frac{\hat{C}p_{pG}}{\hat{C}p_{fGi}} \qquad (2.1.99)$$

$$N_{10} = \frac{UA}{F_i \rho_i \hat{C}p_{fGi}} \qquad (2.1.100)$$

$$N_{11} = \frac{E^\circ}{E_{TN}} \qquad (2.1.101)$$

$$N_{12} = \frac{(-\Delta H_o)[A]_i}{\rho_i \hat{C}p_{fGi} T_i} \qquad (2.1.102)$$

$$N_{13} = \frac{E_0^\circ}{R_{ex} F_i [A]_i 2\mathcal{F}} \qquad (2.1.103)$$

$$N_{14} = Z \qquad (2.1.104)$$

Furthermore, with the following notation for dimensionless temperatures:

$$\theta_o = \frac{T_o}{T_i} \tag{2.1.105}$$

$$\theta_j = \frac{T_j}{T_i} \tag{2.1.106}$$

$$\theta_c = \frac{T_c}{T_i} \tag{2.1.107}$$

$$\theta = \frac{T}{T_i} \tag{2.1.108}$$

the dimensionless steady-state energy balance is then

$$(1-\theta_o) + \frac{N_1 N_2 \{N_6 + \theta N_7 \ln [\sqrt{\frac{0.21(N_{14}-1)}{N_{14}-0.21}} (\frac{1-x}{x})]\} (\theta_j - \theta_o)}{[1 + N_3 + N_5 \exp (\frac{N_4}{\theta})]} =$$

$$\frac{N_1 N_8 \{N_6 + \theta N_7 \ln [\sqrt{\frac{0.21(N_{14}-1)}{N_{14}-0.21}} (\frac{1-x}{x})]\} (\theta-\theta_j) (\frac{N_{14}}{0.233} - 1)}{[1+N_3 + N_5 \exp (\frac{N_4}{\theta})]} +$$

$$+ \left\{1 + \frac{N_1 \{N_6 + \theta N_7 \ln [\sqrt{\frac{0.21(N_{14}-1)}{N_{14}-0.21}} (\frac{1-x}{x})]\}}{[1 + N_3 + N_5 \exp (\frac{N_4}{\theta})]}\right\} N_9 (\theta-\theta_o) +$$

$$+ N_{10} (\theta-\theta_c) -$$

$$-\left\{1 - \frac{N_{11} \{N_6 + \theta N_7 [\ln \sqrt{\frac{0.21(N_{14}-1)}{N_{14}-0.21}} (\frac{1-x}{x})]\}}{[1+N_3+N_5 \exp (\frac{N_4}{\theta})]}\right\} N_{12} N_{13} \left\{N_6 + \theta N_7 \ln [\sqrt{\frac{0.21(N_{14}-1)}{N_{14}-0.21}} (\frac{1-x}{x})]\right\} \tag{2.1.109}$$

Equation (2.1.15), with the same notation, becomes

$$x = \frac{N_{13} \{N_6 + \theta N_7 [\ln \sqrt{\frac{0.21(N_{14}-1)}{N_{14}-0.21}} (\frac{1-x}{x})]\}}{1 + N_3 + N_5 \exp (\frac{N_4}{\theta})}$$

Of the above mentioned dimensionless groups, N_2, N_8 and N_9 have self-evident significance and their importance is relatively minor except for extreme cases when relatively concentrated H_2 is fed to the cell. N_{14}, again, has self-evident significance, its

importance having already been discussed. N_{10} and N_{12} retain their usual (i.e., "non electrical") meaning, namely, number of heat transfer units and dimensionless adiabatic temperature rise. N_4 is an Arrhenius number, with the important difference that its effect is masked by the temperature-independent loads, in such a way that the process kinetics gradually lose the exponential temperature dependence; in other words, contrary to the purely chemical reaction, in which kinetics is a property of the reacting system, in a fuel cell it is both a system property (of the solid electrolyte, though, not of the reacting system) and an externally controllable parameter (by means of R_{ex} we can not only control N_1, but through the combined influence of R_{ex}, d and S we can also control the preexponential factor N_5).

N_1 can be interpreted as a ratio of oxygen mass consumption rate to feed rate, while N_{13} can be viewed as a ratio of moles reacted per unit time to moles fed per unit time. Note, however, that, strictly speaking, the molar consumption rate is $\frac{I}{2\mathcal{F}}$, or $\frac{E_{rev}}{2\mathcal{F}\Sigma R}$, so that a term containing $\frac{E_0^\circ}{2\mathcal{F}R_{ex}}$ has the required form to be interpreted as a molar consumption rate, but can loose its significance if the logarithmic correction to voltage is large; also, note that ΣR has been replaced by R_{ex}, and although the total resistance is related to R_{ex} through N_3 and N_5, it only becomes similar to R_{ex} when the latter is the controlling resistance (i.e., relatively high temperatures and low contact losses).

N_6 is a temperature correction to the reaction's main driving force; it decreases with temperature for exothermic reactions with a negative associated entropy change and viceversa. N_{11} has

no non-electrochemical analogy, and is simply a measure of the relative importance of the entropy variation for the reaction. It approaches 1 for systems with small associated entropy effects, is greater than 1 for exothermic reactions with positive entropy variation, and smaller than 1 for exothermic reactions with negative entropy variation. A large N_{11} implies high efficiency but difficulty to achieve autothermal operation, and viceversa.

In the next section two specific examples of the application of the dimensional form of the governing equations to a system with a given configuration are presented, and this is followed by use of the governing dimensionless numbers as a powerful means of rationally approaching scale-up, design and extrapolation.

2.1.3.5.2 Steady state determination: coupling of material and energy balances

If equation (2.1.90) is rearranged as follows,

$$(1-\frac{E}{E_{TN}})(-\Delta H_o)\frac{I}{2\mathcal{F}} = UA(T-T_c)+F\rho\hat{C}p_{pG}(T-T_o)-F_i\rho_i\hat{C}p_{fGi}(T_i-T_o)+$$
$$=\frac{WI}{2\mathcal{F}}(\frac{Z}{0.233}-1)\hat{C}p_{AirGm}(T-T_j)-\frac{WI}{2\mathcal{F}}\hat{C}p_{O_2Gj}(T_j-T_o) \qquad (2.1.111)$$

The left hand side can be viewed as the net "heat generation" within the fuel cell, while the right hand side is the net heat removal from the fuel cell, via heat interactions and convective enthalpy transport. Equations (2.1.111) and the material balance must be simultaneously satisfied for a steady state to exist. The approach used is illustrated in figure 2.15, with system temperature scanned up to ∿2000°K. System parameters were:

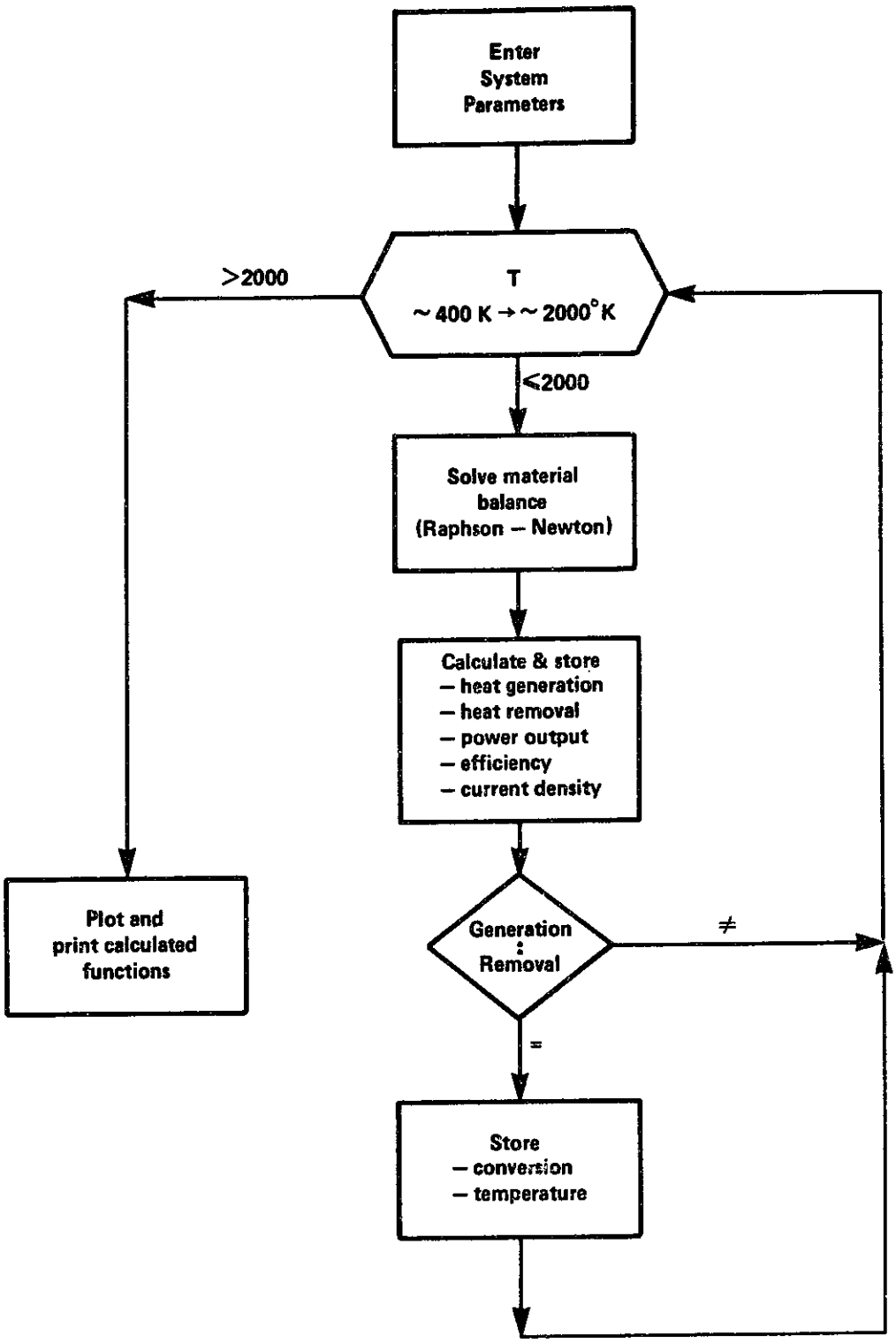

STEADY STATE DETERMINATION
FIGURE 2.15

- feed flow rate at reference conditions
- fuel feed mole fraction
- inlet fuel temperature
- inlet air temperature
- ambient temperature
- ratio of actual to stoichiometric air feed
- electrolyte thickness
- electrolyte area
- contact (electrode) resistance
- external load
- overall heat transfer coefficient
- external to electrode area ratio

Dilute feed has been considered in all cases. The reason for this is the cell's limited fuel-handling capacity, which would lead to extremely low (<5 cc/min) flow rates at reasonable conversions. The flow rates considered here (> 25 cc/min) are within a practical laboratory or pilot scale. Note, however, that ignited operation would be easier with concentrated and low feed rates.

Although all of these parameters were systematically varied (see section 2.1.3.5.4), the order of magnitude of the principal dimensions and feed rate correspond to the cells tested at MIT (see section 2.1.3.5.3 for scale-up). However, it became apparent from the first runs that ignited operation was impossible to achieve unless the single cell was insulated or a stacked arrangement was specified whereby the area for heat interactions with the surroundings associated with each fuel cell was greatly reduced. Appendix III contains some possible stack goemetric arrangements, however, the results are valid for any such geometry as long as the fluid flow characteristics implied in the model are still valid (i.e., well mixed air and fuel chambers), and the numerical values of all the parameters are the same; in other words, they correspond to a pilot or prototype-scaled stack assembly whose individual components are fed in parallel

and are characterized by the specified electrode and electrolyte dimensions, with an overall cell and stack design such that the CSTR assumptions are valid.

The external load associated with each element can be viewed either as the actual load connected to a single, thermally insulated unit or as the equivalent load acting on the elementary fuel cell within a stack. Thus, in figure 2.16 the equivalent load per cell is $R_{ex}/8$ for the first bipolar arrangement and $R_{ex}/2$ for the second bipolar arrangement.

The design of a large-scale electrochemical energy converter is beyond the scope of the present work, however, a brief comment on the fluid-feed arrangement implied by the model is necessary. It is evident that equations (2.1.111) and (2.1.15) were developed for a single reactor and can only be applied to a battery stack if the fluid flow obeys the pattern specified in figure 2.16, with each cell operating under identical conditions. Series feed, on the other hand, cannot be accurately modelled by means of equations (2.1.111) and (2.1.15), unless one is willing to compromise on the accuracy of the predictions by using average temperature and conversion values, and an "equivalent" electrode area, or, alternatively, to apply the equations to a unit composed of a determinate number of cells operating under nearly identical conditions.

Series operation has the advantage of providing a greater driving force, hence, in theory, a greater power output per stack volume, the situation resembling superficially the classic PFR (series flow) - CSTR (parallel flow) alternative. The similarity is not complete, though, since the greater driving force is associated only with the logarithmic component of cell voltage,

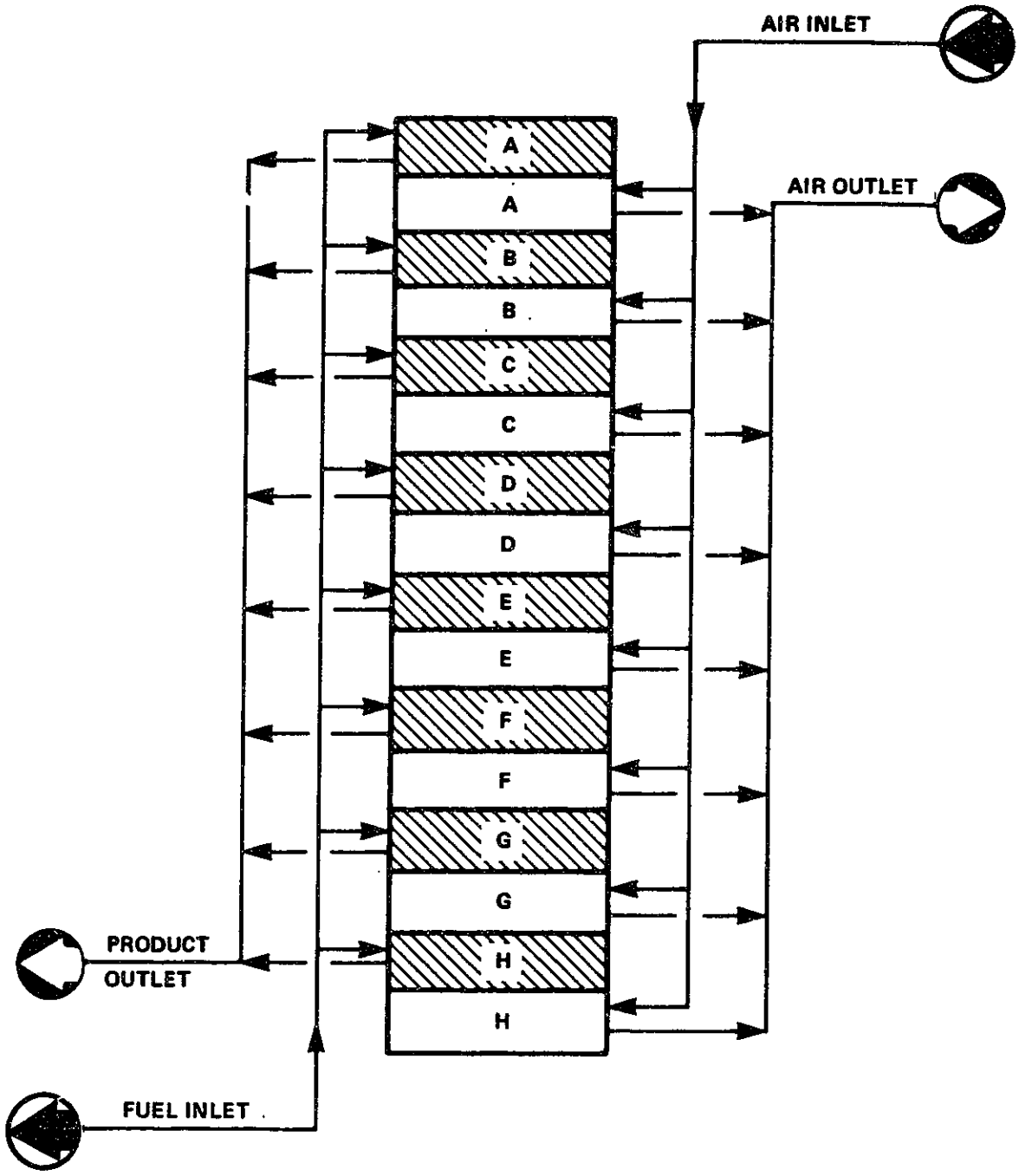

PARALLEL FEED ARRANGEMENT
FIGURE 2.16a

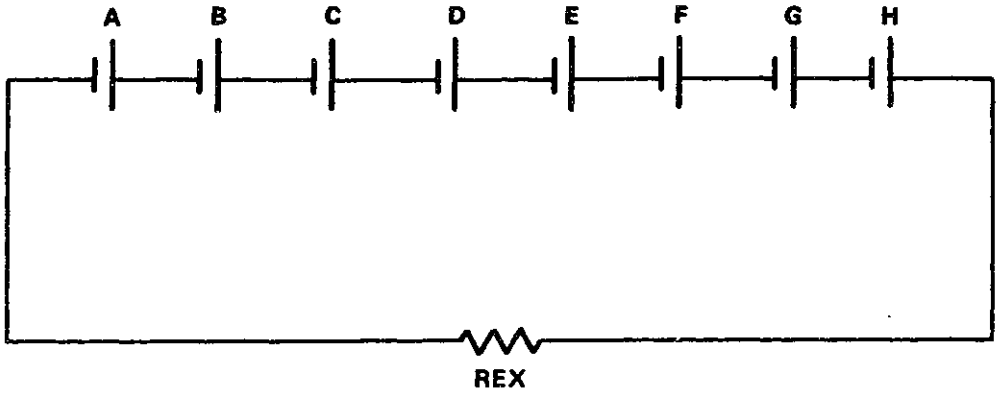

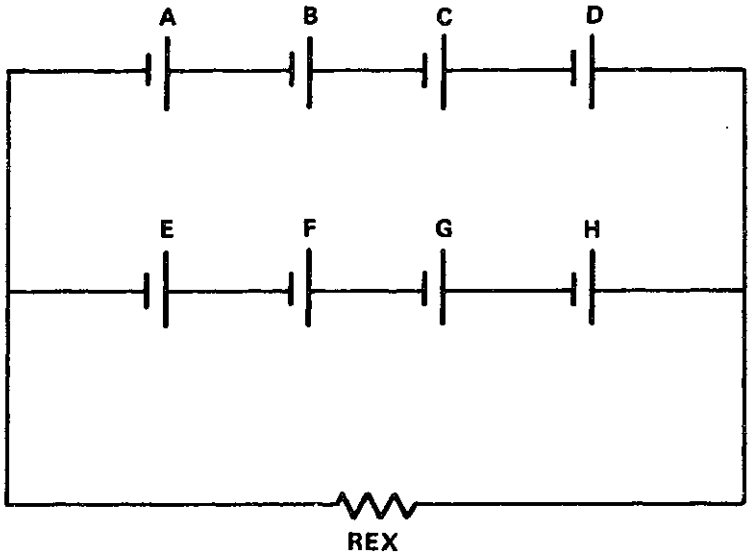

TWO POSSIBLE ELECTRICAL ARRANGEMENTS FOR FIGURE 2.16a
FIGURE 2.16b

which becomes an important fraction of total voltage only at very high conversions, and, with systems characterized by a negative entropy change, at high tempertures. Table 2.2 illustrates this point for the CO/CO_2 system, the temperature dependence being exactly opposite with a positive ΔS system (NH_3 fuel cell). Since the actual voltage will be less than the reversible voltage, the logarithmic term becomes proportionally more important at actual operating conditions.

Consider, however, figure 2.17. In the first case (figure 2.17a), parallel feed is considered. F/4 moles are fed to each cell, and I/4 amperes are produced, under identical conditions, in each cell, with an equivalent external load of R ohms, to achieve the specified conversion. On the other hand, in figure 2.17b the alternative of achieving the required conversion in a series flow arrangement with the same number of reactors is considered. The voltage will now be higher (see table 2.2) and if the same current is to flow through each reactor, R will be correspondingly higher than in figure 2.17a, and decreasing along the series reactors. However, these variations would affect R by roughly the same amount as shown in table 2.2, i.e., variations of 30% are to be expected. This is why, in fig. 2.17b, these loads have been indicated as R. The important fact, however, when one compares the two alternatives, is that the same amount of heat is generated in a reactor that now handles four times the corresponding flow of fuel, though the same flow of air. This must be considered in light of the results to be presented, where it is evident that self-ignited opertion requires a very precise combination of process

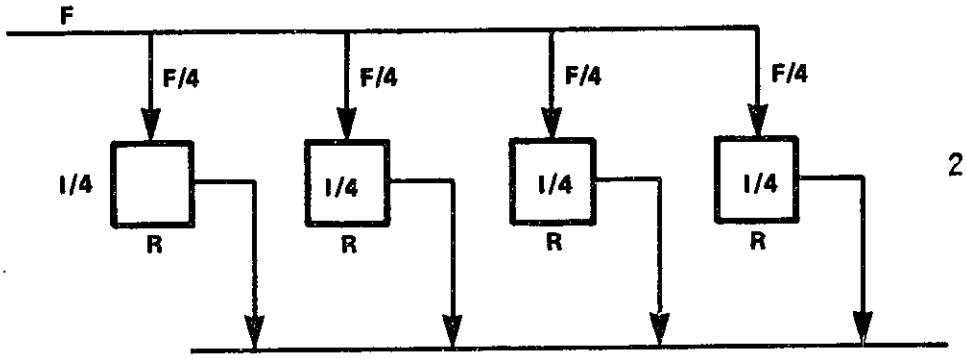

2.17a

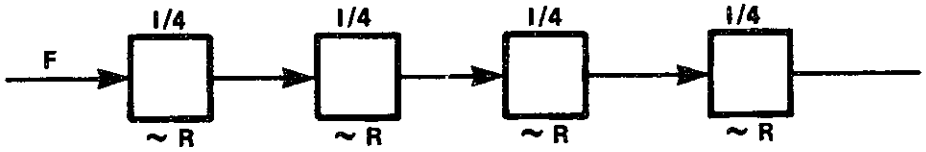

2.17b

PARALLEL VERSUS SERIES FLUID FLOW
FIGURE 2.17

	1300 K			2000 K		
Conversion	E°	$\frac{RT}{2\mathcal{F}}\ln\frac{0.458(1-x)}{x}$	E_{rev}	E°	$\frac{RT}{2\mathcal{F}}\ln\frac{0.458(1-x)}{x}$	E_{rev}
0.1	0.882	0.079	0.961	0.567	0.122	0.689
0.2		0.034	0.916		0.052	0.619
0.3		0.004	0.886		0.006	0.573
0.4		-0.021	0.861		-0.032	0.535
0.5		-0.044	0.838		-0.067	0.500
0.6		-0.066	0.816		-0.102	0.465
0.7		-0.091	0.791		-0.140	0.427
0.8		-0.121	0.761		-0.187	0.380
0.9		-0.167	0.715		-0.257	0.310
0.99		-0.301	0.581		-0.463	0.104

TABLE 2.2

Reversible voltage dependence upon conversion and temperature for the CO/CO_2 system

variables (air flow, external load, external area, feed temperature, etc.). Thus, the effect of the fourfold flow increase would be to correspondingly reduce the dimensionless heat generation, while maintaining a roughly equal heat removal curve (this function would be slightly lower, since air flow rate remains unchanged; however, air flow is only one of the components of the heat removal curve). The obvious conclusion, of course, is that it would be extremely difficult to ignite a system as the one shown in fig. 2.17b. Note that the advantages of series flow as far as cell voltage is concerned are increased as the number of reactors increases (again note the PFR-CSTR analogy), which renders the ignition problem even more difficult (i.e., we operate ever more efficiently as the number of reactors is increased, but the difficulty to achieve self ignited operation within any reactor increases correspondingly as the heat generated per unit flowing matter is lowered). As the number of series-fed reactors is increased, though, provided a sufficiently high degree of stacking and insultation prevent the system from losing heat, ignition will inevitably be attained at a certain feed temperature, for any given set of parameters (load, fuel concentration, etc.), but the degree of stacking, the amount of insulation required, and the number of reactors have been increased with respect to the parallel-feed arrangement. This very qualitative argument serves, however, to point out that the choice of flow-arrangement is by no means a straight-forward one, as consideration of cell voltage alone would suggest; therefore, if the prime objective is the attainment of self-sus-

tained operation at high conversions and generating the maximum possible amount of energy at any given point, a PFR reactor would seem to be the best choice. A great number of series-fed CSTR's, on the other hand, can become quite impractical when compared with the single PFR. Parallel feed, on the other hand, sacrifices power generation effectiveness but achieves ignited operation at high conversions with greater ease than the series counterpart, and requires fewer and smaller reactors.

Having very superficially touched upon the subject of flow arrangements, we now focus attention upon figure 2.18, where the results of three runs such as the one outlined in figure 2.15 are plotted on the same graph, for three different values of the z-parameter. The s-shaped curve is the dimensionless heat generation curve, i.e., the left-hand side of equation (2.1.111) divided by $F_i \rho_i \hat{C}p_{fGi} T_i$. In figure 2.6 it was shown that a high air feed ratio enhances steady state conversion, the effect being greater at higher temperatures. Since heat generation is proportional to current, which in turn is proportional to conversion, the heat generation function shows the influence of air feed ratio, though, as can be seen, the effect is very small, and, moreover, the 2.5 and 6 air feed ratio curves are indistinguishable from each other for all practical purposes. The dimensionless heat removal function (i.e., the right hand side of equation (2.1.111) divided by $F_i \rho_i Cp_{fGi} T_i$) is normally presented in standard reactor engineering books as a straight line. In fact, if, in equation (2.1.111) the air and oxygen terms are dropped, inlet and outlet mass flow rates become

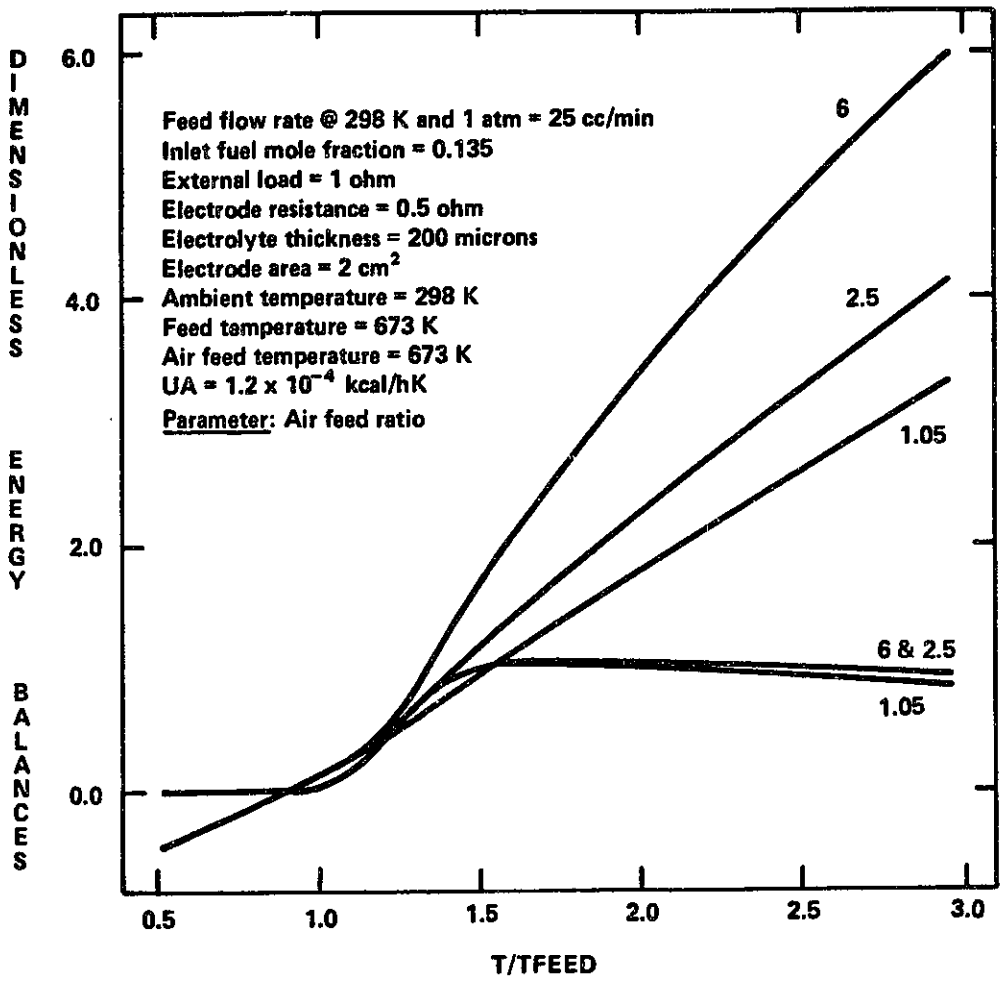

INFLUENCE OF AIR FEED UPON OPERATING POINT (H_2/H_2O CELL)
FIGURE 2.18

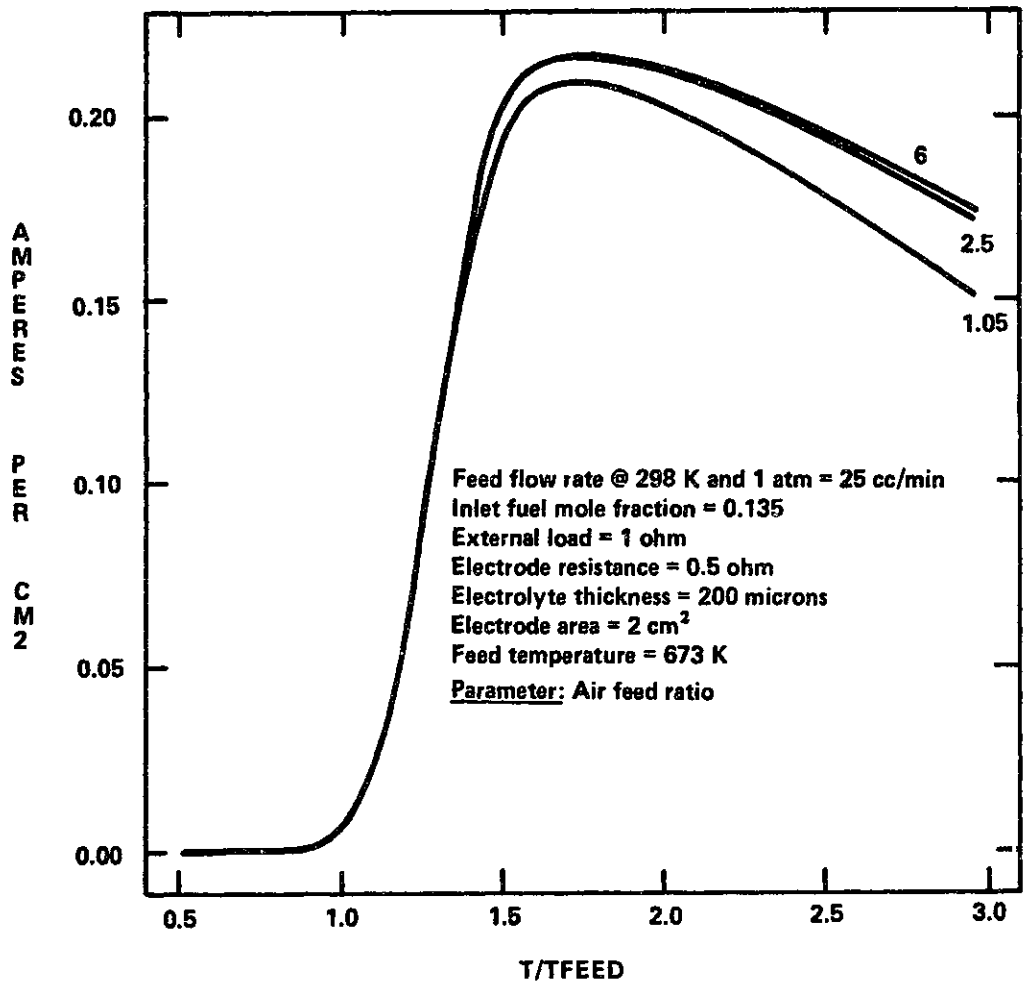

INFLUENCE OF AIR FEED UPON CURRENT OUTPUT (H_2/H_2O CELL)
FIGURE 2.19

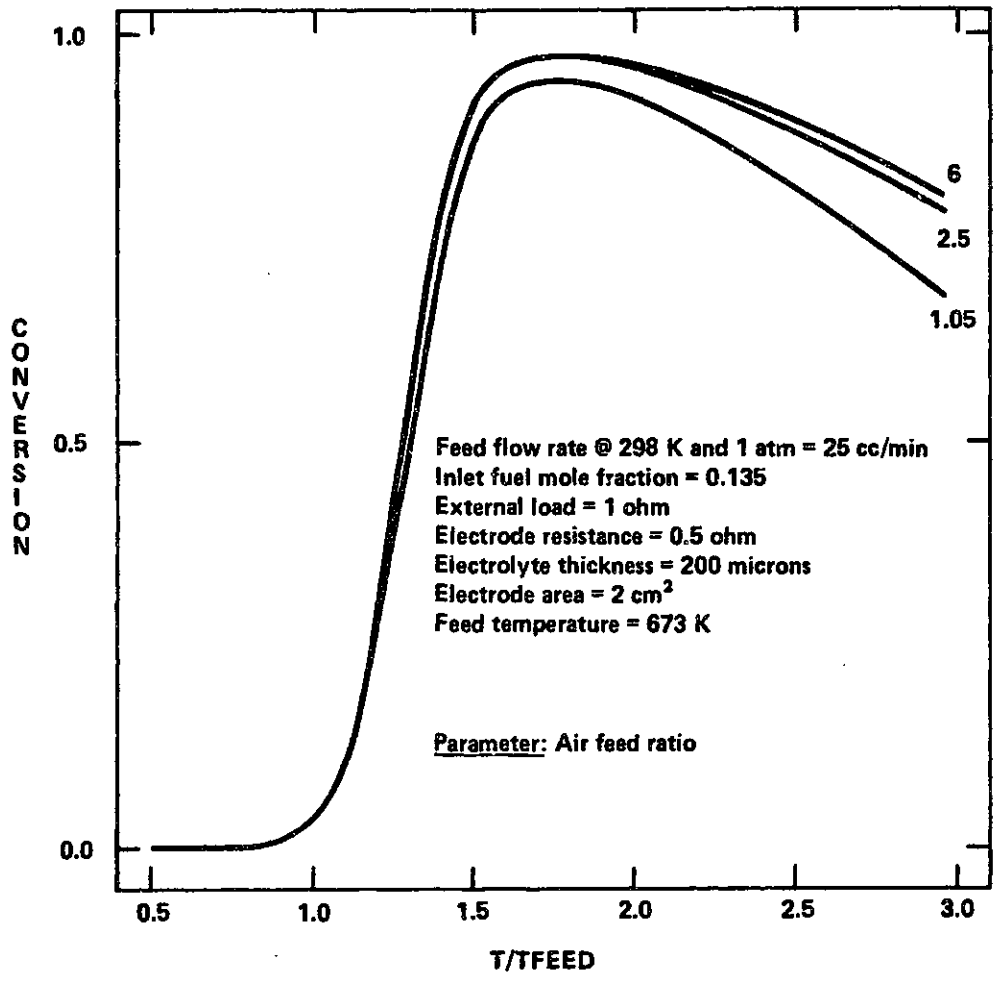

INFLUENCE OF AIR FEED UPON CONVERSION (H_2/H_2O CELL)
FIGURE 2.20

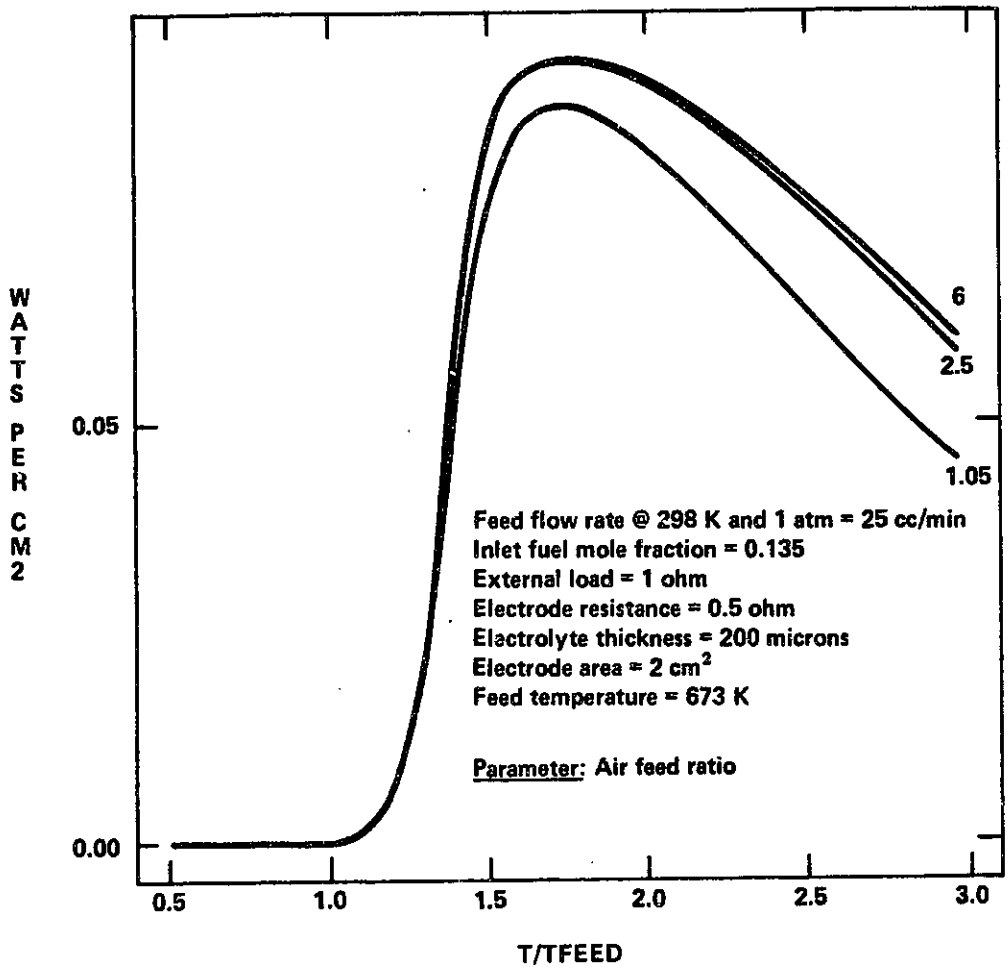

INFLUENCE OF AIR FEED UPON POWER OUTPUT (H_2/H_2O CELL)
FIGURE 2.21

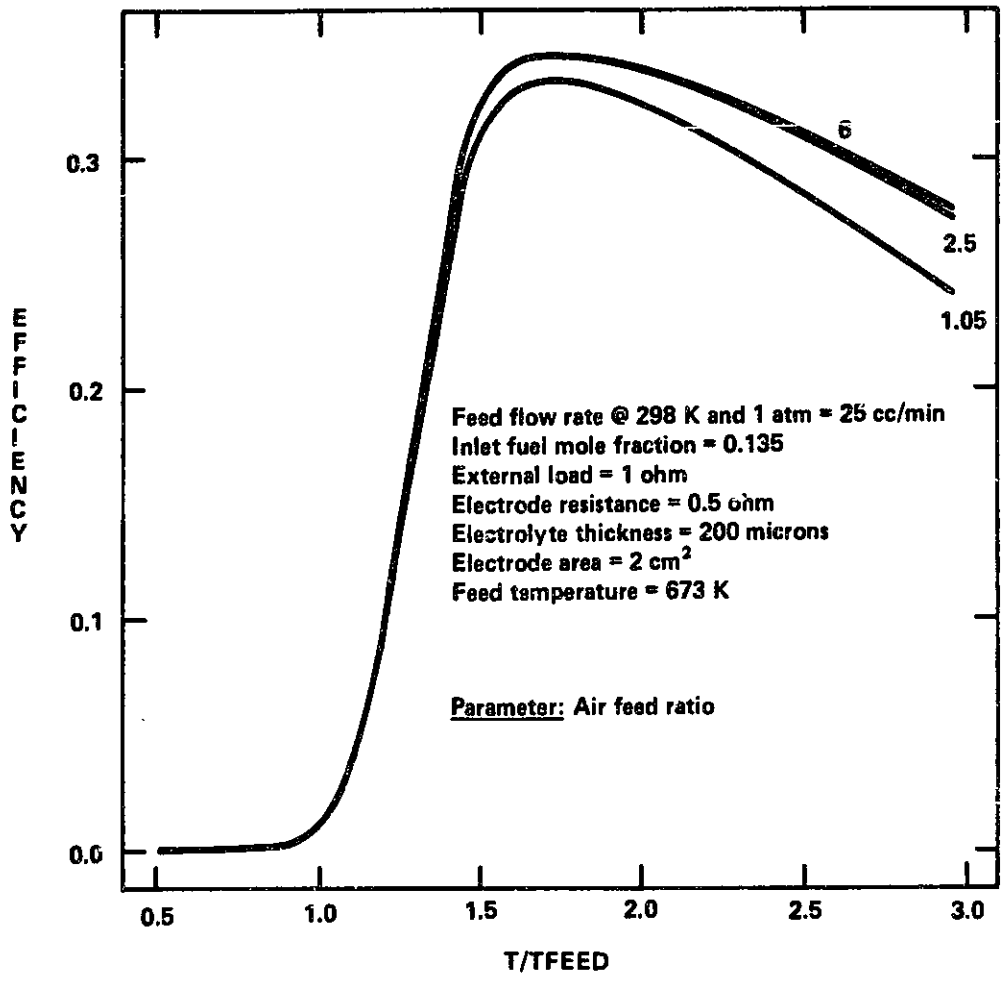

INFLUENCE OF AIR FEED UPON EFFICIENCY (H_2/H_2O CELL)
FIGURE 2.22

equal. If, moreover, constant physical properties are considered, a linear function in T is obtained (and the T_o terms can be dropped). Note, in effect, that the non-linearity of the heat removal line increases as the air feed ratio increases. This is due to the fact that the air feed is not constant but proportional to the current, which is not linear in T (see figure 2.19); in fact, the non-linearity starts at the same dimensionless temperature at which the current curves starts to grow very steeply.

Note that the results given here correspond to parametric runs with (for each run) a constant value of air feed ratio, which means that air flow varies from point to point (hence the non-linearity discussed above). Since the steady state behaviour of the system is being analyzed, a constant air feed ratio means a constant driving force on the cathode, even though the actual air feed changes. We are thus restricting one degree of freedom, with fuel being the only independent feed to the system. Thus the cell shown in Figure 2.3 contains this built-in limitation. Only for a specified steady state can air feed rate to the cell be related to fuel flow, but, in exploring steady state behaviour, air flow must be related to current, hence the significance of an air flow ratio.

The steady states shown in figure 2.18 are summarized in table 2.3.

The corresponding conversion, power output and efficiency vs. temperature curves are shown in figs. 2.20, 2.21 and 2.22. Note, in all cases, the small effect of increasing the air feed ratio from 2.5 to 6, when compared to the 1.05 to 2.5 increase

Air feed ratio (-)	Temperature (dimensionless)	Conversion -	Power output (Watts/cm^2)	Efficiency -	Current density (amps/cm^2)
1.05	0.8915	0.0061	3.765×10^{-5}	2.166×10^{-3}	1.321×10^{-3}
1.05	1.2180	0.3130	9.73×10^{-3}	0.1108	6.945×10^{-2}
1.05	1.5300	0.8954	7.852×10^{-1}	0.3170	0.1987
2.50	0.8915	0.0063	3.961×10^{-5}	2.226×10^{-3}	1.396×10^{-3}
2.50	1.2480	0.3975	1.559×10^{-2}	0.1407	8.819×10^{-2}
2.50	1.3970	0.7593	5.678×10^{-2}	0.2688	0.1685
6.00	0.8915	0.0063	3.984×10^{-6}	2.233×10^{-3}	1.340×10^{-3}

TABLE 2.3: Steady states for figure 2.18

and its related effects (obviously, this does not apply to the heat removal curve). In all cases, as well as in the rest of the examples presented here, a well mixed air chamber is assumed. Thus, for a system with the specified characteristics, an air ratio only slightly above stoichiometric would be the appropriate choice. The detailed final analysis would have to weigh the additional benefits that would be obtained through an additional slight increase in air feed against the increased pumping costs if scale-up were based on these figures. The important conclusion of this analysis is, however, that there is little point in increasing air flow much above stoichiometric requirements, with too high an air flow leading eventually, to unignited operation.

Figure 2.18, in addition, clearly shows that multiple steady states are possible under certain circumstances, a familiar fact in CSTR analysis, though applied here to a very different type of reactor. The issue of steady state multiplicity is fully treated in section 2.1.3.5.4. Also, as is the case in CSTR analysis, when 3 steady states occur, an unstable intermediate steady state is found between an ignited and an unignited steady state.

Note the extremely low value of UA required to achieve self ignited operation. Figure 2.23 illustrates a possible stacked arrangement with parallel fluid flow (2.23.a), while two possible electrical arrangements and the associated electron flows are shown in figures 2.23.b and 2.23.c, namely monopolar (high current-low voltage) and bipolar (high voltage-low current),

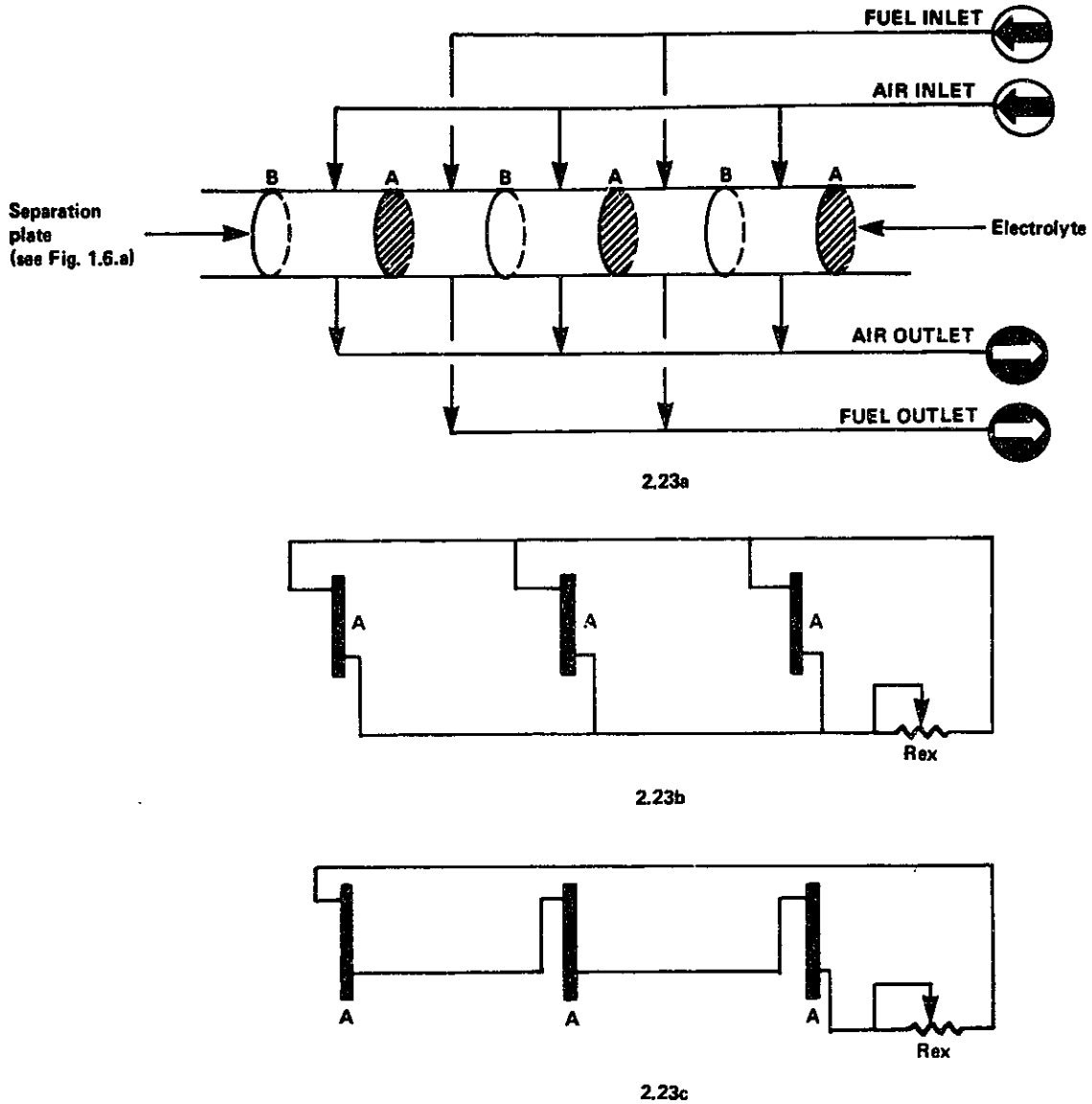

CELL STACK, PARALLEL FEED, MONOPOLAR AND BIPOLAR ARRANGEMENTS
FIGURE 2.23

respectively. For a $2cm^2$ electrode area (a laboratory scale prototype stack, for example), practical considerations set a lower limit to the degree of proximity achievable between successive cells if fluid feed is realized as indicated (this constraint is less severe if an internal through-flow distribution is adopted, though this would considerably increase internal complexity), which means that the stack must be thermally insulated to operate autothermally, or several non-insulated stacks must be grouped together, within an insulated container (see discussion in Appendix III).

In practical terms, a lab-scale experimental stack such as the one illustrated in figure 2.23a, with a 2 cm^2 electrode would be extremely difficult to operate autothermally by itself, and a tube-bundle arrangement within an insulated enclosure would be needed. Difficulties associated with insulation requirements become progressively less critical upon scale-up, since the resulting geometric constraints are much easier to realize in practice (see Appendix III).

In either case, it can be seen, as will be specicifically shown in the next example, that the system is very sensitive to heat losses. Furthermore, the usefulness of the present analysis in providing a first design approach, coupled with the scale-up criteria discussed in section 2.1.3.5.3, lies chiefly in the flexibility with which the designer can arrive at a

satisfactory preliminary design through the systematic variation of any desired parameter.

In figures 2.24 to 2.29, the steady state analysis is repeated, this time for the CO/CO_2 fuel cell, and in order to discuss the effect of external area associated with heat losses upon operating point.

The value of the overall heat transfer coefficient corresponds to a $\sim$4 cm thick insulation with diatomaceous-based insultation. Note that the external to electrode area ratio indicates the necessity to group several stacks together. Both quantitites suggest a solution such as the one illustrated in figure III-2, where a UA value of 1.4 x 10^{-4} Kcal/hm^{2}K has been achieved. The steady states are summarized in table 2.4. Here again, as with the air feed ratio, a point is eventually reached beyond which big changes produce small effects. Thus, although a 0.6 area ratio leads to a totally unacceptable operation, decreasing the area ratio from 0.2 to 0.1 (which, in terms of system geometry would imply doubling the amount of stacking)results in just a $\sim$3% increase in conversion. The reason for this behaviour is associated with the fact that the heat removal function (right hand-side of equation (2.1.111)) is the sum of several terms, the heat interaction with the surroundings being just one of them, and as its contribution is made smaller through heat transfer area reduction, it ceases to be the controlling factor. Figure 2.25 is a "close-up view" of figure 2.24, while figures 2.26

Area ratio	Temperature (dimensionless)	Conversion
0.1	0.9807	0.02752
0.1	1.085	0.1016
0.1	1.605	0.9608
0.2	0.8915	0.00672
0.2	1.174	0.2402
0.2	1.530	0.9356
0.6	0.7578	0.00042

TABLE 2.4:

Steady states for figures 2.24 and 2.25

Feed flow rate @ 298 K and 1 atm = 25 cc/min
Inlet fuel mole fraction = 0.135
External load = 1 ohm
Electrode resistance = 0.5 ohms
Electrolyte thickness = 200 microns
Electrode area = 2 cm^2
Feed temperature = 673 K
Air feed ratio = 2.5
Air feed temperature = 673 K
Ambient temperature = 298 K
Heat transfer coefficient = 3 kcal/hm2K (insulated stack)

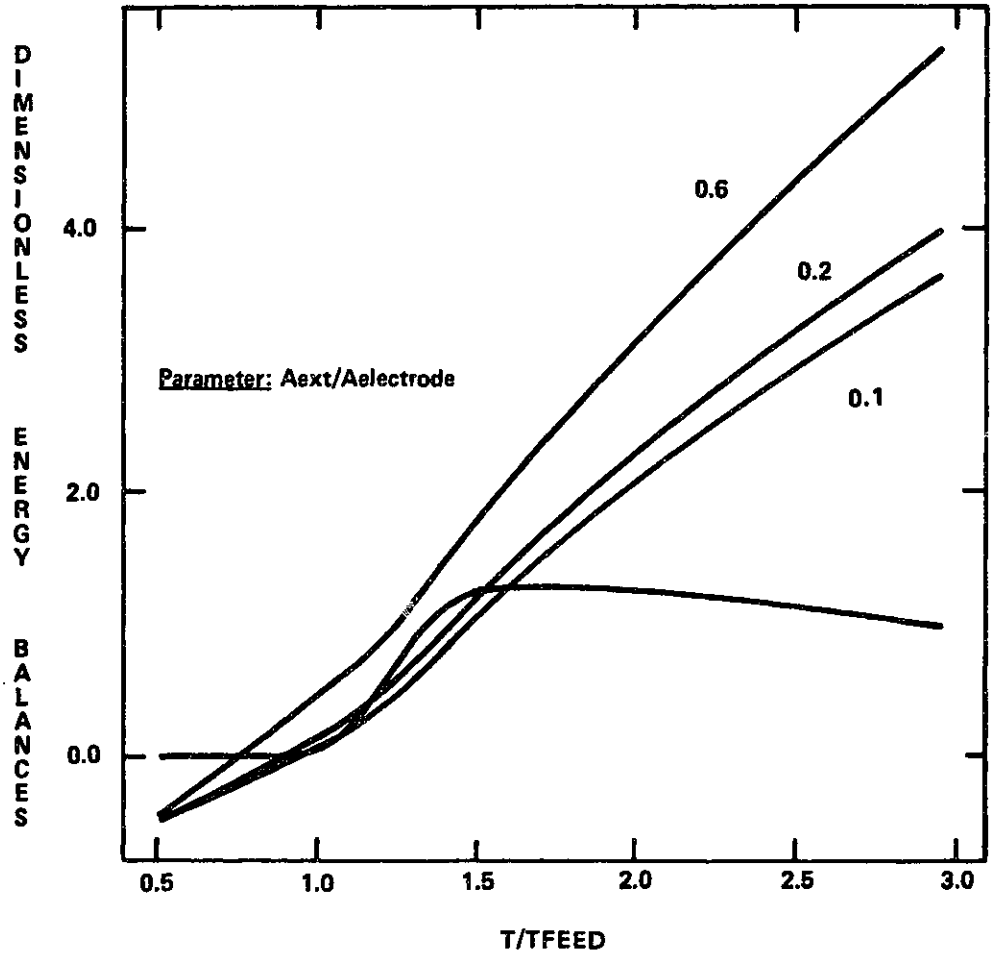

EFFECT OF CELL GEOMETRY UPON OPERATING POINT (CO/CO_2 CELL)
FIGURE 2.24

Feed flow rate @ 298 K and 1 atm = 25 cc/min
Inlet fuel mole fraction = 0.135
External load = 1 ohm
Electrode resistance = 0.5 ohms
Electrolyte thickness = 200 microns
Electrode area = 2 cm^2
Feed temperature = 673 K
Air feed ratio = 2.5
Air feed temperature = 673 K
Ambient temperature = 298 K
Heat transfer coefficient = 3 kcal/hm2K (insulated stack)

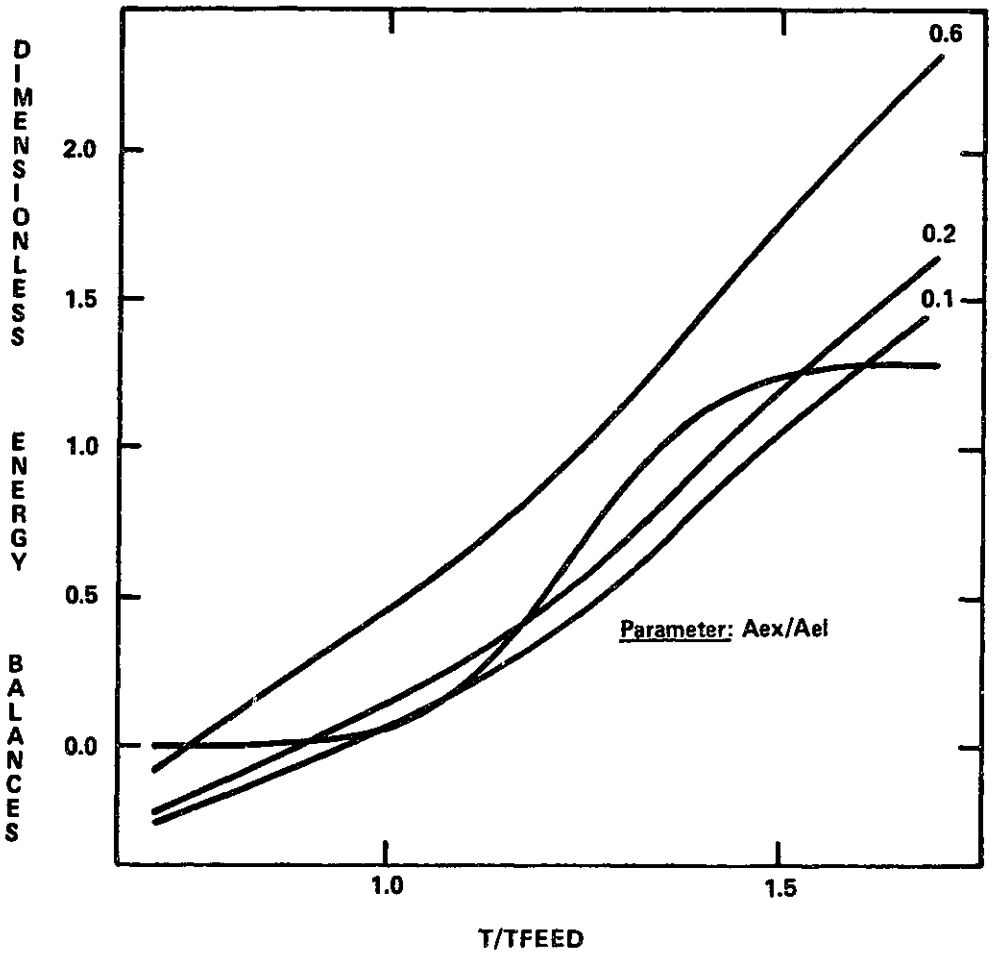

EFFECT OF CELL GEOMETRY UPON OPERATING POINT (CO/CO_2 CELL)
FIGURE 2.25

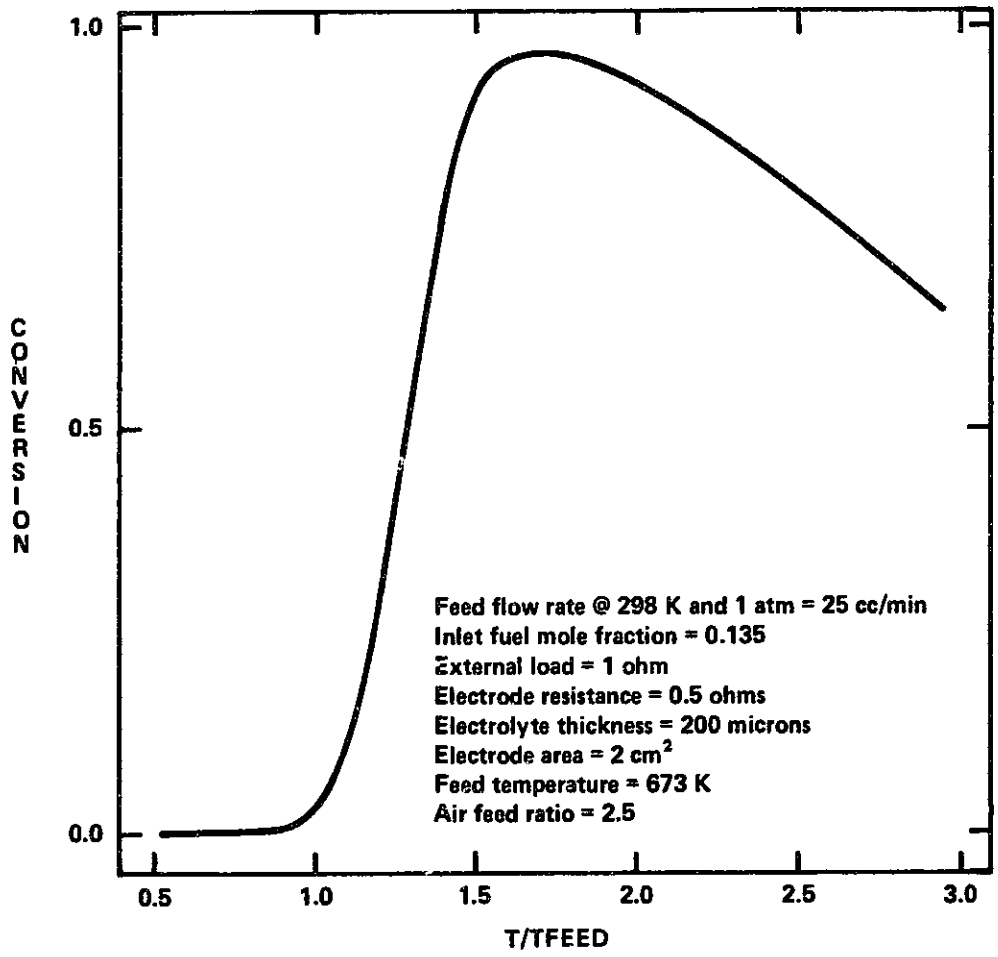

MATERIAL BALANCE (CO/CO_2 CELL)
FIGURE 2.26

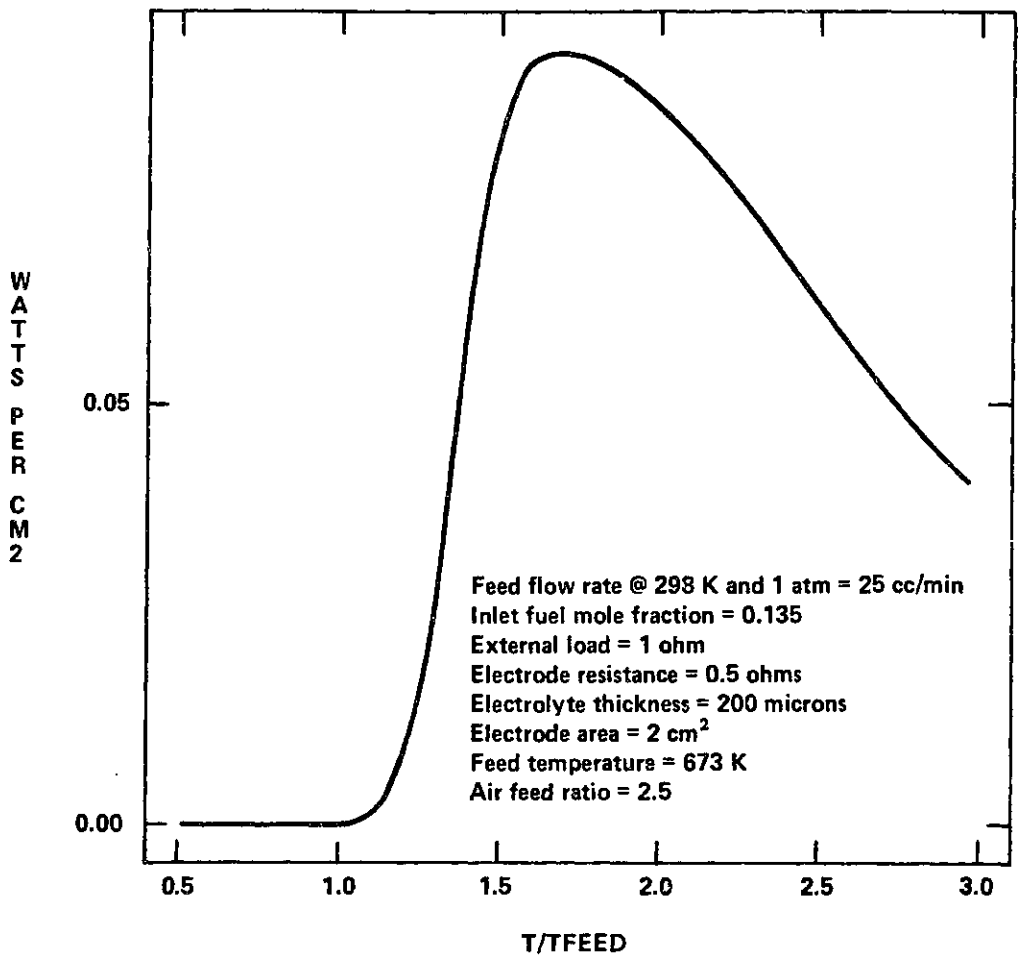

POWER OUTPUT (CO/CO_2 CELL)
FIGURE 2.27

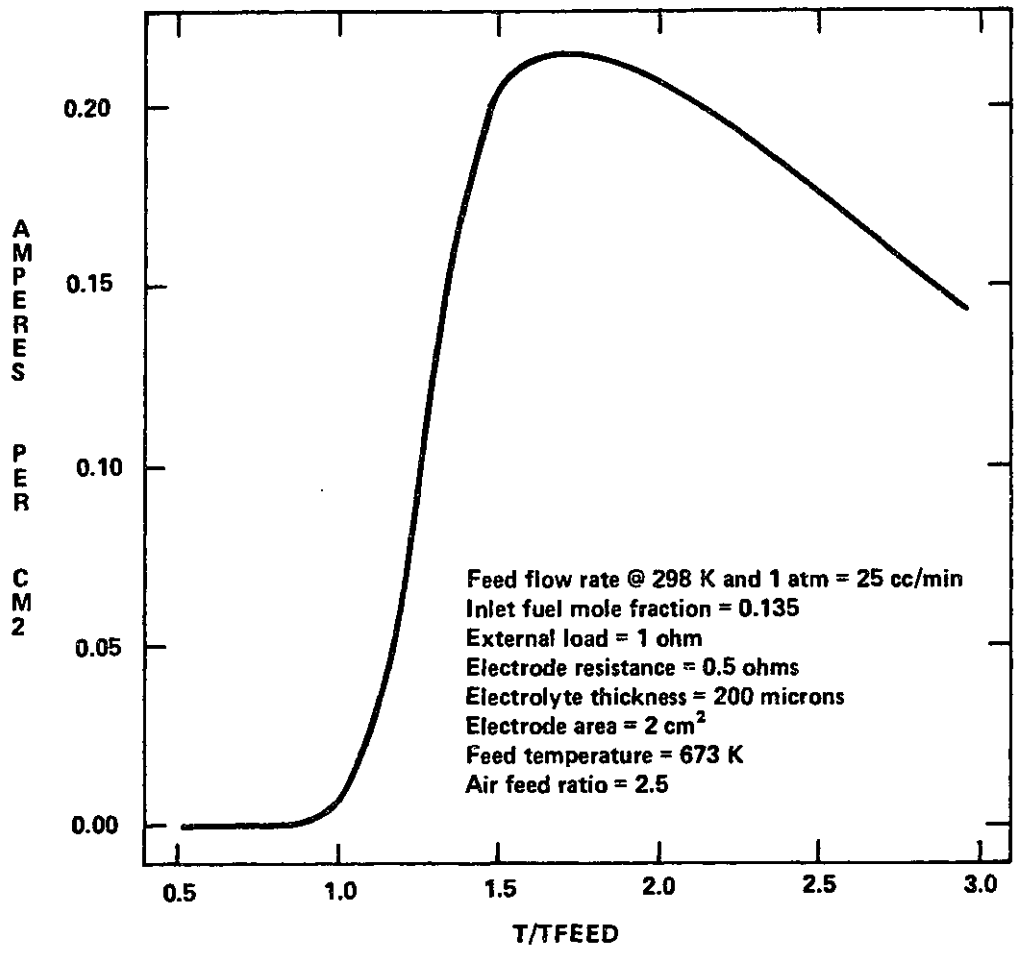

CURRENT OUTPUT (CO/CO_2 CELL)
FIGURE 2.28

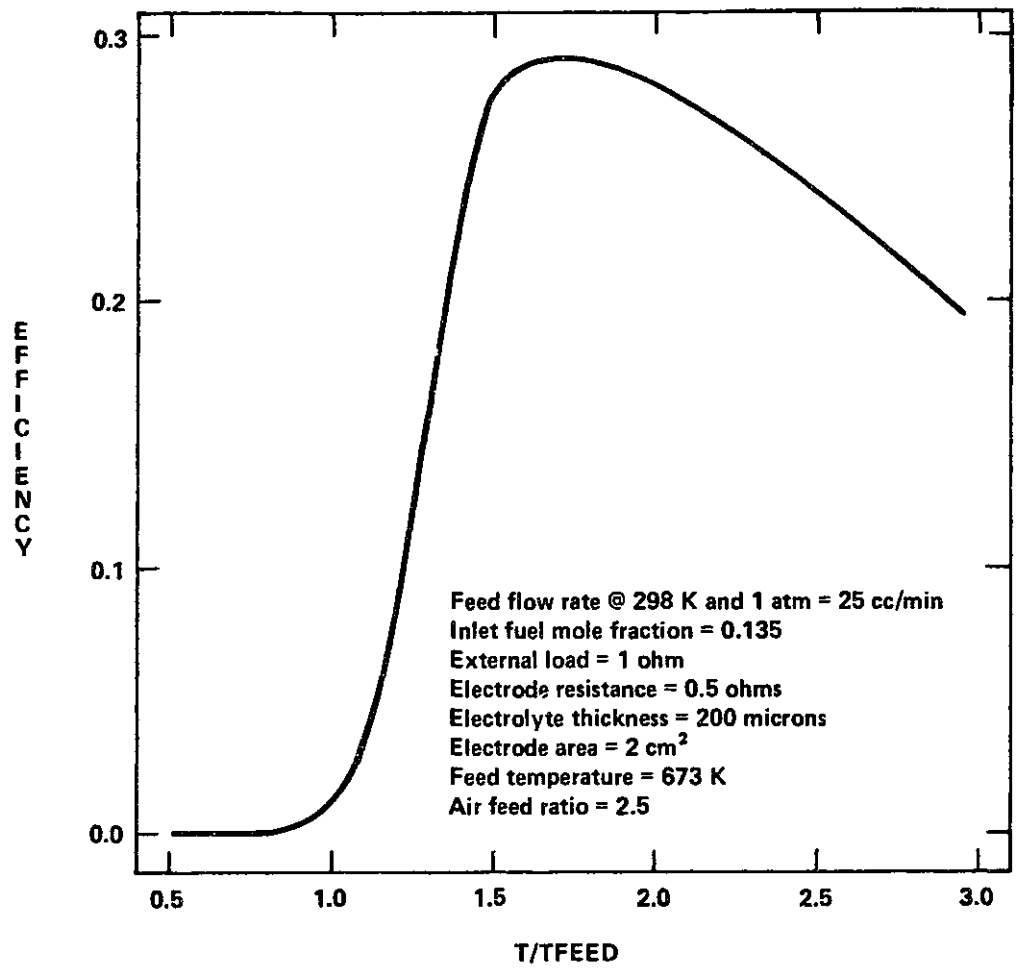

EFFICIENCY (CO/CO_2 CELL)
FIGURE 2.29

to 2.29 show fuel cell steady state performance.

2.1.3.5.3 Application of dimensionless parameters to scale-up

In section 2.1.3.5.1 the dimensionless groups governing reactor behaviour were introduced. They can be classified as follows:

i. dimensionless groups describing the fundamental thermodynamic behaviour of the system

ii. dimensionless groups describing physical properties of the flowing gases (specific heats)

iii. dimensionless groups containing ratios of some important property (either kinetic or thermodynamic) to an equivalent molar or volumetric inlet energy term (RT_i or $\rho_i Cp_i T_i$) (we include N_{12} since $[A]_i$ will be held constant upon scale-up)

iv. dimensionless groups of engineering importance, which contain all the quantities under the designer's control, either related or not to fundamental thermodynamic properties of the reacting system.

v. dimensionless inlet and ambient temperatures.

Among the thermodynamic (group i) dimensionless numbers, N_6 is temperature-dependent and contains information already implied in N_{11} (since it is basically the entropy variation that determines the free energy vs. temperature behaviour). Group ii dimensionless numbers are of relatively small importance, except, as already stated, when fluids with very high (H_2) or very low heat capacities are invovled in high concentrations. Group iii and v numbers are solely dependent upon fuel inlet, air inlet and ambient temperature, and, except for these parameters,

i.	ii.	iii.	iv.	v.
$N_6 = \frac{E^\circ}{E_\delta^\circ}$	$N_2 = \frac{\hat{C}p_{O_2Gj}}{\hat{C}p_{fGi}}$	$N_4 = \frac{E^*}{RT_i}$	$N_1 = \frac{WE_\delta^\circ}{2\pi R_{ex} F_i \rho_i}$	$\theta_c = \frac{T_c}{T_i}$
$N_{11} = \frac{E_\delta^\circ}{E_{TN}}$	$N_8 = \frac{\hat{C}p_{AirGm}}{\hat{C}p_{fGi}}$	$N_7 = \frac{RT_i}{2\pi E_\delta^\circ}$	$N_3 = \frac{R_{el}}{R_{ex}}$	$\theta_j = \frac{T_j}{T_i}$
	$N_9 = \frac{\hat{C}p_{pG}}{\hat{C}p_{fGi}}$	$N_{12} = \frac{(-\Delta H_o)[A]_i}{\rho_i \hat{C}p_{fGi} T_i}$	$N_5 = \frac{r_* d}{SR_{ex}}$	
			$N_{10} = \frac{UA}{F_i \rho_i \hat{C}p_{fGi}}$	
			$N_{13} = \frac{E_\delta^\circ}{R_{ex} F_i [A]_i 2\pi}$	
			$N_{14} = Z$	

TABLE 2.5: Governing dimensionless groups

all of the major engineering variables under the control of the designer are contained in the group iv dimensionless numbers. Furthermore, since intensive properties will be held constant upon scale-up once a suitable operating condition has been found (or chosen), engineering decisions will inevitably focus upon the above mentioned dimensionless groups.

Before discussing the scale-up criteria, it must be added that we are implicitly accepting the validity of the model assumptions to hold upon scale-up, since we are using the same equations. This means that fluid flow and heat transfer are such that well mixed fuel and air compartments, plus the implied heat transfer characteristics that are contained in the air outlet temperature, still hold. This does not necessarily require geometric similarity, so long as the basic well-mixed assumptions hold.

We will now develop the appropriate scale-up criteria. In this section, primed quantities refer to the large unit to be designed, while unprimed quantities refer to the small-scale unit. Therefore, once an appropriate operating point has been selected, let ψ be the fundamental scaling factor which relates the amount of reactants flowing through the large fuel cell per unit time to the corresponding quantity for the pilot-sized unit,

$$\psi = \frac{F_i' \rho_i'}{F_i \rho_i} \tag{2.1.112}$$

Then, to obtain the same temperature and conversion, the governing dimensionless quantities must be equal. Therefore,

$$N_1 = N_1' \tag{2.1.113}$$

Which implies

$$R_{ex}\, F_i \rho_i = Rex'\, F_i' \rho_i' \qquad (2.1.114)$$

Therefore,

$$R_{ex}' = \frac{R_{ex}}{\psi} \qquad (2.1.115)$$

This is a first, very important conclusion. Note that, as illustrated in figure 2.16, R_{ex} is not an actual load, but the equivalent load per cell, and, therfore, the requirement imposed by equation (2.1.115) can be satisfied by means of a suitable electric connection (qualitatively, the number of bipolar cells in series per unit load would increase as ψ).

Equality of N_3 with N_3' leads to

$$\frac{R_{el}'}{R_{ex}'} = \frac{R_{el}}{R_{ex}} \qquad (2.1.116)$$

Therefore

$$R_{el}' = \frac{R_{el}}{\psi} \qquad (2.1.117)$$

Consider, however, figure 2.30. The dotted lines indicate the boundaries (electrical) of a single fuel cell, which <u>include</u> electrolyte <u>and electrode</u> losses, as schematically shown (they are drawn as lumped on one electrode for graphical convenience only). In the first case, as already shown in figure 2.16a and b, a series arrangement of n cells can be reduced, for parallel fluid flow, to a single cell with an "equivalent load" R_{ex}/n, i.e., the equations derived so far can be applied to the single cell with a load $R_{ex/n}$, the total power output being, of course, <u>n times</u> EI. Note, however, that contact and electrode losses do

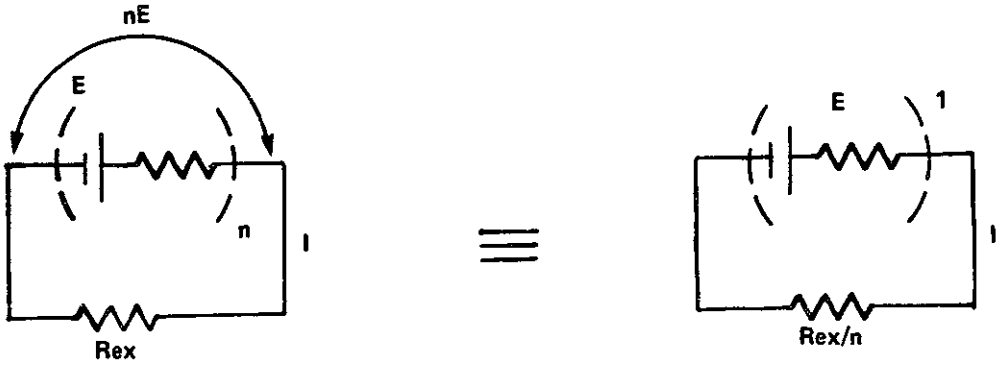

2.30a

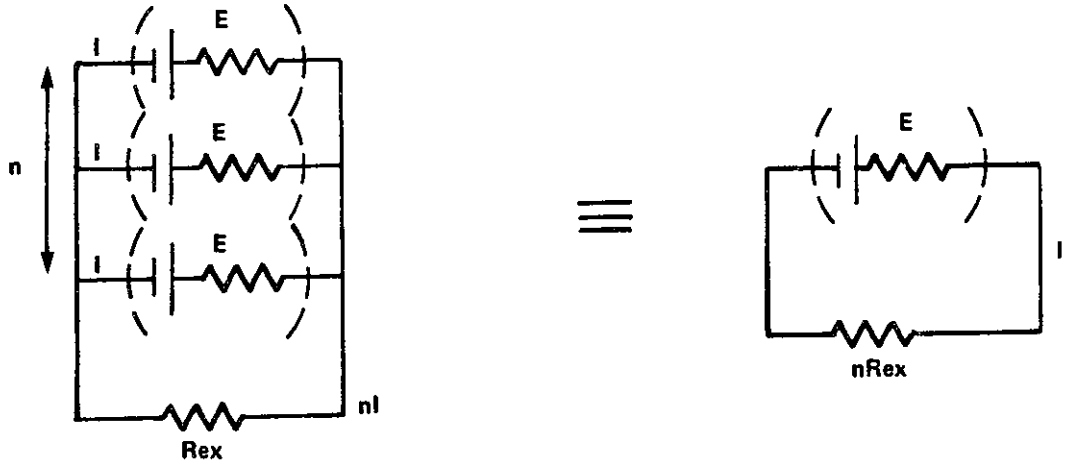

2.30b

ACTUAL CIRCUITS AND EQUIVALENT CIRCUIT PER CELL
FIGURE 2.30

not change, i.e., there is no such thing as an "equivalent electrode loss" per cell for a series arrangement.

In figure 2.30.b, a parallel electrical arrangement is shown. This time, however, the equivalent load is nR_{ex}. In considering the whole circuit, it is obvious that n cells in parallel give rise to an electrode + electrolyte resistance n times smaller than the individual cell's resistance; however, the equivalent loss associated with each cell is, once again, the actual electrode + electrolyte drop; in other words, the single battery operating under identical conditions as each of the n batteries in parallel would be connected to a load nR_{ex} and would have the same resistance as each of the n parallel cells.

The important conclusion is that, while equation (2.1.115) can be satisfied by circuit modifications, equation (2.1.117) cannot. Note that the quantity ψ is not a global scaling factor which relates a single cell's output to a large-scale plant output, but rather the ratio of such rate for the single large-scale cell which will also be part of a stacked arrangement, to the corresponding value of the experimental unit. We are thus scaling up modular elements, the number of which will depend on the desired output.

Returing to equation (2.1.117), therefore, we conclude that, in order to reduce R_{el}, the electrode area must be increased by a factor of ψ. However, it is very important to notice that this is the true "bottleneck" of the scaling-up. In fact, R_{el} groups together three resistances:

i. electrode-electrolyte contact resistance

ii. electrode film resistance

iii. electrode film-current collector contact resistance

While the electrode film resistance can be reduced by increasing electrode area, items i. and iii. also involve localized resistances which cannot be indefinitely reduced, and which will inevitably become controlling as ψ is increased, thus setting an upper bound upon the scaling-up potential of a pilot-sized fuel cell, which, as most constraints associated with engineering decisions, involves primarily economic considerations (in the present case, it is always possible to design an "ideal" current collector with a very small resistance, but this involves a large cross section for the lead wires (bus-bars when scaled-up), expensive silver-coating, etc.).

We will limit the present discussion to the case in which contact and electrode losses are not controlling, i.e., the ψ - proportionality can effectively be achieved. Consideration of N_5 then shows that the electrolyte thickness remains constant upon scale-up. In fact, for scale-up

$$\frac{r_* d}{SR_{ex}} = \left(\frac{r_* d}{SR_{ex}}\right)' \qquad (2.1.118)$$

But, since r_* is an intensive property, and the product SR_{ex} has been held constant (see equations (2.1.115) and (2.1.117), and recall that R_{el} has been reduced by increasing S), we have therefore shown that d is unchanged upon scale-up.

Heat interactions with the surroundings are scaled through N_{10}, and for equal overall coefficients, similarity requires,

again, that A'/A must scale as ψ.

The above discussed design criteria for scale-up lead to a constancy of specific output parameters (power and current per unit area). Consider, in fact, equation (2.1.30), which can be rewritten as follows:

$$\text{Power output} = \frac{E_{rev}^2}{R_{ex}\left[1+N_3+N_5 \exp \frac{N_4}{\theta}\right]} \qquad (2.1.119)$$

Division by S provides, of course, the specific power output. Since N_3, N_4 and N_5 are unchanged, and, for equal operating conditions (θ and x) E_{rev} remains constant; since, moreover, it was shown that SR_{ex} is held constant upon scaling-up, this means that the specific power output is conserved. A similar prrof applies to current density.

We therefore conclude that, within the limits explained above (i.e., electrode and contact losses not controlling), for a given feed temperature and composition, the following scale-up procedures lead to constant intensive process parameters (temperature, conversion, power per unit electrode area, current density):

To increase the fuel-processing capacity of a cell by a factor of ψ

- reduce external effective load by a factor of ψ
- increase electrolyte and electrode areas by a factor of ψ
- hold electrolyte thickness constant
- increase external area by a factor of ψ

Once again, note that this is <u>not</u> an overall plant-scale up factor, but an individual cell scaling factor (for example, to

reduce the external effective load by ψ, we can connect scaled-up cells in series, electrically, and use the same load as for the bench-scale cell, but the production will now be ψ^2 times the small cell's output). Having thus achieved a successful modular deisgn, the desired production can be reached by appropriately connecting the necessary amount of cells, assuming parallel fluid feed applies.

Finally, note that the "bottleneck" described above invovling a limiting value for ψ before contact losses become controlling applies only if parallel fluid flow is specified, in which case a high conversion is necessary in every reactor. Alternately, one can decide upon series fluid flow, in which case conversion per reactor is small, if the limiting ψ consistent with reasonable economic design is low. Thus, it can be seen that one of the reasons which may lead to series flow is the impossibility to process an adequate amount of fluid at high conversion within each single reactor, due to contact losses.

2.1.3.5.4 Steady-state multiplicity

The two cases of steady-state analysis presented in figures 2.18 to 2.23 and 2.24 to 2.29 illustrate some of the insights into fuel cell steady state behaviour provided by the simultaneous consideration of mass and energy balances. It is evident, however, that such an approach is not practical if a more general picture of reactor characteristics under varying conditions is to be obtained. Such an overall picture can, however, be obtained, if the mass and energy balances are simultaneously solved for fuel inlet temperature as a function of reactor

temperature. The general procedure is illustrated in figure 2.31, which should be compared with figure 2.15. Each point on any one of the resulting graphs represents a steady state such as the ones shown in figures 2.24 or 2.18; it is therefore clear that the amount of information conveyed by applying the procedure illustrated in figure 2.31 is much greater than the one shown in any of the figures presented so far, and should therefore be used as a preliminary way of determining satisfactory operating conditions, whereupon the detailed analysis provided by simultaneous solving of heat and material balances for heat generation and removal should follow. In this section the issue of steady state multiplicity is discussed, and the influence of that main parameters on cell performance is analyzed.

Figure 2.32 shows the influence of external load upon the H_2/H_2O cell operating point. An isothermal line has been included to divide the plane into a lower, non-autothermal region, and an upper, self ignited one. Values of heat transfer coefficient and area ratio correspond to a non-insulated stack within an insulated enclosure such that the effective external area for heat transfer associated with each fuel cell is one tenth of the electrode area (see section 2.1.3.5.2 and figure III-2).

The most interesting feature of figure 2.32 is the existence of multiple steady states for the 0.5 and 2 ohm curves. Steady-state multiplicity is a well-known feature of perfectly backmixed reactors. Note that, as the external load becomes smaller, the behaviour of the overall process is controlled by electrolyte resistance (an activated process), and the reactor

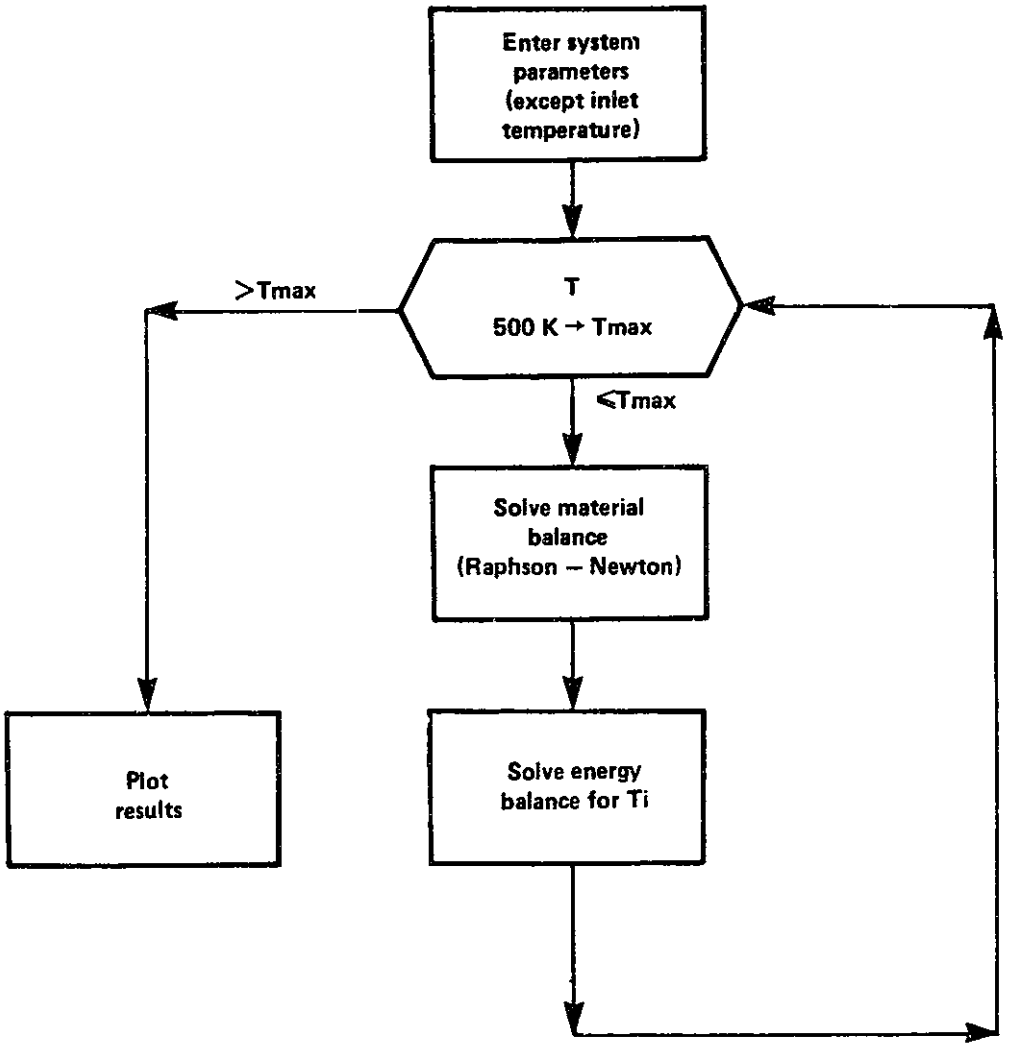

STEADY STATE MULTIPLICITY DETERMINATION
FIGURE 2.31

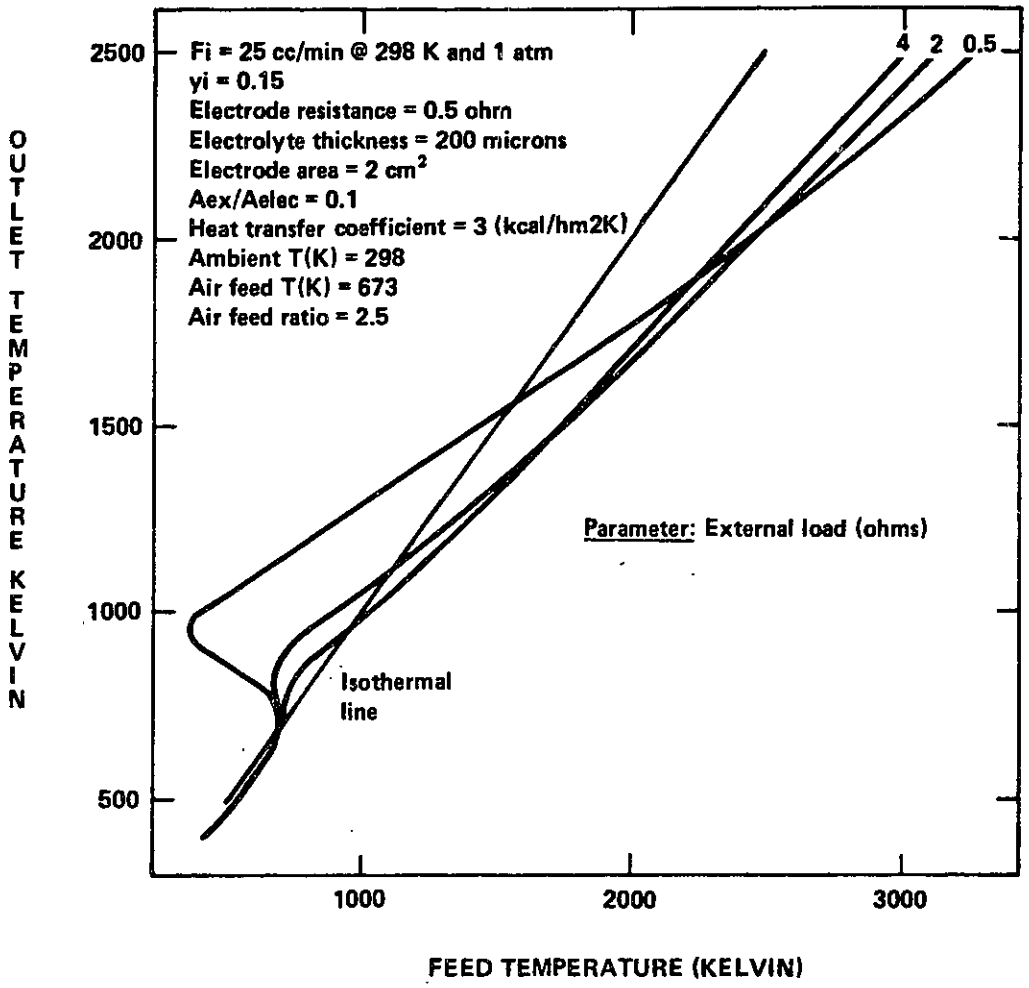

H_2 FUEL CELL MULTIPLICITY
FIGURE 2.32

thus behaves as a "normal" (i.e., non electrochemical) CSTR. At higher temperatures, though, external resistance becomes controlling and the analogy does not hold. Note, in fact, that the region associated with multiplicity, in this and the rest of the examples presented (when changes in system geometry are not considered) involving a wide variation in process parameters, is always roughly circumscribed to an uppper feed temperature ∿700K and a corresponding reactor temperature ∿1200K. The electrolyte resistance's temperature dependence is shown in figure 2.33. For the geometry considered in most cases (200 μm thickness, 2 cm^2 area) it decreases from 437 ohms at 600K to 0.68 ohms at 1000 K. This, therefore, explains why, even within the wide range of values presently considered for the various process parameters, the constancy of electrode geometry imposes a remarkably uniform upper bound upon the region associated with steady state multiplicity, which is, moreover, the region of interest in all cases since ignition is achieved with moderate preheating, and autothermal operation can be considered.

Note the interesting crossing of the constant-load lines in the high temperature region. This is due to the fact that, while it was shown that the external load tends to "stop" the reaction (see figures 2.13 and 2.14), lowering the heat generation curve, it is also true that, coherent with the use of a stoichiometric air feed throughout, related not to fuel flow but to current flow, external load also depresses the heat removal function, since, at higher loads, the air flow is decreased (for a given fuel feed). These two effects are obviously opposite,

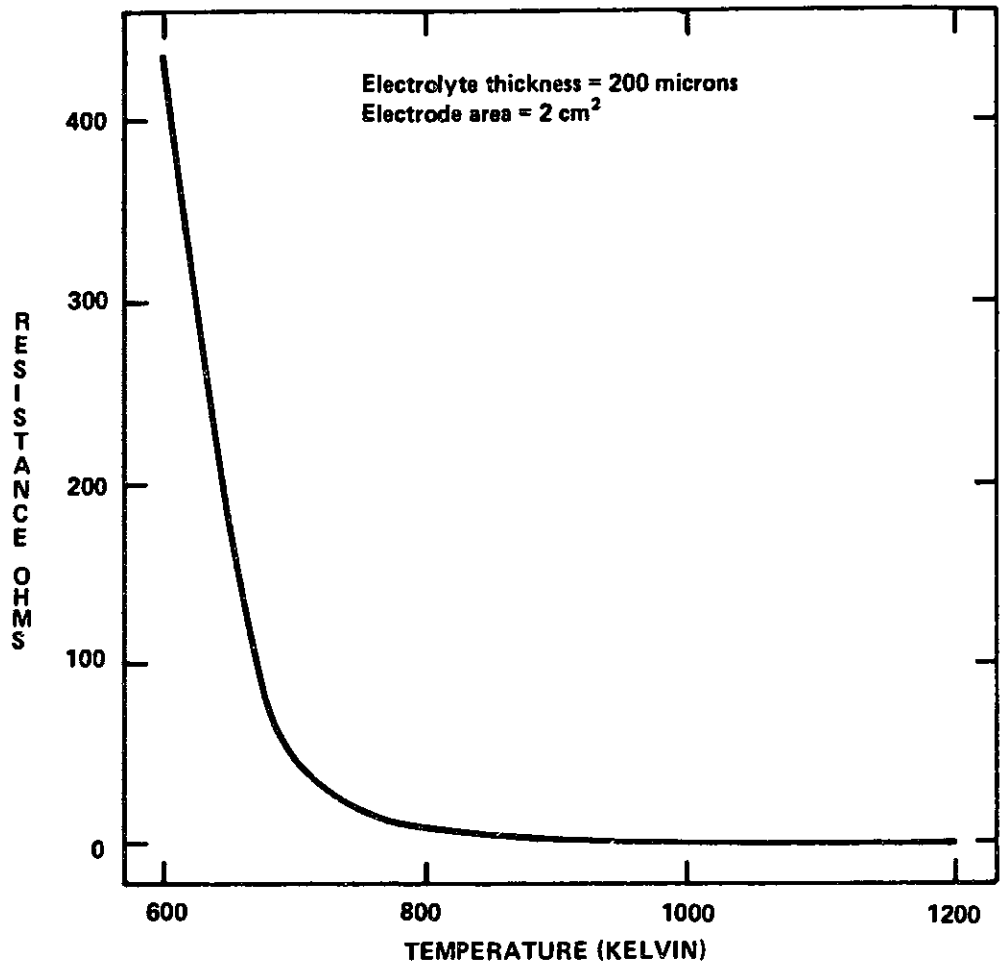

TEMPERATURE DEPENDENCE OF ELECTROLYTE RESISTANCE
FIGURE 2.33

which explains the fact that, for a given inlet temperature, higher outlet temperatures are obtained the lower the external load in the moderate-to-low temperature region (this is the normal, expected behaviour, and predominates in the region of practical interest) while the reverse behaviour is observed at high temperatures; in fact, as can be seen from equation (2.1.111), the stoichiometric component of the heat removal function (air flow) is multiplied by a temperature term, which explains the fact that, at high temperatures, the "abnormal" influence of external load upon operating temperature predominates over the "normal" (depression of heat generation function) behaviour.

Figure 2.34 shows the corresponding analysis for the CO/CO_2 fuel cell. The upper limit of applicability of the model has been reduced in this case (see table 2.4).

Figures 2.35 and 2.36 show an entirely similar behaviour in the case of parametric variation of electrode resistance for the H_2 and CO fuel cells, respectively.

Figures 2.37 and 2.38 illustrate important (and not wholly predictable) effects associated with a change in system geometry. In the first case, electrode area is varied (note the consequent imposed variation of electrode resistance) keeping the rest of the process parameters constant. In particular, the area ratio has been kept constant. Theoretically, increasing electrode area would increase the fuel-processing capacity of the fuel cell and facilitate ignition. In fact, moving along the x-axis, we note that ignition is achieved before for the 5 cm^2 cell than for the 2 cm^2 one; however, the 10 cm^2 and the 2 cm^2 cells attain

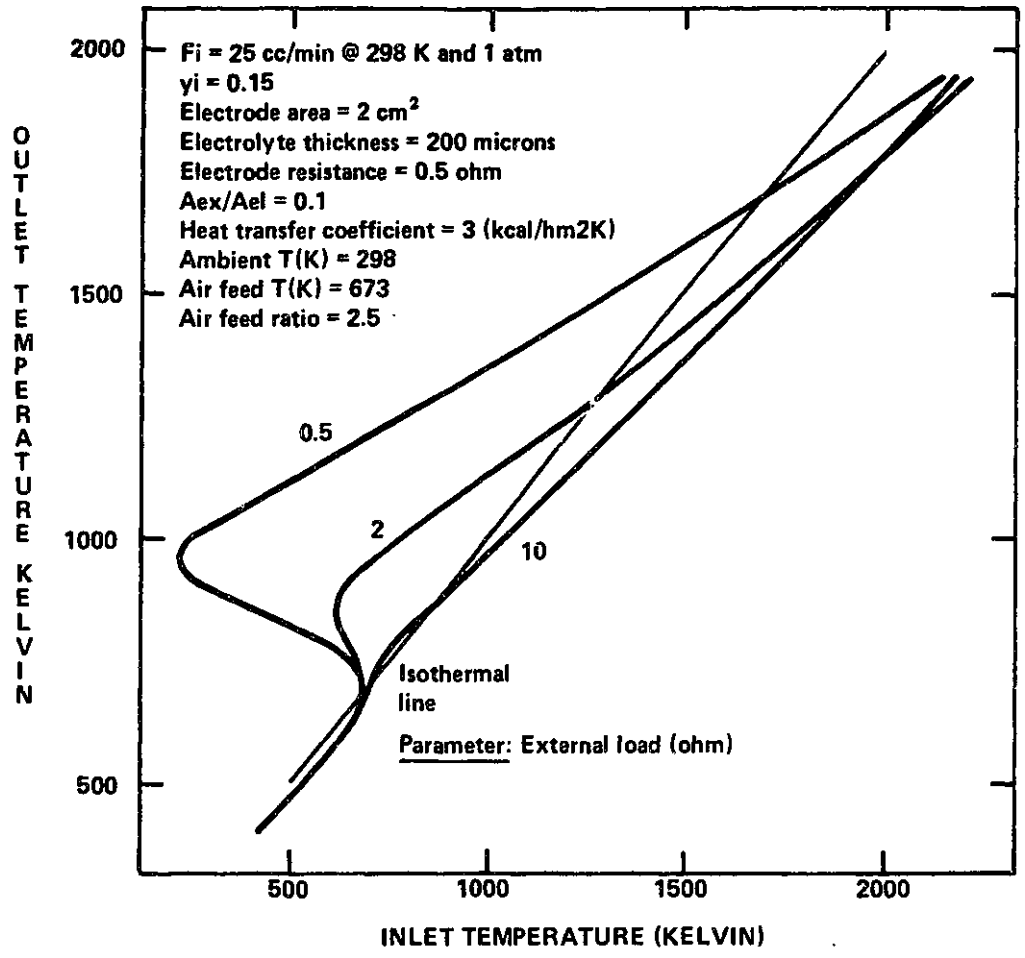

CO/CO_2 FUEL CELL MULTIPLICITY
FIGURE 2.34

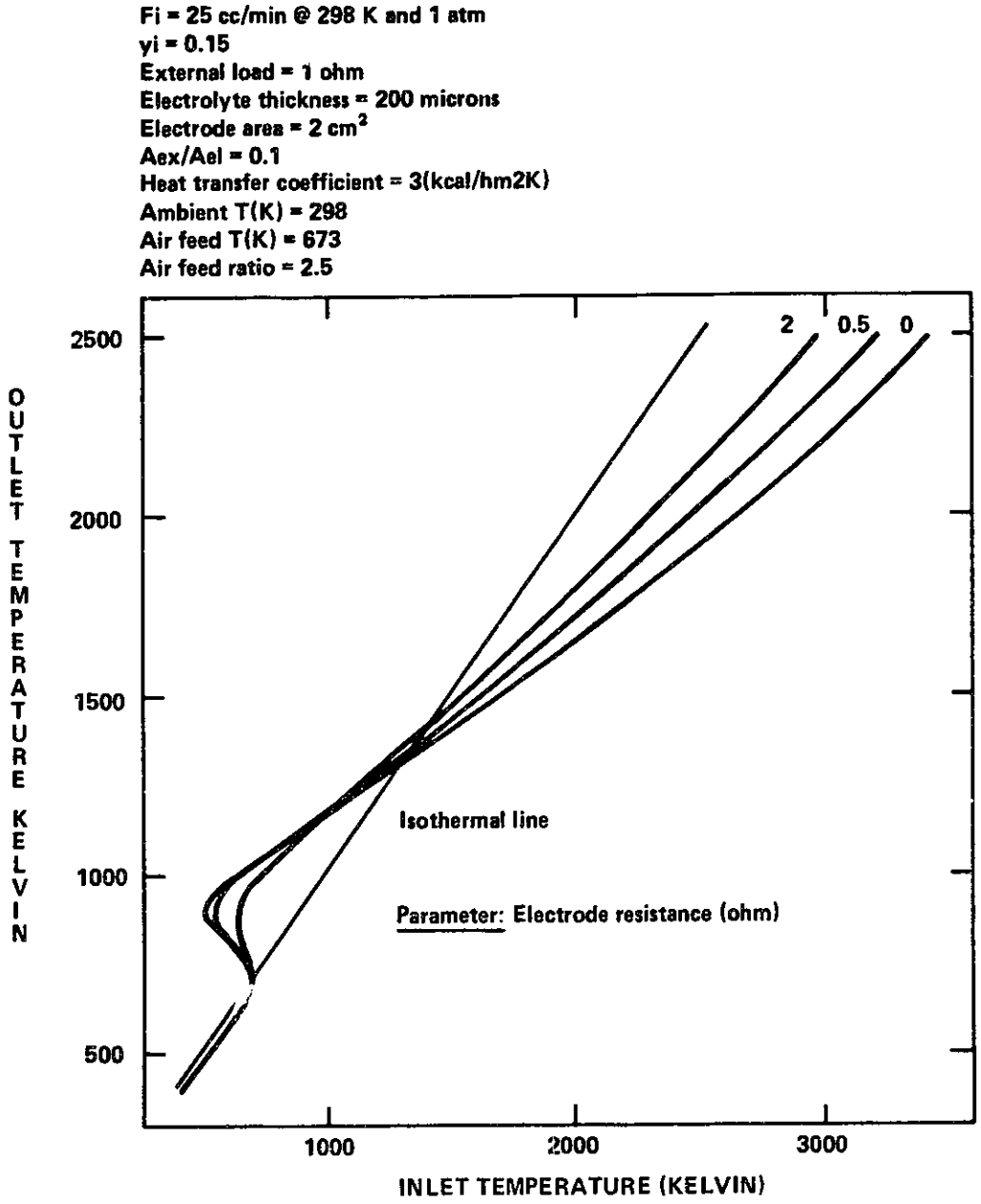

H_2 FUEL CELL MULTIPLICITY
FIGURE 2.35

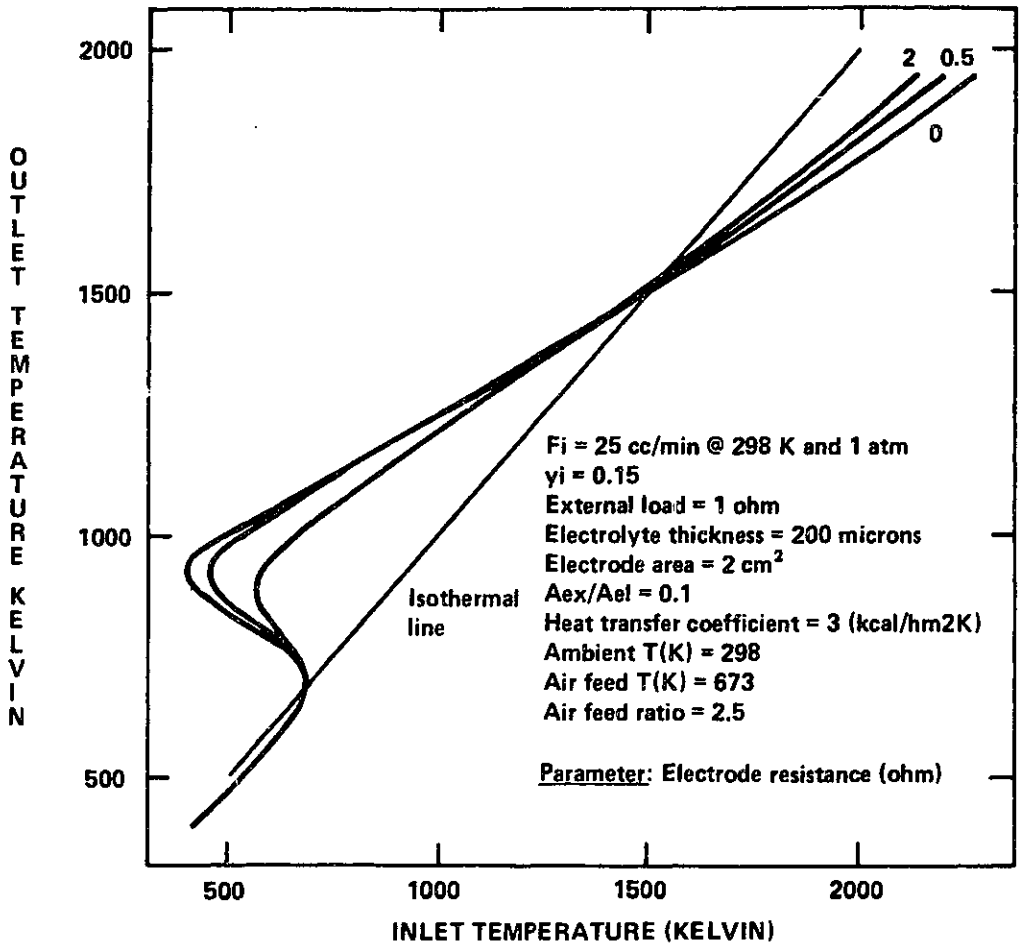

CO/CO_2 FUEL CELL MULTIPLICITY
FIGURE 2.36

ignition at roughly equal temperatures. Moreover, for a given inlet temperature, the outlet temperatures follow a trend which is exactly opposite to the expected one, with the smallest cell achieving a higher temperature. The reason is that the process is not controlled entirely by electrolyte resistance, as it is in the low temperature region, and, therefore, the increased area is offset by increased heat losses associated with a constant area ratio (which means greater external areas not compensated by a greater heat generation). This illustrates the importance of rational use of the scale-up criteria, figure 2.37 being a good example of what not to do when scaling up.

In figure 2.38 the actual external area has been maintained constant by reducing the area ratio when increasing electrode area. The ignition pattern is the expected one; however, note that the three lines coincide along the range of interest. This is due to the fact that curve #1 corresponds to virtually complete conversion, so that no additional fuel can be processed unless fuel flow rate or concentration are increased.

Figures 2.39 and 2.40 illustrate the effect of air feed temperature upon cell steady state operation. The trends are entirely predictable, and the figures self explanatory. The same can be said of figures 2.41 and 2.42, where the effect of air feed ratio is shown.

Figures 2.43 and 2.44 correspond to a parametric scan of the influence of fuel feed upon steady state operation, and an important characteristic of fuel cell behaviour is shown. Equation (2.1.15), the steady state material balance, shows that, except at

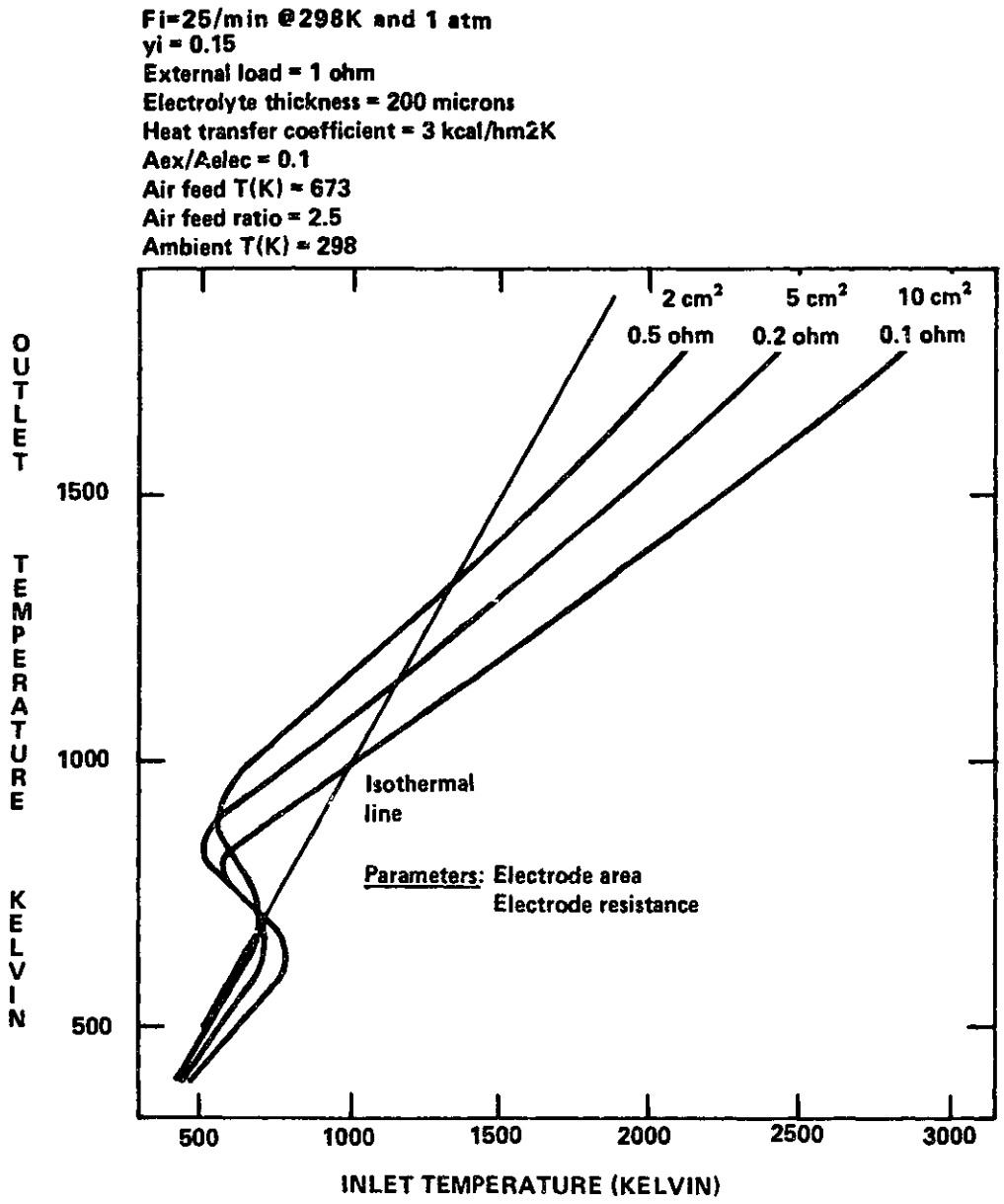

H_2 FUEL CELL MULTIPLICITY
FIGURE 2.37

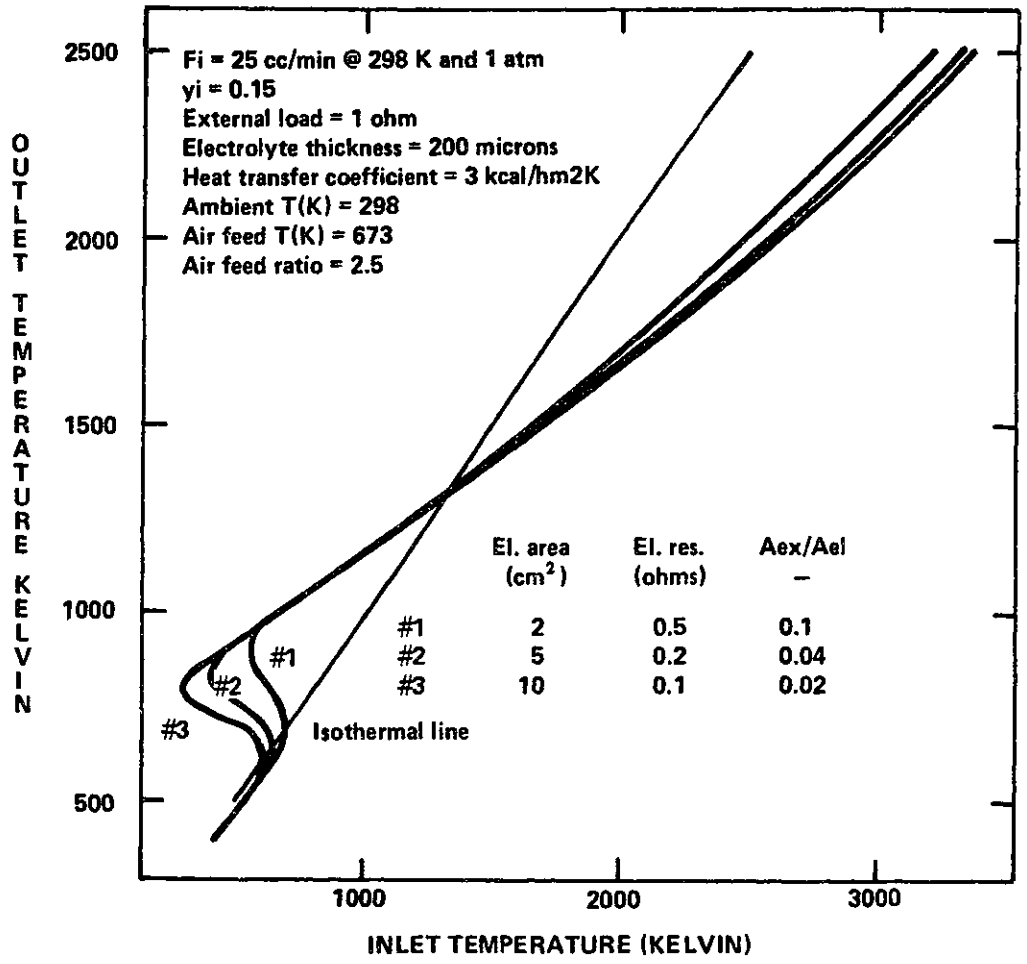

H_2 FUEL CELL MULTIPLICITY
FIGURE 2.38

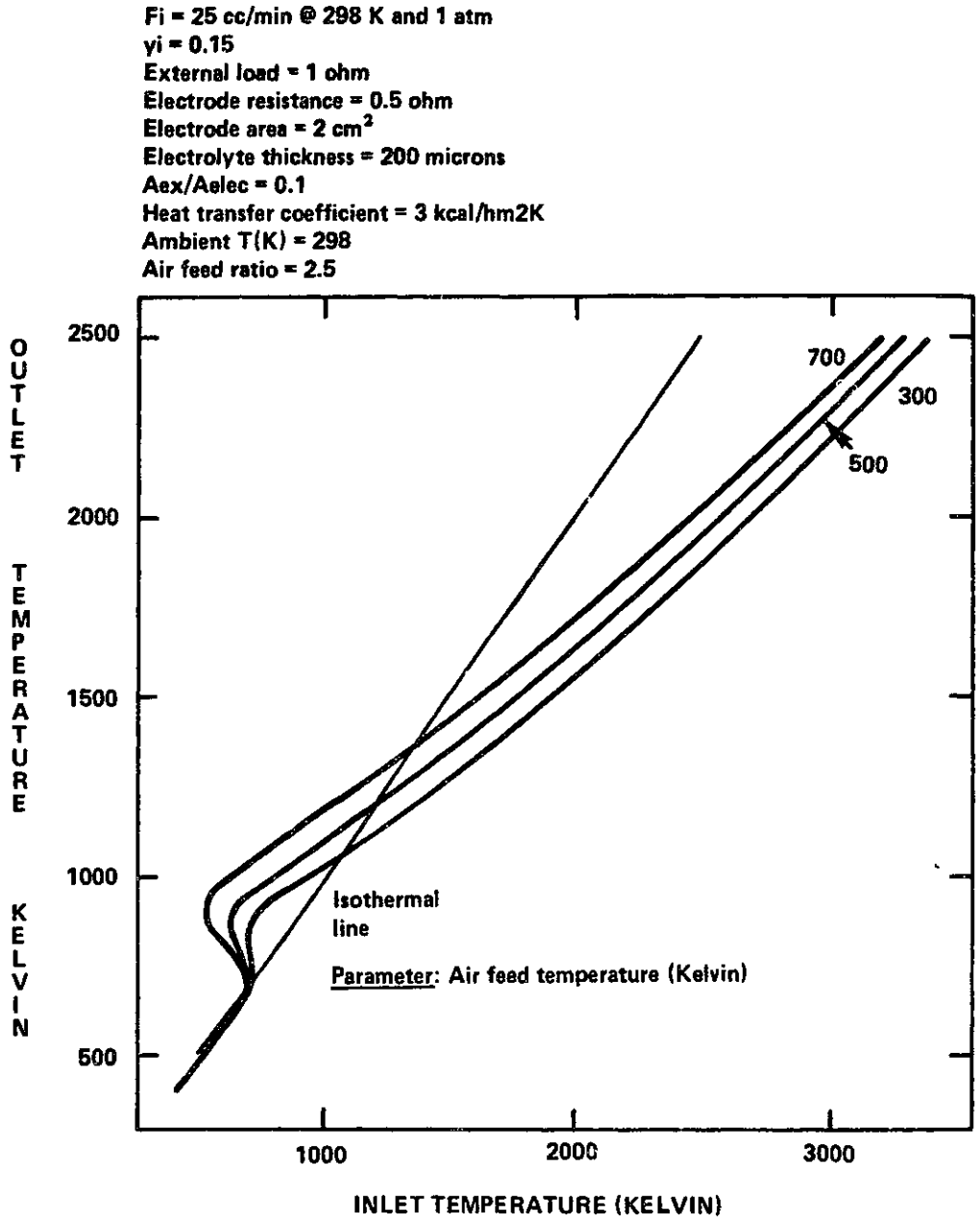

H_2 FUEL CELL MULTIPLICITY
FIGURE 2.39

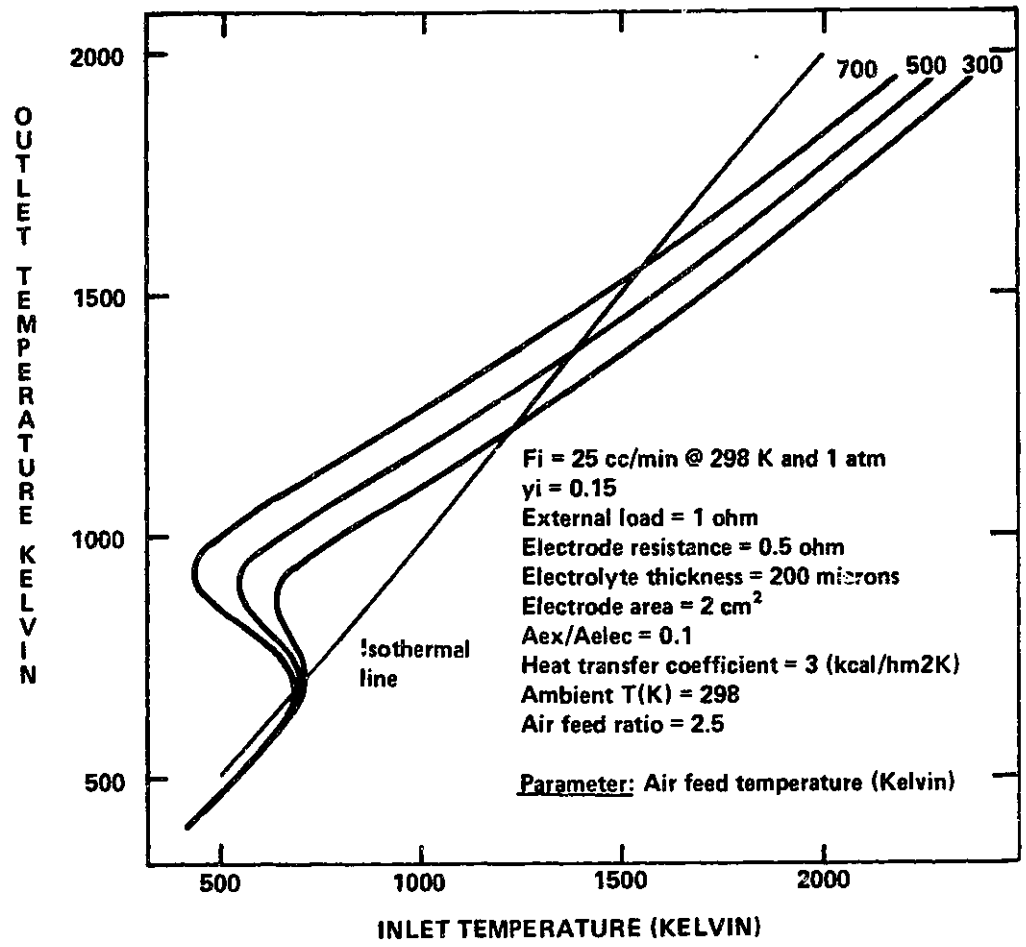

CO/CO_2 FUEL CELL MULTIPLICITY
FIGURE 2.40

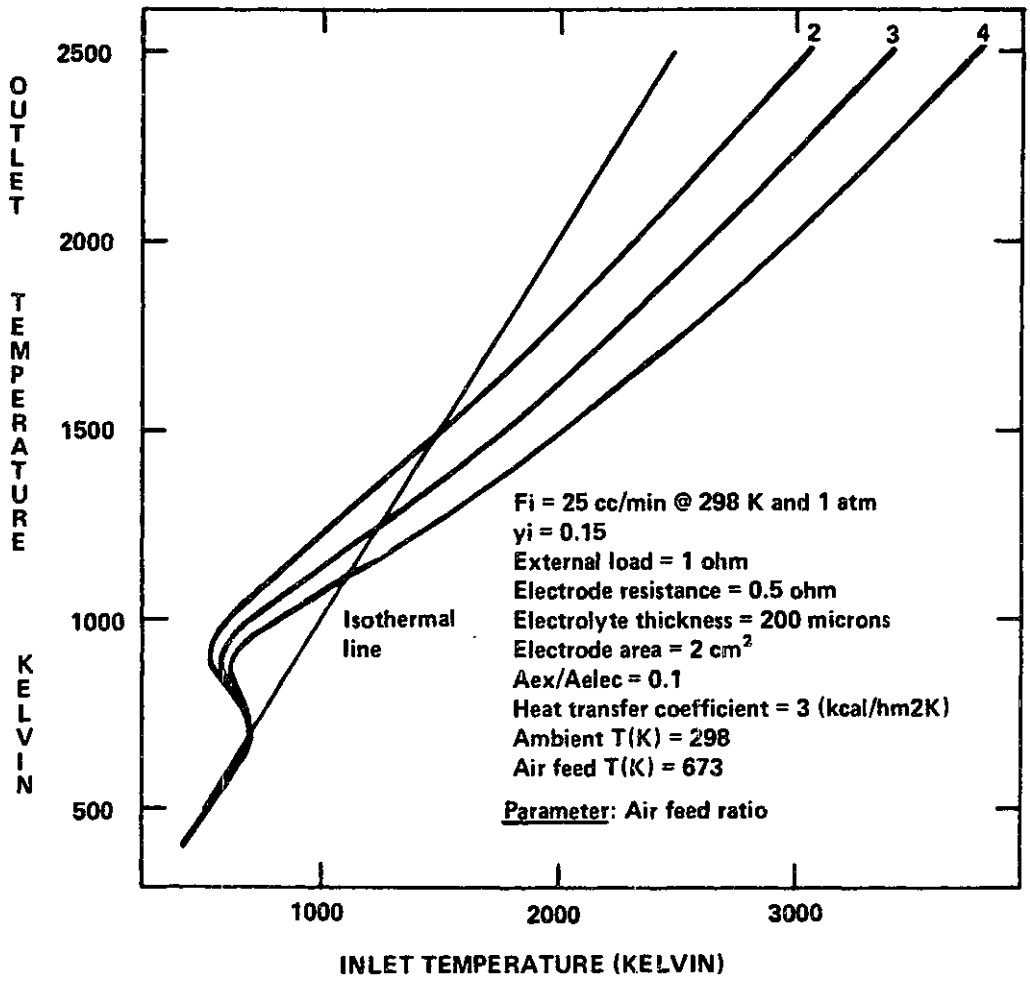

H_2 FUEL CELL MULTIPLICITY
FIGURE 2.41

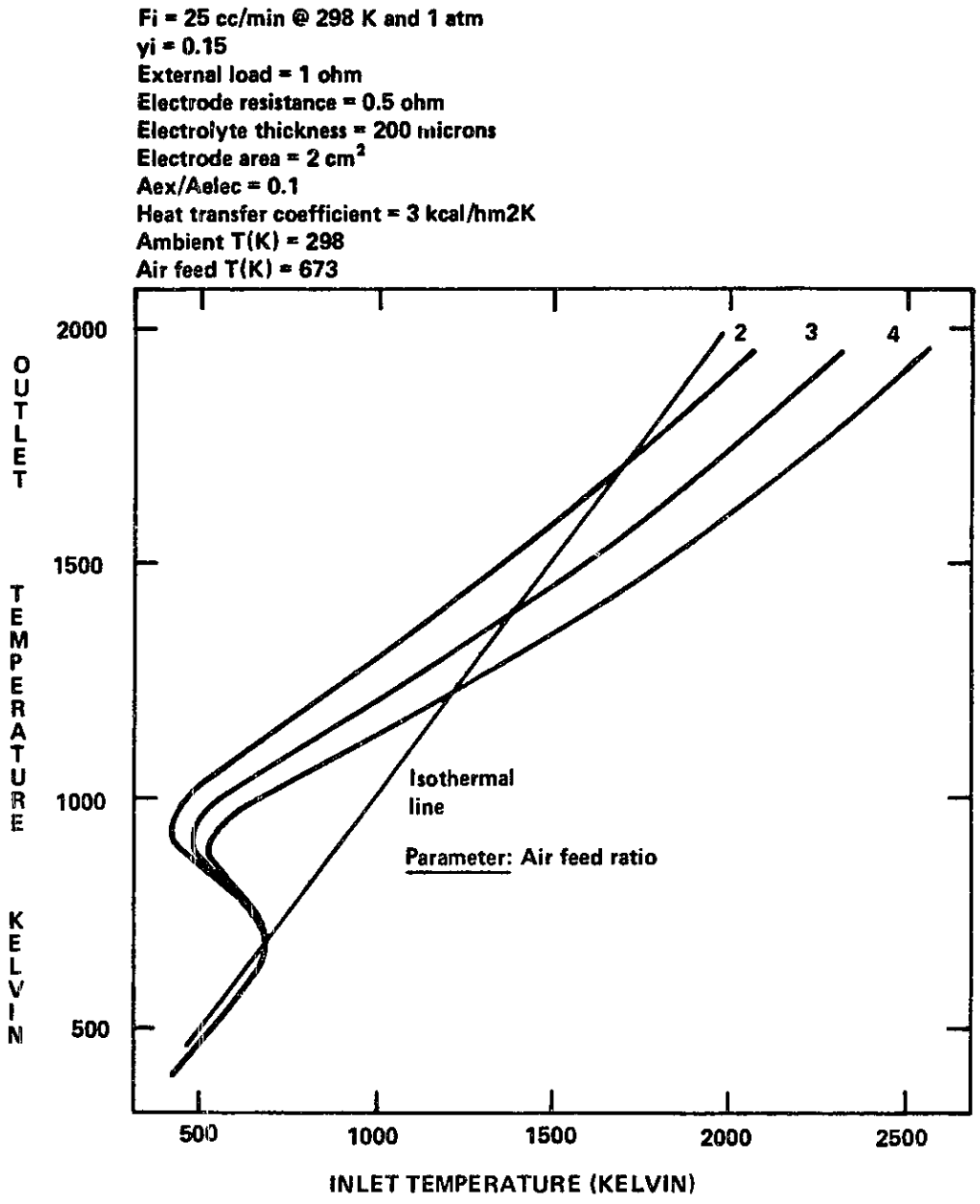

CO/CO_2 FUEL CELL MULTIPLICITY
FIGURE 2.42

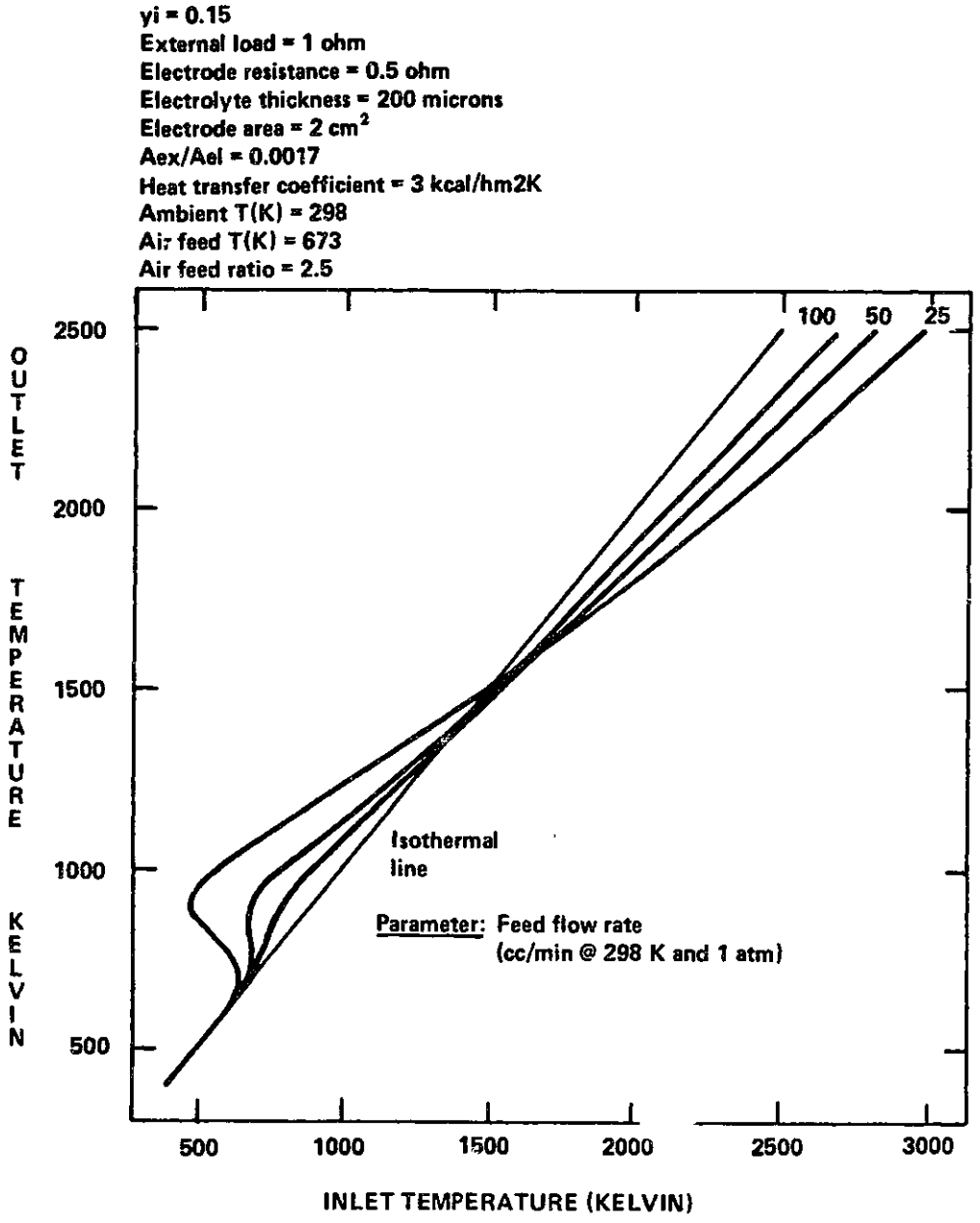

H_2 FUEL CELL MULTIPLICITY
FIGURE 2.43

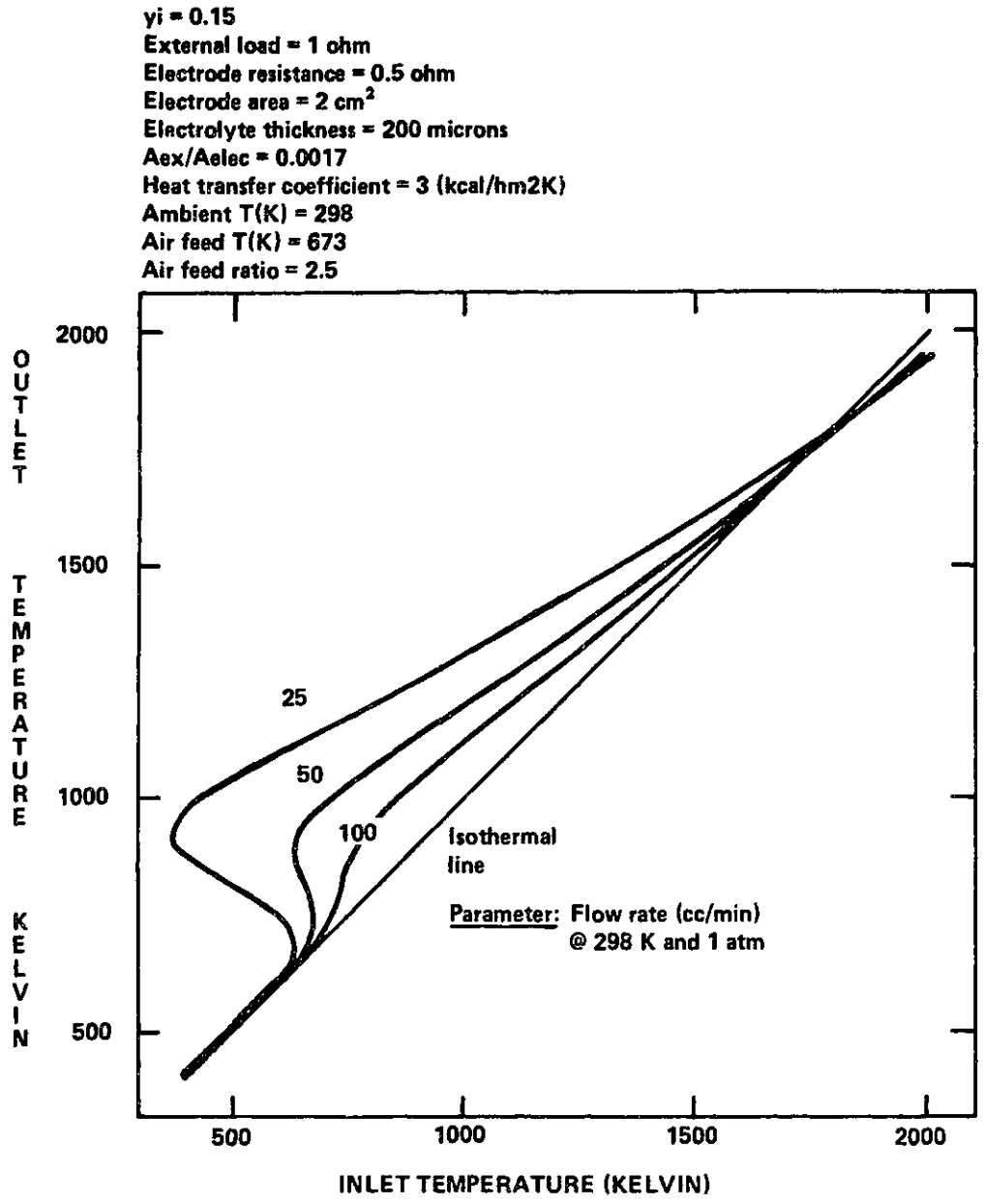

CO/CO_2 FUEL CELL MULTIPLICITY
FIGURE 2.44

extremely high or low values of conversion, when the logarithmic term becomes important, the amount of fuel reacted will be fixed by a combination of external and internal factors. Thus, in close analogy with a standard CSTR, we can consider the electrolyte resistance as a kinetic constant, showing Arrhenius behaviour, which governs cell behaviour at moderate temperatures. If the logarithmic term is neglected, the situation resembles a 0-order reaction. There is no exact equivalent to a holding time, since electrode surface (as opposed to reactor volume) is now the important parameter. However, when the electrolyte resistance is controlling, the conversion will be proportional to the ratio of electrode area to feed flow rate, which is analogous to a holding time. Thus, an internal factor (electrolyte resistance, analogous to a 0-order reaction constant) and an externally fixed parameter (ratio of electrode area to feed rate, analogous to holding time) determine steady state conversion (the E° term can be superficially compared to a pre-exponential factor, though, of course, its thermodynamic significance is very different). However, in the high-temperature region the "internal" factor virtually disappears, and the behaviour of the system is fixed by the external load (for a well-designed cell in which electrode resistance is not significant). Thus, in a very qualitative way, we can say that, when the external load controls the overall cell resistance, the fuel-processing capacity is "externally fixed" within a given moderate temperature interval (E° is not exponential in T but, evidently, is not temperature-independent), and electrode area is no longer

important. In figure 2.43, we see that ignition is facilitated by low flow-rates, and the higher temperatures achieved, in a completely analogous way with a non-electrochemical CSTR, are attributable to the lower heat capacity associated with a lower flow-rate (here, heat capacity is used to denote product of flow rate and heat capacity). At much higher temperatures, the negative entropy change reduces steady-state conversion, and, moreover, as explained above, the fuel processing capacity is externally fixed, signifying that the right hand side of equation (2.1.15) multiplyed by $F_i[A]_i$ (i.e., the moles converted per unit time) is set mainly by R_{ex}, the temperature dependence being not only far from exponential but such that E° (for the systems considered) decreases with T. Under these circumstances, the enthalpy convective transport associated with fuel feed becomes the governing energy term, outweighing reaction and air heating, which is stoichiometric, while heat losses increase due to the greater driving force. The situation is now exactly reversed, the greater heat capacity of the higher feed rates providing the mechanism through which outlet temperature is now higher as the feed gets larger.

Consider again equation(2.1.15). Multplying both sides by $F_i[A]_i$, we obtain, as explained above, the moles of fuel converted per unit time. It can be seen that the only possible fuel-concentration dependence is through the logarithmic term, which is to say that, except for extreme values of fuel concentrations, the dependence is a weak one (the system shows a close to 0 order behaviour). The corresponding effect of fuel feed concentration

upon heat generation is, consequently, not very significant, as was shown in figure 2.10.c. An entirely similar behaviour is evidenced in figures 2.45 and 2.46. The slightly higher effect of fuel concentration at higher temperatures, in the region where external load controls cell behaviour is associated with the physical properties of the stream. In particular, for a fixed flow rate, the product of density and mass heat capacity is lower for H_2 than for the rest of the fluids considered by a factor of ~ 2, which, as explained above, leads to a lower outlet temperature when convective enthalpy transport and heat losses outweigh reaction terms. Schematically, and neglecting temperature dependence of physical properties,

$$T_{out} \sim T_{in} - \frac{\text{Heat losses}}{\text{Flow rate x density x Ht. capacity}}$$

if all other terms are negligible.

Figures 2.47a and 2.47b show the effect of insulation and stacking upon cell performance. In the first case, the heat transfer coefficient is varied from a lower attainable limit (with reasonable materials and thickness) value, to a high-estimate for natural convection, while, in the second case, the non-insulated stack is modelled within a larger multi-stack arrangement of varying compactness whereby the effective area for heat transfer associated with each cell is varied from 1% to 33% of electrode area (see figure III-2).

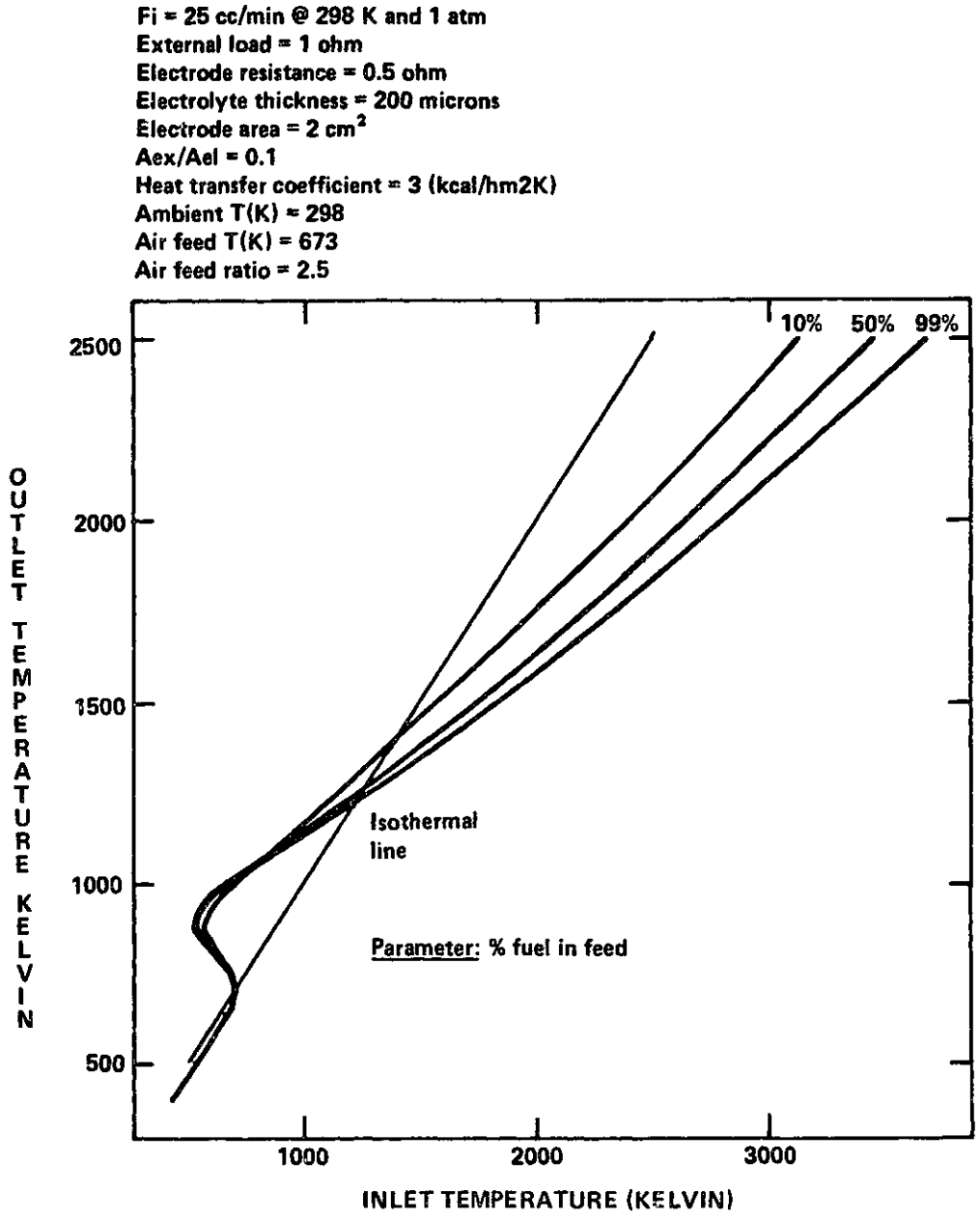

H_2 FUEL CELL MULTIPLICITY
FIGURE 2.45

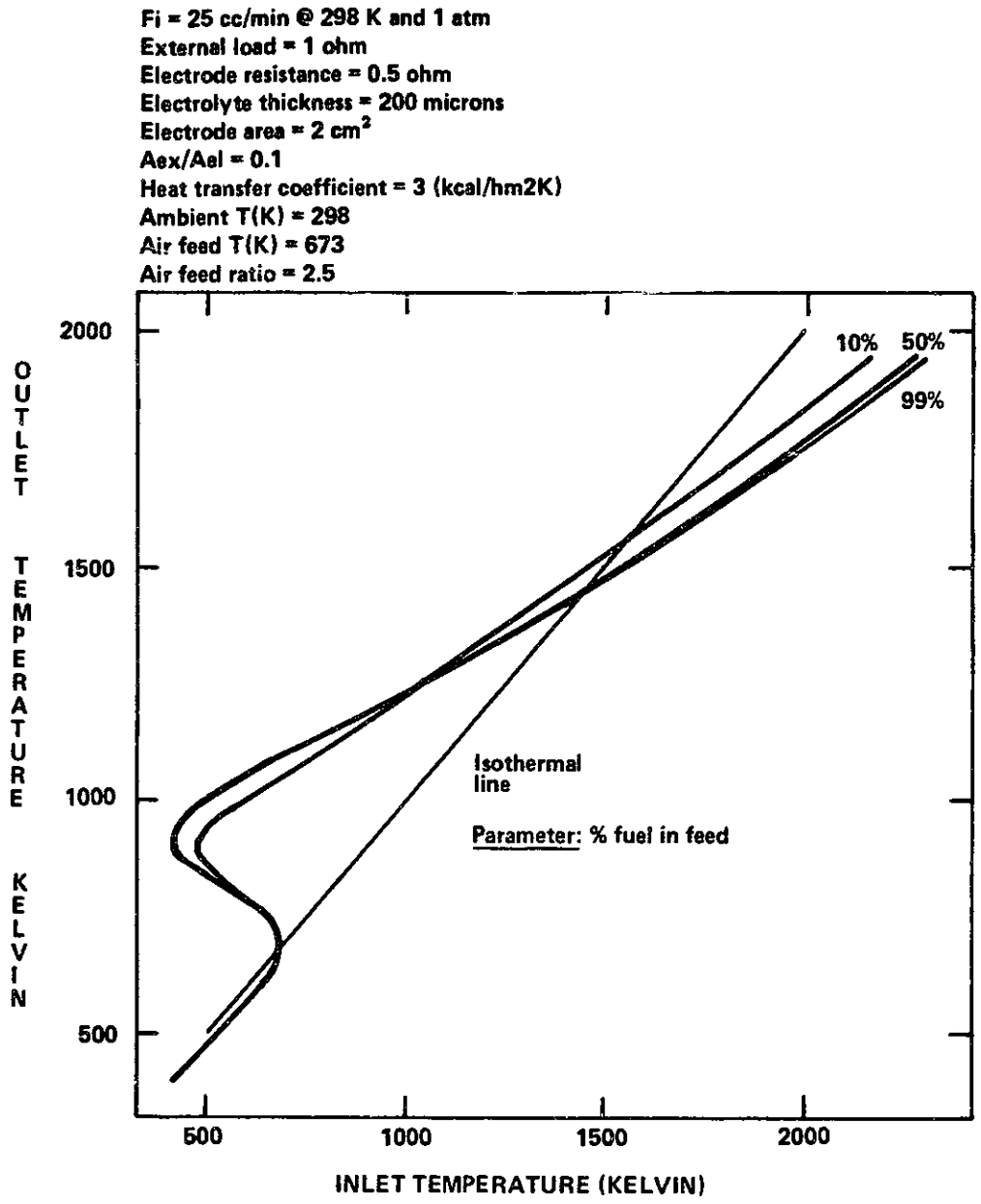

CO/CO_2 FUEL CELL MULTIPLICITY
FIGURE 2.46

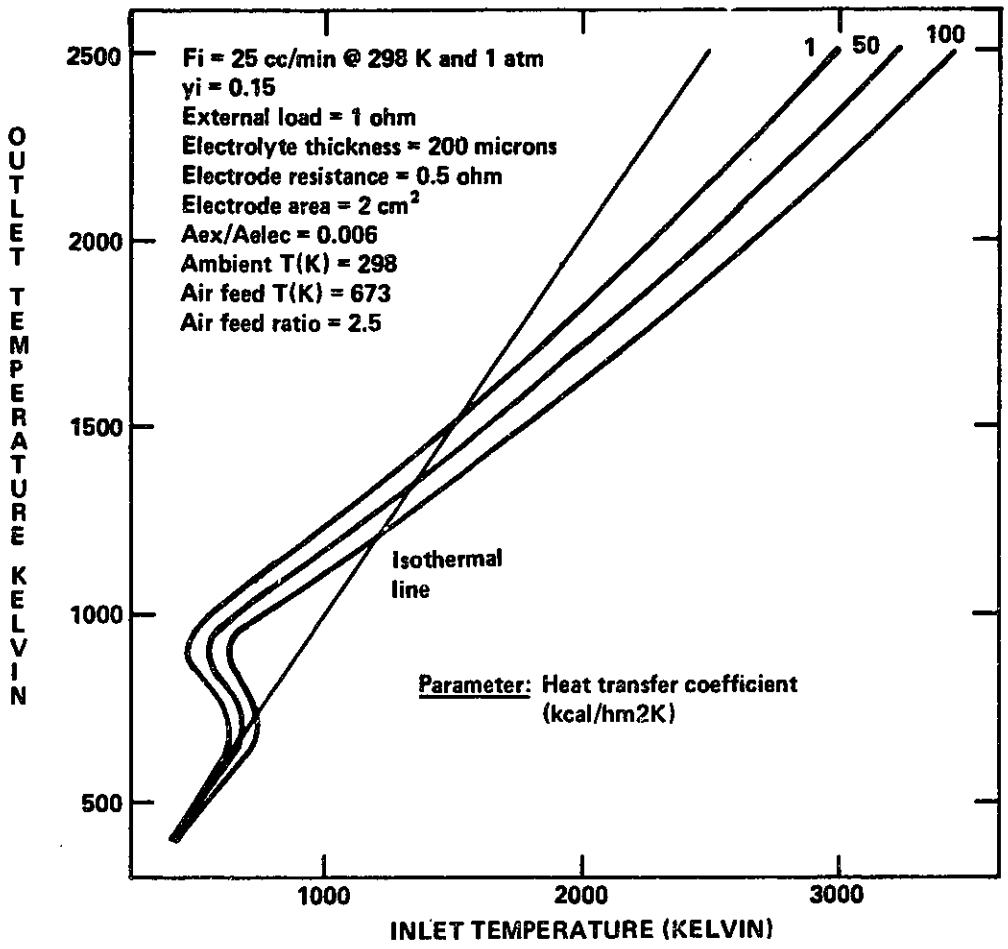

H_2 FUEL CELL MULTIPLICITY
FIGURE 2.47A

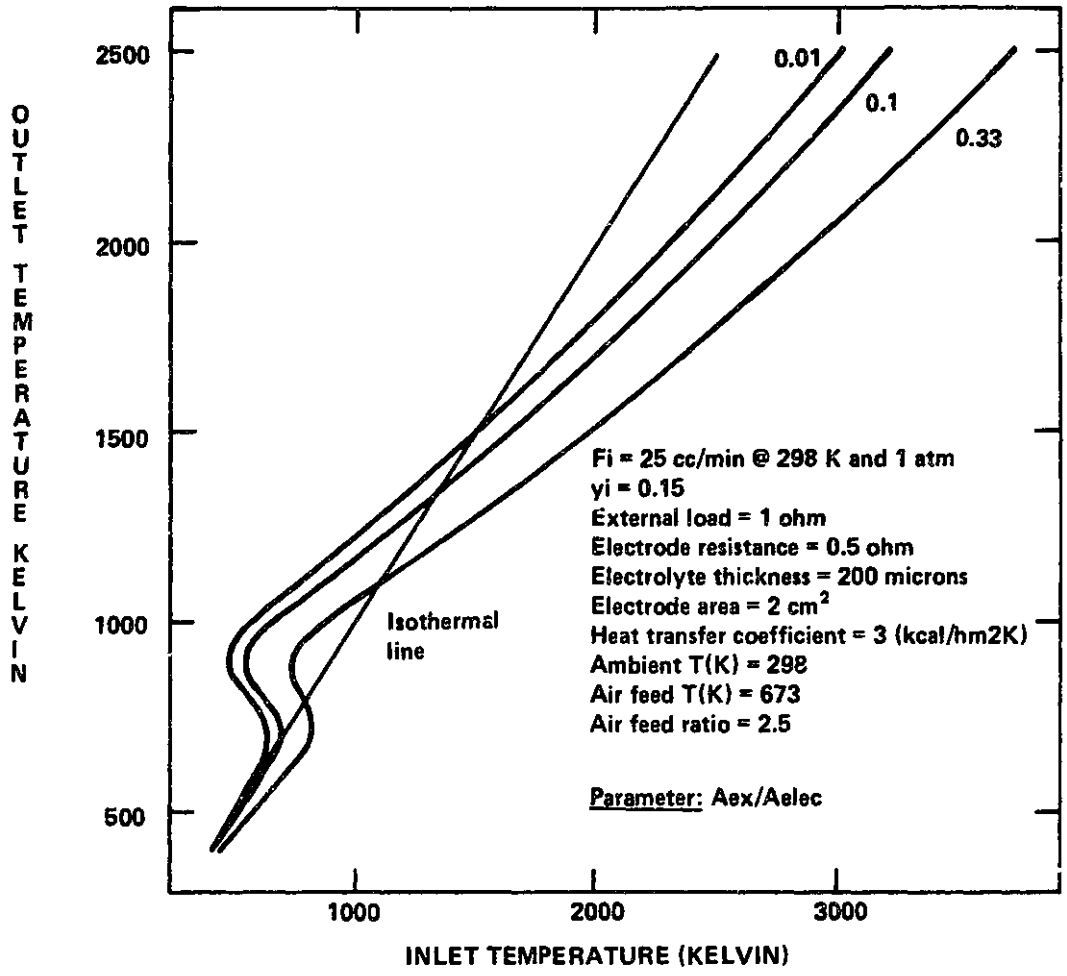

H_2 FUEL CELL MULTIPLICITY
FIGURE 2.47B

2.2 The cross-flow monolith fuel cell

2.2.1 Introduction

Monolithic catalytic converters have been used mainly for automobilie exhaust-control purposes; they were originally proposed for this use by Johnson et al. (1961), the characteristics of the reactor's geometry being such that considerable advantages result from their use when a low pressure drop is required. Satterfield (18) discusses catalytic monoliths and their applications; mathematical modeling of such reactors has been done, among others, by Heck, Wei and Katzer (19), Hegedus (20), and Hlavacek and Votruba (21).

Monoliths (or honeycombs, as they are also called) for catalytic oxidation of auto-exhaust gases consist of an array of parallel channels, numbering anywhere from 30 to 60 per square centimeter, the whole structure being typically made either of magnesia alumina silicate, or ceramic α-alumina, the channels being internally coated with the appropriate catalytic agent.

In the following sections, a mathematical model is presented, together with the corresponding results, whereby a ZrO_2 cross-flow monolith reactor is used as an electrochemical energy converter.

2.2.2 Geometry

The geometry considered is shown in figure 2.48. X,Y,Z and δ can, of course, be varied in a number of ways. The results presented, however, correspond to the following arrangement per monolith

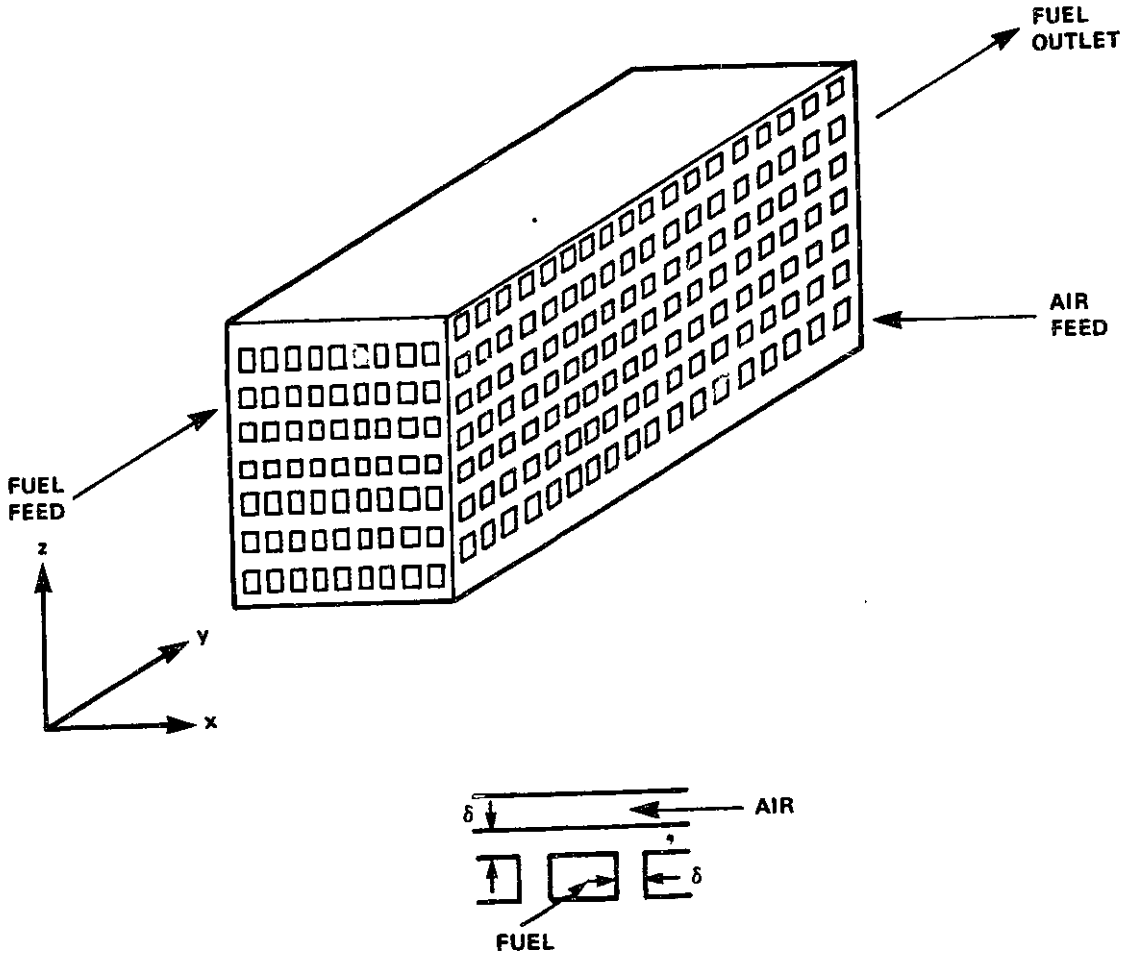

CROSS-FLOW MONOLITH FUEL CELL
FIGURE 2.48

Number of rows in z-dimension: 7

Number of parallel channels per row: 23

Monolith length: 5 cm

Channel cross section: 1 mm^2

Wall thickness (δ): 250 μm

The channels are internally coated with a porous-Pt electrode film, the minimum thickness of which is an important parameter which will be discussed in section 2.2.3. Given the above geometry, which determines the fluid mechanical and transport characteristics of the system, the power generation performance of the fuel cell depends upon the way in which the various channels are connected. This aspect is discussed in the next section.

2.2.3 Electrical arrangement

In figure 2.49a the elementary electrochemical process associated with fuel conversion as it flows along a single channel in the Y (see figure 2.49) direction is shown. $O^{=}$ anions are conducted through the electrolyte wall (thickness δ), and, once on the anodic channel (which runs perpendicular to air channels) react with flowing fuel.

Figure 2.49b shows an arrangement of 4 channels, in which a group of 2 channels (X direction) is connected in series with a similar 2-channel parallel group. Reference should be made to figure 2.48 to relate this circuit with the actual monolith, the same coordinate system having been used in both figures. Connection of all X-channels in a row in parallel between themselves is achieved by painting the row's end with Pt. Thus,

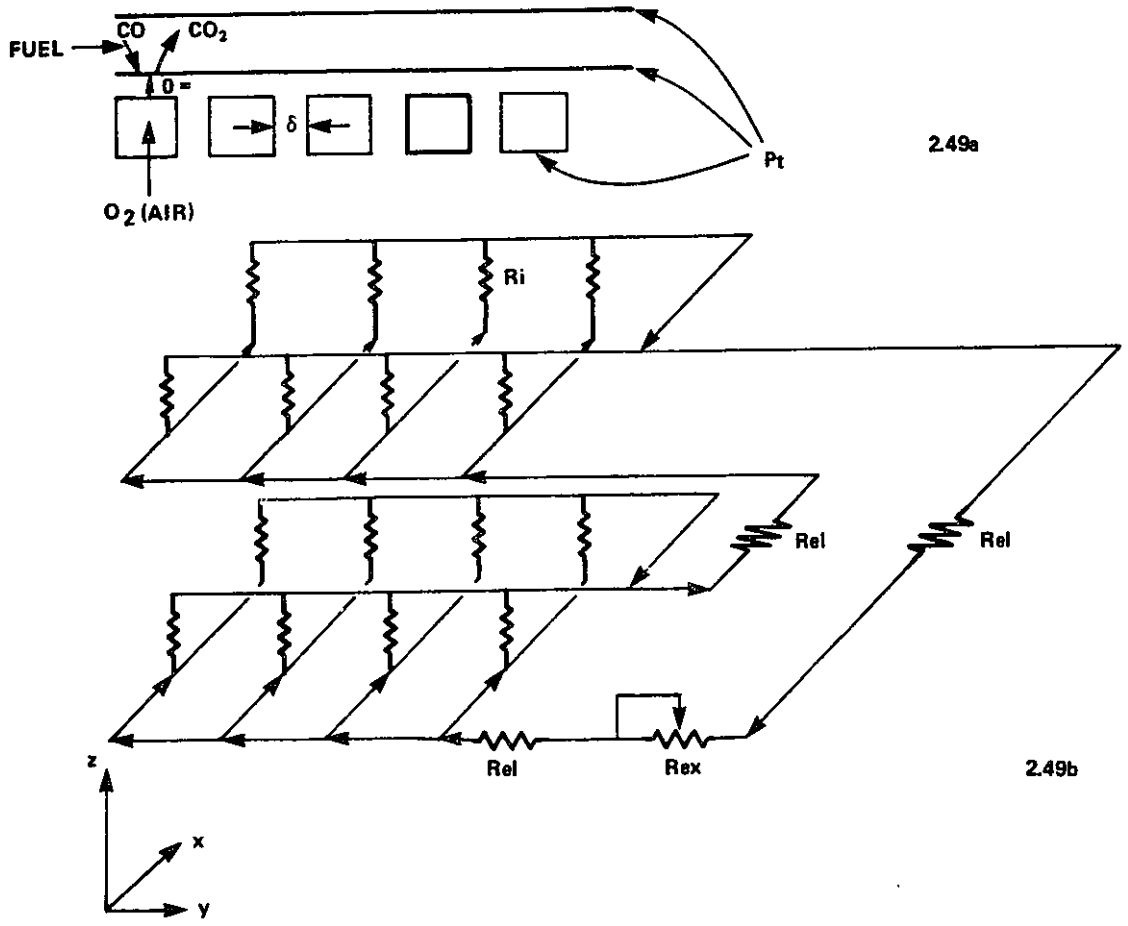

ELEMENTARY REACTION AND SCHEMATIC CIRCUIT
FIGURE 2.49

if each X-row (fuel channels) end face as well as each Y-row (air channels) front face is painted with Pt, and each X-row + Y-row pair connected in series with the next such pair, the circuit can be viewed as consisting of n batteries in series, each battery being composed of an X-row and a Y-row. The possibility of connecting individual channels in series, which would lead, in principle, to higher voltages, is limited by the 250-micron wall thickness available to provide for the actual connection. In fact, even if such a connection were physically possible, the final assembled monolith would inevitably be more of an expensive and complicated experimental curiosity than a prototype of a potentially successful reactor applicable on an industrial scale. In this respect, it must be noted that even the $\sim$ 1.5 mm spacing between alternate rows is insufficient for front face painting, since the possibility of connecting rows in parallel between themselves cannot be safely and completely avoided within such a limited space. This is why the actual reactor currently under construction for experimental purposes at W.R. Grace includes an additional undoped ZrO_2 layer between each battery.

In the brief discussion that follows (up to the beginning of section 2.2.4), the channel is treated as consisting of 40 (for the dimensions presently considered) elementary cells (by which is meant the length of channel associated with a transverse air channel, plus one wall thickness per cell), along which properties are assumed to be uniform. This is equivalent to saying that the reactor behaves as 40 CSTR's in series,

which, as will be explained in section 2.2.5, is not correct, since the results were sensitive to the integration step up to a number of $\sim$ 800 such elementary reactors. However, even with such an idealization, the results summarized in table 2.6 can be used for design purposes, as will be explained below.

In figure 2.49b, therefore, the resistance to anion conduction through the electrolyte is designated as Ri. The relevant cross section for current passage is the channel cross section (since the channels are square), and the corresponding length, the wall thickness. Thus, for the present preliminary calculation, an Ri (with exponential temperature dependence) can be associated, in considering current flow along a fuel channel, with each air channel. A 5-cm long fuel channel "sees" 40 such air channels, and, therefore, 40 Ri's, only four of which are shown in figure 2.49b. The often-invoked fluid flow electrical circuit analogy can be fruitfully employed at this point; in fact, electron flow along the X-direction and electron "distribution" to fuel channels via Ri resistances can be compared to the problem of designing a perforated pipe liquid distributor. Good fluid distribution is achieved when the controlling pressure drop is located at the fluid outlet orifice, in such a way that flow along the distributor does not affect the amount of fluid issuing from each orifice. In fact (22) a good rule of thumb for the design of such devices is the following: "The ratios of kinetic energy of the inlet stream to pressure drop across the outlet hole and of friction loss in the pipe to pressure drop across the outlet hole should be

equal to or less than one-tenth". This guarantees a moldistribution "less than ± 5%." In a completely similar way, electron flow along the X direction should encounter essentially no (ohmic) resistance relative to the magnitude of the Ri resistances. If this were not so, an unnecessary energy inefficiency would be added, and the reactor's performance would be "non-uniform", in the sense that electron flow would not be evenly distributed, but would decrease along X. Similarly, Y-direction flow should also be essentially free of ohmic losses. A minimum electrode thickness can therefore be calculated such that the assumption implicit in figure 2.49b (i.e., no ohmic drop in X or Y directions along air and fuel channels) becomes reasonable. Note that ohmic losses due to electrode-electrolyte contact are "z-direction" loses, and thus are to be added to the Ri's, but they do not affect X or Y direction electron flow. The resistance of porous Pt electrordes used in ZrO_2 fuel cells has been treated by Sverdrup, et al. (23), who found values of about 3 times (sintered electrodes) to 1.5 times (fused electrodes) those corresponding to bulk Pt for the parameter r_{el}/t, where r_{el} is the electrode resistivity and t, the effective electrode film thickness. The approach here will be to calculate a minimum effective film thickness using an electrode resistivity 3 times as big as bulk Pt resistivity.

A conservative estimate can be obtained as follows: consider the longest dimension for current flow (in our case, the Y-dimension). From figure 2.50, it can be seen that the cross sectional area sssociated with an electrode film of t cm deposited on a channel of size ℓ x ℓ cm can be expressed as

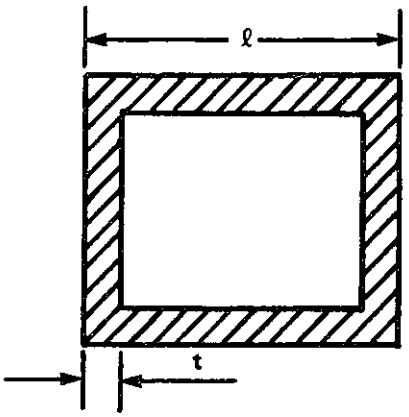

Cross section: $2\ell t + 2[(\ell - 2t)t] \sim 4\ell t$
$\ell \gg t$

CROSS-SECTION FOR CURRENT FLOW
FIGURE 2.50

$$\underline{\text{Transverse section of electrode}} = 2\ell t + 2[(\ell-2t)t] \tag{2.2.1}$$

Considering the microscopic dimensions of t when compared to ℓ, equation (2.2.1) can be simplified to

$$\underline{\text{Transverse section of electrode}} \sim 4\ell t \tag{2.2.2}$$

Therefore, the ohmic drop associated with flow of a current i along a channel of length L through a porous electrode film of thickness t is

$$\Delta V = i \frac{r_{el} L}{4\ell t} \tag{2.2.3}$$

or, in view of the above explained assumption,

$$\Delta V = i \frac{3 r_{pt} L}{4\ell t} \tag{2.2.4}$$

Furthermore, platimun resistivity can be expressed as follows (in ohm-cm)

$$r_{pt} = [10.6 + 0.003927\ (T-293)] \times 10^{-6} \tag{2.2.5}$$

Therefore,

$$\Delta V = \frac{0.75 \times 10^{-2}\ Li}{\ell t} [10.6 + 0.003927\ (T-293)] \tag{2.2.6}$$

Where t is now in microns.

Electrolyte resistance has already been treated in equations 2.1.9 and 2.1.10. The area for current passage is ℓ^2, and the distance through which anion transport takes place is the wall thickness δ. Therefore,

$$R_i = 4.1666 \times 10^{-7} \left(\exp \frac{9700}{T}\right) \frac{\delta}{\ell^2} \tag{2.2.7}$$

where δ is in microns and ℓ in cm. As will be seen when developing the circuit and energy equations, the current distribution along a fuel channel is not uniform. However, for our present estimation purposes, we can say that the current flowing through each R_i is approximately the total current corresponding to one channel divided by the number of air ducts along such a channel. Therefore, letting n denote the number of air ducts along a fuel channel, and, furthermore, letting ε denote an arbitrarily small quantity,

$$\frac{0.75 \times 10^{-2}\ \mathrm{Li}\ [10.6 + 0.003927(T-293)]}{4.1666 \times 10^{-7} \exp\left(\frac{9700}{T}\right)\left(\frac{\delta}{\ell^2}\right)\left(\frac{i}{n}\right)(\ell t)} \leq \varepsilon \qquad (2.2.8)$$

Therefore,

$$t \geq 1.8 \times 10^{4} \left(\frac{L\ell}{\delta}\right)\left(\frac{n}{\varepsilon}\right)\left[\frac{10.6 + 0.003927(T-293)}{\exp\left(\frac{9700}{T}\right)}\right] \qquad (2.2.9)$$

But, from the definition of n (see above),

$$n = \frac{L}{\ell + \delta \times 10^{-4}} \qquad (2.2.10)$$

with δ in microns and ℓ and L in cm.

Therefore, in equation (2.2.9), where δ is in microns, and L and ℓ, in cm,

$$\frac{L\ell n}{\delta} = \frac{L^2}{\delta\left(1 + \frac{10^{-4}\delta}{\ell}\right)} \qquad (2.2.11)$$

Substituting into (2.2.9), we obtain

$$t \geq \frac{1.8 \times 10^{4} L^2}{\delta\varepsilon(1+10^{-4}\delta/\ell)} \left[\frac{10.6 + 0.003927(T-293)}{\exp\frac{9700}{T}}\right] \qquad (2.2.12)$$

Upon substitution of the following values, corresponding to the presently considered geometry,

$L = 5$ cm

$\ell = 0.1$ cm

$\delta = 250$ μm

the required t can be calculated as a function of T and ε. The results are summarized in table 2.6. Therefore, an electrode film thickness of 20 μm, for a uniform temperature of 950 K, would yield an ε of 0.035. This means that, for all practical purposes, the circuit shown in figure 2.49b is an excellent approximation, since all the cells within each battery (one Z-level) can be considered to be in parallel (if t is such that ε is sufficiently small). Note that consideration of Y length as opposed to X length is a conservative criterion. In figure 2.49b, the resistances designated as Rel correspond to local losses associated with inevitable imperfections in the electrode wiring connections, and correspond, physically, to the zones where current flows from the conducting wire to the Pt-painted front faces. Obviously, Rel decreases in direct proportion to the time and material expenditure involved in the realization of such connections.

2.2.4 Electrical circuit equations

To develop the governing relationship for the fuel cell's electric circuit, we first consider figure 2.49b, and let

X = N° of channels in parallel per battery

Y = N° of elementary CSTR's per fuel channel

Z = N° of batteries connected in series

It is necessary, in order to arrive at the correct final equations, to consider firstly the simple case of complete uni-

	$\varepsilon = 0.1$	$\varepsilon = 0.01$	$\varepsilon = 0.001$
T (K)	t (μm)	t (μm)	t (μm)
700	0.168	1.68	16.8
800	0.983	9.83	98.3
900	3.900	39.00	390.0
1000	11.804	118.04	1180.4

TABLE 2.6: Electrode Film Minimum Thickness

formity in the Y-direction, i.e., uniform temperature and fuel concentration. This means that current and resistance are the same throughout. This is obviously a simplification, to be corrected later. Z and X-direction uniformity are also assumed (X-direction uniformity will be discussed in section 2.2.5.1).

Under these assumptions, and considering an elementary fuel cell (by which we mean that longitudinal portion of fuel channel sufficiently small that temperature and conversion can be considered constant, plus, of course, the corresponding part of the air channel) we can write, for the K^{th} such elementary fuel cell,

$$E_K = E_{rev\ K} - I_K R_{iK} \tag{2.2.13}$$

While, for the whole circuit (see fig. 2.49),

$$-X \left(\sum_{K=1}^{Y} I_K \right)(Z+1)R_{el} + Z E_K = X \left(\sum_{K=1}^{Y} I_K \right)R_{ex} \tag{2.2.14}$$

The subscript in E_K can be dropped since the electric arrangement of figure 2.49b implies that not only the X channels, but also the fuel cells within each channel are connected in parallel. This is consistent with the development that led to the neglect of Pt resistance along air and fuel channels. Also, note that X-uniformity is implicit in the form of the two X-containing terms in equations (2.2.14). Therefore,

$$-X\left(\sum_{K=1}^{Y} I_K \right)(Z+1)R_{el} + ZE = X \left(\sum_{K=1}^{Y} I_K \right)R_{ex} \tag{2.2.15}$$

But, if Y-uniformity applies,

$$\sum_{K=1}^{Y} I_K = Y\ I_K \tag{2.2.16}$$

Therefore, keeping subscripts for use in the rigorous equations, although they are not needed under Y uniformity conditions,

$$-XY(Z+1)R_{el}I_K + ZE = XYI_KR_{ex} \tag{2.2.17}$$

Solving for I_K,

$$I_K = \frac{ZE}{XY[(Z+1)R_{el} + R_{ex}]} \tag{2.2.18}$$

Substituting in equation (2.2.13),

$$E = E_{rev,K} - \frac{ZER_{iK}}{XY[(Z+1)R_{el} + R_{ex}]} \tag{2.2.19}$$

Solving for E,

$$E = \frac{XY[(Z+1)R_{el} + R_{ex}]\ E_{rev,K}}{Z\ R_{iK} + XY[(Z+1)R_{el} + R_{ex}]} \tag{2.2.20}$$

Also,

$$I_K = \frac{ZE_{rev,K}}{ZR_{iK} + XY[(Z+1)R_{el} + R_{ex}]} \tag{2.2.21}$$

Equations (2.2.20) and (2.2.21) should be compared with the corresponding CSTR relationships, equations (2.1.6) and (2.1.7). Even though they were deduced under simplifying assumptions which are evidently not true (Y-uniformity), their form does convey important information, and, moreover, the final equations are but numerical modifications of these basic relationships.

Consider now equation (2.2.21) and figure 2.49b. From the latter, it can be seen that, within each battery, elementary fuel cells are connected in parallel (which led to the use of an unsubscripted E in equation (2.2.20)), so that, whatever the changes introudced into the above expressions in order to account for Y non-uniformity, a constant E must result. In order to account for such non-uniformity, let us rewrite equation (2.2.21) as follows:

$$I_K = \frac{Z\ E_{rev,K}}{Z\ R_{iK} + \frac{X(\sum_{K=1}^{Y} I_K)[(Z+1)R_{el}+R_{ex}]}{I_K}} \qquad (2.2.22)$$

The implication is that, under non-uniform conditions, Y can be replaced by $(\sum_{K=1}^{Y} I_K)/I_K$. The argument that follows proves that this intuitively satisfying argument is, indeed, correct. Multiplying through by I_K and simplifying,

$$ZE_{rev,K} = Z\ R_{iK}\ I_K + X\ (\sum_{K=1}^{Y} I_K)[(Z+1)R_{el} + R_{ex}] \qquad (2.2.23)$$

Therefore,

$$E_{rev,K} = R_{iK}I_K + \frac{X(\sum_{K=1}^{Y} I_K)[(Z+1)R_{el} + R_{ex}]}{Z} \qquad (2.2.24)$$

Substituting into equation (2.2.13), and dropping the subscript on E_K,

$$ZE = X(\sum_{K=1}^{Y} I_K)[(Z+1)R_{el} + R_{ex}] \qquad (2.2.25)$$

Equation (2.2.25) is exactly the same as equation (2.2.15). Consider now equation (2.2.20), which can be rewritten under non-uniform conditions in the Y-direction, as follows, with $D(K) = (\Sigma I_K)/I_K$

$$E = \frac{X[(Z+1)R_{el} + R_{ex}]E_{rev,K}(\frac{\sum_{K=1}^{Y} I_K}{I_K})}{Z\ R_{iK}+XD(K)[(Z+1)R_{el} + R_{ex}]} \qquad (2.2.25)$$

Substituting equation (2.2.22) into equation (2.2.25),

$$E = \left\{ \frac{X[(Z+1)R_{el} + R_{ex}](E_{rev,K})(\sum_{K=1}^{Y} I_K)}{Z\ R_{iK}+XD(K)[(Z+1)R_{el} + R_{ex}]} \right\} \times$$

$$\times \left\{ \frac{Z\ R_{iK}+XD(K)[(Z+1)R_{el} + R_{ex}]}{Z\ E_{revK}} \right\} =$$

$$= \frac{X\left(\sum_{K=1}^{Y} I_K\right)\left[(Z+1)R_{el} + R_{ex}\right]}{Z} \qquad (2.2.26)$$

This, again, is identical to (2.2.15). The above arguments show that if Y is substituted by $\left(\sum_{K=1}^{Y} I_K\right)/I_K$ non-uniformity can be accounted for, and the electrical network equations are satisfied. Therfore, equations (2.2.20) and (2.2.21) can finally be rewritten as follows:

$$E = \frac{X\left[(Z+1)R_{el} + R_{ex}\right] E_{rev,K}\left(\sum_{K=1}^{Y} I_K\right)/I_K}{Z\,R_{iK} + X\left[(Z+1)R_{el} + R_{ex}\right]\left(\sum_{K=1}^{Y} I_K\right)/I_K} \qquad (2.2.27)$$

$$I_K = \frac{Z\,E_{rev,K}}{Z\,R_{iK} + X\left[(Z+1)R_{el} + R_{ex}\right]\left(\sum_{K=1}^{Y} I_K\right)/I_K} \qquad (2.2.28)$$

The parameter $\left(\sum_{K=1}^{Y} I_K\right)/I_K$, henceforth called current distribution coefficient, reduces to Y under complete Y-direction uniformity. As will be explained in section 2.2.5.1, the computation involves iterative solution of the governing expressions. One of the nested iteration loops involves convergence of the current distribution pattern, starting from an initial trial assuming Y-direction uniformity, and ending when the current distribution (characterized by a mean and a squared spread) converges to some repetitive pattern, to within a preestablished error. Upon convergence, therefore, a constant E in equation (2.2.27) should be obtained throughout the reactor length. This is indeed what is verified in all cases, the error never exceeding $\pm$ 3.0%.

Before considering the energy and material balances, some equations related to power output will be presented. The monolith's power output can be expressed as follows:

$$P = (X \sum_{K=1}^{Y} I_K)^2 R_{ex} \tag{2.2.29}$$

In designing the reactor, however, it is evident that R_{ex} is a most important parameter in conditioning the reactor's power output, and equation (2.2.29) provides no means of selecting an appropriate value for this parameter. Moreover, contrary to the CSTR case, where an algebraic set of simultaneous equations provides the solution to the material and energy balances, the monolithic fuel cell requires the solution of coupled differential equations. It would therefore be very useful if an estimate of the external load required in order to maximize power output could be obtained in an explicit form. This can be done only if Y-uniformity is assumed. This does not mean that the resulting expression will be actually used in calculating P, but, rather, a useful expression results whereby an estimate of the "optimum" R_{ex} is obtained, besides offering interesting conclusions regarding the way in which power output can be maximized. Under conditions of Y-uniformity, therefore,

$$Y = \frac{\sum_{K=1}^{Y} I_K}{I_K} \tag{2.2.30}$$

$$P = (XYI_K)^2 R_{ex} = (XYI)^2 R_{ex} \tag{2.2.31}$$

Substituting equation (2.2.21) into equation (2.2.31),

$$P = \left\{ \frac{XYE_{rev}Z}{ZR_i + XY[(Z+1)R_{el}+R_{ex}]} \right\}^2 R_{ex} \qquad (2.2.32)$$

Note that subscripts have been dropped since I and E_{rev} are taken as constant. Since we are interested in maximizing P with respect to R_{ex}, we can rewrite equation (2.2.32) as follows,

$$P = \frac{N_1 R_{ex}}{(N_2 + N_3 R_{ex})^2} \qquad (2.2.33)$$

where

$$N_1 = (XZYE_{rev})^2 \qquad (2.2.34)$$

$$N_2 = ZR_i + XY(Z+1)R_{el} \qquad (2.2.35)$$

$$N_3 = XY \qquad (2.2.36)$$

Taking the derivative with respect to R_{ex},

$$\frac{dP}{dR_{ex}} = \frac{N_1(N_2+N_3R_{ex})^2 - 2N_3(N_2+N_3R_{ex})N_1R_{ex}}{(N_2+N_3R_{ex})^4} \qquad (2.2.37)$$

The value of R_{ex} corresponding to maximum power output is therefore, from the above expression,

$$R_{ex}\Big|_{P_{max}} = \frac{N_2}{N_3} = \left(\frac{Z}{XY}\right) R_i + (Z+1)R_{el} \qquad (2.2.38)$$

Even though the actual optimum load cannot be explicitly found and a "parametric scan" of the governing differential equations is necessary, equation(2.2.38) does, however, provide useful qualitative information. In fact, no matter what criterion is adopted to define an "average" temperature (assuming such an average is meaningful, a fact which is rendered dubious in view

of the exponential dependence of R_i upon T), we can see that the optimum load decreases as the operating temperature increases, as well as with the length (through Y) and width (through X) of the monolith, for a constant channel size and electrical arrangement. Again, as in section 2.1.2.6.2, it must be stressed that R_{ex} is not necessarily the actual load, but the "equivalent load" associated with the monolith, and it value depends on the circuit arrangement of the various units.

2.2.5 Energy and Material balance equations

2.2.5.1. Simplifications and order-of-magnitude analysis

Throughout the following discussion, Y denotes distance along a certain direction, y is the mole fraction, x, conversion, and X, number of parallel channels per battery.

Consider, firstly, gaseous fuel-solid electrolyte heat transfer, as depicted in figure 2.51b. With temperature uniform in the X-direction, we can write, for the solid temperature,

$$T_s = T_s(r,Y) \qquad (2.2.39)$$

For a given Y, assume both air and fuel to have the same temperature, T_∞. Furthermore, if air and fuel flows are of similar magnitude, both solid faces will interact with the fluids with essentially equal heat transfer coefficients. The assumption of equal energy-average (or mixed-cup) temperatures will be justified below. With respect to the comparable flow-rates, it will be seen that this is indeed the case. Under the above conditions, the solid temperature profile is symmetrical with

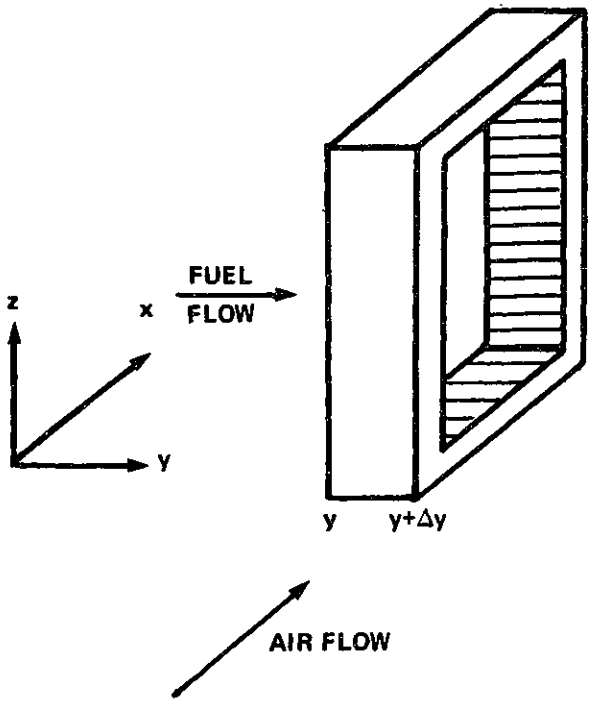

2.51a

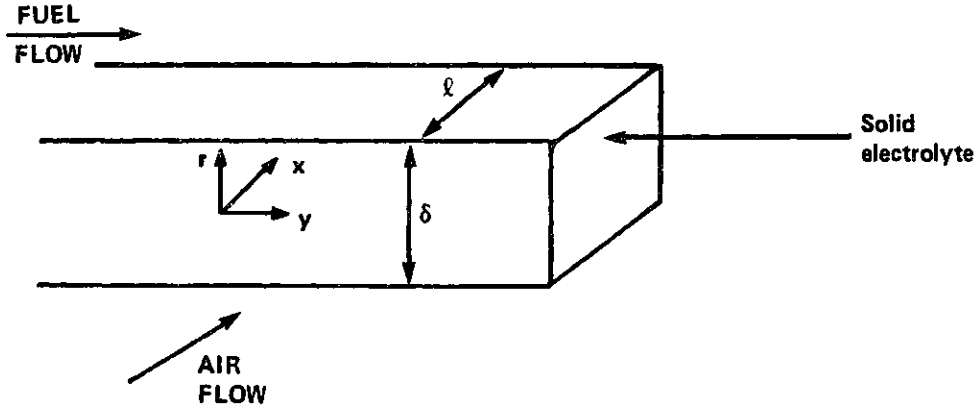

2.51b

COORDINATE SYSTEMS FOR GAS-SOLID INTERACTION
FIGURE 2.51

respect to the centreline. We can define an "area-average" temperature,

$$\ell\delta\overline{T}_s(Y) = 2\ell\int_0^{\delta/2} T_s(r,Y)\,dr \tag{2.2.40}$$

Consequently,

$$\overline{T}_s(Y) = \frac{2}{\delta}\int_0^{\delta/2} T_s(r,Y)\,dr \tag{2.2.41}$$

Next, we can expand $T_s(r,Y)$ about the value @ $r=\delta/2$,

$$T_s(r,Y) = T_s(\tfrac{\delta}{2},Y)+(r-\tfrac{\delta}{2})\left.\frac{\partial T_s(r,Y)}{\partial r}\right|_{r=\delta/2} + \ldots \tag{2.2.42}$$

Considering only linear terms,

$$\overline{T}_s\ (Y) = \frac{2}{\delta}\left\{\int_0^{\delta/2} T_s(\tfrac{\delta}{2},Y)\,dr + \left.\frac{\partial T_s(r,Y)}{\partial r}\right|_{r=\frac{\delta}{2}}\int_0^{\delta/2}(r-\tfrac{\delta}{2})\,dr\right\} \tag{2.2.43}$$

Rearranging,

$$\overline{T}_s(Y) - T_s(\delta/2,Y) = -\frac{\delta}{4}\left.\frac{\partial T_s}{\partial r}\right|_{\delta/2} \tag{2.2.44}$$

But

$$-k_s\left.\frac{\partial T_s}{\partial r}\right|_{\delta/2} = h\,[T_s(\tfrac{\delta}{2},Y)-T_\infty] \tag{2.2.45}$$

Therefore,

$$\overline{T}_s\ (Y) - T_s(\delta/2,Y) = \frac{h\delta/4}{k_s}[(T_s(\delta/2,Y)-T_\infty] \tag{2.2.46}$$

The dimensionless proportionality factor is a Biot number, so we can write

$$\frac{\overline{T}_s(Y)-T_s(\delta/2,Y)}{T_s(\delta/2,Y)-T_\infty} = Bi \tag{2.2.47}$$

Which means that

$$\frac{\bar{T}_s(Y) - T_\infty}{T_s(\delta/2,Y) - T_\infty} = Bi + 1 \qquad (2.2.48)$$

Equation (2.2.48) expresses, of course, the familiar result that solid gradients can be neglected relative to gas gradients if Bi << 1. For fully developed laminar flow in square ducts, subject to a constant wall heating rate boundary condition, we have (24)

$$Nu = 3.608 = \frac{h(4R_H)}{k} \qquad (2.2.49)$$

In our case, $4R_H$ equals the channel side, ℓ. For air @ 1000°K, k = 0.7 mw/cm K. Therefore, for a 1 mm x 1 mm channel,

$$h = \frac{3.608 \times 0.7 \times 10^{-3} \times 10^2}{10^{-3}} = 252.6 \quad \text{joule/sm}^2\text{K} \qquad (2.2.50)$$

For the solid thermal conductivity, we obtain, (25) $k_s \sim 2.09$ joule/sm K. Therefore,

$$Bi = \frac{252.6 \times 250 \times 0.25 \times 10^{-6}}{2.09} = 0.0076 \qquad (2.2.51)$$

for a 250 μm wall thickness. Note that, even if constant wall heating rate is not an exact boundary condition for the problem (though it is a better approximation than the other commonly encountered case, i.e., constant surface temperature), changing this assumption does not lead to appreciable variations in h (the constant temperature condition results in a Nusselt number 16% lower than the one considered). Furthermore, in performing this essentially order-or-magnitude analysis, peripheral non-uniformity of heat flux distribution has been neglected.

For N_2 @ $\sim$ 1000 K (considering that the fuel is normally a stream diluted in N_2) and a typical flow rate per monolith of $\sim$ 600 cc/min @ 298 K and atmospheric pressure, considering a 23 X-channel, 7 batteries monolith, with $\mu \sim 4.2 \times 10^{-5}$ kg/sm,

$$R_e \sim 1.75 \qquad (2.2.52)$$

We thus conclude

i. the flow regime is laminar

ii. radial temperature gradients within the solid can be neglected

The elementary process whereby a fuel molecule is electrochemically oxidized has been described in detail (1). It is evident that mass transfer from the bulk fluid phase to the electrode, and through the electrode's pores to the three phase boundary play a key role in the overall process, and it is important to determine the conditions under which either mechanism can become rate-limiting. As shown in Appendix I, for a 3 μm electrode, bulk-to-electrode transport is the potentially controlling mechanism, against which anion transport must be weighed. The electrolyte film thickness considered here, though, is greater than the one considered in Appendix I (see table 2.6). For a 20 μm-thick electrode film, a bulk-to-electrode mass transfer coefficient of $\sim$40 cm/s (see below, equation (2.2.54)), and an effective diffusivity of 0.09 cm^2/s (see Appendix I), the same calculation as performed in Appendix I yeilds a value of 0.89 for the ratio of bulk-to-electrode transport to diffusion within pores. Thus, although the former is still poten-

tially controlling, both mechanisms are now of roughly equal importance. This illustrates an important trade-off that must be considered between good current distribution (higher values of electrode thickness) and avoiding mass transfer limitations (lower values of electrode thickness). Therefore, for a limiting 20 μm thick electrode film, where bulk-to-electrode transport is still potentially rate-controlling, we can use the following correlation by Hegedus (26), applicable to mass transfer in catalytic monoliths

$$Sh = B\left(1+C\,\frac{4R_H}{L}\,ReSc\right)^{0.45} \qquad (2.2.53)$$

Assuming the peripheral asymmetry does not alter the validity of this equation (i.e., in the present case, only one of the four walls is active, whereas the expression applies for a completely symetrical situation), B can be taken as 2.976, and C, 0.095 (26). As seen above, typical Reynolds numbers are roughly equal to 2. For Sc $\sim$ 1 and a 1 mm x 1 mm channel, we finally obtain Sh $\sim$ 2.98. For CO in N_2, a binary diffusion coefficient at T 900°K and atmospheric pressure can be estimated using the Chapman-Enskog equation and substituting the ideal-gas law (27), to obtain D $\sim$ 1.34 cm^2/s; therefore,

$$k'g = \frac{DSh}{4R_H} \sim 40 \text{ cm/s} \qquad (2.2.54)$$

The molar flow per unit active surface for a completely mass transfer-limited process is therefore:

$$\underline{\text{Specific molar flow:}}\quad k'g[A]_b \text{ moles/sec cm}^2 \qquad (2.2.55)$$

The bulk fuel concentration can be expressed in terms of fuel mole fraction, temperature and pressure. Therefore, for atmospheric pressure, we finally obtain:

$$\underline{\text{Specific molar flow:}}\ \frac{0.487\ y_{Ab}}{T}\ \text{moles/sec cm}^2 \qquad (2.2.56)$$

The actual local rate of fuel transport from the bulk to the reacting zone is, for a current I_K corresponding to the Kth element along a channel, and an integration step of 10^{-3} (dimensionless length units; see section 2.2.5.5), for an ohmic polarized process,

$$\underline{\text{Specific molar flow:}}\ (\frac{I_K}{2\mathcal{F}}) \cdot (\frac{10^4}{L\ \ell})\ \text{moles/sec cm}^2 \qquad (2.2.57)$$

Where ℓ and L (channel width and channel length, respectively) are in cm. Substituting the appropriate values, we obtain

$$\underline{\text{Specific molar flow:}}\ 1.036 \times 10^{-2}\ I_K\ \text{moles/sec cm}^2 \qquad (2.2.58)$$

Typical local current profiles for ignited steady states (see figure 2.69) show a peak at $\sim$ 80% of reactor length. I_K being non-analytical in T or x, we can, however, calculate the ratio of the ohmic to diffusion-controlled processes at the two potentially critical reactor locations, namely, at the local current peak, and at reactor outlet (where x and T are maximum). The results are shown in table 2.7, where the corresponding concentration overpotential has been included. The figures presented in table 2.7 correspond to the two ignited steady states located in the present work characterized by the higher

outlet conversion and temperature (fuel and air feed temperatures 630 K and 650 K, respectively, see figures 2.57 and 2.59). β^{-1} in table 2.7 is the local ratio of ohmic to concentration controlled processes.

Table 2.7 illustrates a very important aspect of rate-controlling mechanisms and their consequences. For all except for the last case analyzed, β is such that the hypothesis of ohmic control seems adequate; nevertheless, in the 650 K feed temperature ignited state, although ohmic control is still potentially rate-determining, the value of β would seem to point towards a mixed regime where both mechanisms are important, even though the activation overpotential is still relatively small. The actual behaviour of the process in this region (i.e., will there be a gradual or a sharp transition from ohmic to mass transfer-controlled rates?) depends on the state of the surface and surface intermediates, and is beyond the scope of the present work. As noted before, oxygen presence in the anodic gas, more than activation overpotential, is to be used as a measure of mass transfer-control. It is useful to stress the difference between chemical and electrochemical reactors when dealing with diffusion limitations, which have a purely kinetic significance in a chemical reactor, constituting a measure of an upper limit of attainable rate, whereas, in an electrochemical reactor a diffusion-controlled operation is also thermodynamically inefficient.

We therefore conclude, in view of table 2.7 and the above brief discussion:

Location	Local current peak		Reactor outlet	
Fuel and air feed T(K)	630	650	630	650
I_K(Amps)	0.0001284	0.000114957	0.0001056	0.000058757
x	0.6863	0.6726	0.9202	0.9845
T(K)	1066	1072.9	1078.7	1092.7
β^{-1}	0.0619	0.0534	0.2024	0.587
ϕ_{conc}(mV)	2.9	2.5	10.5	41.6
$(\frac{E-\phi}{E})$	0.995	0.996	0.983	0.934

TABLE 2.7: Mass transfer limitations in monolith fuel cell

iii. Oxygen-anion conduction, as opposed to bulk-to-interface mass transfer, is the rate-limiting step throughout the present model, and, consequently, fuel concentration can be treated as uniform across any given cross section.

Consider now figure 2.51a. We will now compare Y-direction convective enthalpy transport in the fluid phase to molecular conduction along the solid. For the gaseous phase, we can write,

$$\underline{\text{Enthalpy input @ y:}} \quad F\rho\ \hat{C}p_G(T-T_o)\Big|_Y \tag{2.2.59}$$

$$\underline{\text{Enthalpy output y + } \Delta y\text{:}} \quad F\rho\ \hat{C}p_G(T-T_o)\ \Big|_{Y+\Delta Y} \tag{2.2.60}$$

Assuming ρ, $\hat{C}p_G$ and F remain constant (it is obvious that mass increases along the channel, but even for a pure feed and 100% conversion, mass increase in a CO/CO_2 fuel cell less than 60% so that, within this essentially order-of-magnitude analysis, we can assume an average value), we can write

$$\underline{\text{Net enthalpy output:}} \quad F\ \hat{C}p_G\ \frac{\partial T}{\partial Y}\ \Delta Y \tag{2.2.61}$$

For the solid, on the other hand, we have

$$\underline{\text{Input @ y:}} \quad -A_s k_s\ \frac{\partial T}{\partial Y}\ \Big|_Y \tag{2.2.62}$$

Where A_s is the solid cross section

$$\underline{\text{Output @ y + } \Delta y\text{:}}\ -A_s k_s\ \frac{\partial T}{\partial Y}\Big|_{Y\ +\ \Delta Y} \tag{2.2.63}$$

$$\underline{\text{Net output:}} \quad -A_s k_s\ \frac{\partial^2 T}{\partial Y^2}\ \Delta Y \tag{2.2.64}$$

The characteristic length is the channel length, and we arrive therefore at the following order-of-magnitude expressions

$$F\rho\ \hat{C}p_G \frac{\partial T}{\partial Y} \sim \frac{F\rho\hat{C}p_G T}{L} \tag{2.2.64}$$

$$\left|A_s k_s \frac{\partial^2 T}{\partial Y^2}\right| \sim \frac{A_s k_s T}{L^2} \tag{2.2.65}$$

Dividing both expressions, we obtain an axial Peclet number relating gas to solid energy transport,

$$Pe' = \frac{F\rho\hat{C}p_G\ L}{A_s k_s} \tag{2.2.66}$$

The primed notation on Pe is due to the fact that this Peclet number relates transport in two phases, and, consequently, the reference cross sections are different. For a 1 mm x 1 mm channel with 250 μm walls the solid cross section per channel is 0.875 mm^2 (taking into account the fact that the lateral walls belong 50% to each channel). For a typical 500 cc/min (@ 298 K and 1 atm) feed, and considering the flow rate per channel, we obtain, for a 5 cm long monolith with 7 batteries and 23 X-channels, and with k_s = 2.09 watt/mK, $\hat{C}p_G \sim$ 1000 joule/kg K,

$$Pe' \sim \frac{500 \times 10^{-6}}{60} \cdot \frac{101325 \times 28}{8314.4 \times 298} \cdot \frac{1000 \times 5 \times 10^{-2}}{0.875 \times 10^{-6} \times 2.09} \cdot$$

$$\cdot \frac{1}{23 \times 7} = 1.62 \tag{2.2.67}$$

iv. Therefore, solid-phase transport (conduction) is of the same order as convective gas transport and both must be taken into account in considering the energy equations.

The electric circuit equations (2.2.27) and (2.2.28) were deduced for X-uniform conditions. This, in fact, is the model's major simplification. It was shown in equation (2.2.67) that both conduction and convection must be taken into account

in considering the energy balance along a single channel. Since conduction involves a second order differential equation, the problem's complexity is thus considerably increased, since an initial-value problem is thus transformed into a two-point problem. Since, as will be seen later, the current cannot be expressed in closed form as a function of temperature and conversion, but, rather, includes the current distribution coefficient, which is a function of the current distribution along the whole channel, solution of the energy-balance differential equations involves two embedded iterations: an inner one, whereby integration is repeated until current distribution converges to a repetitive pattern, and an outer loop where the end boundary condition is checked and the whole process repeated for another choice of solid front temperature until the latter condition is verified. The process is schematically shown in figure 2.52.

If, however, X-nonuniformity is introduced, the solution to the problem would become a matricial (as opposed to a vectorial) one, with two such embedded loops to be solved for each Y-location, until the X-problem converges, before the current distribution and end boundary condition are checked and the whole process repeated in the Y-direction (and therefore also in the X-direction at each Y-location). This, of course, is possible in principle. However, the present work being a first attempt at modeling the already complex problem depicted in figure 2.52, it was decided that the additional accuracy was more than offset by the geometric increase in complexity.

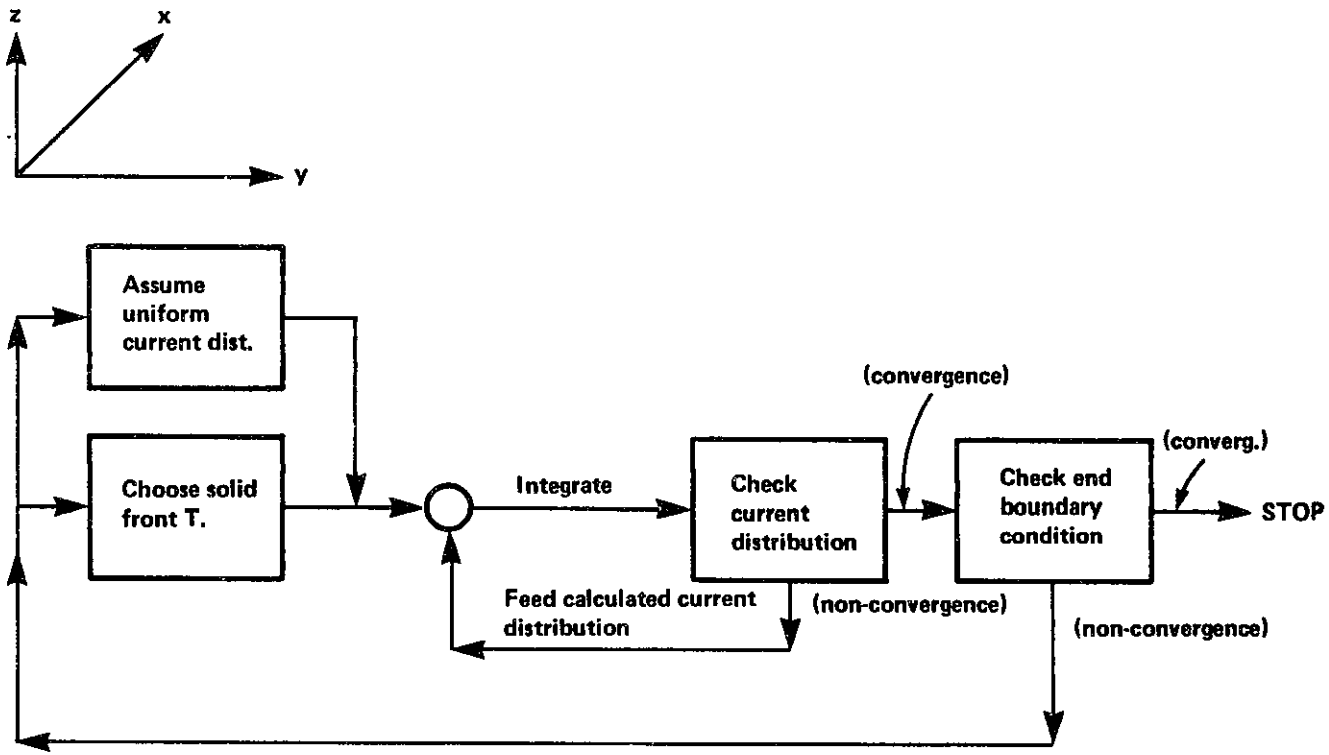

ITERATIVE SCHEME FOR SOLVING ENERGY AND MATERIAL BALANCES
FIGURE 2.52

The global, X and Y nonuniform problem, however, is a logical extension of the present work if more accurate predictions of monolith behaviour are to be obtained. It is very important to note, however, the true meaning of X-uniformity. In fact, such an assumption implies that all channels work under the same conditions. In actual fact, what will happen is that the channels nearest to the air inlet will be cooler, while those farther away will be gradually hotter. In the present model, heat losses to cross flow air have been accounted for by dividing the total load equally among the row of channels connected in parallel in the X-direction, thus the Y-profiles obtained correspond to no actual element of the reactor, but, rather, can be viewed as an "energy-average channel." Thus, it is the uniformity of heat losses, rather than the uniformity in temperature, that constitutes the model's major simplifying assumption and potential source of error.

Consider, in fact, the two normally encountered fully developed laminar flow heat transfer situations: constant wall flux and constant wall temperature. Both cases result in a constant heat transfer coefficient (28), and the qualitative shape of the profiles are depicted in figure 2.53, where the fluid temperature is the energy-average or "mixed-cup" temperature. Thus, it is seen that a constant duty per unit length, as assumed in the present model, requires a rising wall temperature. On the other hand, a constant wall temperature, at constant heat transfer coefficient, leads to an unevently distributed duty. Constant wall temperature can

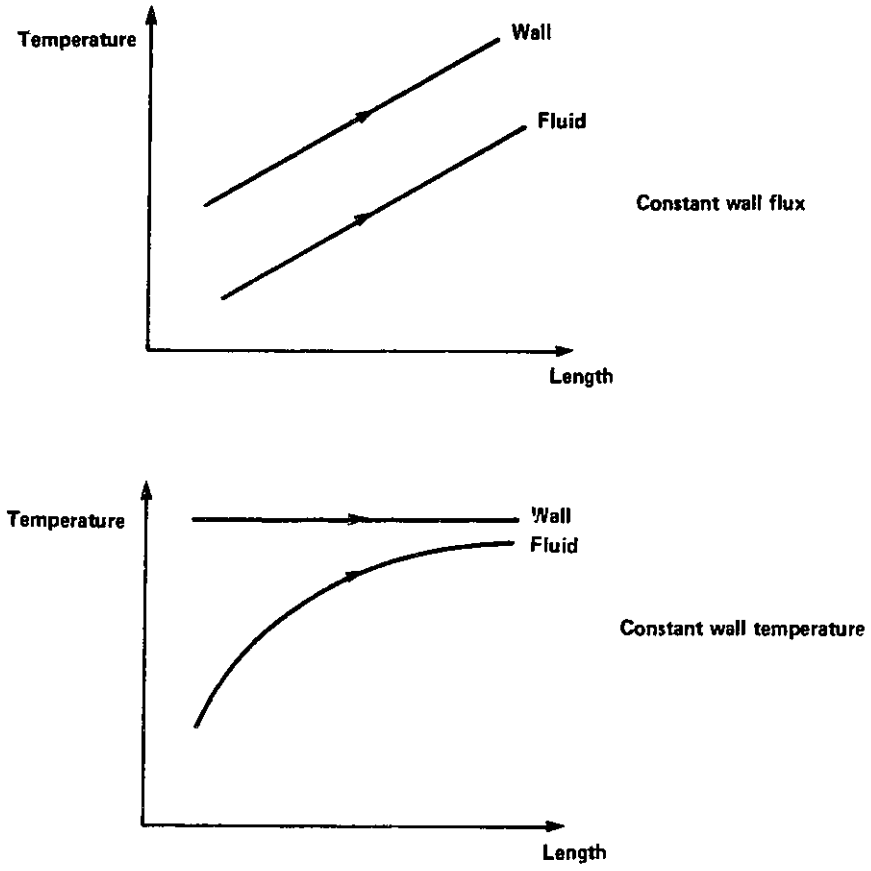

COMMONLY ARISING BOUNDARY CONDITIONS FOR HEAT TRANSFER IN TUBES
FIGURE 2.53

be approached by insulating both lateral walls. Under these conditions, it can be shown that the cross-flow air reaches the wall temperature within a very small transverse distance. In fact, the ratio of solid-to-gas temperature difference at a given location, X, to the same difference at an initial location X = 0 is, for a constant wall temperature,

$$\frac{(T_s-T_g)_X}{(T_s-T_g)_o} = \exp[-\ (\frac{h\ 4\ell X}{F\rho\ \hat{C}p_G})] \qquad (2.2.68)$$

Substituting Nu = 2.976 (24), $\ell = 10^{-3}$ m, $\hat{C}p_G \sim 10^3$ Joule/kgK, a flow-rate of 600 cc/min (298K and 1 atm) in a monolith with 40 Y-channels, 7 Z-batters and 3 cm in the X-direction and % transverse distance as a parameter, we obtain the following results, summarized in table 2.8.

Thus, it can be seen that the extremely low flow-rates involved are such that the gas temperture reaches solid temperature within very short distances. If, therefore, the reactor is insulated at both its lateral walls, the situation will resemble the one depicted in the lower illustration in figure 2.53, and the assumption of an evenly distributed duty is therefore seen to be arbitrary. Solution of the complete problem, with due consideration give to the lateral as well as the terminal boundary conditions, is thus the only means of describing the reactor's behaviour with sufficient accuracy. However, the approach chosen here does make sense from an energy-average point of view, though here, again, it must be stressed that current conduction across the electrolyte is an activated (i.e., highly non-linear) process, hence, extreme

Transverse distance (%)	$[1-\frac{(Ts-Tg)_X}{(Ts-Tg)_o}] : 100$
1	99.73
2	99.999
3	∿1

TABLE 2.8: Gas temperature variation along air channels

caution should be used in interpreting the present results, which presuppose the validity of an overall linear behaviour, implicit in averaging, if electrolyte resistance is controlling.

Note that the results of table 2.8 justify the simplification made in assuming a unique value of T_∞ for air and fuel in equations (2.2.45) to (2.2.48), since both temperatures will be close to the solid temperature.

Finally, before considering the actual governing equations, axial dispersion of heat and mass will be briefly considered. The dimensionless group relating convective transport to molecular conduction is the Peclet number. We can therefore write for heat and mass, respectively,

$$Pe_H = \frac{F\rho\hat{C}p_G L}{k\ A}; \quad Pe = \frac{\langle u\rangle\ L}{D} \tag{2.2.69}$$

where $\langle u\rangle$ is the gas velocity. Upon substitution of typical values,

F = 600 cc/min @ 298 K & 1 atm

$T \sim 1000$ K

L = 5 cm

23 X-channels

7 batteries

$\hat{C}p_G \sim 1000$ Joule/Kg K

A = 1 mm^2

$k \sim 6.5 \times 10^{-2}$ Watt/mK

$D \sim 1.34$ cm^2/S

we obtain $Pe_H = 56.7$, $Pe = 70$

Therefore,

V. We can neglect axial molecular transport of heat and mass in the gaseous phase relative to convective transport.

It is appropriate to sum up all the assumptions and simplifying hypothesis which will be considered in the development of the governing equations.

A - solid temperature is uniform at any given cross section

B - anion conduction through the electrolyte is the rate-determining step

C - consequently, fuel concentration is uniform at any given cross section.

D - axial condution of heat along the reactor walls is of the same order as convective gas-phase transport

E - X-uniformity is assumed and the cross-flow air duty is equally distributed among all channels connected in parallel, at any given Y-location.

F - Axial molecular transport of heat and mass in gaseous phase is negligible relative to convective transport.

G - polarization is exclusively ohmic (equivalent to B)

H - ohmic losses along fuel or air channels are negligible relative to electrolyte resistance.

2.2.5.2 Material balance

For the general reaction $A + \frac{1}{2} O_2 \rightarrow B$, using the same nomenclature as in section 2.1.2.2, we can write, with reference to figure 2.51a, and considering flows per channel, the following A balance:

Rate of disappearance per unit length: $\dot{N}_{Ai} \frac{dx}{dY}$ (2.2.70)

Therefore,

$$\dot{N}_{Ai} \frac{dx}{dY} = \frac{1}{2\mathcal{F}} \frac{dI}{dY} \tag{2.2.71}$$

Consider, however, equation (2.2.28). This expression provides the means whereby current can be calculated, but it involves consideration of a longitudinal element small enough with respect to channel total length such that temperature can be considered constant within the element's length, yet finite in nature. Let therefore Y denote the dimensions of the finite element considered, and let us consider a generic K^{th} such element. Equation (2.2.71) can therefore be rewritten as follows,

$$\dot{N}_{Ai} \frac{dx}{dY}\Big|_K = \left(\frac{1}{2\mathcal{F}}\right)\left(\frac{I_K}{\Delta Y}\right) \tag{2.2.72}$$

It is evident from the form of equation (2.2.72) that the integration will be more accurate the smaller the choice of ΔY. Furthermore, it is very important to note that this finite (as opposed to differential) approach is due to the fact that, in equation (2.2.28), in order to account for Y-nonuniformity, the current distribution coefficient was introduced. This coefficient involves not only the local current (which is in principle analytic in local conversion and temperature), but the total current, which is not, and thus renders the whole expression numerical, rather than analytic; thus writing equation (2.2.71) in closed form as a function of temperature and conversion exclusively is not possible. To shorten notation let D(K) denote the K^{th} element's current distribution coefficient. Then, from equation (2.2.28),

$$I_K = \frac{Z\ E_{rev,K}}{ZR_{iK} + X[(Z+1)R_{el}+R_{ex}]D(K)} \qquad (2.2.73)$$

In the previous section it was shown that the major resistance to heat transfer was interfacial (Bi <<1); we can therefore picture the reaction occuring at the (uniform) solid temperature. Furthermore, in all of the examples to be considered, air is fed in sufficient excess, so that oxygen concentration can be taken as 21% with negligible error. Again, the complete two-dimensional model should also take into consideration X-variation of O_2 concentration. With the above assumptions,

$$E_{rev,K} = E°(T_s) + \frac{RT_s}{2\mathcal{F}} \ln \frac{0.458(1-x)}{x} \qquad (2.2.74)$$

Consideration of the relevant geometry (figure 2.49a) shows the essentially discontinuous nature of the fuel channel, with area available for anion flow periodically interrupted by walls. Since the governing differential equations, must, however, be integrated in a practical way, the above mentioned discontinuity can be easily modelled by defining a "useful length ratio",

$$f = \frac{\ell}{\ell+\delta} \qquad (2.2.75)$$

Therefore, for any channel length considered, the fraction f is available for current passage and reaction (for the presently considered geometry, with ℓ = 1 mm and δ = 250 μm, f = 0.8). Therefore, for a length ΔY,

$$R_{iK} = \frac{4.166 \times 10^{-3}}{f\ \Delta Y\ \ell(1/\delta)} \exp\left(\frac{9700}{T_s}\right) \text{ (ohms)} \qquad (2.2.76)$$

Where δ, ℓ and ΔY must be expressed in cm.

Consequently,

$$I_K = \frac{Z\left[E^\circ(T_s) + \frac{RT_s}{2\mathcal{F}} \ln \frac{0.458(1-x)}{x}\right]}{\frac{4.166 \times 10^{-3} Z\delta}{\Delta Y \, \ell f} \exp\left(\frac{9700}{T_s}\right) + XD(K)\left[(Z+1)R_{el}+R_{ex}\right]} \qquad (2.2.77)$$

Therefore, the derivative of conversion at the K^{th} element can be expressed as

$$\left.\frac{dx}{dY}\right|_K = \left(\frac{1}{\dot{N}_{Ai} 2\mathcal{F} \Delta Y}\right)\left\{\frac{Z\left[E^\circ(T_s) + \frac{RT_s}{2\mathcal{F}} \ln \frac{0.458(1-x)}{x}\right]}{\frac{4.166 \times 10^{-3} Z\delta}{f\Delta Y \, \ell} \exp\left(\frac{9700}{T_s}\right) + XD(K)\left[(Z+1)R_{el}+R_{ex}\right]}\right\} \qquad (2.2.78)$$

Equation (2.2.78) is the material balance differentail equation. Again, it should be noted that its solution involves not only jointly solving it together with the energy equations, but iterative solution until the numerical term D(K) converges to some repetitive pattern, starting from an assumed distribution (uniform in the present work). Obviously, in numerically integrating equation (2.2.78), the integration step will be ΔY.

2.2.5.3. Gas phase energy balance

Consider figure 2.54a, where the dotted line indicates the limits of the control volume for the development of the fuel-phase energy balance. The notation is the same as in section 2.1.2.2. We can therefore write

$$\underline{\text{Enthalpy input @ Y}}: \dot{N}_A[\hat{C}p_A(T_g-T_o)|_Y+H_{oA}] +$$

$$+ \dot{N}_B[\hat{C}p_B(T_g-T_o)|_Y+H_{oB}] + \dot{N}_C[\hat{C}p_C(T_g-T_o)]_Y \qquad (2.2.79)$$

This can be transformed, using the same procedures as in

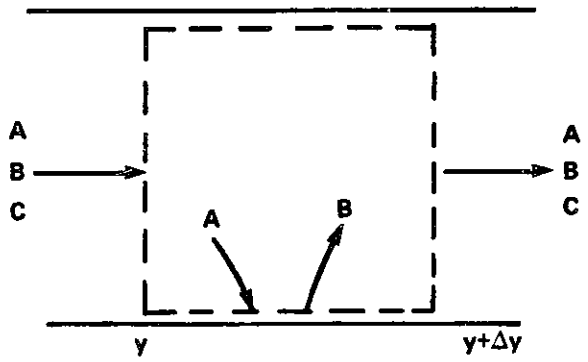

2.54a

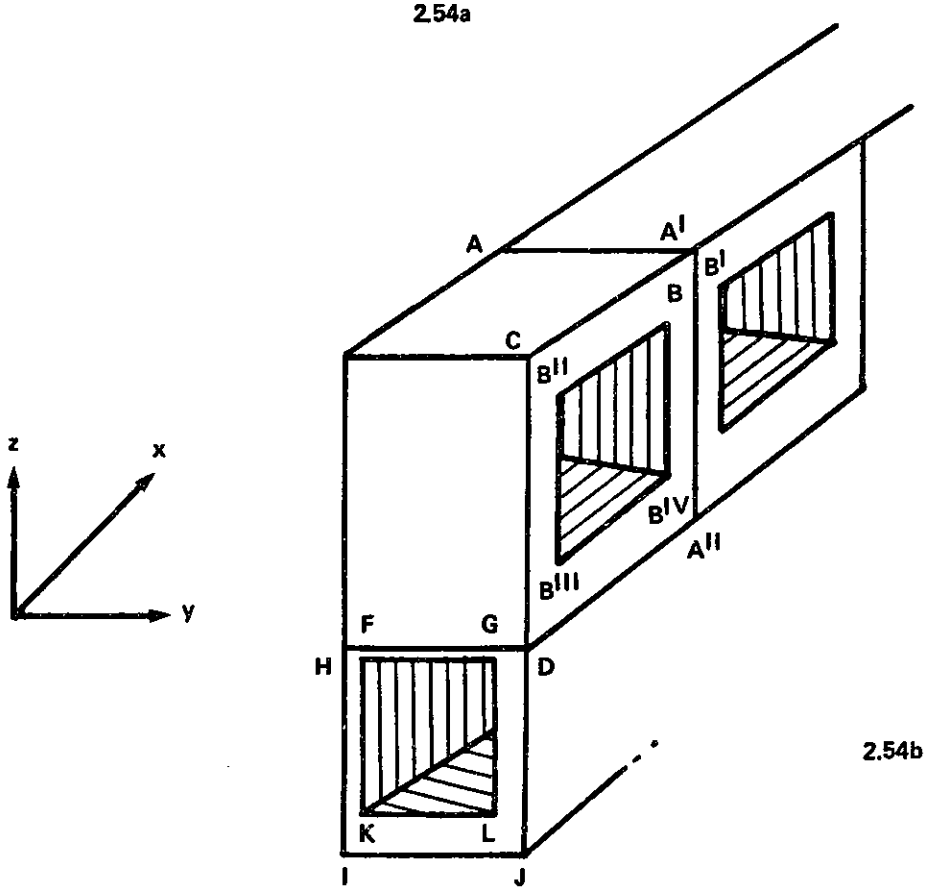

2.54b

CONTROL VOLUMES FOR ENERGY BALANCES
FIGURE 2.54

section 2.1.2.2, to

$$\underline{\text{Enthalpy input @ Y}}: \ (\dot{N}_{Ai}+\dot{N}_c)\,[\hat{C}p_f(T_g-T_o)]_Y + \\ + \dot{N}_{Ai}(1-x)|_Y\, H_{oA}+\dot{N}_{Ai}\,x|_Y\, H_{oB} \qquad (2.2.80)$$

where, as before, $\hat{C}p_f$ denotes the composition-average molar heat capaicity of the fuel stream, temperature-averaged between T_o and T_g.

Therefore, the corresponding output term @ y + Δy is

$$\underline{\text{Enthalpy output @ Y + }\Delta\text{Y}}: \ (\dot{N}_{Ai}+\dot{N}_c)\,[\hat{C}p_f(T_g-T_o)]_{Y+\Delta Y} + \\ + \dot{N}_{Ai}(1-x)|_{Y+\Delta Y}H_{oA}+\dot{N}_{Ai}x|_{Y+\Delta Y}H_{oB} \qquad (2.2.81)$$

The A-flux across the control volume is related to current passage in the interval Y + ΔY, and can be expressed as

$$\underline{\text{A-flux}}: \ \frac{I_K}{2\mathcal{F}}\,[\hat{C}p_A(T_g-T_o)+H_{oA}] \qquad (2.2.82)$$

Similarly,

$$\underline{\text{B-flux}}: \ \frac{I_K}{2\mathcal{F}}\,[\hat{C}p_B(T_s-T_o) + H_{oB}] \qquad (2.2.83)$$

Finally, solid and fuel exchange heat via the convective coefficient h. Thus,

$$\underline{\text{Heat interaction:}} \ \ 4\ell\,\Delta Y\,h\,(T_s-T_g) \qquad (2.2.84)$$

Since each ΔY element has constant properties, it can be compared to a CSTR, and the unsubscripted properties in equations (2.2.82), (2.2.83) and (2.2.84) are outlet (Y+ΔY) properties. Again, note that the validity of this assumption depends upon the choice of a sufficiently small ΔY, keeping, nevertheless, its finite characteristics.

The various terms can now be combined to yield the fuel balance for the K^{th} element,

$$4\ell\Delta Yh(T_s-T_g)+\frac{I_K}{2\mathcal{F}}[\hat{C}p_B(T_s-T_o)+H_{oB}]+(\dot{N}_{Ai}+\dot{N}_c)[\hat{C}p_f(T_g-T_o)]_Y+$$
$$+\dot{N}_{Ai}(1-x)|_Y H_{oA}+\dot{N}_{Ai}x|_Y H_{oB}=\frac{I_K}{2\mathcal{F}}[\hat{C}p_A(T_g-T_o)+H_{oA}]+$$
$$+(\dot{N}_{Ai}+\dot{N}_c)[\hat{C}p_f T_g-T_o)]_{Y+\Delta Y}+\dot{N}_{Ai}(1-x)|_{Y+\Delta Y} H_{oA}+\dot{N}_{Ai}x|_{Y+\Delta Y} H_{oB}$$

(2.2.85)

Rearranging, and noting that the specific heat terms can be taken out of the derivatives without any appreciable error,

$$(\dot{N}_{Ai}+\dot{N}_c)\hat{C}p_f\frac{dTg}{dY}\Big|_K=4\ell h(T_s-T_g)+$$
$$+\frac{Z[E^\circ(T_s)+\frac{RT_s}{2\mathcal{F}}\ln\frac{0.458(1-x)}{x}][\hat{C}p_B(T_s-T_o)-\hat{C}p_A(T_g-T_o)]}{\left\{\frac{4.1666\times10^{-3}Z\delta}{\Delta Y\ \ell f}\exp(\frac{9700}{T_s})+XD(K)[(Z+1)R_{el}+R_{ex}]\right\}(2\mathcal{F}\Delta Y)}$$

(2.2.86)

Equation (2.2.86) is the fuel energy balance. Note the cancellation of the reference enthalpy terms and the consequent disappearance of the heat of reaction. This agrees with the conclusion whereby gas-solid interaction takes place via h, while actual reaction takes place in the solid phase. Again, upon numerically integrating equation (2.2.86), the integration step is ΔY. The balance refers to the Kth element.

2.2.5.4 Solid energy balance

Figure 2.54b depicts the essential geometrical elements involved in the consideration of the solid energy balance. Line AA'A" has no actual physical significance, but, instead,

shows the solid boundaries associated with one channel. Thus, if δ = 250 μm, BB' = 250μm and half of this width belongs to each channel. Thus, the solid cross section per fuel channel is outwardly bounded by A'CDA". and internally bounded by BB^{II} $B^{III}B^{IV}$. The assumed X-uniformity implies, of course, infinite X-direction solid conduction. In the present work, therefore, the solid corresponding to an air channel (i.e., bounded by FKLGDJIH) is treated as isothermal in the X-direction with Y-variation from air channel to air channel dictated by the solid energy balance. Interaction with air channels is via convection to cross flow air. The ZrO_2 layer which, as explained in section 2.2.3, separates successive batteries, is assumed to act as an insulator, so that batteries do not interact in the Z-direction.

Consider now a longitudinal element of length ΔY, and let the current associated with it be I_K, given by equation (2.2.77). The oxygen flow to this element is therefore,

$$\underline{O_2 \text{ molar flow to } K^{th} \text{ element}} = \frac{I_K}{4\mathcal{F}} \qquad (2.2.87)$$

As explained in section 2.2.5.1, modeling of an "energy-average" channel involves uniformity of X-direction air-heating duties. Therefore, with T_{Airj} denoting air feed temperature,

$$\underline{O_2 \text{ enthalpy flow to } K^{th} \text{ element}} = (\frac{I_K}{4\mathcal{F}})\hat{Cp}_{O_2}(T_{Airj}-T_o) \qquad (2.2.88)$$

Note, however, that oxygen enthalpy input is negligible with respect to heat of reaction, therefore, the error involved in

using T_{Airj} is very small, and the contribution of this enthalpy flux would not change the energy balance if X nonuniformity were introduced. Let the total air feed per monolith by $\dot{N}_{Air}$ moles per second. Therefore, $\dot{N}_{Air}/Z$ moles are fed to each battery. Since the governing equations will be integrated along the Y-direction, the air flow, which is discontinuous in Y, must be transformed into an equivalent continuous flow. Therefore,

$$\underline{\text{Transverse air flow per battery per unit Y-length}} = \frac{\dot{N}_{air}}{ZL} \qquad (2.2.89)$$

Consequently, the amount of air that flows across the X-direction without being transported across the electrolyte, for a length ΔY, is

$$\underline{\text{Unreacted air in a length } \Delta Y} = \frac{\dot{N}_{air}\ \Delta Y}{ZL} - \frac{XI_K}{4\mathcal{F}} \qquad (2.2.90)$$

The simplifying assumption of X-uniformity will now be introduced. As shown in table 2.22, air exits the monolith at wall temperature in the cases currently considered (that is, unless air excess is such that the wall temperature is not reached). Assuming air heating to be equally distributed among the X-channels, we can write

$$\underline{\text{Air heating duty per channel in a length } \Delta Y:}$$

$$\frac{1}{X}\left[\frac{\dot{N}_{Air}\ \Delta Y}{ZL} - \frac{XI_K}{4\mathcal{F}}\right] \hat{C}p_{Air}(T_s - T_{Airj}) \qquad (2.2.91)$$

Equation (2.2.91) is the expression of assumed X-uniformity, and transforms the rigorous approach into an "energy-average channel" problem. It should be evident that it contains the source of any major discrepencies between the model's predictions and the reactor's actual performance. The rigorous 2-dimensional model would replace such equation by the gas and solid X-direction differential equations.

The A and B fluxes shown in figure 2.54a must now be taken into consideration. Equations (2.2.82) and (2.2.83) apply, so we rewrite

$$\underline{\text{A-flux}} : \frac{I_K}{2\mathcal{F}} \left[\hat{Cp}_A(T_g - T_o) + H_{oA}\right] \qquad (2.2.82)$$

$$\underline{\text{B-flux}} : \frac{I_K}{2\mathcal{F}} \left[\hat{Cp}_B(T_s - T_o) + H_{oB}\right] \qquad (2.2.83)$$

For solid axial conduction, we can write,

$$\underline{\text{Input @ Y}}: \quad - k_s A_s \left.\frac{dT_s}{dY}\right|_Y \qquad (2.2.92)$$

$$\underline{\text{Output @ Y + } \Delta Y}: \quad - k_s A_s \left.\frac{dT_s}{dY}\right|_{Y+\Delta Y} \qquad (2.2.93)$$

Next, the work interactions must be accounted for. Contrary to the CSTR case, in which electrode resistance was inseparable from electrolyte resistance and was appropriately considered within the control volume, in the present case contact resistance is negligible with respect to Ri ($\sim$0.5 Ω vs. $\sim$200 Ω for a length associated with an air channel) ohmic drops along the channel can be neglected, and the "electrode" resistances are now "concentrated" and <u>outside</u> the control volume shown in figure 2.54b. Thus, the work interaction

considered is not 100% useful work, since part of this energy will be expended in overcoming R_{el}-losses. On the other hand, the voltage considered here includes only electrolyte ohmic drop, while, in the CSTR case, the voltage includes also R_{el}-losses.

Work interaction: EI_K (2.2.94)

Heat interaction with fuel: $4h\,\Delta Y\ell(T_s-T_g)$ (2.2.95)

Combining all the terms, we finally have

$$\frac{I_K}{4\mathcal{F}}\hat{Cp}_{O_2}\,(T_{airj}-T_o)+\frac{I_K}{2\mathcal{F}}[\hat{Cp}_A(T_g-T_o)+H_{oA}]-k_sA_s\frac{dT_s}{dY}\Big|_Y=$$

$$=-k_sA_s\frac{dT_s}{dY}\Big|_{Y+\Delta Y}+\frac{I_K}{2\mathcal{F}}[\hat{Cp}_B(T_s-T_o)+H_{oB}]+4h\Delta Y\ell(T_s-T_g)+$$

$$+\frac{1}{X}\left[\frac{\dot{N}_{Air}\,\Delta Y}{ZL}-\frac{XI_k}{4\mathcal{F}}\right]\hat{Cp}_{Air}(T_s-T_{Airj})+EI_K \qquad (2.2.96)$$

Rearranging,

$$-k_sA_s\frac{d^2T_s}{dY^2}\Big|_K=\frac{I_K}{2\mathcal{F}\Delta Y}\left\{(-\Delta H_o)\left(1-\frac{E}{E_{TN}}\right)-\hat{Cp}_B(T_s-T_o)+\hat{Cp}_A(T_g-T_o)+\right.$$

$$\left.+\frac{\hat{Cp}_{O_2}}{2}(T_{Airj}-T_o)\right\}-4h\,\ell(T_s-T_g)-$$

$$-\frac{\hat{Cp}_{Air}(T_s-T_{Airj})}{X}\left[\frac{\dot{N}_{Air}}{ZL}-\frac{XI_K}{4\mathcal{F}\Delta Y}\right] \qquad (2.2.97)$$

where E_{TN} ("thermoneutral voltage") $=(-\Delta H_o)/2\mathcal{F}$. Equation (2.2.97) is the solid-phase energy balance, and it can be expressed as a function of temperature, conversion and current distribution coefficient exclusively upon substitution of equations (2.2.74),(2.2.77) and (2.2.27), to yield, finally, for the Kth element,

$$-k_s A_s \frac{d^2T_s}{dY^2} = \left\{ \frac{\left[E^\circ(T_s) + \frac{RT_s}{2\mathcal{F}} \ln \frac{0.458(1-x)}{x}\right] Z}{\left\{\frac{4.166 \times 10^{-3}\delta\, Z}{f\, \Delta y \ell} \exp\left(\frac{9700}{T_s}\right) + XD(K)\left[(Z+1)R_{el} + R_{ex}\right]\right\} 2\mathcal{F}\Delta Y} \right\} \times$$

$$\times \left\{ (-\Delta H_o)\left[1 - \frac{XD(K)\left[(Z+1)R_{el}+R_{ex}\right]\left[E^\circ(T_s) + \frac{RT_s}{2\mathcal{F}} \ln \frac{0.458(1-x)}{x}\right]\left(\frac{1}{E_{TN}}\right)}{\frac{4.166 \times 10^{-3} Z\delta}{f\, \Delta Y\, \ell} \exp\left(\frac{9700}{T_s}\right) + XD(K)\left[(z+1)R_{el}+R_{ex}\right]} \right] - \right.$$

$$\left. - \hat{C}p_B(T_s - T_o) + \hat{C}p_A(T_g - T_o) + \frac{\hat{C}p_{O_2}}{2}(T_{Airj} - T_o) \right\} -$$

$$- 4h\,\ell(T_s - T_g) - \frac{\hat{C}p_{Air}(T_s - T_{air})}{X} \left\{ \frac{\dot{N}_{Air}}{ZL} - \right.$$

$$\left. - \frac{XZ\left[E^\circ(T_s) + \frac{RT_s}{2\mathcal{F}} \ln \frac{0.458\,(1-x)}{x}\right]\left(\frac{1}{4\mathcal{F}\Delta Y}\right)}{\frac{4.166 \times 10^{-3} Z\delta}{\Delta Y\, \ell f} \exp\left(\frac{9700}{T_s}\right) + XD(K)\left[(Z+1)R_{el}+R_{ex}\right]} \right\} \qquad (2.2.98)$$

2.2.5.5 Integration and boundary conditions

Equations (2.2.98),(2.2.86) and (2.2.78) were non-dimensionalized and integrated via a fourth order Runge-Kutta method. Figure 2.52 shows the iterative procedure employed. The current distribution coefficient was initially assumed to be equal for all elements, and the calculated coefficient compared with the previous value; the inner loop's convergence condition was arbitrarily set as a relative variation of less than 10^{-3} for both the mean current per element and the sum of squares of the spread of the current distribution with respect to uniformity

$$\frac{\left|\left[\frac{\sum_{K=1}^{m} I_K}{m}\right]_i - \left[\frac{\sum_{K=1}^{m} I_K}{m}\right]_{i-1}\right|}{\left[\frac{\sum_{K=1}^{m} I_K}{m}\right]_{i-1}} \leq 10^{-3} \qquad (2.2.99)$$

$$\frac{\left|\left\{\sum_{K=1}^{m}\left[(I_K/\sum_{K=1}^{m} I_K)-1/m\right]^2\right\}_i - \left\{\sum_{K=1}^{m}\left[(I_K/\sum_{K=1}^{m} I_K)-1/m\right]^2\right\}_{i-1}\right|}{\left\{\sum_{K=1}^{m}\left[(I_K/\sum_{K=1}^{m} I_K)-1/m\right]^2\right\}_{i-1}} \leq 10^{-3}$$

(2.2.100)

Here, K denotes the Kth element along the integration, i, the number of current distribution iterations (internal loop in figure 2.52), and $\bar{m}$, the reciprocal of integration step (i.e., number of elements per channel).

The step size for the results to be presented was 10^{-3} (dimensionless length), results being sensitive to step size

for steps larger than 1.25×10^{-3} (a rather surprising result in view of the fact that each integration step represents a CSTR).

The gas energy and material equations being first order, they require only an initial condition. For energy we have, with θ representing dimensionless temperature referred to gas feed temperature,

$$\theta_G(0) = 1 \qquad (2.2.101)$$

while, for conversion,

$$x(0) = 0 \qquad (2.2.102)$$

However, the initial condition for conversion cannot be used for voltage calculation purposes, since it gives rise to an infinite voltage which is physically meaningless. In the actual reactor, the initial voltage will be mainly determined by the trace CO_2 content in the inlet fuel; however, even if 100% purity were acheived, a finite CO_2 concentration would exist due to backmixing (although this has been neglected since $Pe \sim 70$, the non-backmixed condition is only true for $Pe = \infty$). Thus, in the results presented, the voltage in the first integration step was calculated assuming 0.1% CO_2 in the fuel stream, though this was not used for material balance calculations (i.e., only the logarithmic component of the driving force in the first step was calculated using 0.1% CO_2, but the inlet conversion was taken as 0). The influence of this arbitrary initial CO_2 concentration was, of course, negligible, and the results were insensitive to variations of this parameter even when its value was set at 0.001% for sensitivity testing

purposes. Note, furthermore, that the negligible influence of the trace initial CO_2 concentration for voltage calculations,

i. is guaranteed by the small integration step.

ii. is to be expected in any realistic model, since it is clear that the overall reactor's performance will not be influenced by the trace impurities present in the fuel feed.

iii. is even smaller for the ignited steady states (which are the ones of practical interest), since this trace CO_2 content is infinitesimal with respect to conversions achieved in the reactor for ignited operation, but is of the same order of the unignited conversions. Thus, the model's predictions increase in accuracy as the reactor's regime changes from unignited to ignited. Even in the former case, however, no significant influence of this parameter was detected upon variation down to 0.001%.

For the solid energy balance, both ends were treated as insulated. The solid's front temperature, therefore, was the parameter varied in order to achieve a zero slope at the reactor's outlet, starting with the chosen solid front temperature and a zero slope at the reactor's inlet. If another front boundary condition is imposed upon the system (for example, stagnation flow of the gas as it encounters the uninsulated solid), then the calculation would be exactly analogous, but now the trial solid temperature imposes an initial slope different than zero, according to the usual boundary condition (where h can be modified to include radiation)

$$k_s \frac{dT_s}{dY} = h(T_s - T_g) \qquad (2.2.103)$$

(note signs, coherent with the coordinate system chosen, see figure 2.48). The matching outlet slope, however, would still be zero for all practical purposes, since solid and gas temperatures are practically equal throughout the reactor, except at the inlet (see results). The present model applies to a reactor still in the process of being assembled. Air and fuel feed is one of the many practical aspects under consideration, the issue being particularly important when one takes into due account the potentially explosive mixtures involved. At present, one of the possibilities considered is to feed the actual monolith through an approximately 1-in layer of porous insulating material (Fiberfax) which allows the flow of gas, the length being such as to allow good gas distribution. Another possible alternative is to feed the reactor via an "inert" (i.e., without catalyst or electrical connections) feed monolith. The choice not having yet been made, it was decided, nevertheless, to model the monolith as being insulated in the ends, and gas inlet temperature to the reactor was treated as an independent parameter. A feed monolith kept at the required inlet gas temperature, plus a short length of insulating material which uncouples solid and gas inlet temperatures (see figure 2.55) would therefore satisfy the boundary conditions used in the present model. Adequate choice of the short insulator, moreover, would help achieve good sealing and mechanical contact between both monoliths. Feeding the gas through a porous insulator, on the other hand, though clearly satisfying the insulation requirement, transforms the inlet gas temperature from an arbitrary parameter to a point in the

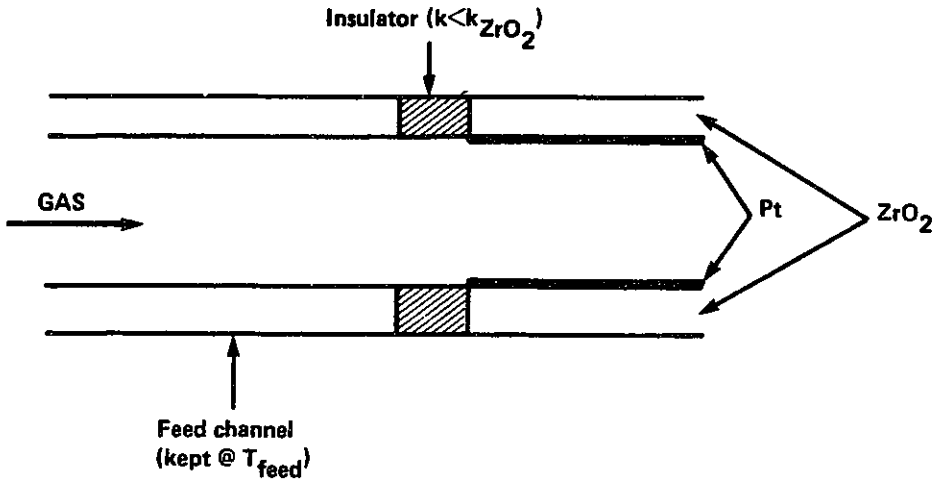

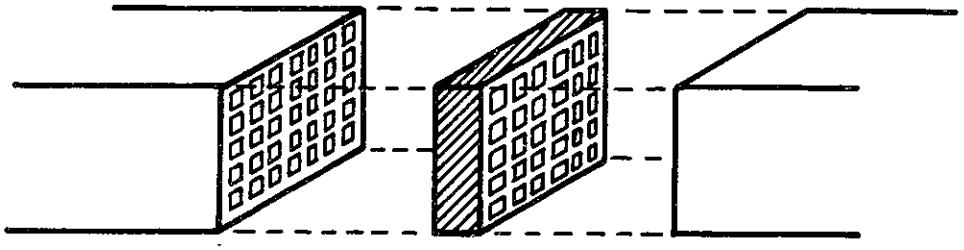

FEED ARRANGEMENT CONSIDERED IN MODEL
FIGURE 2.55

temperature profile that would result from the joint integration of equations (2.2.98),(2.2.86) and (2.2.78), coupled with the differential energy balance across the porous solid. However, in the absence of chemical reaction, there must be a linear relation between the temperatures of the gas at both ends of the porous insulator, in such a way that all the qualititative features of reactor behaviour explained below should still hold true even for this feed design.

The program used to solve the governing equations (see Appendix IV, MONOLITH program) contains two basic sections, the last of which is schematically shown in figure 2.52. The initial section prompts the user for the following main inputs (see program for complete list of inputs required):

1. Fuel feed temperature
2. Air feed temperature
3. Fuel mole fraction @ reactor inlet
4. Air feed ratio
5. Contact resistance
6. Number of parallel channels per battery
7. Number of batteries in series per monolith
8. Channel length
9. Channel cross section
10. Wall thickness
11. Nusselt number
12. Desired final conversion
13. Guess for operating temperature

Items 1,2,3,4,5,6,7,8,9,10,12 and 13 (the latter to calculate optimum load at the assumed operating temperature, see equation

(2.2.38)) are used to calculate an overall energy balance and the corresponding fuel and air requirements, the resulting temperature is then compared with the initial guess; the user then decides whether to repeat the calculation or to introduce a new guess for the overall energy-average temperature. Each time the program calculates the corresponding "optimum" load and power output. When the user decides that satisfactory convergence has been achieved, the program gives the possibility to alter the calculated flows and external load. Note that, contrary to the case of the CSTR cell, when air feed was a direct multiple of cell current, here one can only fix an air feed ratio for the first part of the program, which treats the cell as a lumped-parameter system. However, in the actual integration of the differential equations, the air feed is not recalculated. Excess air was such that no appreciable error results in considering a constant driving force on the cathodic side. However, at lower air feeds, this may lead to error. Figures 2.56 to 2.71, therefore, are characterized by a fixed air-to-fuel ratio, as opposed to the CSTR-multiplicity figures, where the air-to-current ratio was fixed.

Solid and gas thermal conductivities were treated as constant. Note, however, that the former is not of great importance, insofar as the virtual equality of gas and solid temperatures is mainly due to the low gas flow rates involved, so that the temperature dependence of gaseous thermal conductivity would have virtually no effect on the gasous profile.

Heat transfer between gas an solid was modelled through a laminar Nusselt number for fully developed flow and constant heat generation per unit length.

2.2.6 Results

As shown in section 2.2.5.1, axial molecular conduction of heat through the solid cannot be neglected when compared with convective enthalpy transport via gas flow, this rather unusual situation arising due to the fact that the gas flows involved are very low. This introduces into the governing equations a second order differential equation, physically implying a finite measure of backmixing, and, mathematically, transforming a straightforward initial value problem into a two point boundary condition one. Furthermore, a reactor posessing backmixing deviates from ideal plug flow behavior and shows characteristics intermediate between the opposing PFR and CSTR extremes, approaching the latter as the mixing effects predominate over the plug flow behaviour.

For the conditions considered in the examples to follow, multiple steady states were found to characterize reactor behaviour, even though the gas flow is such that axial dispersion of heat and mass can be neglected (Peclet numbers). The values of the parameters used are summarized in table 2.9.

Figure 2.56 illustates the behaviour of the differential equations involved. The dimensionless first derivative of solid temperature at reactor outlet is plotted against the assumed solid front temperature. For any given end boundary condition (0 slope in the present case), it follows that there can either be 1 or 3 steady states. Ignited operation is achieved upon raising the gas feed temperature.

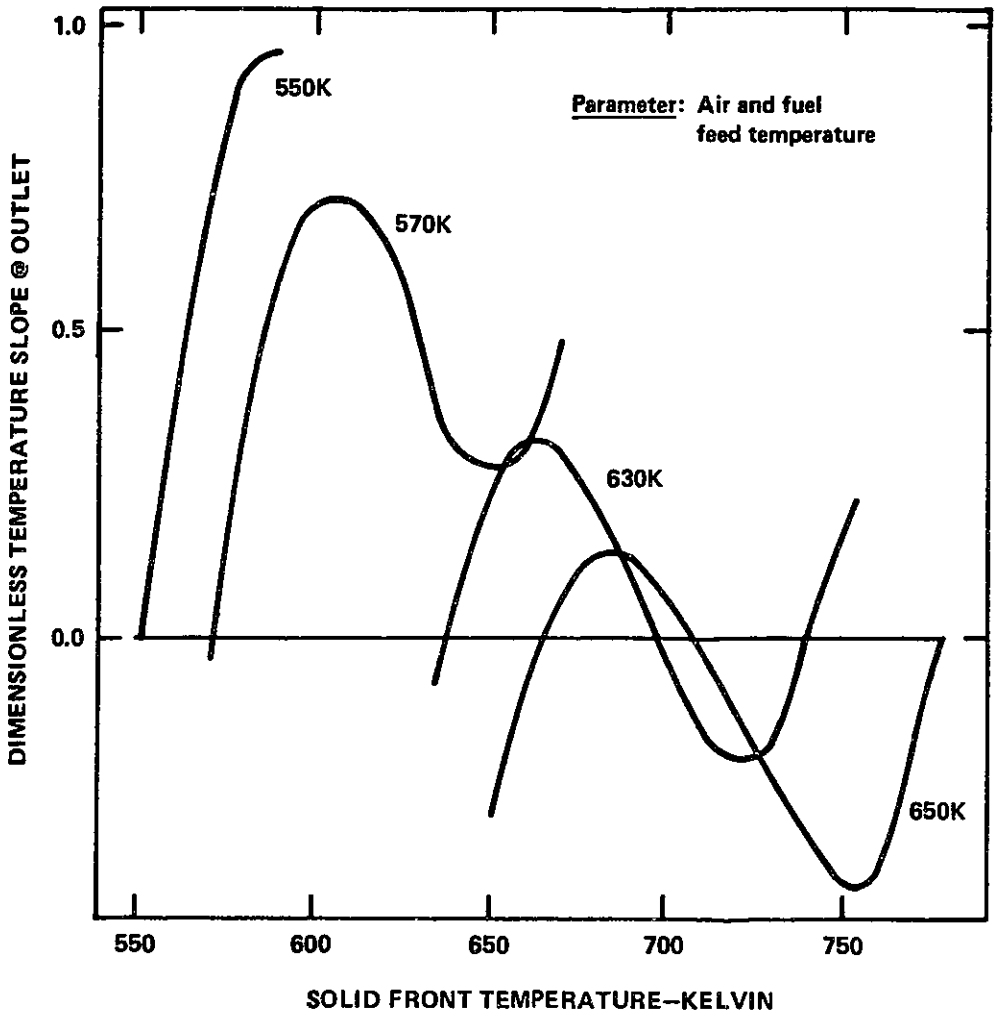

BEHAVIOUR OF MATCHING BOUNDARY CONDITION
FIGURE 2.56

Fuel feed (cc/min @ 298K & 1 atm)	= 500
Air feed (cc/min @ 298K & 1 atm)	= 600
Fuel mole fraction @ inlet	= 0.15 (diluent N_2)
External load (ohms)	= 2.5
Concentrated contact losses(each),(ohms)	=0.1
Parallel channels per battery	= 23
Series batteries per monolith	= 7
Channel length (cm)	= 5
Channel cross section (mm^2)	= 1
Wall thickness	= 250 μm
ZrO_2 thermal conductivity (watt/mK)	= 2.09

TABLE 2.9: Parameters used in figures 2.56 through 2.71

Figure 2.57 shows the steady state outlet fuel temperature as a function of fuel (and air) feed temperature. Points indicated by triangles on the graph correspond to values actually calculated, while the straight line is the reference, isothermal line. It is important to note that, for the conditions specified in table 2.9, ignited steady states corresponding to feed temperatures above 660 K gave rise to numerical problems. These originate from the fact that, at the high temperature-high conversion conditions involved, the driving force (reversible voltage) tends to zero, and, without an otherwise unnecessary futher reduction in the integration step, the conversion drops along the channel, which is meaningless. Also, the introduction of a default value for high conversions was necessary. Therefore, to investigate the behaviour of the cell in this region it is necessary to consider

i. a smaller integration step.

ii. an extended model which also covers operation under mass transfer limited conditions.

The preliminary results so far obtained in this region, however, point towards the inconvenience of operation under such conditions, since the driving force tends to zero, which means that very little additional power output is to be obtained through a further increase in fuel and air inlet temperatures. However, further work is required in this region. Although, as explained above, the actual steady state for a feed temperature of 670 K was not located, the behaviour of the end matching condition shown in figure 2.58 clearly shows

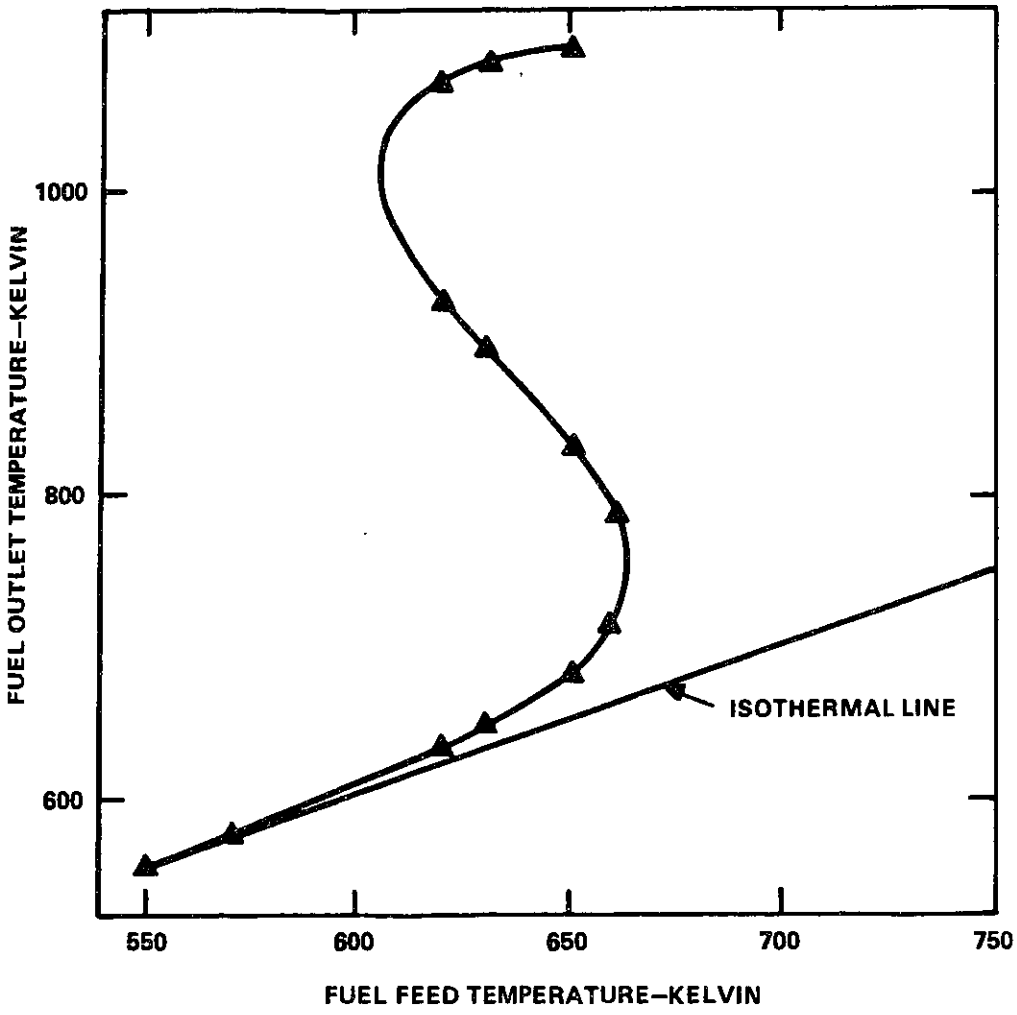

STEADY STATE MULTIPLICITY IN MONOLITH CELL
FIGURE 2.57

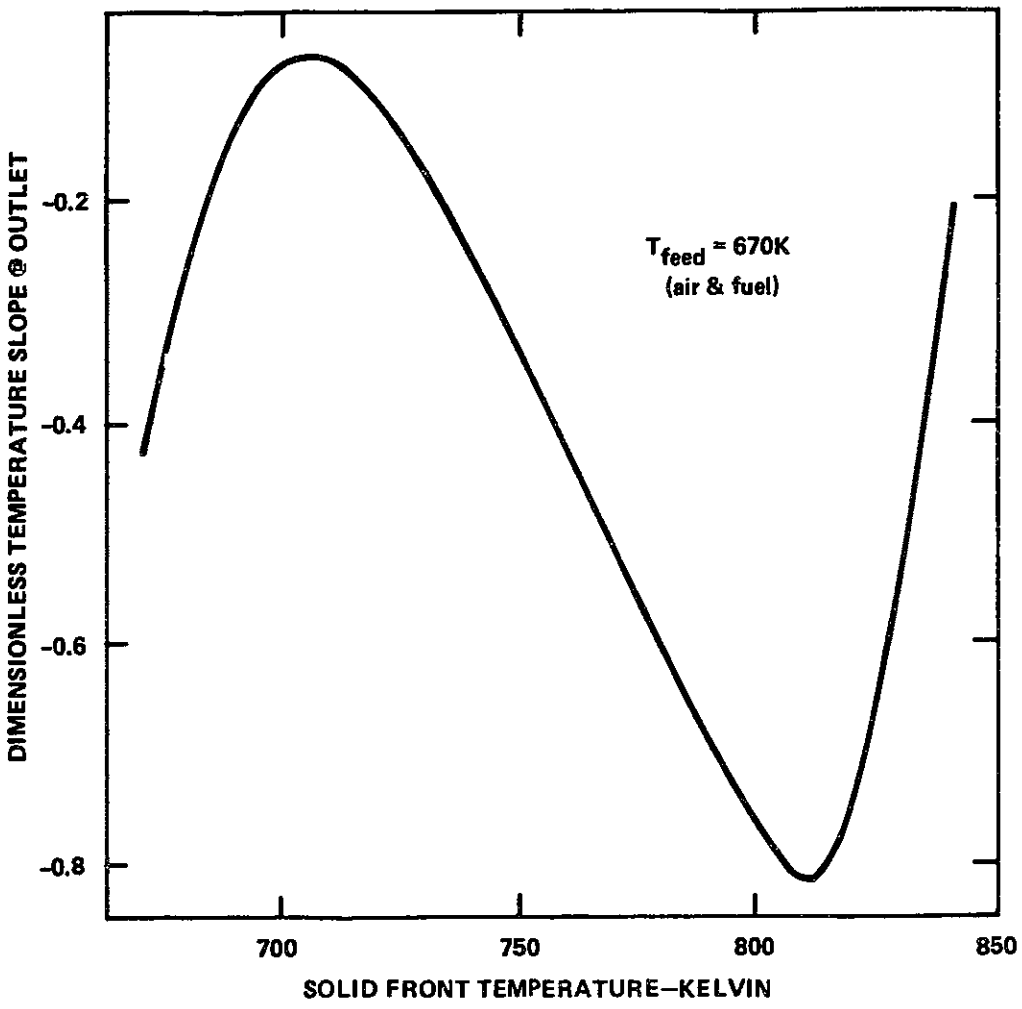

EXISTENCE OF IGNITED STEADY STATE
FIGURE 2.58

that there are no multiple steady states. The curve is interrupted at the upper limit where numerical problems were encountered.

Figure 2.59 shows the outlet conversion vs. inlet temperature curve, while figure 2.60 illustates the corresponding power output curve. The numerical values are summarized in table 2.10.

The results presented so far characterize reactor behaviour by a single point, i.e., outlet parameters. However, it is obvious that this is not a lumped parameter system, and each steady state is characterized by a profile rather than a point. The unignited, intermediate and ignited conversion, current and temperature profiles associated with feed temperatures of 630 K and 650 K (see table 2.10) are shown in figures 2.61 to 2.68. The steep rise in gas temperature at reactor inlet tends to mask the zero slope intial condition specified for solid temperature. This can be easily explained upon writing a differential energy balance for the solid at reactor inlet; it can then be seen that heat condution along the solid (which requires a temperature gradient) provides the energy required by the interaction with the gas (part of the heat comes also from reaction, but this is very limited at reactor inlet due to the low temperatures and correspondingly high resistances involved). Furthermore, the plots show one out of every five points actually calculated. A modified version of the program with every calculated point plotted clearly showed the zero intial slope.

Finally, figure 2.69 shows the current associated with each integration step versus length, or, in other words, the differential current increase versus length for the ignited state

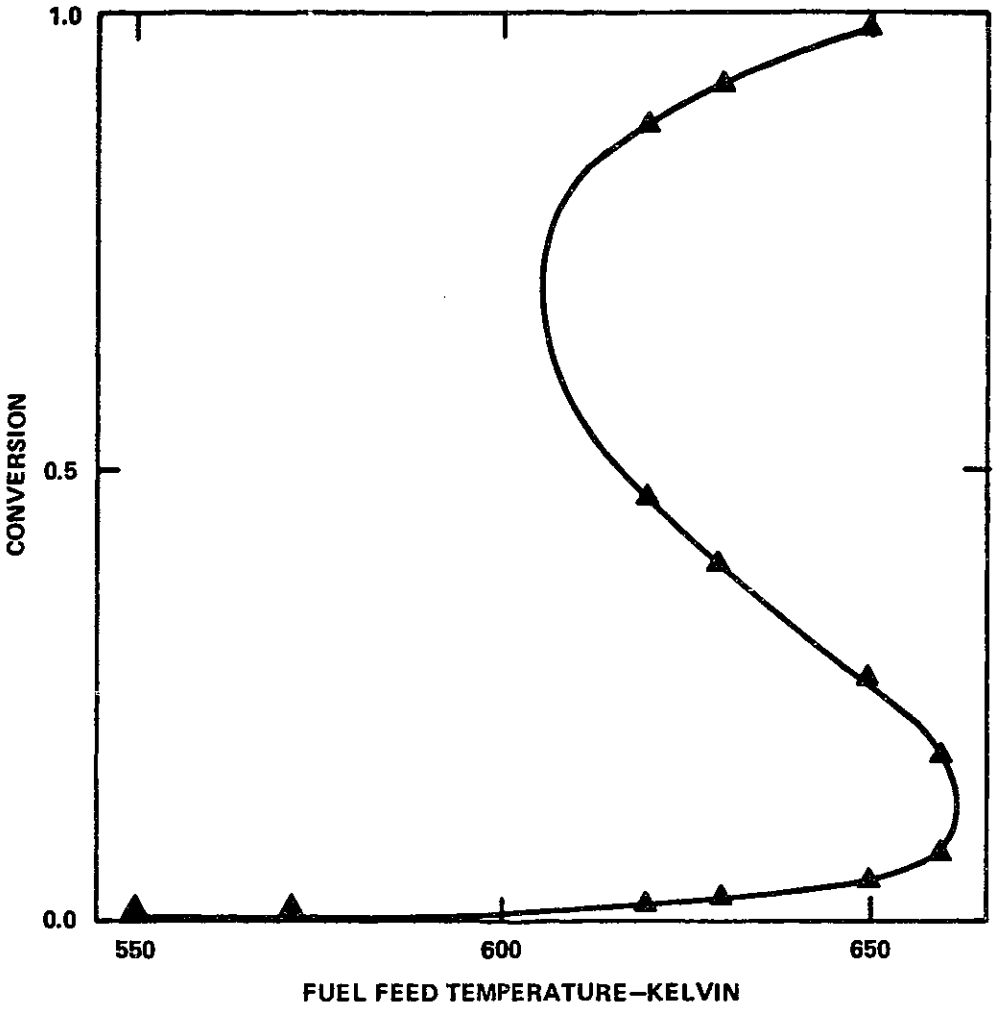

STEADY STATE MULTIPLICITY IN MONOLITH CELL
FIGURE 2.59

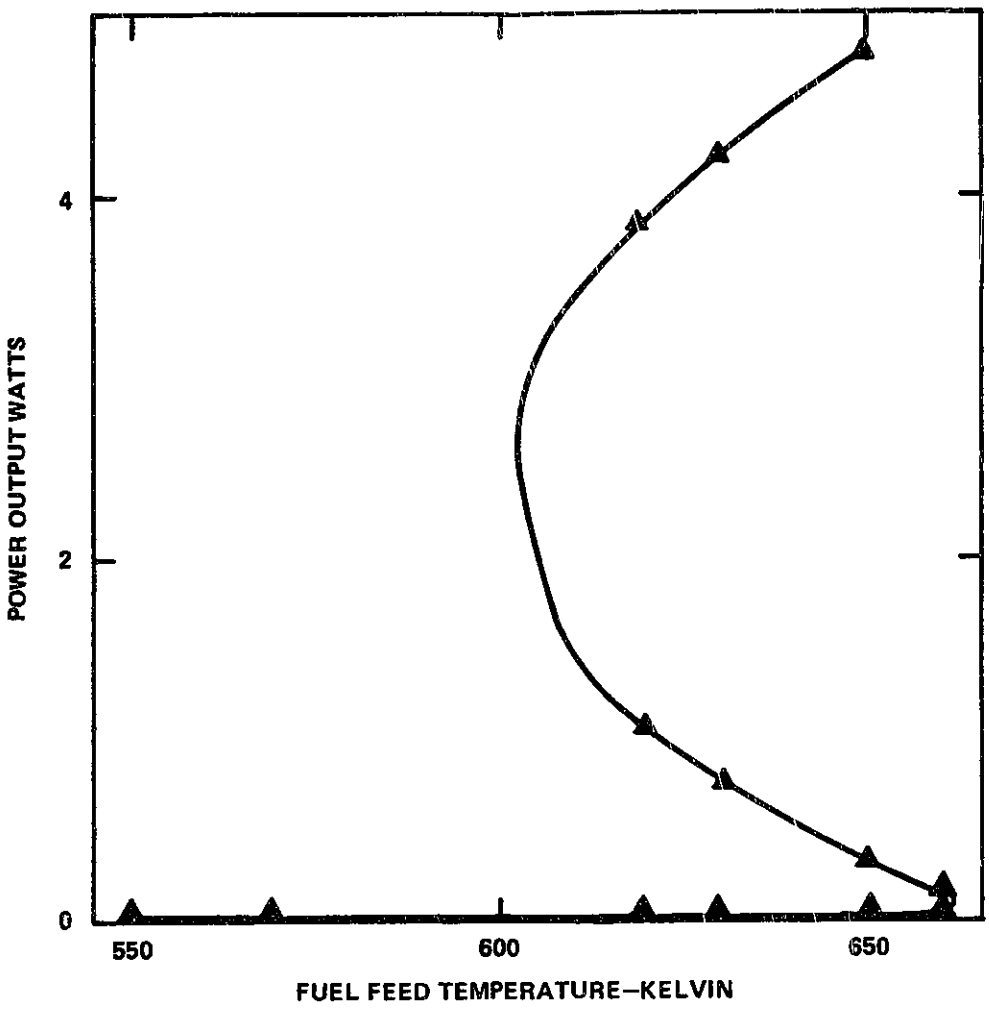

STEADY STATE MULTIPLICITY IN MONOLITH CELL
FIGURE 2.60

Air & fuel feed temp. (K)	Solid front temperature (K)	Fuel outlet temperature (K)	Conversion (-)	Power output (watts)
550	550.75	551.6	0.001955	1.898×10^{-5}
570	571.37	572.6	0.003669	6.685×10^{-5}
620	626	631.9	0.0165	1.353×10^{-3}
620	691.8	927.6	0.465	1.076
620	722.7	1070	0.8804	3.953
630	638.1	646.3	0.02253	2.522×10^{-3}
630	698	896.7	0.3937	0.7714
630	740	1080	0.9213	4.219
650	665	682	0.04514	0.01012
650	708.2	831.5	0.2611	0.3385
650	779	1093	0.9845	4.815
660	684.3	713.3	0.07482	0.02782
660	707.5	787.1	0.1805	0.162

Table 2.10: Steady states for Figures 2.57, 2.59, 2.60

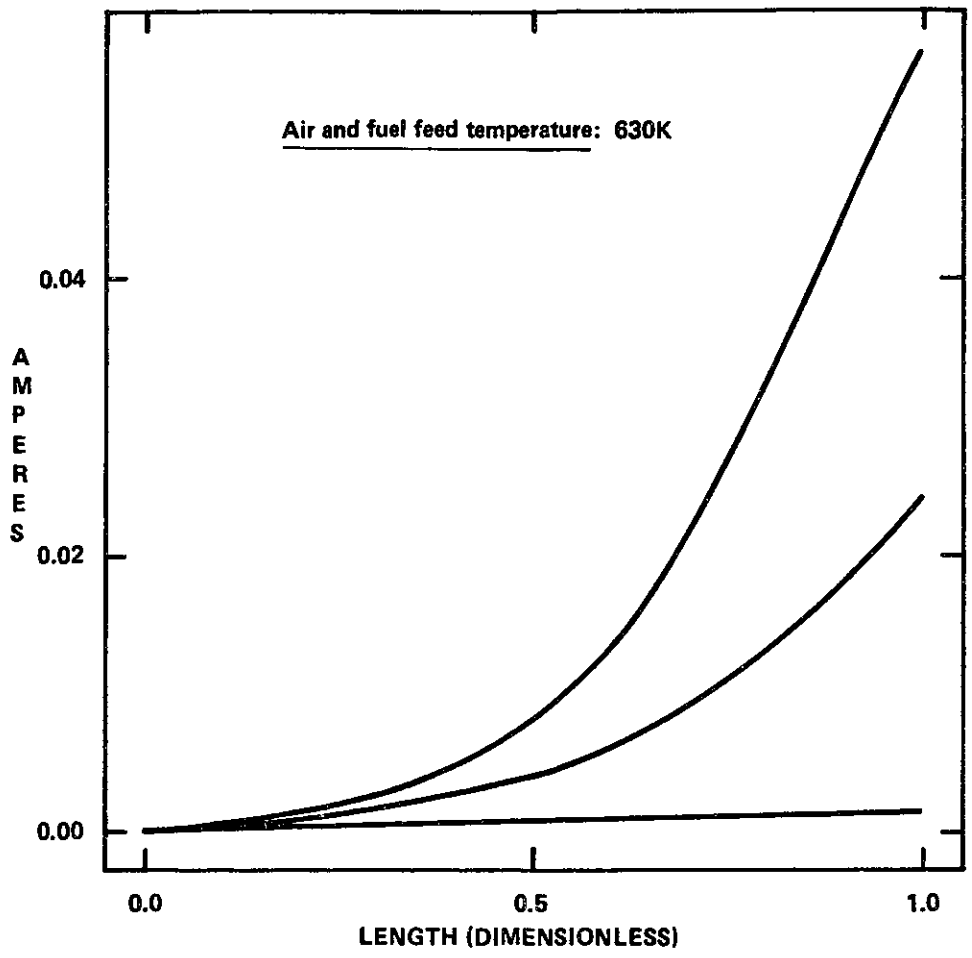

ACCUMULATED CURRENT PROFILES ALONG A MONOLITH CHANNEL
FIGURE 2.61

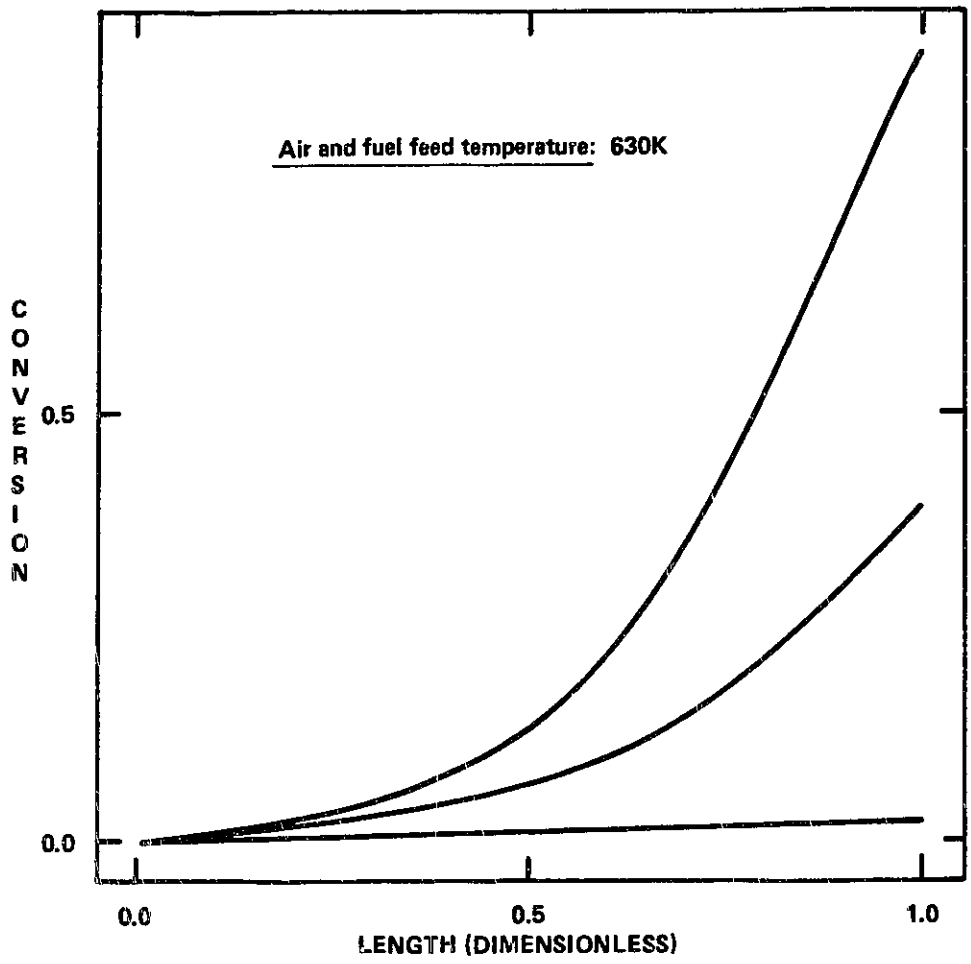

CONVERSION PROFILES ALONG A MONOLITH CHANNEL
FIGURE 2.62

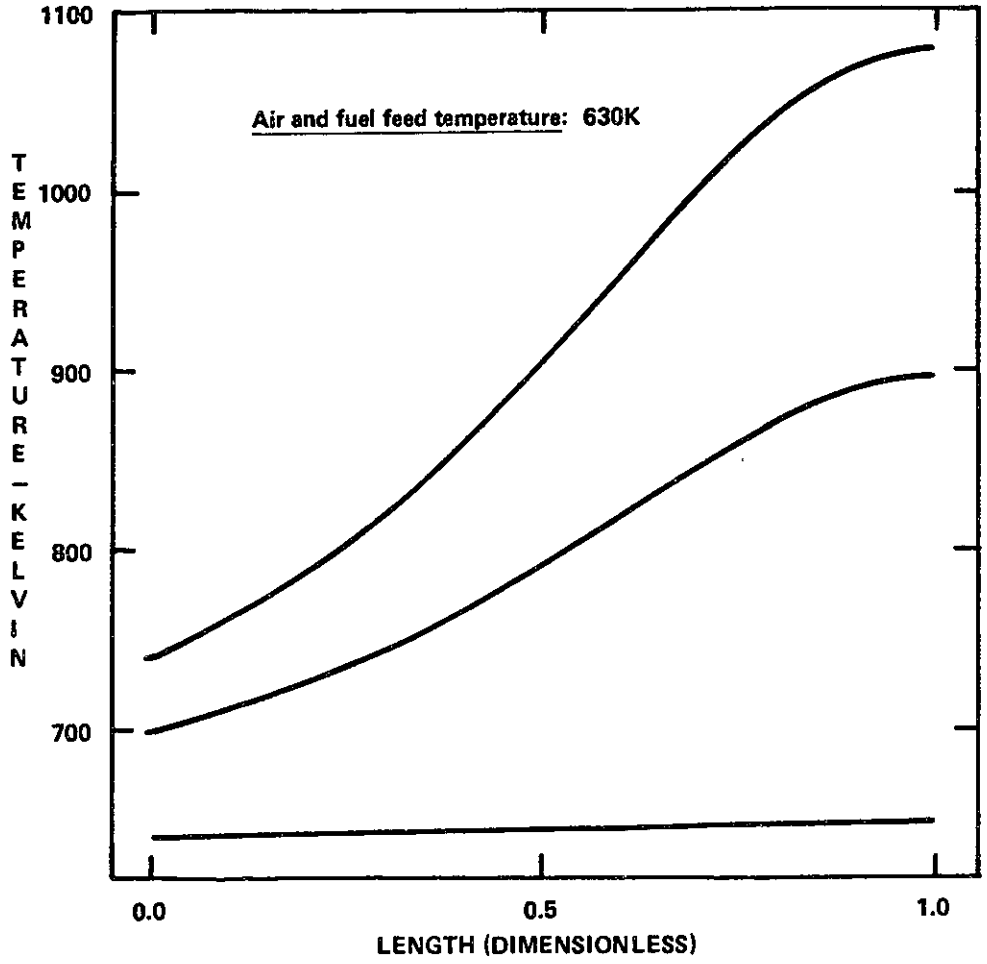

SOLID TEMPERATURE PROFILES
FIGURE 2.63

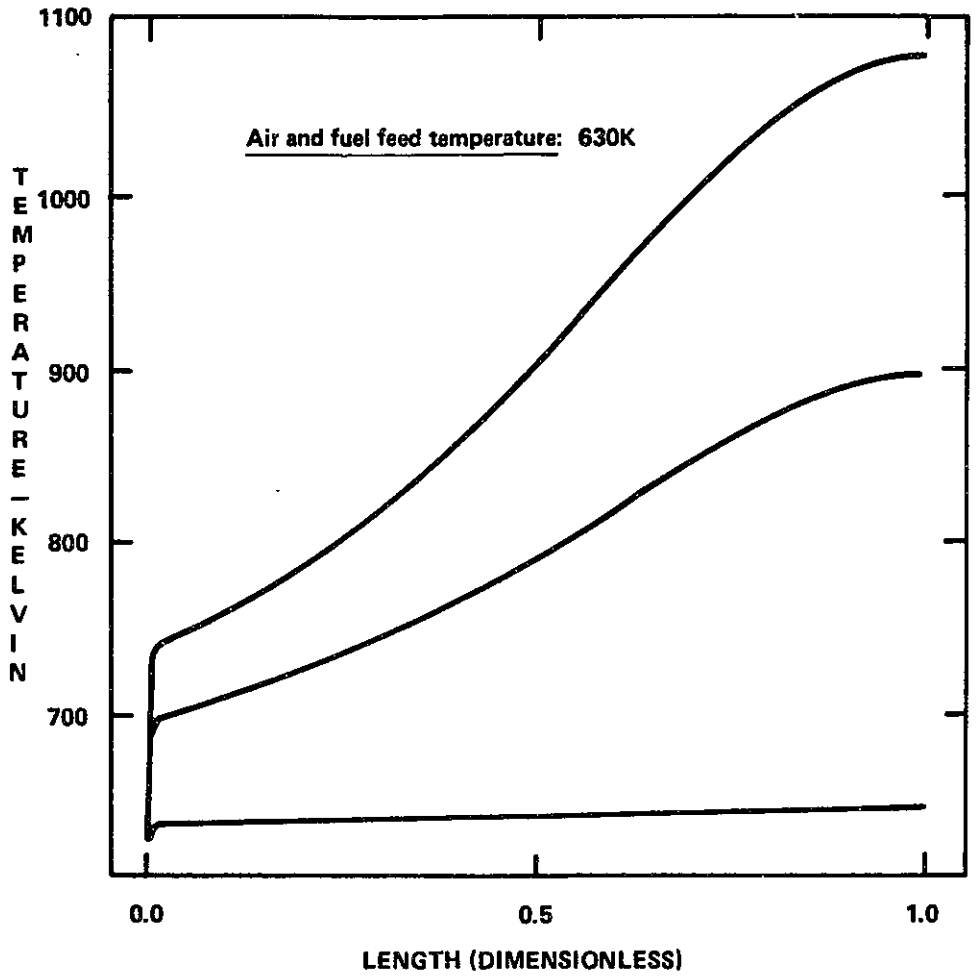

GAS TEMPERATURE PROFILES
FIGURE 2.64

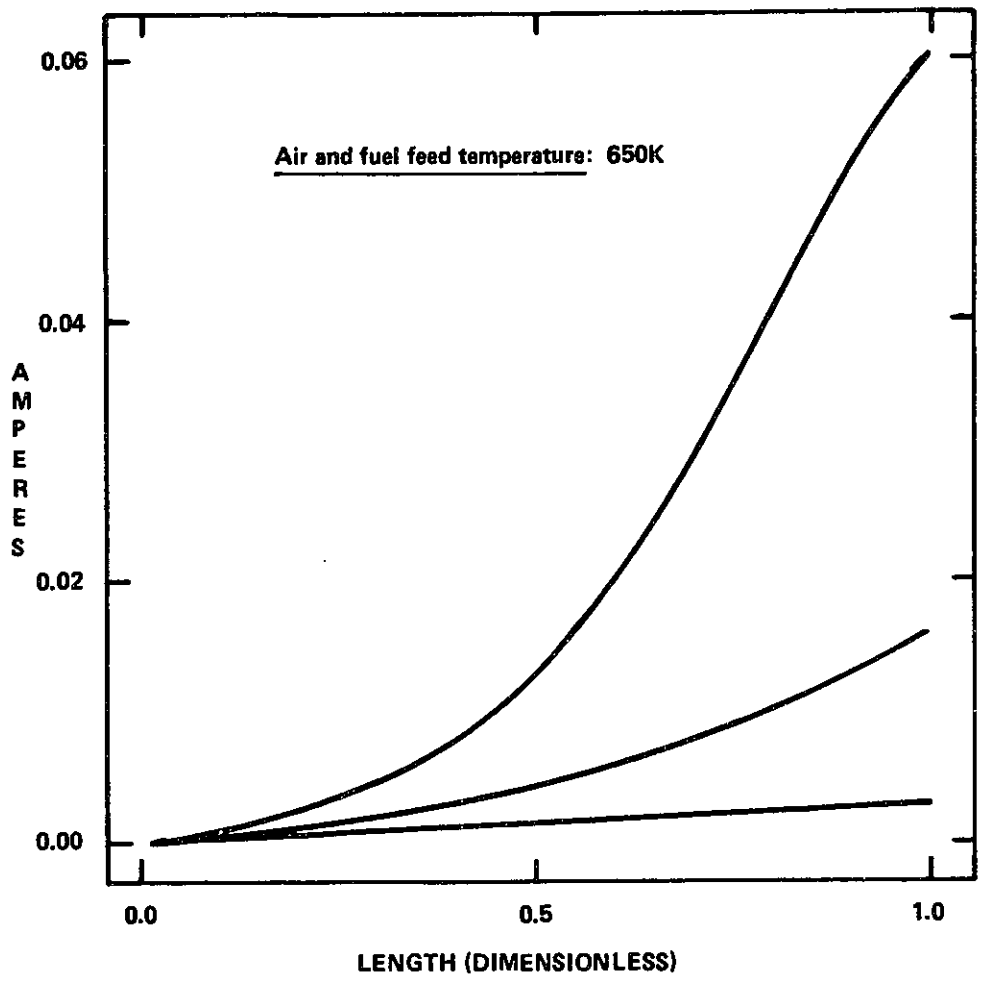

ACCUMULATED CURRENT PROFILES ALONG A MONOLITH CHANNEL
FIGURE 2.65

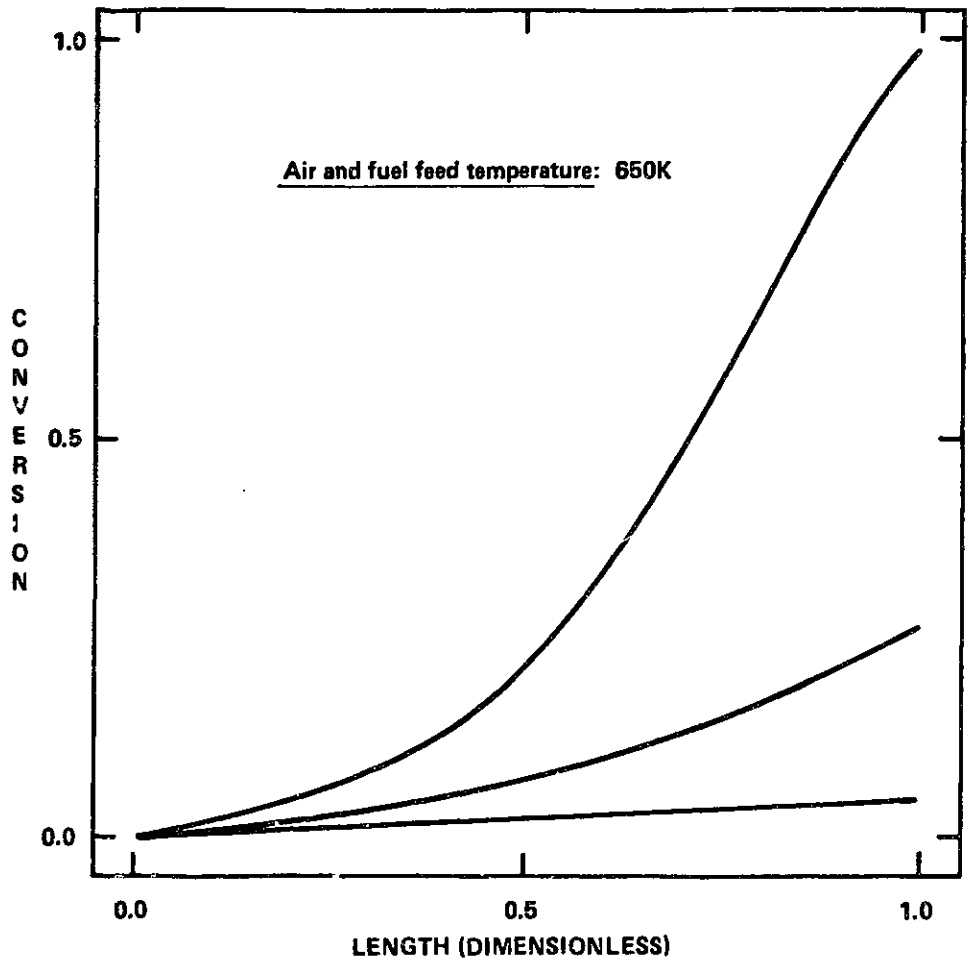

CONVERSION PROFILES ALONG A MONOLITH CHANNEL
FIGURE 2.66

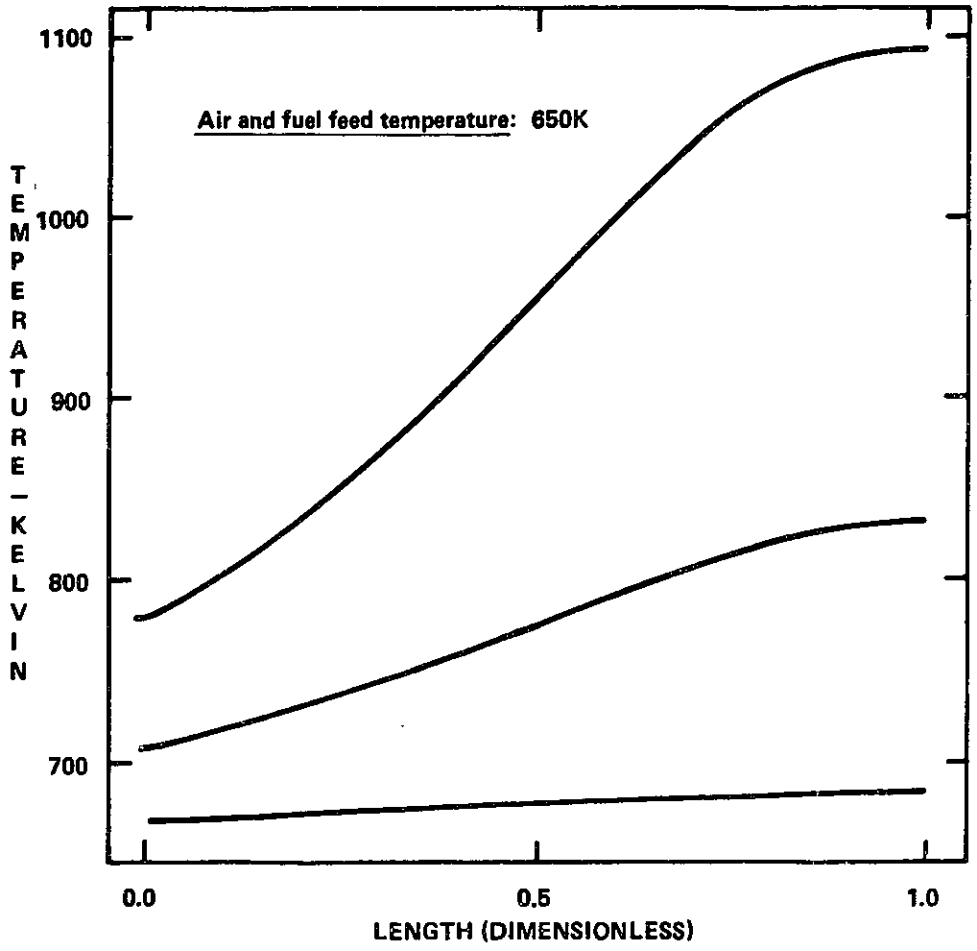

SOLID TEMPERATURE PROFILES
FIGURE 2.67

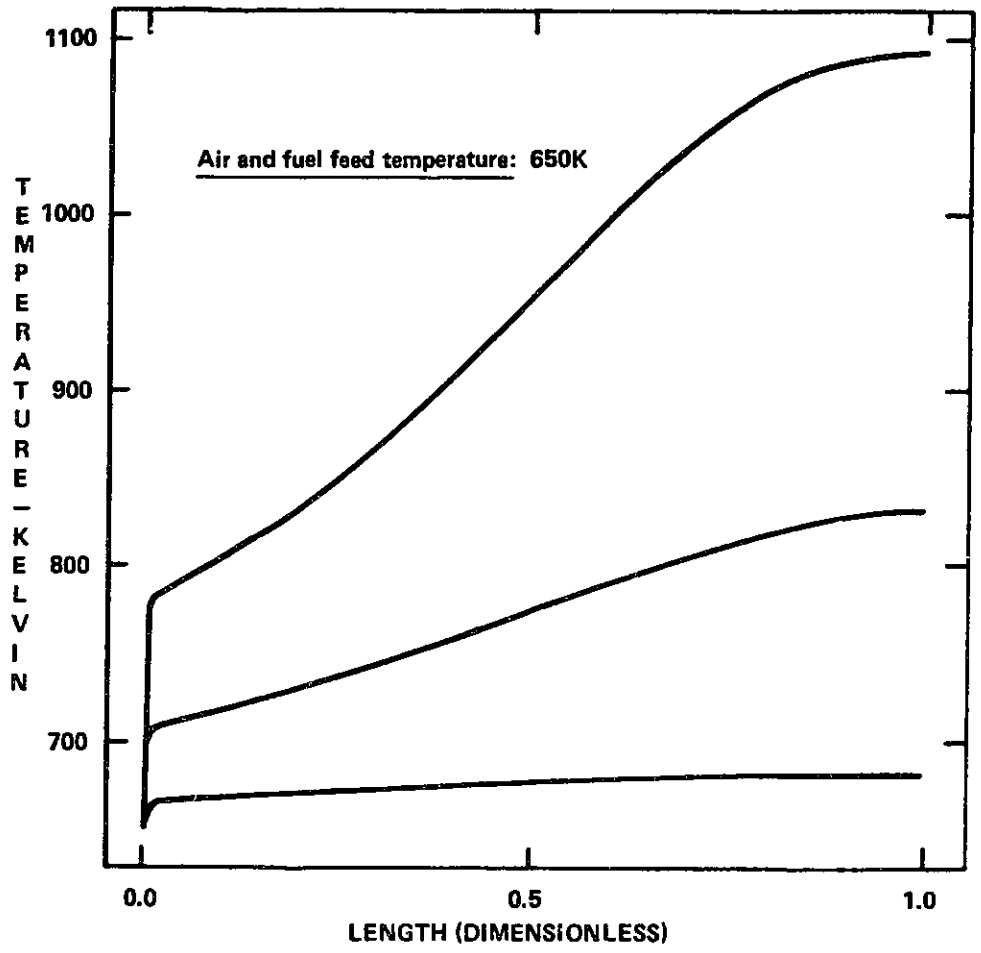

GAS TEMPERATURE PROFILES
FIGURE 2.68

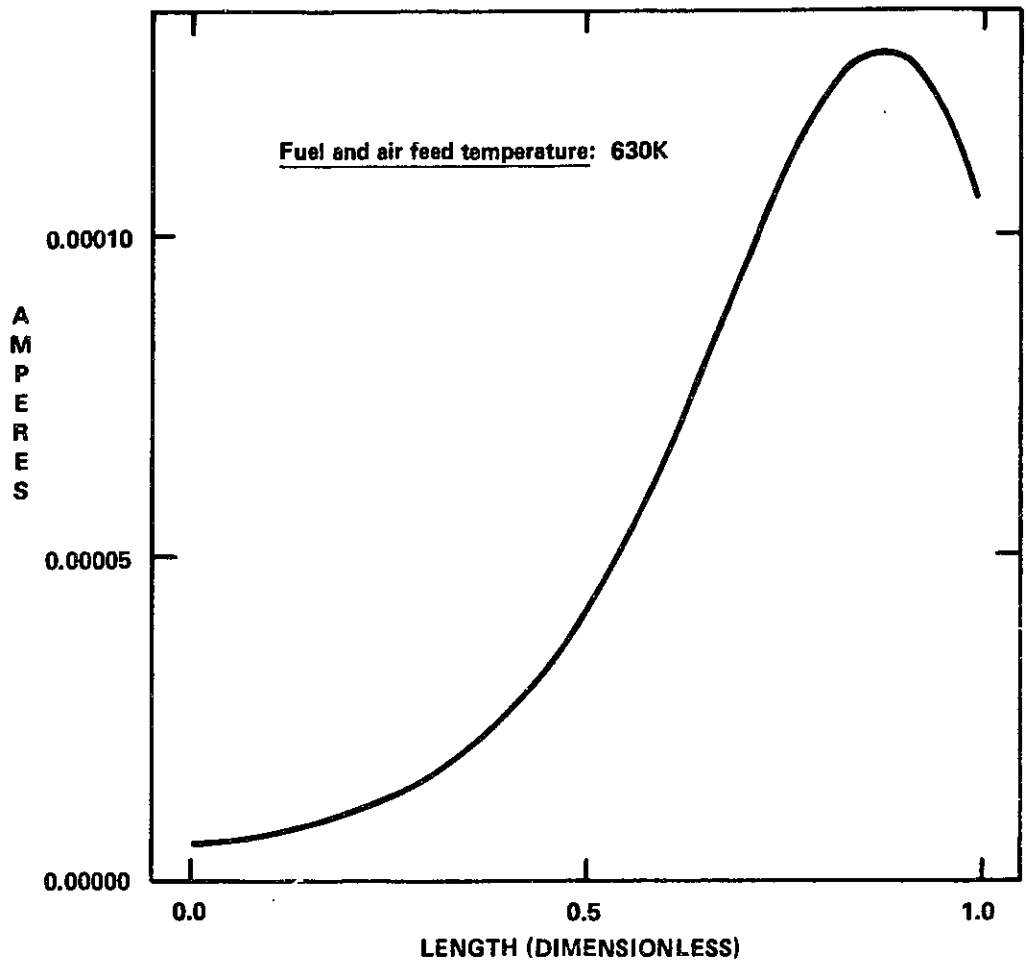

CURRENT DISTRIBUTION ALONG MONOLITH CHANNEL (IGNITED STATE)
FIGURE 2.69

corresponding to a feed temperature of 630 K. Figure 2.70 (i.e., the upper curve in figure 2.61) is simply the integral of figure 2.69. Figure 2.71 shows the reversible voltage along a channel for the same ignited state. The actual voltage was 0.61 V. As explained in section 2.2.4, this voltage should be constant. However, since the current distribution loop is closed to within a certain error (see section 2.2.5.5) the constancy of actual voltage is also subject to minor variations. In the present case, the percentage error between maximum and minimum voltage along the channel was 0.49%. Note the opposing trends of current and reversible voltage. These can be easily interpreted by means of equation (2.2.28); in fact the exponential temperature dependence of R_i far outweighs the decreasing reversible voltage, the current variation along the channel following the variations in reversible voltage only at high temperatures, when the electrolyte reistance becomes unimportant.

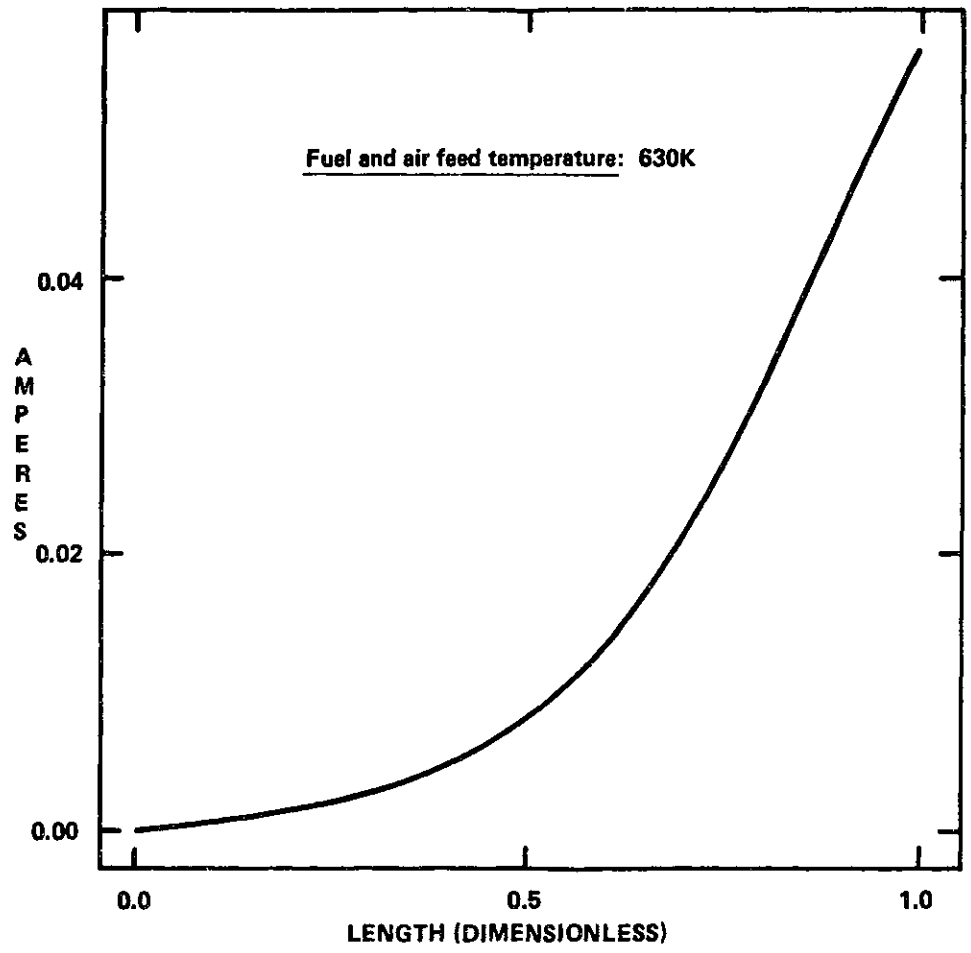

ACCUMULATED CURRENT ALONG MONOLITH CHANNEL (IGNITED STATE)
FIGURE 2.70

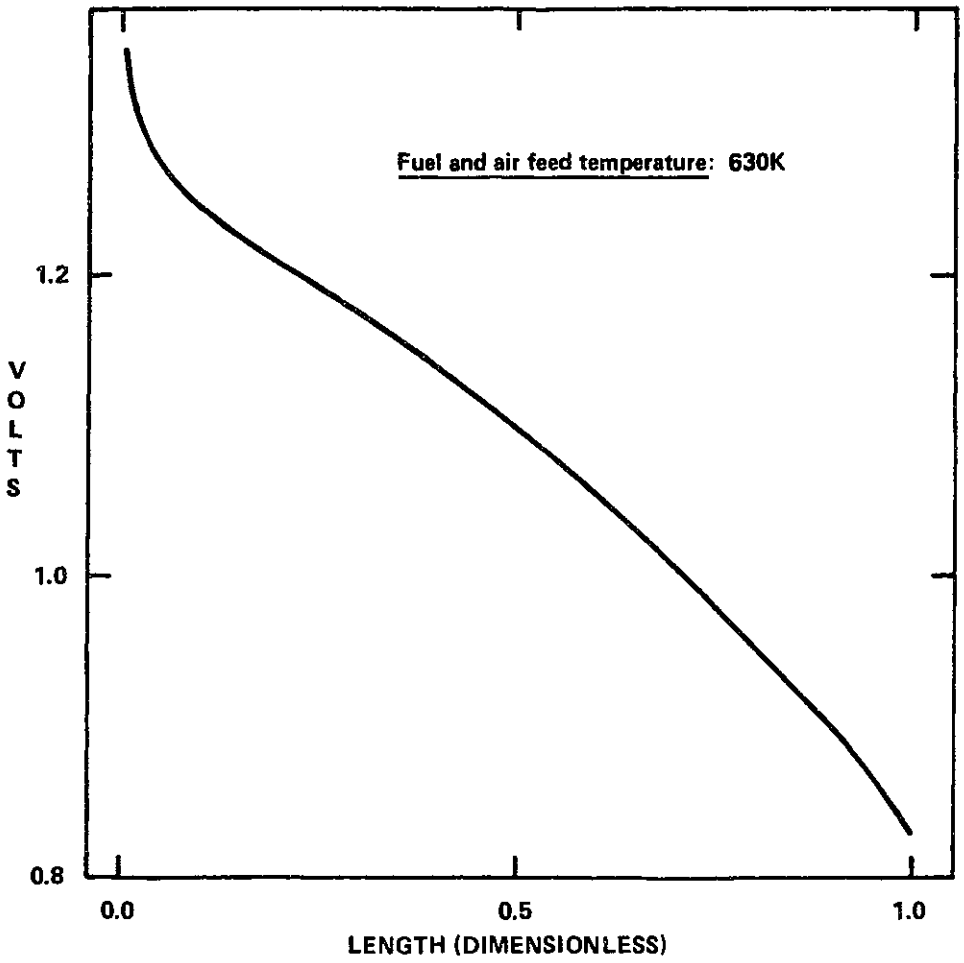

REVERSIBLE VOLTAGE VS LENGTH (IGNITED STATE)
FIGURE 2.71

3. CONCLUSIONS

3.1. CSTR model

- Application of standard thermodynamic and reactor engineering analysis to high temperature fuel cells has led to the formulation of the governing material and energy steady state equations for such type of reactors.
- The governing dimensionless groups have been derived, and the consequent scale-up criteria have been presented. The practical limits for equipment scale-up have been identified through the use of the governing dimensionless groups.
- Within the limits largely imposed by the "bottleneck" factor in cell scale-up (electrode resistance), a 1 watt, 10 cm^2 module can realistically be designed as a component in a stacked arrangement. Suggestions for the actual design of such a unit are given in this work (see Appendix III).
- As the detailed discussions in Appendix III show, the 10 cm^2 module's design (though not to the extent that characterized the 2 cm^2 module's design) is largely determined by the insulation requirements. Possible alternatives for the design of such a prototype could be either a close-stacked, internally fed insulated modular stack, or a tube-bundle arrangement (figure III-2).
- The fundamental importance of electrode and contact resistances in limiting the possiblity of increasing the fuel processing capacity per cell has been shown; for parallel feed the resulting manifolding complexity is the major limiting factor.
- For the process parameters, and geometries analyzed, the conditions whereby H_2 fuel cells can operate at 97%+ conversion,

with simultaneous maximization of current density and power output to $\sim$ 0.2 Amps/cm^2 and $\sim$0.1 watts/cm^2, respectively, in a self ignited way, have been identified through the use of the governing material and energy balances.

- The above conclusions would also apply to a CO cell with a sutiable electrocatalyst that would reduce or elminate activation overpotential (addition of < 3% H_2 in the CO feed would have the same effect).
- A gas feed arrangement which leads to virtual elmination of concentration overpotential has been presented, and a design method of sufficient generality has been outlined.
- The opposing trends of efficiency and power output, power output and autothermal operation, efficiency and conversion, have been thoroughly analyzed, and the fundamental importance of the entropy change associated with the reaction under consideration in determining the performance of the fuel cell has been explained.
- Steady state multiplicity for high temperature cells has been demonstrated.

3.2 Cross-flow monolith cell

- The feasibility of employing a monolith reactor as a fuel cell has been shown. This represents a new concept of great potentiality for practical applications.
- As with the CSTR cell, results pertaining to CO as a fuel are to be interpreted as a limiting behaviour with a suitable catalyst.
- Parametric analysis has not yet been performed, so that the power output figures presented are not necessarily optimum. For a monlith reactor with the dimensions and electrical

arrangement considered, a 5 watt power output and 98% conversion can be expected.

- Within the simplifications implied by the model, a very interesting behaviour has been found whereby a tubular reactor shows steady state multiplicity. The influence of feed temperature on multiplicity has been explored and results have been presented.
- Compared with the CSTR fuel cell, this reactor presents the potential advantage of a greater power per unit volume and simplicity.
- The influence of heat losses has not been investigated, a perfect insulation has been assumed.

4. SUGGESTIONS FOR FUTURE WORK

4.1 CSTR model

In the experimental area, major goals of research should be:

- testing of a suitable electrolyte arrangement such that structural strength and low ohmic losses can be simultaneously achieved. A metallic frame serving both as a current collector and as a structural unit would allow the successful operation of a cell such as the one shown in figure 1.6b.
- reduction of contact and electrode losses
- finding a suitable electrocatalyst for CO or hydrocarbon systems.
- construction and testing of a modular stack with unitary dimensions as per section 3.1 (10 cm^2 per module).

From a theoretical point of view, attention should focus on the application of the equations derived in the present work to design purposes. The feasibility of operating medium-to-large scale units should be investigated. The consequences of all of the main trends and relationships which have been shown to characterize fuel cell behaviour should be integrated into a design project. Only then can the overall possibilities of high temperature fuel cells be evaluated realistically. Of fundamental importance within this project would be the consideration of the optimum fluid flow arrangement. It might be necessary to develop new models if process conditions deviate from the assumed fluid flow. The limited fuel processing capacity per cell suggests the convenience of studying the plug flow reactor.

Also, the material and energy balances should be extended

to consider activation overpotential, not as a design-oriented project, but, rather, to assess the relative importance of this source of inefficiency.

Other stoichiometries and reacting systems should be investigated (modeling in currently being done at MIT on SO_2 fuel cells). As can be seen from the equations and results presented, attention in the present work has focused on steady state behaviour; the complete picture of cell behaviour can only be grasped if transient behaviour and stability are analyzed. Some work in this field has already been done, and computer simulations have been performed, but a systematic approach is needed.

Possible alternatives for successful autothermal operation should be investigated, two approaches that should be explored are:

- introduction of small amounts of O_2 with the fuel stream.
- operation under low-flow, concentrated fuel, conditions (this is merely an extension of the present work to other process conditions).

4.2 Cross-flow monolith fuel cell

The cell is currently being tested, so that any suggestions for future experimental work must await the results.

From the mathematical modeling point of view, though, much can be done:

- the development of a two-dimensional model, taking into account X-nonuniformity is both a useful and challenging problem.
- within the present one-dimensional model, the following tasks can be listed, in order of increasing complexity:

i. extensive use should be made of the present model, in order to thoroughly explore the influence of the main process and geometric parameters, as was done with the CSTR model.

ii. introduce new boundary conditions and temperature-dependent solid thermal conductivity.

iii. take into account the discontinuous nature of the phenomena involved as the fuel flows along a channel. This would require a periodic switching of the governing differential equations along the reactor's length.

APPENDIX I

Mass transfer limitations in CSTR cell

Let A generically denote the fuel. Then, for a mass transfer limited process, the rate of fuel transport to the electrode surface is (assuming external diffusion limitations)

$$\dot{N}_A = k'g\ S[A]_b \qquad (I\text{-}1)$$

where S is the electrode surface, k'g is a mass transfer coefficient, and $[A]_b$ refers to bulk gas-phase conditions. Referring to figure 1.6, the relevant problem can be modelled as stagnation flow, which, neglecting end effects, can, for the present analysis, be regarded as occuring on a semi-infinite plate. Analytical solutions for the corresponding heat transfer problem exist, and, therefore, k'g can be estimated through the heat transfer-mass transfer analogy. For Prandtl numbers not far removed from unity, the Nusselt number can be expressed as (28)

$$Nu = 0.57\ Re_{\ell'}^{1/2}\ Pr^{0.4} \qquad (I\text{-}2)$$

where

$$Re_{\ell'} = \frac{(C'\ell')\ell'}{\nu} \qquad (I\text{-}3)$$

Therefore,

$$h = 0.57\ Pr^{0.4}\ k\ \sqrt{C'/\nu} \qquad (I\text{-}4)$$

Where k is the gas mean thermal conductivity. C' (29) is the ratio of gas velocity at feed tube outlet to feed tube-electrode distance. Making use of the heat-mass transfer analogy, we can rewrite equation (I.4) as follows

$$k'g = 0.57\ (Sc)^{0.4}\ D\ \sqrt{C'/\nu} \qquad (I\text{-}5)$$

where D is now the molecular diffusivity of the fuel in the

TABLE I-1: Physical properties for equation I-5

	H_2 fuel cell	CO fuel cell
Sc(-)	0.205	0.740
D (cm^2/s)	6.76	1.870
ν (cm^2/s)	1.39	1.39

diluent gas (N_2 in the present case). For a typical 1100 K temperature, we have the physical properties (density and viscosity are those of N_2) illustrated in Table I-1; therefore,

$$k'g]_{CO} = 0.801 \sqrt{C'} \qquad \text{(I-6)}$$

$$k'g]_{H_2} = 1.734 \sqrt{C'} \qquad \text{(I-7)}$$

where k'g is in cm/s, and C' in sec^{-1}.

The flow rate being fixed by process conditions, the designer has two variables that can be manipulated in order to enhance the rate of mass transfer to the electrode surface, namely, feed tube-to electrode distance, and, if necessary, feed tube restriction orifice diameter. Letting F denote feed rate in cc/min, at 298K and 1 atmosphere, D' the fuel feed tube's restriction orifice, in mm, and t' the distance in mm, between feed tube tip and electrode surface, for a 1100K temperature,

$$C' = \left(\frac{1100F}{60x298}\right) \cdot \frac{4 \times 10^2}{\pi (D')^2} \cdot \frac{10}{t'} = \frac{78.33F}{(D')^2 t'} \qquad \text{(I-8)}$$

Therefore,

$$k'g]_{CO} = 7.089 \sqrt{F} \left(\frac{1}{D' \sqrt{t'}} \right) \qquad \text{(I-9)}$$

$$k'g]_{H_2} = 15.347 \sqrt{F} \left(\frac{1}{D' \sqrt{t'}} \right) \qquad \text{(I-10)}$$

For a fuel feed mole fraction y_i, conversion x and 1100K, we have, for atmospheric pressure,

$$[A]_b = 1.108 \times 10^{-5} y_i (1-x) \qquad \text{(I-11)}$$

Therefore,

$$\left.\frac{\dot{N}_A}{S}\right]_{CO} = 7.855 \times 10^{-5}\, y_i(1-x)\, \sqrt{F}\, \left(\frac{1}{D'\sqrt{t'}}\right) \qquad \text{(I-12)}$$

$$\left.\frac{\dot{N}_A}{S}\right]_{H_2} = 1.7 \times 10^{-4}\, y_i(1-x)\, \sqrt{F}\, \left(\frac{1}{D'\sqrt{t'}}\right) \qquad \text{(I-13)}$$

As can be seen from the examples presented throughout this work, the maximum current acheivable for the range of variables considered is roughly 0.2 Amperes/cm^2. To calculate the actual rate for an ohmic controlled process, we can use the concept implied in equation (2.1.3) and write

$$\frac{\dot{N}_A}{S} = 6.812 \times 10^{-7}\, \frac{F\, yi\, x}{S}\ \text{g mol/s cm}^2 \qquad \text{(I-14)}$$

It is evident, from equations (I.12) and (I.13), that a good design for a CO cell would guarantee good operation for a H_2 cell, due to the latter's almost fourfold higher diffusivity. For a 25 cc/min (@ 298 K and 1 atm) feed, and y_i = 0.15, a 0.8 mm restriction orifice and a 0.8 mm separation between feed tube and electrode, dividing equation (I-12) by (I-14) at various levels of conversion provides the ratio of mass transfer to anionic conduction for the sepcificed parameters, which should be always greater than unity. These results are shown in Table I-2, where β is the ratio of mass transfer-controlled rate to current flow limited rate, with S = 2 cm^2.

The parameters used in calculating Table I-2 are listed in Table I-3.

TABLE I-2: Ratio of mass transfer-limited rate to ohmic-controlled rate

x	βH_2	$\phi_{conc,anode}$ (mV)	βCO	$\phi_{conc,anode}$ (mV)
0.90	15.5	3.2	7.16	7.1
0.92	12.13	4.1	5.61	9.3
0.94	8.90	5.6	4.11	13.2
0.98	2.84	20.6	1.32	67.2
0.99	1.41	58.5	0.65	-

TABLE I-3: Parameters used in Table I-2

y_i	inlet fuel mole fraction	0.15
D'	feed tube restriction orifice diameter	0.8 mm
t'	feed tube-electrode distance	0.8 mm
F	feed rate (@298 K and 1 atm)	25 cc/min
T	cell temperature	1100K

The fuel velocity across the orifice is 3 m/s, and the mass transfer coefficients

$$k'_{g_{CO}} \sim 50 \quad cm/s$$

$$k'_{g_{H_2}} \sim 107 \quad cm/s$$

Finally, in order to guarantee mass transfer-free operation, the bulk-to-electrode transport rate must be related to reactant transport within the porous electrode. Assuming, therefore, that reaction takes place at the so called "triple points"(i.e., three-phase boundary points where electrode, electrolyte and gas are in contact), the fuel molecules must not only diffuse from the bulk gas phase to the external electrode surface, but must, in addition, diffuse along the catalyst pores to the electrolyte surface. For the electrodes under consideration, the following quantities apply:

porosity (conservative estimate) $\sim$ 10%

pore diameter $\sim$ 1 μm

film thickness $\sim$ 3 μm

Under these conditions, and for a typical temperature of 1100K, the controlling mechanism for diffusion is molecular (as opposed to Knudsen) diffusion, as can be seen by substitution in the defining equation for Knudsen diffusivity

$$D_K = 9.7 \times 10^3 \, r\left(\frac{T}{M}\right)^{0.5} \qquad (I.15)$$

where r is the pore diameter (cm), M, the fuel's molecular weight, and D_K is in cm^2/s.

The effective diffusivity for fuel transport in the electrocatalyst's pores is therefore the molecular diffusivity (see table I.1) multiplied by the geometric factor characterizing the porous electrode,

$$D_{eff} = \frac{D\varepsilon}{\delta} \qquad (I.16)$$

where ε is the electrode's porosity, and δ the tortuosity factor, which accounts for deviations between an idealized straight, cylindrical pore, and the electrode's actual pores. For a conservative 10% porosity, and a tortuosity factor of 2, we obtain, from table I.1,

$$D_{eff,\ H_2} = 0.34\ cm^2/S$$
$$D_{eff,CO} = 0.09\ cm^2/S$$

Therefore, in order to compare bulk-to-electrode diffusion with diffusion along the pores, we calculate the following ratio

$$\frac{\text{Bulk-to-electrode transport}}{\text{Diffusion within pores}} = \frac{k'g}{D_{eff}/b} \qquad (I.17)$$

where b is the electrode film thickness. Substituting the calculated values for the mass transfer coefficients, we obtain

$$\left[\frac{k'g}{D_{eff}/b}\right]_{H_2} = 0.044$$

$$\left[\frac{kg}{D_{eff}/b}\right]_{CO} = 0.167$$

It can thus be seen that the relatively large pore size, coupled with the extremely thin electrode thickness lead to a situation

where bulk-to-electrode mass diffusion, as opposed to diffusion along electrode pores, is the controlling factor to be considered in designing a cell which is essentially free of concentration overpotential (for the above specified electrode configuration; this is not, obviously, a general statement, and each case should be analyzed individually).

From Table I-2 and the above discussion, assigning a cathodic concentration overpotential equal to the anodic one (which, it can be shown, is conservative with the air feeds considered here), for a 1100 K temperature, 0.5 ohm electrode resistance, 200 μm electrolyte and 2 cm^2 electrode projected area, concentration losses are less than 10% of the combined losses for conversions up to 98% (H_2) and 96.5% (CO).

Entirely similar calculations apply to the cathodic side of the fuel cell, where the problem is less critical in view of the excess air considered in most cases.

APPENDIX II

Activation overpotential

As shown in equation (1.8), all sources of overpotential whereby the fuel cell's output voltage departs from the open circuit value represent sources of thermodynamic inefficiency, and research and design efforts should be directed towards their reduction. In Appendix I one such design was presented, leading to the virtual elimination of concentration overpotential. The model presented in the present work, however, also treats the cell as an ideal, non-polarizable device, in connection with activation overpotential. The validity of such an assumption will be briefly discussed here.

Activation overpotential, arising from the fact that electrodic processes take place at a finite rate, with the resulting situation of an electrodic surface that is not, as required by Nernst's equation, in equilibrium can be expressed, in the region of high overpotentials (4), as

$$\phi_{act} = \frac{RT}{\alpha n \mathcal{F}} \ln \left(\frac{i}{i_o}\right) \qquad \text{(II.1)}$$

where α is an empirically determined quantity, usually assumed to be 0.5, i is the current density, and i_o, the exchange current density, or, in other words, the equal and opposite rates at which the elementary process under consideration and its reverse take place under equilibrium conditions. It therefore follows that i_o is a kinetic (as opposed to thermodynamic) quantity; it can, in fact, be regarded as a rate constant for the reaction, and, as such, can be varied through two independent means:

i. selection of the correct electrocatalyst, which leads

to a lowering of the activation energy barrier.

ii. temperature, which exponentially accelerates activated processes.

i being greater than i_o, it is apparent, from equation (II.1) that, in order to minimize activation overpotential, one should select an appropriate combination of electrode and temperature (compatible with the overall process requirements) such that i_o is as high as possible. It follows that, in general, activation overpotential becomes more important the lower the operating temperature of the fuel cell. This represents an important advantage of high temperature fuel cells over their moderate-to-low temperature counterparts.

ZrO_2-based fuel cells operating at 1273 K with Pt electrodes have been built and operated (16) with H_2 as a fuel under what was observed to be an activation overpotential-free regime. This is coherent with the findings of Etsell and Flengas (15), who investigated the overpotential behaviour of stabilized ZrO_2 cells equipped with Pt electrodes and found "almost pure resistance polarization" for H_2-H_2O operation in the 700°C to 1100°C range.

CO-CO_2 cells, on the other hand, are still unsatisfactory from the activation overpotential viewpoint, since the source of thermodynamic inefficiency is still present at high temperatures (15,16). Not surprisingly, therefore, much research in electrocatalysis is directed towards finding appropriate electrodes for CO and hydrocarbons. For a CO-CO_2 cell, it has been reported (16) that addition of small (<5%) quantity of H_2, or, alternatively, 3% H_2O and coating the fuel feed tube with sintered

Cr_2O_3 (which catalyzes the water-gas shift reaction) lead to a substantial drop in activation overpotential.

The present day situation, therefore, is such that, for H_2 as a fuel, activation losses have been eliminated in high temperature fuel cells, and, while this is not the case for CO or hydrocarbons, it is also evident that, in order to fully exploit the inherent thermodynamic advantages of direct electrochemical energy conversion, this goal must be approached, if not completely achieved.

It is with these considerations in mind that the present work was developed. All results pertaining to H_2 cells are therefore coherent with present day technology; the corresponding CO results should be viewed as extrapolations, describing the idealized behaviour of such a system, which can nowadays only be approached, but will have to be achieved if such cells are to be applied commercially.

APPENDIX III

Some trends and ideas on design

The steady-state analysis (see, for example, figure 2.18) for the 2 cm^2 fuel cell indicated a value of 1.2×10^{-4} Kcal/hK for the product of the overall heat transfer coefficient and external surface area in order to achieve self-sustained operation. For a cylindrical tube of radius r_1, and an insulation radius r_2, assuming the insulation to be the controlling heat-transfer resistance (i.e., conservatively assuming the whole ΔT across the insulation), the heat flux per unit length of tube, for an overall driving force ΔT, is

$$\text{Specific heat flux: } \left(\frac{2\pi k}{\ln \frac{r_2}{r_1}}\right) \Delta T \quad \text{(energy/time-length)} \qquad \text{(III-1)}$$

where k is the insulation's thermal conductivity. Using the calculated 1.2×10^{-4} kcal/hK value and SI units, for a length s(mm) associated with an elementary cell within a stacked assembly, the design equation then becomes

$$\ln \frac{r_2}{r_1} = 45.02\ ks \qquad \text{(III-2)}$$

$$r_2 = r_1 \exp (45.02\ ks)\Big]_{2 cm^2 cell} \qquad \text{(III-3)}$$

Before calculating any cell arrangement, it is useful to consider a 10 cm^2 cell (see section 2.1.3.5.3 for scale-up limits). According to the criteria developed in section 2.1.3.5.3, the number of heat transfer units is unchanged upon scale-up, so that the UA product scales as the electrode area. Therefore,

$$r_2 = r_1 \exp (9.004\ k\ s)\Big]_{10\ cm^2 cell} \qquad \text{(III-4)}$$

Comparison of equations (III-3) and (III-4) shows the expo-

nentially increasing difficulty in insulating progressively smaller cells. For a 0.05 W/mK thermal conductivity (intermediate between aerogel and fine diatomaceous powder), and considering internal radii of 0.8 and 1.78 cm for the 2 cm^2 and the 10 cm^2 cells, respectively table III-1 gives the required insulation thickness as a function of the length of each cell.

The extremely close parallel stacking required has important consequences on the feed arrangement of such a fuel cell. In fact, considering either a 1 mm per cell (2 cm^2) or a 2 mm per cell (10 cm^2) design, the feed arrangement suggested in figure 2.23 cannot be realistically realized as shown (i.e., from the outside of the cylindrical stack). A possible design is shown in figure III.1 (the second figure is in exploded view). The orifice in the distribution channel should be designed according to the principles outlined in Appendix I, with additional consideration to fluid distribution. The orifice in the outlet channel sets the slight operating overpressure. Note that, with the extremely low inter-cell distances specified, the design shown in figure 1.6b is the only rational solution. Care should therefore be taken in interpreting the results, if applied to this cell, as figures per cell.

Two fundamental facts must be taken into account in analyzing these geometric characteristics. In the first place, note that the "bottleneck" scale-up factor (see section 2.1.3.5.3) imposes an upper limit on cell size, which is disadvantageous in view of the fact that, as shown above, insulation constraints tend to disappear exponentially as cell size is increased. Thus, for a medium-sized reactor in which contact and electrode losses have been virtually eliminated (which is not impossible

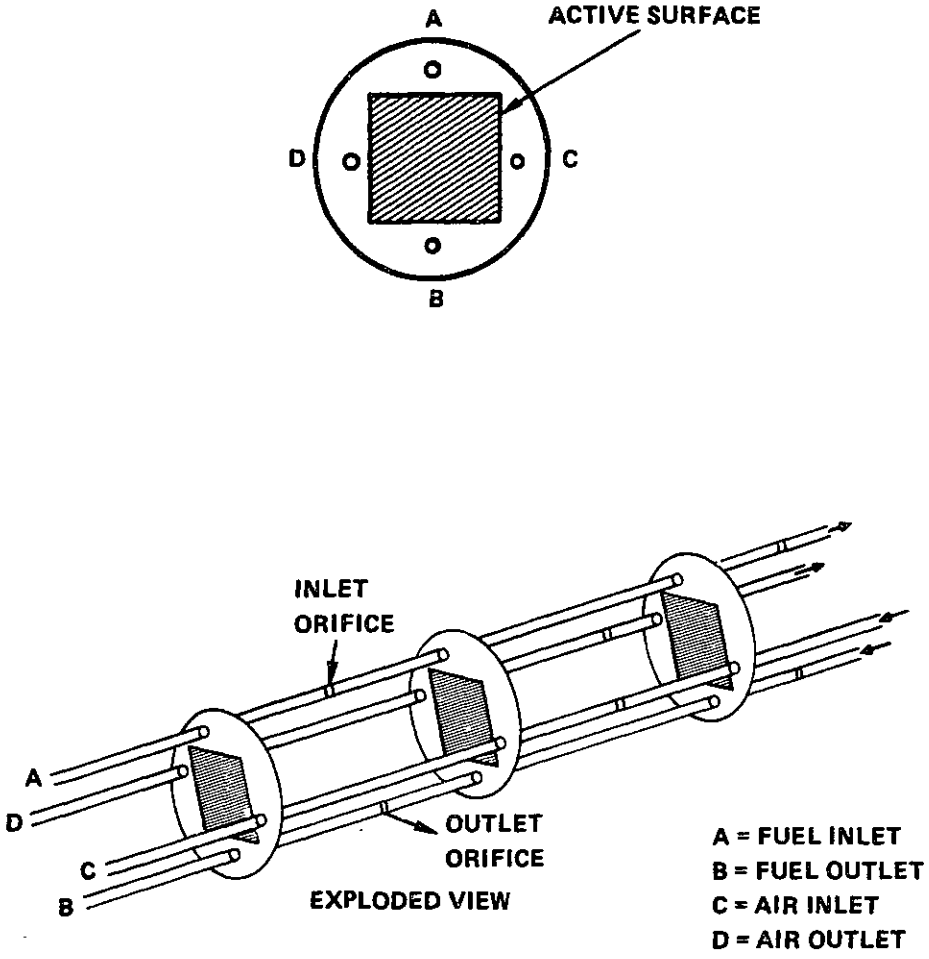

ARRANGEMENT FOR SMALL SIZED STACKS
FIGURE III-1

S (mm)	r_2 (cm) 2 cm^2 cell	r_2 (cm) 10 cm^2 cell
1	7.60	2.79
2	72.16	4.38
3	-	6.87
4	-	10.78
5	-	16.91

Table III-1: Total (cell + insulation) radius as a function of cell spacing

but costly), the internal channels can be eliminated and a feed arrangement such as the one shown in figure 1.6a (easily adaptable to series flow) can easily be realized. We thus conclude that, if electrode-associated losses can be eliminated, cell design is governed by constraints other than heat losses as size is increased.

Secondly, in all of the steady state analyses presented (and in most of the multiplicity graphs), a 2 cm^2 cell was considered, since this corresponds to the size currently being operated at MIT. Feed dilution was necessary in order to achieve high conversions while operting with flow rates easily achievable and controllable under laboratory conditions. Undiluted feed would have resulted in very low and difficult to measure and control rates per cell (<5 cc/min) if operation of a single cell for experimental purposes is considered. However, if scale-up is not restricted by electrode losses, operation with pure or nearly pure feed can be realized for greater cell sizes, in which case self ignited operation would be greatly facilitated, and the constraints and dimensions shown here may not hold true.

The maximum number of modular elements per stack is limited by fluid distribution and pressure drop considerations. For a 25 cc/min feed per cell (@ 298 K and 1 atm), and a maximum velocity of 3 m/s in the distributor channel, a 5 mm-diameter distribution tube can handle, at 1000 K, the feed corresponding to 42 cells (2 cm^2 electrode). The inlet orifice to each cell would have to be such that fluid distribution is assured (i.e., pressure drop along channel should be negligible with respect to the concentrated loss across the orifice). A 0.80 mm orifice

would result in a 6 m/s velocity, entirely adequate for this purpose. The corresponding pressure drop is less than 1 mmwc. For a 10 cm^2 modular stack, and a 10 mm-diameter distribution channel, the corresponding number of cells is 34.

For a 0.1 W/cm^2 power density, considering a 1 mm spacing for the 2 cm^2 module and 2 mm for the 10 cm^2 module, with the corresponding insulation thicknesses, and applying an overall correction factor of 0.5 to allow for the fact that the cell's cross section contains a "non-useful fraction", we finally obtain 8.4 watts @ 5.5 KW/m^3 for the 42-2cm^2 cell stack, and 34 watts @ 41.5 KW/m^3 for the 34-10 cm^2 cell stack.

Note that the requirements of extremely low heat losses imposed the close stacking discussed above. This, however, represents only one of the many possible approaches to the problem. In fact, the design formulae were derived from equation (III-1) which is based on a single, independent stack, insulated in such a way that the energy balance requirements are satisfied. Another approach is to effectively reduce the heat exchange area per cell not through cell spacing alone, but by considering a bundle of unisnulated cylindrical stacks within an insulated, closed container. Such an approach is illustrated in figure III-2. It is clear, in this case, that the size of such unit is limited by the complexity of manifolding, assuming parallel feed. On the other hand, a series feed would, if anything, be even more complex.

Referring to figure III-2, an experimental 10-stack unit

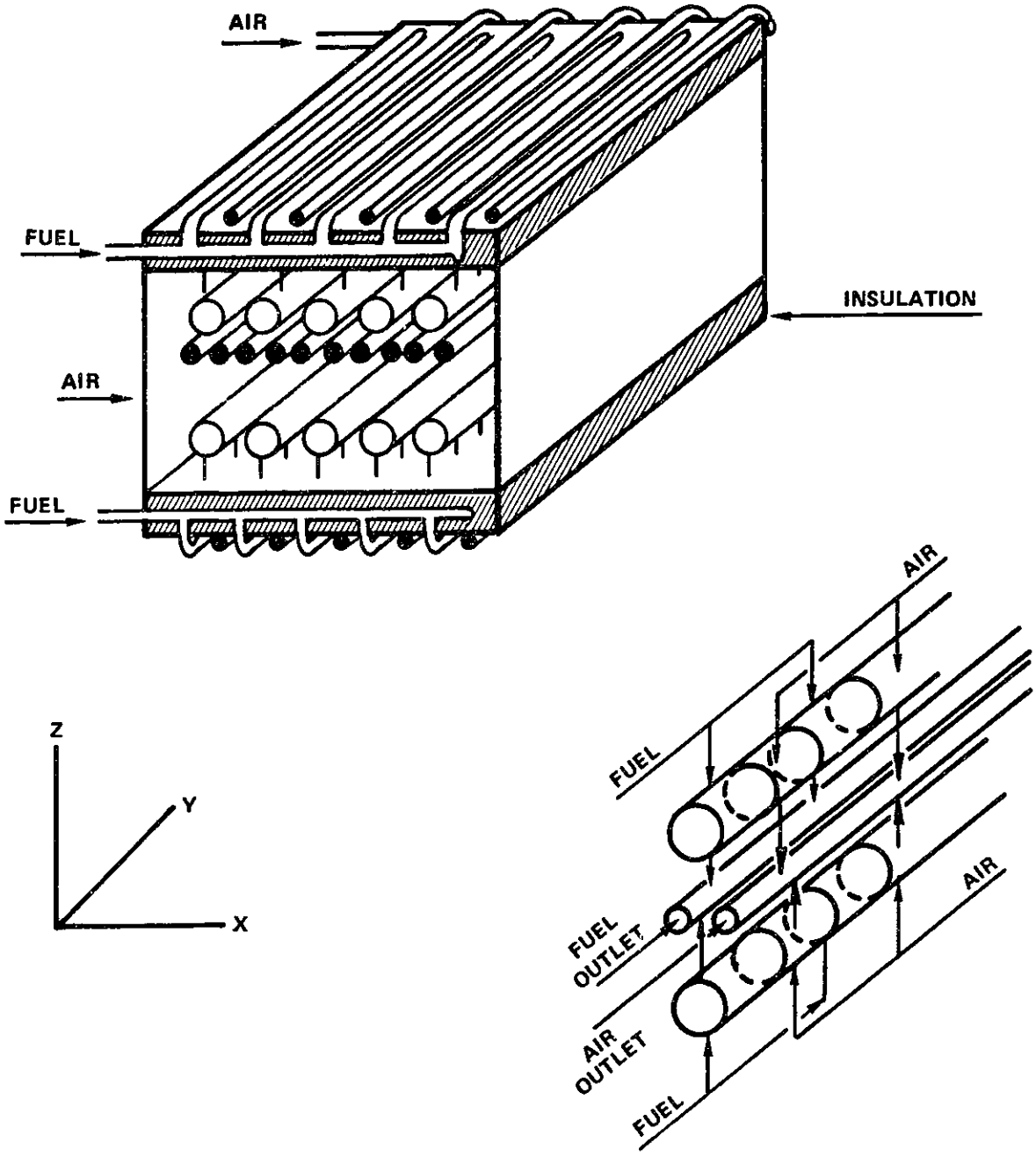

TUBE BUNDLE — PARALLEL FEED ARRANGEMENT
FIGURE III-2

(2x5) with 2 cm^2 elements separated by a 4 mm spacing (see figure 1.6b but without insulation), with a 4 cm insulation thickness (not required on z-y faces, since units can be stacked in the x direction), and a 40 cm depth (including 4 cm insulating layers at both xz faces), would have the following characteristics:

Active area per stack: $\frac{2cm^2}{cell} \times \frac{1\ cell}{0.4\ cm} \times 32\ cm = 160\ cm^2/stack$

Active area per unit: $160\ \frac{cm^2}{stack} \times 10\ \frac{stacks}{unit} = 1600\ cm^2$

Z-height (including insulation): $\sim$ 14 cm

X-width: $\sim$ 10.5 cm

Y-depth (including insulation): $\sim$ 40 cm

Total exposed area excluding z-y faces: $\sim$ 1134 cm^2

External/Electrode area ratio: 0.70

Power generated @ 0.1 W/cm^2: 160 w

Power density: 27 Kw/m^3

This is not necessarily an optimum, and lower area ratios can obviously be acheived, depending upon the designer's ingenuity, but this certainly shows the feasibility of such an alternative. For a 0.05 W/mK insulator, the resulting heat transfer coefficient would be $\sim$ 1 Kcal/h m^2K. Fuel and air outlet channels would be 1.3 cm in diameter, for a gas velocity $\sim$ 1.6 m/S @ 1000 K. Note that X-stacking of units is required in order to minimize heat losses from Y-Z faces. If, however, a single unit is considered, all faces should be insulated, and a better insulator with slightly increased thickness would be needed.

APPENDIX IV

CO/CO_2 material & energy balances

DCSTR1 program

```
C DCSTR1 CALCULATES THE MATERIAL BALANCE (CONVERSION VS. TEMPERATURE)
C FOR THE CO/CO2 FUEL CELL.POWER DENSITY,CURRENT DENSITY,EFFICIENCY,HEAT
C GENERATION AND HEAT REMOVAL VS TEMPERATURE FUNCTIONS ARE ALSO CALCULATED
C THE PROGRAM ALSO LOCATES STEADY STATES AND GIVES THE CORRESPONDING
C CONVERSION AND TEMPERATURE VALUES

      COMPILER DOUBLE PRECISION
      COMPILER NOSTACK
      DIMENSION T(500),TEMP(500),CONVN(500),QGEN(500),QREM(500),POWDEN
     L(500),EFF(500),CURDEN(500),PIFF(500)
      CALL FOPEN (3,'PARAMETERS')
      CALL FOPEN (4,'OUTPUT')
      CALL FOPEN(20,'STABILITY')
      CALL APPEND (5,'PLCON',3,IERR)
      CALL APPEND (16,'PLHT',3,IERR)
      CALL APPEND (18,'PLEFF',3,IERR)
      CALL APPEND (17,'PLPOUT',3,IERR)
      CALL APPEND(19,'PLCURD',3,IERR)

C ENTER PROCESS VARIABLES

      ACCEPT "INLET FLOW @ 298K & 1 ATM(CC/MIN)=",UFRATE
      ACCEPT "EXTERNAL CIRCUIT LOAD(OHMS)=",REX
      ACCEPT "INLET FUEL MOLE FRACTION=",YO
      ACCEPT "ELECTROLYTE THICKNESS(MICRONS)=",UD
      ACCEPT "ELECTRODE AREA(CM2)=",AREA
      ACCEPT "ELECTRODE RESISTANCE(OHMS)=",REL
      ACCEPT "FEED TEMPERATURE(KELVIN)=",TFEED
      ACCEPT "OVERALL HEAT TRANSFER COEFFICIENT(KCAL/HM2K)=",COEFF
      ACCEPT "RATIO OF EXTERNAL TO ELECTRODE AREA=",RATIO
      ACCEPT "AMBIENT TEMPERATURE(KELVIN)=",TCOOL
      ACCEPT "AIR FEED TEMPERATURE(KELVIN)=",TFEEDO
      ACCEPT"STOICHIOMETRIC RATIO FOR AIR FEED=",STCH

C ACOIL IS THE AREA ASSOCIATED WITH HEAT INTERACTIONS PER UNIT CELL(CM2)
C D IS THE ELECTROLYTE THICKNESS IN CM
C PN1 AND PN2 ARE CONSTANTS APPEARING IN THE DIMENSIONLESS ENERGY & MATERIAL
C BALANCES
C CPI(JOULES/KG*K)IS THE TEMPERATURE-AVERAGED INLET FUEL SPECIFIC HEAT
C CIN2 AND CICO ARE FUNCTIONS THAT CALCULATE THE INTEGRAL OF THE MOLAR SPE-
C IFIC HEATS OF N2 & CO FROM 298.15K TO GIVEN TEMPERATURE,UNITS FOR SPECIFIC
C HEATS BEING CAL/MOLE*K
C PNCOOL IS THE NUMBER OF HEAT TRANSFER UNITS
C YO2 IS THE OXYEN MOLE FRACTION IN THE WELL-MIXED CATHODE
C YN2 IS THE N2 MOLE FRACTION IN THE WELL MIXED CATHODE
C PMAIR IS THE RESULTING AIR MOLECULAR WEIGHT

      ACOIL=RATIO*AREA
      D=1.0E-04*UD
```

```
      PN1=3.276E-04*TFEED/(UFRATE*YO*REX)
      PN2=4.167E-03*D/(AREA*REX)
      CPI=(149.5286*((1.0-YO)*CIN2(TFEED)+YO*CICO(TFEED)))/(TFEED-298.15)
      PNCOOL=6097.117*COEFF*ACOIL/(CPI*UFRATE)
      PN13=REL/REX
      YO2=.21*(STCH-1.)/(STCH-.21)
      YN2=1.-YO2
      PMAIR=(28.84*STCH-6.72)/(STCH-.21)

C FEED TEMPERATURE CANNOT EXCEED MAXIMUM SCANNED OUTLET TEMPERATURE
      IF(TFEED.GT.2000.0)GO TO 108

C SET LOWER & UPPER LIMITS FOR TEMPERATURE SCANNING
      TSTART=5.0*AINT(TFEED/10.0)
      L=AINT((2000.-(TSTART+10.0))/10.0)+1

C EXTERNAL LOOP SCANS TEMPERATURE FROM LOWER TO UPPER LIMITS
      DO 69 J=1,L
      T(J)=TSTART+10.0*FLOAT(J)
      THETA=T(J)/TFEED
      TORY=TFEED*THETA

C B AND A ARE FUNCTIONS OF TEMPERATURE ONLY IN THE MATERIAL BALANCE EQN.
C DELG IS A FUNCTION THAT CALCULATES THE GIBBS FREE ENERGY CHANGE PER MOLE
C OF FUEL FOR ANY GIVEN TEMPERATURE(JOULES/MOLE)
      B=3.9408E-05*DELG(TORY)/(THETA*REX*UFRATE*YO*(1.+PN13+PN2*DEXP(9700./
     LTORY)))-DLOG(DSQRT(YO2))*PN1/(1.+PN13+PN2*DEXP(9700./TORY))
      A=PN1/(1.0+PN13+PN2*DEXP(9700.0/TORY))

      TYPE "RAPHSON NEWTON ITERATION"
      TYPE "B=",B
      TYPE "THETA=",THETA

C INITIAL GUESS
      X=1.0E-13
      IF(ABS(A*DLOG((1.0-X)/X)-X/THETA-B).LT.1.0E-12) GO TO 90

C RAPHSON-NEWTON ITERATION STARTS
      DO 70 K=1,150
      XNEW=X+(A*DLOG((1.0-X)/X)-X/THETA-B)/(A/((1.0-X)*X)+1.0/THETA)

C CONVERSION MUST BE BOUNDED BETWEEN 0 AND 1
      IF(XNEW.LE.1.0E-12)XNEW=1.0E-12
      IF(XNEW.GE.9.9999999999E-01)XNEW=9.9999999999E-01
      XI=A*DLOG((1.0-XNEW)/XNEW)-XNEW/THETA
      TYPE "XNEW=",XNEW
      TYPE "XI=",XI
      X=XNEW

C CHECK CALCULATION CLOSURE
```

```
        IF(ABS(XI-B).LT.1.0E-12) GO TO 90

70    CONTINUE

C PROGRAM STOPS DUE TO NON-CONVERGENCE AFTER 150 ITERATIONS
        WRITE(4,82) THETA
        GO TO 100

C NORMAL EXIT OF RAPHSON-NEWTON LOOP
  90    XS=X

C PMOLWT IS THE FUEL OUTLET MOLECULAR WEIGHT
C PN5 IS THE RATIO OF OUTLET TO INLET SPECIFIC HEATS
C VOLT IS THE ACTUAL CELL VOLTAGE
C WAGNER WAS A RENOWNED GERMAN COMPOSER,AND IS PRESENTLY THE LOGARITHMIC
C TERM IN THE NERNST EXPRESSION FOR REVERSIBLE VOLTAGE
C AMP IS THE CURRENT PRODUCED BY THE FUEL CELL
C AIRDTY IS THE DIMENSIONLESS AMOUNT OF ENERGY REQUIRED TO HEAT THE NITRO-
C GEN PLUS THE UNREACTED OXYGEN FROM INLET TO OUTLET TEMPERATURE
C CICO2 AND CICO ARE FUNCTIONS THAT CALCULATE THE INTEGRAL OF MOLAR SPE-
C CIFIC HEAT(CAL/MOLE*K) FROM 298.15 TO THE INDICATED TEMPERATURE

        PMOLWT=44.0*YO*XS+28.0*(1.0-YO*XS)
        CP=YO*XS*CICO2(TORY)+YO*(1.0-XS)*CICO(TORY)+(1.0-YO)*CIN2(TORY)
        PN5=(4186.8*CP/(PMOLWT*CPI))/(TORY-298.15)
        VOLT=(-5.181E-06*DELG(TORY)+4.3079793E-05*TORY*DLOG(DSQRT(YO2)*(1.-XS)
     L/XS))/(1.+PN13+PN2*DEXP(9700./TORY))
        WAGNER=DLOG(DSQRT(YO2)*(1.-XS)/XS)
        AMP=(-DELG(TORY)*5.181E-06+4.308E-05*TORY*WAGNER)/(REX+REL+
     L(4.167E-07*UD/AREA)*DEXP(9700.0/TORY))
        TM=.5*(TFEEDO+TORY)
        AIRDTY=18196.47326*(TORY-TFEEDO)*AMP*(STCH/.233-1.)*(1./PMAIR)*(YO2*CI
     LO2(TM)+YN2*CIN2(TM))/((TM-298.15)*CPI*UFRATE*TFEED)

C UGEN IS THE DIMENSIONLESS HEAT GENERATION
C UREM IS THE DIMENSIONLESS HEAT REMOVAL
C DELH IS THE ENTHALPY CHANGE PER MOLE OF FUEL (JOULE/MOLE)
C POWDEN IS THE POWER PER UNIT ELECTRODE AREA (WATTS/CM2)
C EFF IS THE RATIO OF ACTUAL TO THERMONEUTRAL VOLTAGE
C CURDEN IS THE CURRENT DENSITY(AMPS/CM2)

        UGEN=AMP*(1.-193000.*VOLT/(-DELH(298.15)))*271.63456*(-DELH(298.15))/
     L(UFRATE*CPI*TFEED)
        UREM=(1.+4.346*AMP/UFRATE)*PN5*(THETA-298.15/TFEED)-(1.-298.15/TFEED)+
     LPNCOOL*(THETA-TCOOL/TFEED)-(4.346*AMP/UFRATE)*CIO2(TFEEDO)*130.8375*(
     LTFEEDO-298.15)/(CPI*TFEED*(TFEEDO-298.15))+AIRDTY
        POWDEN(J)=REX*(AMP**2)/AREA
        EFF(J)=193000.*VOLT/(-DELH(298.15))
        TEMP(J)=THETA
        CURDEN(J)=AMP/AREA
```

```
      CONVN(J)=XS
      QGEN(J)=UGEN
      QREM(J)=UREM
      KOUNT=J

C THE NEXT SECTION OF THE PROGRAM LOOKS FOR STEADY STATES
      IF(J.GT.1)GO TO 700
      PIFF(J)=QREM(J)-QGEN(J)
      IF(ABS(PIFF(J)).GT.1.0E-06) GO TO 69
      TSTEAD=TEMP(J)
      XSTEAD=CONVN(J)
      GO TO 402
 700  IF(ABS(QGEN(J)-QREM(J)).GT.1.0E-06) GO TO 400
      PIFF(J)=0.0
      IF((PIFF(J).EQ.0.0).AND.(PIFF(J-1).EQ.0.0)) GO TO 69
      TSTEAD=TEMP(J)
      XSTEAD=CONVN(J)
      GO TO 402
 400  PIFF(J)=QREM(J)-QGEN(J)
      IF((PIFF(J)*PIFF(J-1)).GE.0.0)GO TO 69
      TSTEAD=(TEMP(J)+TEMP(J-1))/2.0
      XSTEAD=(CONVN(J)+CONVN(J-1))/2.0

C STEADY STATE SEARCH SECTION ENDS

C CALCULATED VALUES ARE STORED FOR PLOTTING AND PRINTING

 402  WRITE(20,800)
      WRITE(20,801) TSTEAD,XSTEAD
  69  CONTINUE
      WRITE(3,83)UPRATE,REX,YO,UD,AREA,REL,TFEED,COEFF,RATIO,TCOOL,TFEEDO,STCH
      WRITE(4,85)
      WRITE(4,86)(TEMP(K),CONVN(K),QGEN(K),QREM(K),POWDEN(K),K=1,KOUNT)
      WRITE(4,87)
      WRITE(4,88)(TEMP(K),EFF(K),CURDEN(K),K=1,KOUNT)
      WRITE(5,200)(TEMP(K),CONVN(K),K=1,KOUNT)
      WRITE(16,201)(TEMP(K),QGEN(K),K=1,KOUNT)
      WRITE(16,201)(TEMP(K),QREM(K),K=1,KOUNT)
      WRITE(17,203)(TEMP(K),POWDEN(K),K=1,KOUNT)
      WRITE(18,204)(TEMP(K),EFF(K),K=1,KOUNT)
      WRITE(19,205)(TEMP(K),CURDEN(K),K=1,KOUNT)
      GO TO 100
 108  WRITE(4,202)
 202  FORMAT('0','FEED TEMPERATURE EXCEEDS PROGRAM VALIDITY RANGE')
  82  FORMAT('0','NON CONVERGENCE AT 150 ITERATIONS AT THETA=',G11.4)
  83  FORMAT('1','INLET FLOW @ 298K & 1 ATM(CC/MIN)=',G11.4/' ','EXTERNAL CIR
     LCUIT LOAD(OHMS)=',G11.4/' ','INLET FUEL MOLE FRACTION=',G11.4/' ','ELEC
     LTROLYTE THICKNESS(MICRONS)=',G11.4/' ','ELECTRODE AREA(CM2)=',G11.4/' ',
     L'ELECTRODE RESISTANCE(OHMS)=',G11.4/' ','FEED TEMPERATURE(KELVIN)=',G11.4
     L/' ','OVERALL HEAT TRANSFER COEFFICIENT(KCAL/HM2K)=',G11.4/' ','EXTER
```

```
     LNAL TO ELECTRODE AREA RATIO=',G11.4/' ','AMBIENT TEMPERATURE(KELVIN)=',G
     L11.4/' ','AIR FEED TEMPERATURE(KELVIN)=',G11.4/' ','ACTUAL/STOICHIOMETR
     LIC AIR FEED RATIO=',G11.4)
  85  FORMAT('0',2X,'DIM"LESS TEMPERATURE',9X,'CONVERSION',10X,'DIM"LESS
     D HEAT GEN"N',3X,'DIM"LESS HEAT REMOVAL',4X,'POWER DENSITY(W/CM2)')
  86  FORMAT('0',5(7X,G11.4,6X))
  87  FORMAT('1',8X,'DIMENSIONLESS TEMPERATURE',22X,'EFFICIENCY',22X,'CURRENT
     L DENSITY(AMP/CM2)')
  88  FORMAT('0',3(15X,G11.4,14X))
 200  FORMAT(' ',G11.4,',',G11.4)
 201  FORMAT(' ',G11.4,',',G11.4)
 203  FORMAT(' ',G11.4,',',G11.4)
 204  FORMAT(' ',G11.4,',',G11.4)
 205  FORMAT(' ',G11.4,',',G11.4)
 800  FORMAT('1','STEADY STATE')
 801  FORMAT('0','T/TFEED=',G11.4/' ','CONVERSION=',G11.4)
 100    CALL RESET
      STOP
        END

)
```

```
  FUNCTION DDELTG
C DELG COMPUTES THE GIBBS FREE ENERGY CHANGE PER MOLE OF FUEL(JOULES/MOLE)
C  FOR ANY GIVEN TEMPERATURE

        COMPILER DOUBLE PRECISION
        COMPILER NOSTACK
        FUNCTION DELG(Z)
        DELG=4.1868*(8.75E 04/Z+23.25*Z-0.2*Z*DLOG(Z)-3.1E-04*(Z**2)-68310.38)
        RETURN
        END

) FUNCTION DDELTH
C DELH COMPUTES THE ENTHALPY CHANGE PER MOLE OF FUEL (JOULE/MOLE) FOR
C ANY GIVEN TEMPERATURE

        COMPILER DOUBLE PRECISION
        COMPILER NOSTACK
        FUNCTION DELH(Z)
        DELH=4.1868*(1.75E05/Z+0.2*Z+3.1E-04*(Z**2)-68310.38)
        RETURN
        END

)
```

```
  FUNCTION DCICO
C CICO CALCULATES THE INTEGRAL OF CO MOLAR HEAT CAPACITY(CAL/MOLE*K) FROM
C 298K TO ANY GIVEN TEMPERATURE

        COMPILER DOUBLE PRECISION
        COMPILER NOSTACK
        FUNCTION CICO(Z)
        CICO=6.79*Z+4.9E-04*(Z**2)+0.11E 05/Z-2104.89
        RETURN
        END

) FUNCTION DCICO2
C CICO2 COMPUTES THE INTEGRAL OF CO2 MOLAR HEAT CAPACITY(CAL/MOLE*K) FROM
C 298K TO ANY GIVEN TEMPERATURE

        COMPILER DOUBLE PRECISION
        COMPILER NOSTACK
        FUNCTION CICO2(Z)
        CICO2=10.57*Z+1.05E-03*(Z**2)+2.06E 05/Z-3935.711
        RETURN
        END

) FUNCTION DCIN2
C CIN2 COMPUTES THE INTEGRAL OF N2 MOLAR HEAT CAPACITY(CAL/MOLE*K) FROM
C 298K TO ANY GIVEN TEMPERATURE

        COMPILER DOUBLE PRECISION
        COMPILER NOSTACK
        FUNCTION CIN2(Z)
        CIN2=6.83*Z+4.5E-04*(Z**2)+0.12E 05/Z-2116.615
        RETURN
        END

) FUNCTION DCIO2
C CIO2 COMPUTES THE INTEGRAL OF OXYGEN MOLAR HEAT CAPACITY(CAL/MOLE*K) FROM
C 298K TO ANY GIVEN TEMPERATURE

        COMPILER DOUBLE PRECISION
        COMPILER NOSTACK
        FUNCTION CIO2(Z)
        CIO2=7.16*Z+5.0E-04*(Z**2)+0.4E 05/Z-2313.36
        RETURN
        END

)
```

CO/CO_2 multiplicity

MULTIP program

```
C MULTIP SOLVES FOR FUEL INLET TEMPERATURE AS A FUNCTION OF REACTOR
C TEMPERATURE,SCANNED BETWEEN APPROPIATE LOWER & UPPER LIMITS

      COMPILER DOUBLE PRECISION
      COMPILER NOSTACK
      CALL APPEND(1,'MANY',3,IERR)
      CALL FOPEN(2,'VARIABLES')
      CALL FOPEN(3,'WARNING')

C ENTER PROCESS PARAMETERS
      ACCEPT"INLET FLOW @ 25C & 1 ATM=",UFRATE
      ACCEPT"EXTERNAL CIRCUIT LOAD(OHMS)=",REX
      ACCEPT"INLET FUEL MOLE FRACTION=",YO
      ACCEPT"ELCTRODE GAP(MICRONS)=",UD
      ACCEPT"ELECTRODE AREA(CM2)=",AREA
      ACCEPT"ELECTRODE RESISTANCE(OHMS)=",REL
      ACCEPT"OVERALL HEAT TRANSFER COEFFICIENT(KCAL/HM2K)=",COEFF
      ACCEPT"RATIO OF EXTERNAL TO ELECTRODE AREA=",RATIO
      ACCEPT"AMBIENT TEMPERATURE(KELVIN)=",TCOOL
      ACCEPT"AIR FEED TEMPERATURE(KELVIN)=",TFEEDO
      ACCEPT"STOICHIOMETRIC RATIO FOR AIR FEED=",STCH
      WRITE(2,2)UFRATE,REX,YO,UD,AREA,REL,COEFF,RATIO,TCOOL,TFEEDO,STCH

C ACOIL IS THE AREA ASSOCIATED WITH HEAT INTERACTIONS PER CELL(CM2)
C D IS THE ELECTROLYTE THICKNESS IN CM
C CGUESS IS THE TEMPERATURE AVERAGE HEAT CAPACITY OF THE FUEL FEED STREAM
C (JOULES/KG*K) FOR AN INITIAL GUESS OF 1650K FOR FUEL INLET TEMPERATURE
C THIS VARIABLE IS NECESSARY SINCE IT IS AN IMPLICIT FUNCTION OF T THROUGH
C CIN2 & CICO
C CIN2 & CICO ARE FUNCTIONS THAT CALCULATE THE INTEGRAL OF THE MOLAR HEAT
C CAPACITIES OF N2 & CO(CAL/MOLE*K) FROM 298K TO ANY GIVEN TEMPERATURE
      ACOIL=RATIO*AREA
      D=1.E-04*UD
      PN2=4.1666E-03*D/(AREA*REX)
      PN13=REL/REX
      CGUESS=.1106*((1.-YO)*CIN2(1650.)+YO*CICO(1650.))

C OUTLET TEMPERATURE SCANNING STARTS
      DO 69 I=1,32
      T=350.+50.*FLOAT(I)

C MATERIAL BALANCE IS SOLVED THROUGH NEWTON-RAPHSON'S METHOD
C A & B ARE FUNCTIONS OF TEMPERATURE EXCLUSIVELY
C YO2 IS THE OXYGEN MOLE FRACTION IN THE WELL MIXED CATHODE
      A=(1./(1.+PN13+PN2*DEXP(9700./T)))*(-3.9408E-05*DELG(T))/(REX*UFRATE*YO)

      YO2=.21*(STCH-1.)/(STCH-.21)
      B=(1./(1.+PN13+PN2*DEXP(9700./T)))*(-3.27655E-04*DLOG(DSQRT(YO2)))*T
     L/(REX*UFRATE*YO)
```

```
        C=(1./(1.+PN13+PN2*DEXP(9700./T)))*3.27655E-04*T/(REX*UFRATE*YO)
        PLEFT=A-B
        TYPE"RAPHSON-NEWTON ITERATION"
        TYPE"LEFT HAND SIDE=",PLEFT
        TYPE"TEPERATURE(KELVIN)=",T

C INITIAL GUESS FOR CONVERSION
        X=1.E-13
        IF(ABS(PLEFT-X-C*DLOG((1.-X)/X)).LT.1.E-12)GO TO 90

C RAPHSON NEWTON ITERATION STARTS
        DO 70 K=1,150
        XNEW=X-(X-C*DLOG((1.-X)/X)-PLEFT)/(1.+C/(X*(1.-X)))

C CONVERSION MUST BE BOUNDED BETWEEN 0 & 1
        IF(XNEW.LE.1.E-12)XNEW=1.E-12
        IF(XNEW.GT.9.9999999999E-01)XNEW=9.9999999999E-01

        RHS=XNEW-C*DLOG((1.-XNEW)/XNEW)
        TYPE"XNEW=",XNEW
        TYPE"RIGHT HAND SIDE=",RHS
        X=XNEW

C CHECK CALCULATION CLOSURE
        IF(ABS(PLEFT-RHS).LT.1.E-12)GO TO 90

  70    CONTINUE

C PROGRAM STOPS DUE TO NON CONVERGENCE AFTER 150 ITERATIONS
        TYPE"NON-CONVERGENCE AFTER 150 ITERATIONS"
        WRITE(3,1)T,RHS,PLEFT,X
        GO TO 100

C NORMAL EXIT FROM NEWTON RAPHSON LOOP
  90    XS=X

C VOLT IS THE REVERSIBLE(NERNST) VOLTAGE @ CELL CONDITIONS
C AMP IS THE CELL'S CURRENT OUTPUT
C PMOLWT IS THE FUEL MOLECULAR WEIGHT @ CELL(=OUTLET) CONDITIONS
C DELG IS A FUNCTION THAT COMPUTES THE GIBBS FREE ENERGY CHANGE PER MOLE
C OF FUEL(JOULE/MOLE) AT ANY GIVEN TEMPERATURE
        VOLT=-5.1813E-06*DELG(T)+4.3079793E-05*T*DLOG(DSQRT(YO2)*(1.-X)/X)
        AMP=VOLT/(REX*(1.+PN13+PN2*DEXP(9700./T)))
        PMOLWT=44.*YO*XS+28.*(1.-YO*XS)

C SINCE INLET TEMPERATURE IS ALSO CONTAINED IN THE FUEL'S SPECIFIC HEAT,
C THE SOLUTION INVOLVES AN ITERATIVE SCHEME WITH AN INITIAL SPECIFIC HEAT
C CALCULATED @ 1650K
        CPI=CGUESS
        PREV=1650.
```

```
      CP=(YO*XS*CICO2(T)+YO*(1.-XS)*CICO(T)+(1.-YO)*CIN2(T))*4186.8/(PMOLWT*
     L(T-298.15))

C INLET TEMPERATURE CALCULATION LOOP
      DO 71 J=1,150

C PMAIR IS THE EXCESS AIR'S MOLECULAR WEIGHT
C YO2 IS THE OXYGEN MOLE FRACTION IN THE WELL MIXED CATHODE
C YN2 IS THE NITROGEN MOLE FRACTION IN THE WELL MIXED CATHODE
C CIO2,CICO2 ARE FUNCTIONS THAT COMPUTE THE INTEGRAL OF MOLAR SPECIFIC
C HEAT(CAL/MOLE*K) FROM 298K TO ANY GIVEN TEMPERATURE
C DELH COMPUTES THE ENTHALPY CHANGE PER MOLE OF FUEL(JOULES/MOLE) @ ANY
C GIVEN TEMPERATURE
      PMAIR=(28.84*STCH-6.72)/(STCH-.21)
      YN2=1.-YO2
      TM=.5*(T+TFEEDO)
      PN5=CP/CPI
      Z1=6097.117*COEFF*ACOIL*(T-TCOOL)/(CPI*UFRATE)+(18196.473*AMP/PMAIR)*(
     LSTCH/.233-1.)*(T-TFEEDO)/(TM-298.15)*(YO2*CIO2(TM)+YN2*CIN2(TM))/(CPI*
     LUFRATE)
      Z2=PN5*(T-298.15)*(1.+4.346*AMP/UFRATE)
      AUX1=2.0934*(TFEEDO-298.15)*CIO2(TFEEDO)/(TFEEDO-298.15)
      AUX2=AMP*REX*193000./(-DELH(298.15))
      AUX3=271.6346*AMP/(CPI*UFRATE)
      Z3=AUX3*(AUX1+(1.-AUX2)*(-DELH(298.15)))
      TIN=Z2+Z1-Z3+298.15

C CALCULATED & PREVIOUS INLET TEMPERATURE ARE COMPARED;CONVERGENCE IS
C ACHEIVED WHEN THE DIFFERENCE IS LESS THAN 1K;OTHERWISE,THE ITERATION
C IS REPEATED AFTER COMPUTING THE INLET FUEL SPECIFIC HEAT @ CALCULATED
C INLET TEMPERATURE
      TYPE"CALCULATED INLET TEMPERATURE(KELVIN)=",TIN
      IF(ABS(TIN-PREV).LE.1.)GO TO 91
      CPI=(149.2586*((1.-YO)*CIN2(TIN)+YO*CICO(TIN)))/(TIN-298.15)
      PREV=TIN
 71   CONTINUE

C PROGRAM STOPS IF TEMPERATURE DOES NOT CONVERGE AFTER 150 TRIALS
      TYPE"NON-CONVERGENCE AFTER 150 ITERATIONS"
      WRITE(3,3)T,TIN
      GO TO 100

C NORMAL EXIT FROM ITERATION
 91   TINLET=TIN

C STORE DATA FOR PRINTING & PLOTTING
      WRITE(1,4)TINLET,T
 69   CONTINUE
  1   FORMAT('0','RAPHSON-NEWTON ITERATION DOES NOT CONVERGE'/' ','TEM
     LPERATURE(KELVIN)=',G11.4/' ','RIGHT HAND SIDE OF EXPRESSION=',G11.4/
```

```
     L' ','LEFT HAND SIDE OF EXPRESSION=',G11.4/' ','CONVERSION=',G11.4)
   2    FORMAT('1','INLET FLOW @ 25C & 1 ATM(CC/MIN)=',G11.4/' ','EXTER
     LNAL CIRCUIT LOAD(OHMS)=',G11.4/' ','INLET FUEL MOLE FRACTION=',G11.4/
     L' ','ELECTRODE GAP(MICRONS)=',G11.4/' ','ELECTRODE AREA(CM2)=',G11.4/
     L' ','ELECTRODE RESISTANCE(OHMS)=',G11.4/' ','OVERALL HEAT TRANSFER CO
     LEFFICIENT(KCAL/HM2K)=',G11.4/' ','RATIO OF EXTERNAL TO ELECTRODE AREA=
     L',G11.4/' ','AMBIENT TEMPERATURE(KELVIN)=',G11.4/' ','AIR FEED TEMPE
     LRATURE(KELVIN)=',G11.4/' ','AIR FEED RATIO=',G11.4)
   3    FORMAT('0','INLET TEMPERATURE DOES NOT CONVERGE'/' ','OUTLET TEM
     LPERATURE(KELVIN)=',G11.4/' ','INLET TEMPERATURE(KELVIN)=',G11.4)
   4    FORMAT(1X,G11.4,',',G11.4)
  100   CALL RESET
        STOP
        END

)
```

```
   FUNCTION DDELTG
C DELG COMPUTES THE GIBBS FREE ENERGY CHANGE PER MOLE OF FUEL(JOULES/MOLE)
C   FOR ANY GIVEN TEMPERATURE

         COMPILER DOUBLE PRECISION
         COMPILER NOSTACK
         FUNCTION DELG(Z)
         DELG=4.1868*(8.75E 04/Z+23.25*Z-0.2*Z*DLOG(Z)-3.1E-04*(Z**2)-68310.38)
         RETURN
         END

) FUNCTION DDELTH
C DELH COMPUTES THE ENTHALPY CHANGE PER MOLE OF FUEL (JOULE/MOLE)  FOR
C ANY GIVEN TEMPERATURE

         COMPILER DOUBLE PRECISION
         COMPILER NOSTACK
         FUNCTION DELH(Z)
         DELH=4.1868*(1.75E05/Z+0.2*Z+3.1E-04*(Z**2)-68310.38)
         RETURN
         END

)
```

```
  FUNCTION DCICO
C CICO CALCULATES THE INTEGRAL OF CO MOLAR HEAT CAPACITY(CAL/MOLE*K) FROM
C 298K TO ANY GIVEN TEMPERATURE

        COMPILER DOUBLE PRECISION
        COMPILER NOSTACK
        FUNCTION CICO(Z)
        CICO=6.79*Z+4.9E-04*(Z**2)+0.11E 05/Z-2104.89
        RETURN
        END

) FUNCTION DCICO2
C CICO2 COMPUTES THE INTEGRAL OF CO2 MOLAR HEAT CAPACITY(CAL/MOLE*K) FROM
C 298K TO ANY GIVEN TEMPERATURE

        COMPILER DOUBLE PRECISION
        COMPILER NOSTACK
        FUNCTION CICO2(Z)
        CICO2=10.57*Z+1.05E-03*(Z**2)+2.06E 05/Z-3935.711
        RETURN
        END

) FUNCTION DCIN2
C CIN2 COMPUTES THE INTEGRAL OF N2 MOLAR HEAT CAPACITY(CAL/MOLE*K) FROM
C 298K TO ANY GIVEN TEMPERATURE

        COMPILER DOUBLE PRECISION
        COMPILER NOSTACK
        FUNCTION CIN2(Z)
        CIN2=6.83*Z+4.5E-04*(Z**2)+0.12E 05/Z-2116.615
        RETURN
        END

) FUNCTION DCIO2
C CIO2 COMPUTES THE INTEGRAL OF OXYGEN MOLAR HEAT CAPACITY(CAL/MOLE*K) FROM
C 298K TO ANY GIVEN TEMPERATURE

        COMPILER DOUBLE PRECISION
        COMPILER NOSTACK
        FUNCTION CIO2(Z)
        CIO2=7.16*Z+5.0E-04*(Z**2)+0.4E 05/Z-2313.36
        RETURN
        END

)
```

H_2/H_2O material & energy balances

CSTR2 program

```
C CSTR2 CALCULATES THE MATERIAL BALANCE(CONVERSION VS. TEMPERATURE)
C FOR THE H2/H2O FUEL CELL.POWER DENSITY,CURRENT DENSITY,EFFICIENCY,HEAT
C GENERATION AND HEAT REMOVAL VS TEMPERATURE FUNCTIONS ARE ALSO CALCULATED
C THE PROGRAM ALSO LOCATES STEADY STATES AND GIVES THE CORRESPONDING
C CONVERSION AND TEMPERATURE VALUES

      COMPILER DOUBLE PRECISION
      COMPILER NOSTACK
      DIMENSION T(500),TEMP(500),CONVN(500),QGEN(500),QREM(500),POWDEN
     L(500),EFF(500),CURDEN(500),PIFF(500)
      CALL FOPEN (3,'PARAMETERS')
      CALL FOPEN (4,'OUTPUT')
      CALL FOPEN(20,'STABILITY')
      CALL APPEND (5,'PLCON',3,IERR)
      CALL APPEND (16,'PLHT',3,IERR)
      CALL APPEND (18,'PLEFF',3,IERR)
      CALL APPEND (17,'PLPOUT',3,IERR)
      CALL APPEND(19,'PLCURD',3,IERR)

C ENTER PROCESS VARIABLES

      ACCEPT "INLET FLOW @ AMBIENT CONDITIONS(CC/MIN)=",UFRATE
      ACCEPT "EXTERNAL CIRCUIT LOAD(OHMS)=",REX
      ACCEPT "INLET FUEL MOLE FRACTION=",YO
      ACCEPT "ELECTROLYTE THICKNESS(MICRONS)=",UD
      ACCEPT "ELECTRODE AREA(CM2)=",AREA
      ACCEPT "ELECTRODE RESISTANCE(OHMS)=",REL
      ACCEPT "FEED TEMPERATURE(KELVIN)=",TFEED
      ACCEPT "OVERALL HEAT TRANSFER COEFFICIENT(KCAL/HM2C)=",COEFF
      ACCEPT "RATIO OF EXTERNAL TO ELECTRODE AREA=",RATIO
      ACCEPT "AMBIENT TEMPERATURE(KELVIN)=",TCOOL
      ACCEPT "AIR FEED TEMPERATURE(KELVIN)=",TFEEDO
      ACCEPT"STOICHIOMETRIC RATIO FOR AIR FEED=",STCH

C ACOIL IS THE AREA ASSOCIATED WITH HEAT INTERACTIONS PER UNIT CELL(CM2)
C D IS THE ELECTROLYTE THICKNESS IN CM
C PN1 AND PN2 ARE CONSTANTS APPEARING IN THE DIMENSIONLESS ENERGY & MATERIAL
C BALANCES
C CPI(JOULES/KG*K)IS THE TEMPERATURE-AVERAGED INLET FUEL SPECIFIC HEAT
C CIN2 AND CIH2 ARE FUNCTIONS THAT CALCULATE THE INTEGRAL OF THE MOLAR SPE-
C CIFIC HEATS OF N2 & H2 FRO 298K TO GIVEN TEMPERATURE,UNITS FOR SPECIFIC
C HEATS BEING CAL/MOLE*K
C PNCOOL IS THE NUMBER OF HEAT TRANSFER UNITS
C YO2 IS THE OXYGEN MOLE FRACTION IN THE WELL MIXED CATHODE
C PMAIR IS THE RESULTING AIR MOLECULAR WEIGHT

      ACOIL=RATIO*AREA
      D=1.0E-04*UD
      PN1=3.276E-04*TFEED/(UFRATE*YO*REX)
```

```
      PN2=4.167E-03*D/(AREA*REX)
      CPI=((4186.8/(28.-26.*YO))*((1.-YO)*CIN2(TFEED)+YO*CIH2(TFEED)))/(TFEED-
     L298.15)
      PNCOOL=(170718.301/(28.-26.*YO))*COEFF*ACOIL/(CPI*UFRATE)
      PN13=REL/REX
      YO2=.21*(STCH-1.)/(STCH-.21)
      YN2=1.-YO2
      PMAIR=(28.84*STCH-6.72)/(STCH-.21)

C FEED TEPERATURE CANNOT EXCEED MAXIMUM SCANNED OUTLET TEMPERATURE
      IF(TFEED.GT.2000.0)GO TO 108

C SET LOWER & UPPER LIMITS FOR TEMPERATURE SCANNING
      TSTART=5.0*AINT(TFEED/10.0)
      L=AINT((2000.-(TSTART+10.0))/10.0)+1

C EXTERNAL LOOP SCANS TEMPERATURE FROM LOWER TO UPPER LIMITS
      DO 69 J=1,L
      T(J)=TSTART+10.0*FLOAT(J)
      THETA=T(J)/TFEED
      TORY=TFEED*THETA

C B AND A ARE FUNCTIONS OF TEMPERATURE ONLY IN THE MATERIAL BALANCE EQN.
C DELG IS A FUNCTION THAT CALCULATES THE GIBBS FREE ENERGY CHANGE PER MOLE
C OF FUEL FOR ANY GIVEN TEMPERATURE(JOULES/MOLE)
      B=3.9408E-05*DELG(TORY)/(THETA*REX*UFRATE*YO*(1.+PN13+PN2*DEXP(9700./
     LTORY)))-DLOG(DSQRT(YO2))*PN1/(1.+PN13+PN2*DEXP(9700./TORY))
      A=PN1/(1.0+PN13+PN2*DEXP(9700.0/TORY))
      TYPE "RAPHSON NEWTON ITERATION"
      TYPE "B=",B
      TYPE "THETA=",THETA

C INITIAL GUESS
      X=1.0E-13
      IF(ABS(A*DLOG((1.0-X)/X)-X/THETA-B).LT.1.0E-12) GO TO 90

C RAPHSON NEWTON ITERATION STARTS
      DO 70 K=1,150
      XNEW=X+(A*DLOG((1.0-X)/X)-X/THETA-B)/(A/((1.0-X)*X)+1.0/THETA)

C CONVERSION MUST BE BOUNDED BETWEEN 0 AND 1
      IF(XNEW.LE.1.0E-12)XNEW=1.0E-12
      IF(XNEW.GE.9.9999999999E-01)XNEW=9.9999999999E-01
      XI=A*DLOG((1.0-XNEW)/XNEW)-XNEW/THETA
      TYPE "XNEW=",XNEW
      TYPE "XI=",XI
      X=XNEW

C CHECK CALCULATION CLOSURE
```

```
        IF(ABS(XI-B).LT.1.0E-12) GO TO 90
70    CONTINUE

C PROGRAM STOPS DUE TO NON-CONVERGENCE AFTER 150 ITERATIONS
        WRITE(4,82) THETA
        GO TO 100

C NORMAL EXIT FROM RAPHSON-NEWTON LOOP
  90    XS=X

C PMOLWT IS THE FUEL OUTLET MOLECULAR WEIGHT
C PN5 IS THE RATIO OF OUTLET TO INLET SPECIFIC HEATS
C VOLT IS THE ACTUAL CELL VOLTAGE
C WAGNER IS THE LOGARITHMIC TERM IN THE NERNST EXPRESSION FOR CELL VOLTAGE
C AMP IS THE CURRENT GENERATED BY THE FUEL CELL
C AIRDTY IS THE DIMENSIONLESS AMOUNT OF ENERGY REQUIRED TO HEAT THE NITRO-
C GEN PLUS THE UNREACTED OXYGEN FROM INLET TO OUTLET TEMPERATURE
C CIO2 AND CIH2O ARE FUNCTIONS THAT CALCULATE THE INTEGRAL OF MOLAR SPE-
C CIFIC HEAT (CAL/MOLE*K) FROM 298K TO THE INDICATED TEMPERATURE

        PMOLWT=18.*YO*XS+2.*YO*(1.-XS)+28.*(1.-YO)
        CP=YO*XS*CIH2O(TORY)+YO*(1.0-XS)*CIH2(TORY)+(1.0-YO)*CIN2(TORY)
        PN5=(4186.8*CP/(PMOLWT*CPI))/(TORY-298.15)
        VOLT=(-5.181E-06*DELG(TORY)+4.3079793E-05*TORY*DLOG(DSQRT(YO2)*(1.-XS)
     L/XS))/(1.+PN13+PN2*DEXP(9700./TORY))
        WAGNER=DLOG(DSQRT(YO2)*(1.-XS)/XS)
        AMP=(-DELG(TORY)*5.181E-06+4.308E-05*TORY*WAGNER)/(REX+REL+
     L(4.167E-07*UD/AREA)*DEXP(9700.0/TORY))
        TM=.5*(TFEEDO+TORY)
        AIRDTY=509501.2516*(TORY-TFEEDO)*AMP*(STCH/.233-1.)*(1./PMAIR)*(YO2*CI
     LO2(TM)+YN2*CIN2(TM))/((TM-298.15)*CPI*UFRATE*TFEED*(28.-26.*YO))

C UGEN IS THE DIMENSIONLESS HEAT GENERATION
C UREM IS THE DIMENSIONLESS HEAT REMOVAL
C DELH IS THE ENTHALPY CHANGE PER MOLE OF FUEL(JOULE/MOLE)
C POWDEN IS THE POWER PER UNIT ELECTRODE AREA(WATTS/CM2)
C EFF IS THE RATIO OF ACTUAL TO THERMONEUTRAL VOLTAGE
C CURDEN IS THE CURRENT DENSITY(AMPS/CM2)

        UGEN=AMP*(1.-193000.*VOLT/(-DELH(298.15)))*7605.7677*(-DELH(298.15))/
     L(UFRATE*CPI*TFEED*(28.-26.*YO))
        UREM=(1.+121.692*AMP/(UFRATE*(28.-26.*YO)))*PN5*(THETA-298.15/TFEED)-(1.

     L-298.15/TFEED)+PNCOOL*(THETA-TCOOL/TFEED)-(121.692*AMP/(UFRATE*(28.-26.*

     LYO)))*CIO2(TFEEDO)*130.8375*(TFEEDO-298.15)/(CPI*TFEED*(TFEEDO-298.15))+

     LAIRDTY

        POWDEN(J)=REX*(AMP**2)/AREA
```

```
        EFF(J)=193000.*VOLT/(-DELH(298.15))
        TEMP(J)=THETA
        CURDEN(J)=AMP/AREA
        CONVN(J)=XS
        QGEN(J)=UGEN
        QREM(J)=UREM
        KOUNT=J

C THE NEXT SECTION OF THE PROGRAM LOOKS FOR STEADY STATES
        IF(J.GT.1)GO TO 700
        PIFF(J)=QREM(J)-QGEN(J)
        IF(ABS(PIFF(J)).GT.1.0E-06) GO TO 69
        TSTEAD=TEMP(J)
        XSTEAD=CONVN(J)
        GO TO 402
 700  IF(ABS(QGEN(J)-QREM(J)).GT.1.0E-06) GO TO 400
        PIFF(J)=0.0
        IF((PIFF(J).EQ.0.0).AND.(PIFF(J-1).EQ.0.0)) GO TO 69
        TSTEAD=TEMP(J)
        XSTEAD=CONVN(J)
        GO TO 402
 400  PIFF(J)=QREM(J)-QGEN(J)
        IF((PIFF(J)*PIFF(J-1)).GE.0.0)GO TO 69
        TSTEAD=(TEMP(J)+TEMP(J-1))/2.0
        XSTEAD=(CONVN(J)+CONVN(J-1))/2.0

C STEADY STATE SEARCH SECTION ENDS
C CALCULATED VALUES ARE STORED FOR PLOTTING AND PRINTING
 402    WRITE(20,800)
        WRITE(20,801) TSTEAD,XSTEAD
  69  CONTINUE
        WRITE(3,83)UFRATE,REX,YO,UD,AREA,REL,TFEED,COEFF,RATIO,TCOOL,TFEEDO,STCH

        WRITE(4,85)
        WRITE(4,86)(TEMP(K),CONVN(K),QGEN(K),QREM(K),POWDEN(K),K=1,KOUNT)
        WRITE(4,87)
        WRITE(4,88)(TEMP(K),EFF(K),CURDEN(K),K=1,KOUNT)
        WRITE(5,200)(TEMP(K),CONVN(K),K=1,KOUNT)
        WRITE(16,201)(TEMP(K),QGEN(K),K=1,KOUNT)
        WRITE(16,201)(TEMP(K),QREM(K),K=1,KOUNT)
        WRITE(17,203)(TEMP(K),POWDEN(K),K=1,KOUNT)
        WRITE(18,204)(TEMP(K),EFF(K),K=1,KOUNT)
        WRITE(19,205)(TEMP(K),CURDEN(K),K=1,KOUNT)
        GO TO 100
 108    WRITE(4,202)
 202    FORMAT('0','FEED TEMPERATURE EXCEEDS PROGRAM VALIDITY RANGE')
  82  FORMAT('0','NON CONVERGENCE AT 150 ITERATIONS AT THETA=',G11.4)
  83  FORMAT('1','INLET FLOW @ AMBIENT CONDITIONS(CC/MIN)=',F7.2/
     R' ','EXTERNAL CIRCUIT LOAD(OHMS)=',E10.3/' ','INLET FUEL MOLE FRACTION
     R=',F5.3/' ','ELECTRODE GAP(MICRONS)=',F7.2/' ','ELECTRODE CROSS SECTI
```

```
     RON(CM**2)=',F6.2/' ','ELECTRODE RESISTANCE(OHMS)=',F6.2/' ','FEED TEM
     RPERATURE(KELVIN)=',F7.2/' ','OVERALL HEAT TRANSFER COEFFICIENT(KCAL/(H*M*
     R*2*K))=',F7.2/' ','AREA RATIO=',F8.4/' ','COOLANT TEMP
     LERATURE(KELVIN)=',F7.2/' ','AIR FEED TEMPERATURE(KELVIN)=',F7.2/' ',
     L'AIR FEED RATIO=',G11.4)
  85  FORMAT('0',2X,'DIM"LESS TEMPERATURE',9X,'CONVERSION',10X,'DIM"LESS
     D HEAT GEN"N',3X,'DIM"LESS HEAT REMOVAL',4X,'POWER DENSITY(W/CM2)')
  86  FORMAT('0',5(7X,G11.4,6X))
  87  FORMAT('1',8X,'DIMENSIONLESS TEMPERATURE',22X,'EFFICIENCY',22X,'CURRENT
     L DENSITY(AMP/CM2)')
  88  FORMAT('0',3(15X,G11.4,14X))
 200  FORMAT(' ',G11.4,',',G11.4)
 201  FORMAT(' ',G11.4,',',G11.4)
 203  FORMAT(' ',G11.4,',',G11.4)
 204  FORMAT(' ',G11.4,',',G11.4)
 205  FORMAT(' ',G11.4,',',G11.4)
 800  FORMAT('1','STEADY STATE')
 801  FORMAT('0','T/TFEED=',G11.4/' ','CONVERSION=',G11.4)
 100    CALL RESET
      STOP
        END

)
```

```
  FUNCTION DELG
C DELG CALCULATES THE MOLAR GIBBS FREE ENERGY CHANGE(JOULES/MOLE)
C AT ANY GIVEN TEMPERATURE

        COMPILER DOUBLE PRECISION
        COMPILER NOSTACK
        FUNCTION DELG(Z)
        DELG=4.1868*(-56704.085-46925./Z+2.535*Z*DLOG(Z)-7.0739*Z+3.945E-04*(
     LZ**2)-2.233E-07*(Z**3))
        RETURN
        END

) FUNCTION DELH
C DELH CALCULATES THE MOLAR ENTHALPY CHANGE(JOULES/MOLE)
C AT ANY GIVEN TEMPERATURE

        COMPILER DOUBLE PRECISION
        COMPILER NOSTACK
        FUNCTION DELH(Z)
        DELH=4.1868*(-93850./Z-2.535*Z-3.945E-04*(Z**2)+4.4666E-07*(Z**3)-56704.

     L085)
        RETURN
        END

)
```

```
  FUNCTION CIO2
C CIO2 COMPUTES THE INTEGRAL OF MOLAR HEAT CAPACITY(CAL/MOLE*K)
C OF O2 FROM 298K TO ANY GIVEN TEMPERATURE

        COMPILER DOUBLE PRECISION
        COMPILER NOSTACK
        FUNCTION CIO2(Z)
        CIO2=7.16*Z+5.0E-04*(Z**2)+0.4E 05/Z-2313.36
        RETURN
        END

) FUNCTION CIN2
C CIN2 COMPUTES THE INTEGRAL OF THE MOLAR HEAT CAPACITY(CAL/MOLE*K)
C OF N2 FROM 298K TO ANY GIVEN TEMPERATURE

        COMPILER DOUBLE PRECISION
        COMPILER NOSTACK
        FUNCTION CIN2(Z)
        CIN2=6.83*Z+4.5E-04*(Z**2)+0.12E 05/Z-2116.615
        RETURN
        END

) FUNCTION CIH2
C CIH2 COMPUTES THE INTEGRAL OF MOLAR HEAT CAPACITY(CAL/MOPLE*K) FROM
C 298K TO ANY GIVEN TEMPERATURE (FOR H2)


        COMPILER DOUBLE PRECISION
        COMPILER NOSTACK
        FUNCTION CIH2(Z)
        CIH2=6.62*Z+4.05E-04*(Z**2)-2009.7548
        RETURN
        END

) FUNCTION CIH2O
C CIH2O CALCULATES THE INTEGRAL OF MOLAR HEAT CAPACITY (CAL/MOLE*K)
C  OF H2O(g) FROM 298K TO ANY GIVEN TEMPERATURE

        COMPILER DOUBLE PRECISION
        COMPILER NOSTACK
        FUNCTION CIH2O(Z)
        CIH2O=8.22*Z+7.5E-05*(Z**2)+4.4666E-07*(Z**3)-2469.298
        RETURN
        END

)
```

H_2/H_2O multiplicity

MULTH2 program

```
C MULTH2 SOLVES FOR FUEL INLET TEMPERATURE AS A FUNCTION OF REACTOR
C TEMPERATURE,SCANNED BETWEEN APPROPRIATE LOWER & UPPER LIMITS

      COMPILER DOUBLE PRECISION
      COMPILER NOSTACK
      CALL APPEND(1,'MANY',3,IERR)
      CALL FOPEN(2,'VARIABLES')
      CALL FOPEN(3,'WARNING')

C ENTER PROCESS PARAMETERS
      ACCEPT"INLET FLOW @ 25C & 1 ATM=",UFRATE
      ACCEPT"EXTERNAL CIRCUIT LOAD(OHMS)=",REX
      ACCEPT"INLET FUEL MOLE FRACTION=",YO
      ACCEPT"ELCTRODE GAP(MICRONS)=",UD
      ACCEPT"ELECTRODE AREA(CM2)=",AREA
      ACCEPT"ELECTRODE RESISTANCE(OHMS)=",REL
      ACCEPT"OVERALL HEAT TRANSFER COEFFICIENT(KCAL/HM2C)=",COEFF
      ACCEPT"RATIO OF EXTERNAL TO ELECTRODE AREA=",RATIO
      ACCEPT"AMBIENT TEMPERATURE(KELVIN)=",TCOOL
      ACCEPT"AIR FEED TEMPERATURE(KELVIN)=",TFEEDO
      ACCEPT"STOICHIOMETRIC RATIO FOR AIR FEED=",STCH
      WRITE(2,2)UFRATE,REX,YO,UD,AREA,REL,COEFF,RATIO,TCOOL,TFEEDO,STCH

C ACOIL IS THE AREA ASSOCIATED WITH HEAT INTERACTIONS PER CELL(CM2)
C D IS THE ELECTROLYTE THICKNESS IN CM
C CGUESS IS THE TEMPERATURE AVERAGE HEAT CAPACITY OF THE FUEL FEED STREAM
C (JOULES/KG*K) FOR AN INITIAL GUESS OF 1650K FOR FUEL INLET TEMPERATURE
C THIS VARIABLE IS NECESSARY SINCE IT IS AN IMPLICIT FUNCTION OF T THROUGH
C CIN2 & CIH2
C CIN2 & CIH2 ARE FUNCTIONS THAT CALCULATE THE INTEGRAL OF THE MOLAR HEAT
C CAPACITIES OF N2 & H2 (CAL/MOLE*K) FROM 298K TO ANY GIVEN TEMPERATURE
      ACOIL=RATIO*AREA
      D=1.E-04*UD
      PN2=4.1666E-03*D/(AREA*REX)
      PN13=REL/REX
      CGUESS=(3.09709/(28.-26.*YO))*((1.-YO)*CIN2(1650.)+YO*CIH2(1650.))

C OUTLET TEMPERATURE SCANNING STARTS
      DO 69 I=1,43
      T=350.+50.*FLOAT(I)

C MATERIAL BALANCE IS SOLVED THROUGH NEWTON-RAPHSON'S METHOD
C A & B ARE FUNCTIONS OF TEMPERATURE EXCLUSIVELY
C YO2 IS THE OXYGEN MOLE FRACTION IN THE WELL MIXED CATHODE
      A=(1./(1.+PN13+PN2*DEXP(9700./T)))*(-3.9408E-05*DELG(T))/(REX*UFRATE*YO)

      YO2=.21*(STCH-1.)/(STCH-.21)
      B=(1./(1.+PN13+PN2*DEXP(9700./T)))*(-3.27655E-04*DLOG(DSQRT(YO2)
     L))*T/(REX*UFRATE*YO)
```

```
        C=(1./(1.+PN13+PN2*DEXP(9700./T)))*3.27655E-04*T/(REX*UFRATE*YO)
        PLEFT=A-B
        TYPE"RAPHSON-NEWTON ITERATION"
        TYPE"LEFT HAND SIDE=",PLEFT
        TYPE"TEPERATURE(KELVIN)=",T

C INITIAL GUESS FOR CONVERSION
        X=1.E-13
        IF(ABS(PLEFT-X-C*DLOG((1.-X)/X)).LT.1.E-12)GO TO 90

C RAPHSON-NEWTON ITERATION STARTS
        DO 70 K=1,150
        XNEW=X-(X-C*DLOG((1.-X)/X)-PLEFT)/(1.+C/(X*(1.-X)))

C CONVERSION MUST BE BOUNDED BETWEEN 0 AND 1
        IF(XNEW.LE.1.E-12)XNEW=1.E-12
        IF(XNEW.GT.9.9999999999E-01)XNEW=9.9999999999E-01
        RHS=XNEW-C*DLOG((1.-XNEW)/XNEW)
        TYPE"XNEW=",XNEW
        TYPE"RIGHT HAND SIDE=",RHS
        X=XNEW

C CHECK CALCULATION CLOSURE
        IF(ABS(PLEFT-RHS).LT.1.E-12)GO TO 90
  70    CONTINUE

C PROGRAM STOPS DUE TO NON-CONVERGENCE AFTER 150 ITERATIONS
        TYPE"NON-CONVERGENCE AFTER 150 ITERATIONS"
        WRITE(3,1)T,RHS,PLEFT,X
        GO TO 100

C NORMAL EXIT FROM RAPHSON-NEWTON LOOP
  90    XS=X

C VOLT IS THE REVERSIBLE VOLTAGE @ CELL CONDITIONS
C AMP IS THE CELL'S CURRENT OUTPUT
C PMOLWT IS THE FUEL MOLECULAR WEIGHT @ CELL CONDITIONS
C DELG IS A FUNCTION THAT COMPUTES THE GIBBS FREE ENERGY CHANGE PER MOLE
C OF FUEL (JOULE/MOLE) AT ANY GIVEN TEMPERATURE
        VOLT=-5.1813E-06*DELG(T)+4.3079793E-05*T*DLOG(DSQRT(YO2)*(1.-X)/X)
        AMP=VOLT/(REX*(1.+PN13+PN2*DEXP(9700./T)))
        PMOLWT=16.*YO*XS+28.-26.*YO

C SINCE INLET TEMPERATURE IS ALSO CONTAINED IN THE FUEL'S SPECIFIC HEAT,
C THE SOLUTION INVOLVES AN ITERATIVE SCHEME WITH AN INITIAL SPECIFIC HEAT
C CALCULATED @ 1650K
        CPI=CGUESS
        PREV=1650.
        CP=(YO*XS*CIH2O(T)+YO*(1.-XS)*CIH2(T)+(1.-YO)*CIN2(T))*4186.8/(PMOLWT*
     L(T-298.15))
```

```
C INLET TEMPERATURE CALCULATION LOOP
      DO 71 J=1,150

C PMAIR IS THE EXCESS AIR'S MOLECULAR WEIGHT
C YN2 IS THE NITROGEN MOLE FRACTION IN THE WELL MIXED CATHODE
C CIO2 & CIH2O ARE FUNCTIONS THAT COMPUTE THE INTEGRAL OF MOLAR SPECIFIC
C HEAT(CAL/MOLE*K) FROM 298K TO ANY GIVEN TEMPERATURE
C DELH COMPUTES THE ENTHALPY CHANGE PER MOLE OF FUEL(JOULE/MOLE) @ ANY
C GIVEN TEMPERATURE

      PMAIR=(28.84*STCH-6.72)/(STCH-.21)
      YN2=1.-YO2
      TM=.5*(T+TFEEDO)
      PN5=CP/CPI
      Z1=(170719.276/(28.-26.*YO))*COEFF*ACOIL*(T-TCOOL)/(CPI*UFRATE)+(5.09501

     L25E05*AMP/PMAIR)*(STCH/.233-1.)*(T-TFEEDO)/(TM-298.15)*(YO2*CIO2(TM)+YN

     L2*CIN2(TM))/(CPI*UFRATE*(28.-26.*YO))

      Z2=PN5*(T-298.15)*(1.+(121.688/(28.-26.*YO))*AMP/UFRATE)
      AUX1=2.0934*(TFEEDO-298.15)*CIO2(TFEEDO)/(TFEEDO-298.15)
      AUX2=AMP*REX*193000./(-DELH(298.15))
      AUX3=(7605.7688/(28.-26.*YO))*AMP/(CPI*UFRATE)
      Z3=AUX3*(AUX1+(1.-AUX2)*(-DELH(298.15)))
      TIN=Z2+Z1-Z3+298.15

C CALCULATED & PREVIOUS INLET TEMPERATURE ARE COMPARED;CONVERGENCE IS
C ACHEIVED WHEN THE DIFFERENCE IS LESS THAN 1K;OTHERWISE,THE ITERATION
C IS REPEATED AFTER COMPUTING THE INLET FUEL SPECIFIC HEAT @ CALCULATED
C INLET TEMPERATURE
      TYPE"CALCULATED INLET TEMPERATURE(KELVIN)=",TIN
      IF(ABS(TIN-PREV).LE.1.)GO TO 91
      CPI=(4186.8*((1.-YO)*CIN2(TIN)+YO*CIH2(TIN)))/((TIN-298.15)*(28.-26.*YO))
      PREV=TIN
 71   CONTINUE

C PROGRAM STOPS IF TEMPERATURE DOES NOT CONVERGE AFTER 150 TRIALS
      TYPE"NON-CONVERGENCE AFTER 150 ITERATIONS"
      WRITE(3,3)T,TIN
      GO TO 100

C NORMAL EXIT FROM ITERATION
 91   TINLET=TIN

C STORE DATA FOR PRINTING AND PLOTTING
      WRITE(1,4)TINLET,T
 69   CONTINUE
  1   FORMAT('0','RAPHSON-NEWTON ITERATION DOES NOT CONVERGE'/' ','TEM
```

```
     LPERATURE(KELVIN)=',G11.4/' ','RIGHT HAND SIDE OF EXPRESSION=',G11.4/
     L' ','LEFT HAND SIDE OF EXPRESSION=',G11.4/' ','CONVERSION=',G11.4)
   2    FORMAT('1','INLET FLOW @ 25C & 1 ATM(CC/MIN)=',G11.4/' ','EXTER
     LNAL CIRCUIT LOAD(OHMS)=',G11.4/' ','INLET FUEL MOLE FRACTION=',G11.4/
     L' ','ELECTRODE GAP(MICRONS)=',G11.4/' ','ELECTRODE AREA(CM2)=',G11.4/
     L' ','ELECTRODE RESISTANCE(OHMS)=',G11.4/' ','OVERALL HEAT TRANSFER CO
     LEFFICIENT(KCAL/HM2K)=',G11.4/' ','RATIO OF EXTERNAL TO ELECTRODE AREA=
     L',G11.4/' ','AMBIENT TEMPERATURE(KELVIN)=',G11.4/' ','AIR FEED TEMPE
     LRATURE(KELVIN)=',G11.4/' ','EXCESS AIR RATIO=',G11.4)
   3    FORMAT('0','INLET TEMPERATURE DOES NOT CONVERGE'/' ','OUTLET TEM
     LPERATURE(KELVIN)=',G11.4/' ','INLET TEMPERATURE(KELVIN)=',G11.4)
   4    FORMAT(1X,G11.4,',',G11.4)
  100   CALL RESET
        STOP
        END

)
```

```
  FUNCTION DELG
C DELG CALCULATES THE MOLAR GIBBS FREE ENERGY CHANGE(JOULES/MOLE)
C AT ANY GIVEN TEMPERATURE

        COMPILER DOUBLE PRECISION
        COMPILER NOSTACK
        FUNCTION DELG(Z)
        DELG=4.1868*(-56704.085-46925./Z+2.535*Z*DLOG(Z)-7.0739*Z+3.945E-04*(
     LZ**2)-2.233E-07*(Z**3))
        RETURN
        END

) FUNCTION DELH
C DELH CALCULATES THE MOLAR ENTHALPY CHANGE(JOULES/MOLE)
C AT ANY GIVEN TEMPERATURE

        COMPILER DOUBLE PRECISION
        COMPILER NOSTACK
        FUNCTION DELH(Z)
        DELH=4.1868*(-93850./Z-2.535*Z-3.945E-04*(Z**2)+4.4666E-07*(Z**3)-56704.

     L085)
        RETURN
        END

)
```

```
  FUNCTION CIO2
C CIO2 COMPUTES THE INTEGRAL OF MOLAR HEAT CAPACITY(CAL/MOLE*K)
C OF O2 FROM 298K TO ANY GIVEN TEMPERATURE

        COMPILER DOUBLE PRECISION
        COMPILER NOSTACK
        FUNCTION CIO2(Z)
        CIO2=7.16*Z+5.0E-04*(Z**2)+0.4E 05/Z-2313.36
        RETURN
        END

) FUNCTION CIN2
C CIN2 COMPUTES THE INTEGRAL OF THE MOLAR HEAT CAPACITY(CAL/MOLE*K)
C OF N2 FROM 298K TO ANY GIVEN TEMPERATURE

        COMPILER DOUBLE PRECISION
        COMPILER NOSTACK
        FUNCTION CIN2(Z)
        CIN2=6.83*Z+4.5E-04*(Z**2)+0.12E 05/Z-2116.615
        RETURN
        END

) FUNCTION CIH2
C CIH2 COMPUTES THE INTEGRAL OF MOLAR HEAT CAPACITY(CAL/MOPLE*K) FROM
C 298K TO ANY GIVEN TEMPERATURE (FOR H2)


        COMPILER DOUBLE PRECISION
        COMPILER NOSTACK
        FUNCTION CIH2(Z)
        CIH2=6.62*Z+4.05E-04*(Z**2)-2009.7548
        RETURN
        END

) FUNCTION CIH2O
C CIH2O CALCULATES THE INTEGRAL OF MOLAR HEAT CAPACITY (CAL/MOLE*K)
C  OF H2O(g) FROM 298K TO ANY GIVEN TEMPERATURE

        COMPILER DOUBLE PRECISION
        COMPILER NOSTACK
        FUNCTION CIH2O(Z)
        CIH2O=8.22*Z+7.5E-05*(Z**2)+4.4666E-07*(Z**3)-2469.298
        RETURN
        END

)
```

Monolith fuel cell

MONOLITH program

```
C MONOLITH SOLVES THE GOVERNING MATERIAL & ENERGY BALANCES FOR THE
C CROSS FLOW MONOLITH CELL.THE INTEGRATION METHOD IS A 4th ORDER RUNGE-
C KUTTA ALGORITHM.

      COMPILER DOUBLE PRECISION
      COMPILER NOSTACK
      DIMENSION DIST(1000),VECT1(210),VECT2(210),VECT3(210),
     LVECT5(210),VECT6(1000),VECT7(210),VECT8(210),VECT9(210),
     LVECT4(210),VECT0(1000)


      COMMON A1,A2,A3,A4,A5,A6,A7,TAIR,TFEED,RQRD,YO,
     LPN,X,REX,REL,RECIP,A9,A10,PL,A12

C FILE ACCUM STORES ACCUMULATED CURRENT VS REACTOR AXIAL DIMENSION
C FILE PLOTCUR STORES LOCAL CURRENT VS REACTOR AXIAL DIMENSION
C FILE PLOTX STORES CONVERSION VS REACTOR AXIAL DIMENSION
C FILE PLOTS STORES SOLID TEMPERATURE VS REACTOR AXIAL DIMENSION
C FILE PLOTG STORES GAS TEMPERATURE VS REACTOR AXIAL DIMENSION
C FILE OUTPUT STORES MAIN OUTPUT VALUES AFTER CONVERGENCE
C FILE ERROR CONTAINS THE VARIOUS ERROR,DEFAULT CONDITION & WARNING MESSAGES
C THAT MAY BE GENERATED DURING THE EXECUTION OF THE PROGRAM
C FILE PARAMETERS CONTAINS THE MAIN PROCESS PARAMETERS
C FILE EXCPECTED CONTAINS THE EXCPECTED PERFORMANCE OF THE MONOLITH AS
C CALCULATED @ END OF PRELIMINARY ITERATIONS
C FILE VOLTREV STORES REVERSIBLE VOLTAGE VS REACTOR AXIAL DIMENSION
C FILE VOLTACT STORES ACTUAL VOLTAGE VS REACTOR AXIAL DIMENSION

      CALL FOPEN(27,'EXCPECTED')
      CALL FOPEN(28,'PARAMETERS')
      CALL FOPEN(20,'ERRORS')
      CALL FOPEN(21,'OUTPUT')
      CALL FOPEN(22,'PLOTS')
      CALL FOPEN(24,'PLOTX')
      CALL FOPEN(25,'PLOTCUR')
      CALL FOPEN(26,'ACCUM')
      CALL FOPEN(29,'VOLTREV')
      CALL FOPEN(30,'VOLTACT')
      CALL FOPEN(35,'PLOTG')

C ENTER MAIN PROCESS VARIABLES

      ACCEPT "NUSSELT NUMBER=",PNUSS
      ACCEPT"FEED TEMPERATURE(KELVIN)=",TFEED
      ACCEPT "AMBIENT TEMPERATURE FOR FLOW RATE REFERENCE(KELVIN)=",TREF
      ACCEPT "INLET FUEL MOLE FRACTION=",YO
      ACCEPT "CHANNEL CROSS SECTION(MM2)=",AREA
      ACCEPT "WALL THICKNESS(MICRONS)=",DELTA
      ACCEPT "AIR TEMPERATURE(KELVIN)=",TAIR
```

```
      ACCEPT "CONTACT RESISTANCE(OHM)=",REL
      ACCEPT "NUMBER OF CHANNELS IN X DIMENSION=",X
      ACCEPT "CHANNEL LENGTH(CM)=",PL
      ACCEPT "NUMBER OF BATTERIES IN SERIES=",PN
      ACCEPT "GUESS TEMPERATURE (FOR LOAD DETERMINATION)-(KELVIN)=",TGUESS

C RECIP IS A REAL WHOLE NUMBER EQUAL TO RECIPROCAL OF INTEGRATION STEP
C RECIP MUST BE A MULTIPLE OF 200. AND CANNOT EXCEED 1000. WITH THE
C PRESENT DIMENSION DECLARATION

      ACCEPT "NUMBER OF DISCRETE ELEMENTS IN A CHANNEL(WHOLE NO.)=",RECIP
      ACCEPT "DESIRED CONVERSION=",GOAL
      ACCEPT "STOICHIOMETRIC RATIO FOR AIR FEED=",EXC
      ACCEPT "ZIRCONIA THERMAL CONDUCTIVITY(WATTS/MK)=",COND
      ACCEPT "MAXIMUM NUMBER OF ITERATIONS FOR CURRENT DIST. LOOP=",MAX

C CALCULATE SOLID CROSS SECTION PER CHANNEL(M2)
      SAREA=1.E-06*(2.*(1.E-03*DELTA*DSQRT(AREA)+5.E-04*DELTA*(2.E-03*DELTA
     L+DSQRT(AREA)))

C CALCULATE HEAT TRANSFER COEFFICIENT,WITH CONSTANT GAS PROPERTIES(JOULES/SM2K)
      COEFF=PNUSS*55./DSQRT(AREA)

C THE FOLLOWING SECTION OF THE PROGRAM CALCULATES THE OPTIMUM EXTERNAL LOAD &
C FEED RATE REQUIRED IN ORDER TO ACHEIVE THE DESIRED CONVERSION @ A TEMPERATURE
C TGUESS,MAXIMIZING POWER OUTPUT,FOR THE ABOVE SPECIFIED GEOMETRIC & ELECTRICAL
C CONFIGURATION
C A PRELIMINARY DO LOOP CHECKS THE OPERATING TEMPERATURE LEVEL & REPEATS
C THE CALCULATION UNTIL A SATISFACTORY CONVERGENCE(JUDGED BY THE OPERATOR)
C IS ACHEIVED

 1    RI=(4.1666E-05*DELTA/AREA)*DEXP(9700./TGUESS)

C CALCULATE NUMBER OF REPETITIVE(CHANNEL+WALL)UNITS ALONG A CHANNEL
C THIS SHOULD NOT BE CONFUSED WITH RECIPROCAL OF INTEGRATION STEP
      UNITS=10.*PL/(DSQRT(AREA)+1.E-03*DELTA)

C CALCULATE EXTERNAL LOAD THAT MAXIMIZES POWER OUTPUT FOR SPECIFIED ASSUMED
C UNIFORM CONDITIONS
      REXl=PN*RI/(X*UNITS)+(PN+1.)*REL

C CALCULATE THE POSSIBLE EXTREME VALUES OF THE LOGARITHMIC TERM OF THE RE-
C VERSIBLE VOLTAGE;MINIMUM CONVERSION IS TAKEN AS 0.001
      ZMIN=4.308E-05*TGUESS*DLOG((1.-GOAL)*0.4582/GOAL)
      ZMAX=4.308E-05*TGUESS*DLOG(999.*0.4582)
      EAVG=-5.181E-06*DELG(TGUESS)+(ZMIN+ZMAX)/2.

C CALCULATE THE CURRENT FLOWING THROUGH AN ELEMENT @ TGUESS & WITH REXl
      AMPAVG=PN*EAVG/(PN*RI+X*UNITS*(REXl+(PN+1.)*REL))
```

```
C CALCULATE MOLES REACTED PER CHANNEL PER MINUTE
      RTED=UNITS*AMPAVG*3.1088E-04

C CALCULATE MOLES REQUIRED PER CHANNEL PER MINUTE
      RQRD=RTED/(GOAL*YO)

C CALCULATE FEED PER MONOLITH @ REFERENCE CONDITIONS (CC/MIN)
      RATE1=((RQRD*PN*X*28.)/0.341227)*TREF

C CALCULATE O2 CROSSFLOW (MOLES/CHANNEL*MINUTE)
      RTEDO2=.5*RTED

C CALCULATE PRODUCT OF INLET MASS FLOW RATE & AVERAGE HEAT CAPACITY
C (JOULE/SEC K)
      HTCAP1=.519*RQRD

C CALCULATE TOTAL AIR STOICHIOMETRIC REQUIREMENT (MOLES/MIN)-21%O2 IN AIR
      STOICH=.5*RTED*PN*X/.21

C CALCULATE ACTUAL AIR FLOW RATE @ REFERENCE CONDITIONS (CC/MIN PER MONOLITH)
      RATE2=STOICH*EXC*82.0567*TREF

C CALCULATE TOTAL AIR MOLAR FLOW RATE (MOLES/SEC PER MONOLITH)
      STCH1=STOICH*EXC/60.

C CALCULATE PRODUCT OF PROPORTIONAL AIR MASS FLOW & AVERAGE HEAT CAPACITY
C (JOULES/SEC K) PER CHANNEL (CONSTANT GAS PROPERTIES)
      HTCAP2=32.77*STCH1/(X*PN)

C CALCULATE EXCPECTED POWER OUTPUT (WATTS)
      POWER=((UNITS*AMPAVG*X)**2)*REX1

C THE FOLLOWING SECTION COMPARES THE CALCULATED & GUESSED TEMPERATURES
C & PROMPTS THE USER TO DECIDE WHETHER OR NOT TO MAKE A NEW GUESS
C 1st CALCULATE HEAT GENERATION PER UNIT CELL(WATTS)
C CALCULATE ACTUAL VOLTAGE(OHMS)
      EACT1=EAVG*UNITS*X*(REX1+(PN+1.)*REL)/(PN*RI+UNITS*X*(REX1+(PN+1.)*REL))

      QGEN=(1.-EACT1/(-5.181E-06*DELH(298.15)))*(-DELH(298.15))*(5.181E-06*
     LAMPAVG)

C CALCULATE ESTIMATED TOTAL HEAT GENERATION (WATTS)
      QTOT=UNITS*QGEN

C CALCULATE SOLID TEMPERATURE
      TCALC=(QTOT+HTCAP1*TFEED+HTCAP2*TAIR)/(HTCAP1+HTCAP2)

      TYPE "INITIAL GUESS FOR SOLID TEMPERATURE(KELVIN)=",TGUESS
      TYPE "CALCULATED SOLID TEMPERATURE(KELVIN)=",TCALC
      TYPE "CALCULATED OPTIMUM RESISTANCE @ TGUESS(OHMS)=",REX1
```

```
      TYPE "CALCULATED POWER OUTPUT(WATTS)=",POWER
      TYPE "FEED PER MONOLITH(CC/MIN @ 298K & 1 ATM)=",RATE1
      TYPE "AIR FEED PER MONOLITH(CC/MIN @ 298K & 1 ATM)=",RATE2

C THE USER NOW DECIDES WHETHER OR NOT TO TRY A NEW PRELIMINARY ITERATION

      ACCEPT "WANT NEW ITERATION?(1=YES;0=NO)",IFATE
      IF(IFATE.EQ.0) GO TO 2
      ACCEPT "NEW GUESS TEMPERATURE FOR LOAD DETERMINATION=",TGUESS
      GO TO 1
 2    WRITE(27,500) POWER,REX1,GOAL,AMPAVG,EACT1,TGUESS,TCALC,RATE1,RATE2,EXC
      CALL FCLOS(27)

C THE USER NOW DECIDES WHAT  ARE THE ACTUAL FLOW RATES AND LOAD
C MODEL ASSUMES 21% O2 THROUGHOUT TRANSVERSE CHANNEL,SMALL AIR RATES
C SHOULD THEREFORE NOT BE USED IF MEANINGFUL RESULTS ARE DESIRED
      ACCEPT"MODIFICATION COEFFICIENT FOR FUEL FLOW=",ZMOD1
      ACCEPT"MODIFICATION COEFFICIENT FOR AIR FLOW=",ZMOD2
      RATE1=RATE1*ZMOD1
      RATE2=RATE2*ZMOD2
      RQRD=RQRD*ZMOD1
      STCH1=STCH1*ZMOD2
      TYPE"CALCULATED LOAD=",REX1
      ACCEPT"ACTUAL LOAD=",REX
      WRITE(28,501) TFEED,YO,RATE1,RATE2,X,PL,PN,DELTA,AREA,TREF,REX,PNUSS

C HAVING CLOSED THE PRELIMINARY ESTIMATION LOOP,THE PROGRAM NOW PROCEEDS
C TO INTEGRATE THE GOVERNING DIFFERENTIAL EQUATIONS.THERE ARE THREE EMBEDDED
C LOOPS:AN INTERNAL (INEGRATION) LOOP ,AT THE END OF WHICH CURRENT DISTRIBU-
C TION IS VERIFIED & RECALCULATED,THE RESULTS BEING FED BACK TO THE INTEGRA-
C TION LOOP UNTIL THE CURRENT DISTRIBUTION CONVERGES TO SOME REPETITIVE PATTERN
C ,THE END BOUNDARY CONDITION IS THEN VERIFIED & THE WHOLE PROCESS REPEATED
C IF NECESSARY.

C THE ORIGINAL CURRENT DISTRIBUTION IS ASSUMED TO BE UNIFORM;THE FOLLOWING LOOP
C ASSIGNS AN EQUAL CURRENT DISTRIBUTION PARAMETER TO EACH ELEMENTARY UNIT (NOT
C TO BE CONFUSED WITH ELEMENTARY FUEL CELL OF SIZE=CHANNEL WIDTH ,BUT,IN THIS
C CASE,TOTAL LENGTH DIVIDED BY INTEGRATION STEP)

      NNN=INT(RECIP/200.)
      M=INT(RECIP)
      DO 5 IDIST=1,M
      DIST(IDIST)=RECIP
 5    CONTINUE

C THE DIMENSIONAL & DIMENSIONLESS PARAMETERS NECESSARY IN ORDER TO
C INTEGRATE THE DIFFERENTIAL EQUATIONS ARE NOW CALCULATED

C A1 IS THE DIMENSIONLESS COEFFICIENT OF THE LOGARITHMIC TERM
C IN NERNST'S EQUATION
```

```
      A1=4.307979E-05*TFEED

C A2 IS A DIMENSIONLESS RATIO OF PREEXPONENTIAL ELECTROLYTE RESISTANCE (MULTIPLI

C ED BY THE NUMBER OF SERIES BATTERIES) TO EXTERNAL & CONTACT RESISTANCE.IN EVA-

C LUATING THE ELECTROLYTE RESISTANCE,THE APPROPIATE CROSS SECTION FOR CURRENT P-

C ASSAGE IS INTRODUCED.

      A2=(4.1666E-06*DELTA*PN/(DSQRT(AREA)*(REX+(PN+1.)*REL)))*(RECIP/PL)

C A3 IS A DIMENSIONAL CONSTANT HAVING UNITS OF RECIPROC AL AMPERES.
      A3=-5.181E-08*(DELH(298.15)*PL/(COND*SAREA*TFEED))*RECIP

C A4 IS THE ARRHENIUS NUMBER FOR THE ELECTROLYTE RESISTANCE, CALCULATED @ TFEED

      A4=9700./TFEED

C A5 IS A GEOMETRIC FACTOR WHICH ALLOWS FOR THE FACT THAT NOT ALL OF THE SURFA-
C CE IS AVAILABLE FOR OXYGEN PASSAGE,DUE TO FINITE WALL THICKNESS

      A5=DSQRT(AREA)/(DSQRT(AREA)+1.E-03*DELTA)


C A6 & A7 ARE DIMENSIONLESS CONSTANTS APPEARING IN THE ENERGY BALANCE
      A6=STCH1*PL*1.E-02/(X*PN*COND*SAREA)
      A7=1.E-02*PL/(COND*SAREA)

C A9 THROUGH A12 ARE CONSTANTS APPEARING IN THE ENERGY EQUATIONS
      A9=PN*RECIP*PL*2.59067E-08/(COND*SAREA)
      A10=4.E-07*DSQRT(AREA)*COEFF*(PL**2)/(COND*SAREA)
      A12=4.E-03*DSQRT(AREA)*COEFF

C SET LIMIT FOR NUMBER OF INTEGRATIONS ALONG REACTOR

      II=INT(RECIP)

C SET INTEGRATION STEP

      H=1./RECIP

C SINCE 0 CO2 WOULD GIVE RISE TO AN INFINITE VOLTAGE ,WE INTRODUCE A REALISTIC
C VALUE FOR CO2 @ L=0,& KEEP IT OUT OF MATERIAL BALANCE CALCULATIONS

      ACCEPT "ENTER A SMALL(APPROX.0.1%) QUANTITY FOR CO2 @ L=0  ",TRACE

C SET BOUNDARY VALUE CHECK COUNTER TO 1
```

```
        L=1

C THE SOLID FRONT FACE TEMPERATURE IS GUESSED @ EACH ITERATION,AND MUST SATISFY
C THE END BOUNDARY CONDITION

        ACCEPT "SOLID FRONT TEMPERATURE(KELVIN)=",TFRONT
        IF(L.EQ.1)GO TO 20
  301   KP=INT(RECIP)
        DO 302 KR=1,KP
        DIST(KR)=RECIP
  302   CONTINUE


C THE PROGRAM TREATS EITHER INSULATED OR NON-INSULATED BOUNDARY COND'S.

   20   ACCEPT"BOUNDARY?(1=INSULATED;0=NON.INS) ",IBOUND
        IF(IBOUND.EQ.1)GO TO 699

C THE STAGNATION HEAT TRANSFER COEFFICIENT FOR THE NON-INSULATED CONDITION
C IS FIRSTLY CALCULATED (UNITS=JOULE/SM2K)

        STAGH=18.5*DSQRT(RATE1*TFEED/(TREF*DELTA))
        SLOPE=(STAGH*PL*1.E-02/COND)*(TFRONT/TFEED-1.)
        GO TO 698

C FOR THE INSULATED CONDITION,THE SLOPE OF THE SOLID TEMPERATURE PROFILE IS
C SET TO 0 @ REACTOR INLET

  699   SLOPE=0.

C CURRENT DISTRIBUTION LOOP STARTS

  698   DO 7 K=1,MAX

C THE INITIAL CHANNEL TOTAL CURRENT IS SET TO 0

        AMPTOT=0.

C SET THE PRODUCT OF LOCAL CURRENT & VOLTAGE TO 0

        PROD=0.

C THE DIMENSIONLESS LENGTH IS SET TO 0.

        AXIS=0.
        NK=1
C CINTEGRATION PROPER STARTS

        DO 8 I=1,II
```

```
C THE DIFFERENTIAL EQUATIONS ARE INTEGRATED VIA A 4TH ORDER RUNGE-KUTTA METHOD
C A IS THE DIMENSIONLESS FIRST DERIVATIVE OF THE SOLID TEMPERATURE WITH RES-
C PECT TO REACTOR LENGTH(TEMPERATURES ARE REFERRED TO TFEED;LENGTHS TO REACTOR
C LENGTH)
C B IS THE DIMENSIONLESS SOLID TEMPERATURE
C C IS THE DIMENSIONLESS GAS TEMPERATURE
C D IS THE CONVERSION

      IF(I.GT.1) GO TO 9

C THE FIRST INTEGRATION STEP IS DIFFERENT FROM THE OTHER ONES

      B=TFRONT/TFEED
      A=SLOPE
      C=1.

C XFIC IS A FICTITIOUS CONVERSION DUE TO THE PRESENCE OF CO2,WHICH IS ONLY USED
C FOR INITIAL VOLTAGE CALCULATION & IS SUBSEQUENTLY KEPT OUT OF THE MATERIAL
C BALANCE

      XFIC=TRACE/YO
      D=XFIC

C BEFORE EACH DERIVATIVE EVALUATION,THE CONVERSION IS CHECKED,AND,IF NEEDED,
C DEFAULT VALUES ARE INTRODUCED IN ORDER NOT TO STOP THE INTEGRATION.THE DE-
C FAULT CONDITION IS LOCATED & RECORDED

 9    O=D
      NI=1
      GO TO 69
 800  D=O
      AS1=H*DA(B,C,D,DIST(I))
      BS1=H*DB(A)
      CG1=H*DC(B,C,D,DIST(I))
      DX1=H*DD(B,D,DIST(I))
      O=D+DX1/2.
      NI=2
      GO TO 69
 801  ZN=O
      AS2=H*DA(B+BS1/2.,C+CG1/2.,ZN,DIST(I))
      BS2=H*DB(A+AS1/2.)
      CG2=H*DC(B+BS1/2.,C+CG1/2.,ZN,DIST(I))
      DX2=H*DD(B+BS1/2.,ZN,DIST(I))
      O=D+DX2/2.
      NI=3
      GO TO 69
 802  AU=O
      AS3=H*DA(B+BS2/2.,C+CG2/2.,AU,DIST(I))
      BS3=H*DB(A+AS2/2.)
      CG3=H*DC(B+BS2/2.,C+CG2/2.,AU,DIST(I))
```

```
        DX3=H*DD(B+BS2/2.,AU,DIST(I))
        O=D+DX3/2.
        NI=4
        GO TO 69
 803    ZR=O
        AS4=H*DA(B+BS3/2.,C+CG3/2.,ZR,DIST(I))
        BS4=H*DB(A+AS3/2.)
        CG4=H*DC(B+BS3/2.,C+CG3/2.,ZR,DIST(I))
        DX4=H*DD(B+BS3/2.,ZR,DIST(I))
        A=A+(AS1+2.*AS2+2.*AS3+AS4)/6.
        B=B+(BS1+2.*BS2+2.*BS3+BS4)/6.
        C=C+(CG1+2.*CG2+2.*CG3+CG4)/6.
        GO TO 701
  69    IF(O.LE.1.E-06) GO TO 900
        GO TO 700
 900    O=1.E-06
        GO TO (800,801,802,803) NI
 700    IF(O.GT.9.999999E-01) GO TO 600
        GO TO (800,801,802,803) NI
 600    O=9.999999E-01
        GO TO (800,801,802,803) NI

C INITIAL CONVERSION SET TO 0(XFIC IS ONLY FOR VOLTAGE CALCULATION)

 701    IF(I.GT.1) GO TO 10
        D=(DX1+2.*DX2+2.*DX3+DX4)/6.
        IF(D.GT.1.E-06) GO TO 11
        D=1.E-06
        GO TO 11
  10    D=D+(DX1+2.*DX2+2.*DX3+DX4)/6.
        IF(D.LE.1.E-06) GO TO 703
        GO TO 704
 703    D=1.E-06
        GO TO 11
 704    IF(D.LT.9.999999E-01) GO TO 11
        D=9.999999E-01
  11    AXIS=AXIS+H
        T=TFEED*B
        RES=REX+(PN+1.)*REL

C CALCULATE CURRENT FOR THE ITH ELEMENT
C CONC CALCULATES THE LOGARITHMIC TERM IN THE VOLTAGE EXPRESSION

        CUR=((-5.181E-06*DELG(T))+A1*B*CONC(D))*PN/(RES*(X*DIST(I)+(A2/
     LA5)*DEXP(A4/B)))

C CALCULATE THE ACCUMULATED CURRENT

        AMPTOT=AMPTOT+CUR
```

```
C CALCULATE LOCAL REVERSIBLE & ACTUAL VOLTAGES

        EREV=-5.181E-06*DELG(T)+4.3079792E-05*T*CONC(D)
        EACT=EREV-(CUR*DEXP(9700./T)*4.1666E-06*DELTA/(DSQRT(AREA)*A5*PL
     L))*RECIP

C CALCULATE THE SUM OF PRODUCTS OF CURRENT TIMES VOLTAGE

        PROD=PROD+EACT*CUR
        VECT6(I)=CUR
        VECT0(I)=AXIS
        IF(((I/NNN)*NNN).NE.I)GO TO 401

        TYPE "LENGTH=",AXIS
        TYPE "SOLID TEMPERATURE=",B
        TYPE "GAS TEMPERATURE=",C
        TYPE "CONVERSION=",D
        TYPE "       "
        VECT1(NK)=AXIS
        VECT2(NK)=A
        VECT3(NK)=B*TFEED
        VECT4(NK)=C*TFEED
        VECT5(NK)=D
        VECT7(NK)=AMPTOT
        VECT8(NK)=EREV
        VECT9(NK)=EACT
        NK=NK+1
 401    CONTINUE
   8    CONTINUE

C THE NEW CURRENT DISTRIBUTION PARAMETERS ARE CALCULATED.EACH INTEGRATION IS
C CHARACTERIZED BY A MEAN & A 2ND MOMENT WHICH ARE COMPARED TO THE PREVIOUS
C VALUES.CONVERGENCE IS ACHEIVED WHEN THE RELATIVE VARIATION BETWEEN SUCCE-
C SSIVE INTEGRATIONS IS LESS THAN .001 , BOTH FOR THE MEAN & FOR THE SUM OF
C SQUARES OF VARIATIONS BETWEEN RECIPROCALS OF CURRENT DISTRIBUTION
C COEFFICIENT(I.E.LOCAL OVER TOTAL CURRENT) AND THE MEAN CURRENT PER
C ELEMENT

        PMEAN=AMPTOT/RECIP
        SIGMA=0.
        DO 12 KK=1,II
        SIGMA=(VECT6(KK)/AMPTOT-1./RECIP)**2+SIGMA
  12    CONTINUE

C THE INITIAL COMPARISON IS BETWEEN THE ASSUMED UNIFORM DISTRIBUTION AND THE
C 1st ITERATION

        IF(K.GT.1) GO TO 14

C THE ASSUMED DISTRIBUTION ASSIGNED AMPAVG AMPERES TO EACH ELEMENTARY CELL;
```

```
C THIS MUST BE COMPARED WITH AMPTOT/UNITS(INTEGRATION STEP IS NOT NECESSARI-
C LY EQUAL TO THE RECIPROCAL OF THE NUMBER OF ELEMENTARY CELLS).THE ASSUMED
C 2nd MOMENT IS,OF COURSE,0 FOR THE 1ST ITERATION

        TEST1=(ABS(AMPTOT/UNITS-AMPAVG))/AMPAVG
        TEST2=SIGMA
        IF((TEST1.LT.1.E-03).AND.(TEST2.LT.1.E-03))GO TO 15

C STORE MEAN & 2ND MOMENT FOR NEXT COMPARISON

        PREV1=PMEAN
        PREV2=SIGMA
        TRIST=AMPTOT/UNITS
        TYPE "DISTRIBUTION ITERATION #1"
        TYPE "ASSUMED MEAN CURRENT PER UNIT CELL(AMPS)=",AMPAVG
        TYPE "CALCULATED MEAN CURRENT PER UNIT CELL(AMPS)=",TRIST
        TYPE "CALCULATED 2nd MOMENT OF DISTRIBUTION=",SIGMA
        TYPE "          "

C CALCULATE NEW CURRENT DISTRIBUTION

  17    DO 16 MM=1,M
        DIST(MM)=AMPTOT/VECT6(MM)
  16    CONTINUE
        GO TO 99
  14    IF(((ABS(SIGMA-PREV2)/PREV2).LT.1.E-03).AND.((ABS(PMEAN-PREV1)/PREV1).LT
     L.1.E-03))GO TO 15
        TYPE "DISTRIBUTION ITERATION #=",K
        TYPE "PREVIOUS MEAN CURRENT PER UNIT ELEMENT(AMPS)=",PREV1
        TYPE "CALCULATED MEAN CURRENT PER UNIT ELEMENT(AMPS)=",PMEAN
        TYPE "PREVIOUS 2ND MOMENT OF DISTRIBUTION=",SIGMA
        TYPE "                    "
        PREV1=PMEAN
        PREV2=SIGMA
        GO TO 17
 99     CONTINUE
   7    CONTINUE
        TYPE "TOO MANY ITERATIONS IN CURRENT DISTRIBUTION LOOP"
        WRITE(20,18) L
        GO TO 100

C CHECK KHIRCHOFF'S LAW
C DROP1 IS THE PRODUCT OF THE SQUARE OF THE TOTAL CHANNEL CURRENT,TIMES THE
C NUMBER OF CHANNELS IN THE X DIMENSION,TIMES THE EXTERNAL LOAD
 15     DROP1=X*REX*(AMPTOT**2)

C DROP2 IS THE PRODUCT OF THE SQUARE OF THE TOTAL CHANNEL CURRENT,TIMES THE
C NUMBER OF CHANNELS IN THE X DIMENSION,TIMES N+1 CONTACT RESISTANCES
```

```
      DROP2=(PN+1.)*X*REL*(AMPTOT**2)

C DROP3 IS THE PRODUCT SUM OF THE PRODUCTS OF THE CELL EMF'S TIMES LOCAL
C CURRENT,MULTIPLIED BY THE NUMBER OF BATTERIES IN SERIES

      DROP3=PN*PROD

C DIFF IS THE PERCENTAGE ERROR IN THE ALGEBRAIC SUM OF THE EMF'S

      DIFF=((DROP3-DROP2)-DROP1)*100./DROP1
      TYPE "PERCENTAGE ERROR IN KHIRCHOFF'S LAW=",DIFF

C THE END BOUNDARY CONDITION IS VERIFIED ACCORDING TO THE PHYSICAL SITUATION
C (INSULATED OR NON-INSULATED)

      IF(IBOUND.EQ.1)GO TO 697
      ENDSLP=-.4*PL*(B-C)/COND
      TYPE "FIRST DERIVATIVE OF SOLID TEMPERATURE @ OUTLET=",A
      TYPE"CALCULATED SLOPE FROM BOUNDARY CONDITION=",ENDSLP
      CHECK=100.*ABS((ENDSLP-A)/ENDSLP)
      TYPE"PERCENTAGE ERROR IN B.C.=",CHECK
      GO TO 696
697   TYPE"FIRST DERIVATIVE OF SOLID TEMPERATURE @ OUTLET=",A
696   ACCEPT"OTHER ITERATION DESIRED?(1=YES;0=NO)",IEND
      IF(IEND.EQ.0) GO TO 19
      ACCEPT "NEW GUESS FOR FRONT TEMPERATURE(KELVIN)=",TFRONT
      L=L+1
      GO TO 301
19    LUN=NK-1

C PUISSE IS THE POWER OUTPUT,BFIN IS THE ABSOLUTE OUTLET TEMPERATURE

      PUISSE=((AMPTOT*X)**2)*REX
      BFIN=TFEED*C
      WRITE(21,70) BFIN,PUISSE,D
      WRITE(28,21)COND,H,TFRONT,TRACE
      WRITE(22,22)
      WRITE(22,29)(VECT1(MN),VECT3(MN),MN=1,LUN)
      WRITE(35,35)
      WRITE(35,29)(VECT1(MN),VECT4(MN),MN=1,LUN)
      WRITE(24,24)
      WRITE(24,29)(VECT1(MN),VECT5(MN),MN=1,LUN)
      WRITE(25,25)
      WRITE(25,29)(VECT0(MN),VECT6(MN),MN=1,II,NNN)
      WRITE(26,26)
      WRITE(26,29)(VECT1(MN),VECT7(MN),MN=1,LUN)
      WRITE(29,30)
      WRITE(29,29)(VECT1(MN),VECT8(MN),MN=1,LUN)
      WRITE(30,31)
      WRITE(30,29)(VECT1(MN),VECT9(MN),MN=1,LUN)
```

```
  500   FORMAT('1','EXCPECTED POWER OUTPUT(WATTS)=',G11.4/' ','EXTERNAL LOAD(OH
     LMS)=',G11.4/' ','CONVERSION=',G11.4/' ','AVERAGE CURRENT PER UNIT ELEME
     LNTARY CELL(AMPS-@TGUESS)=',G11.4/' ','AVERAGE ACTUAL VOLTAGE ACROSS EAC
     LH ELEMENTARY CELL(VOLTS-@TGUESS)=',G11.4/' ','ASSUMED SOLID OPERATING
     L TEMPERATURE(KELVIN)=',G11.4/' ','CALCULATED MEAN SOLID TEMPERAT
     LURE(KELVIN)=',G11.4/' ','CALC.FUEL FEED RATE PER MONOLITH(CC/MIN @
     L298K & 1 ATM=',G11.4/' ','CALC.AIR FEED RATE PER MONOLITH(CC/MIN @ 2
     L98K & 1 ATM=',G11.4/' ','EXCESS AIR RATIO FOR PRESENT CALC.=',G11.4)
  501   FORMAT('1','FEED TEMPERATURE(KELVIN)=',G11.4/' ','INLET FUEL MOLE FRAC
     LTION=',G11.4/' ','FUEL FEED RATE PER MONOLITH(CC/MIN @ REFERENCE CONDS.
     L)=',G11.4/' ','AIR FEE
     LD RATE PER MONOLITH(CC/MIN @ REFERENCE CONDS.)=',G11.4/' ','NUMBER OF
     L CHANNELS IN X DIRECTION=',G11.4/' ','CHANNEL LENGTH(CM)=',G11.4/' ','
     LNUMBER OF BATTERIE IN SERIES=',G11.4/' ','WALL THICKNESS(MICRONS)=',G
     L11.4/' ','CHANNEL CROSS SECTION(MM2)=',G11.4/' ','REFERENCE TEMPERATU
     LRE FOR FEED FLOW RATE(KELVIN)=',G11.4/' ','LOAD(OHMS)=',G11.4/' ',
     L'NUSSELT#=',G11.4)
   18   FORMAT('1','MAXIMUM ALLOWED NUMBER OF ITERATIONS EXCEEDED'/' ','CURRENT
     L INDICATION OF BOUNDARY LOOP COUNTER=',I3)
   70   FORMAT('1','FUEL OUTLET TEMPERATURE(KELVIN)=',G11.4/' ','POWER OUTPUT
     L PER MONOLITH(WATTS)=',G11.4/' ','OUTLET CONVERSION=',G11.4)
   21   FORMAT('1','SECONDARY PARAMETERS'/' ','ZIRCONIA THERMAL CONDUCTI
     LVITY(WATTS/M K)=',G11.4/' ','INTEGRATION STEP=',G11.4/' ','SOLID FRO
     LNT TEMPERATURE(KELVIN)=',G11.4/' ','TRACE CO2 MOLE FRACTION @ L=0=',
     LG11.4)
   22   FORMAT(1X,'SOLID TEMPERATURE VS LENGTH'/' ','LENGTH'/' ','TEMPERATURE'/
     L' ','SYMB 99.'/' ','END')
   24   FORMAT(1X,'CONVERSION VS LENGTH'/' ','LENGTH'/' ','CONVERSION'/' ','SYM
     LB 99.'/' ','END')
   25   FORMAT(1X,'CURRENT DISTRIBUTION'/' ','LENGTH'/' ','LOCAL CURRENT'/
     L' ','SYMB 99.'/' ','END')
   26   FORMAT(1X,'ACCUMULATED CURRENT'/' ','LENGTH'/' ','AMPERES'/' ','SYMB
     L 99.'/' ','END')
   29   FORMAT(1X,G11.4,',',G15.8)
   30   FORMAT(1X,'REVERSIBLE VOLTAGE VS LENGTH'/' ','LENGTH'/' ','VOLTAGE-
     LVOLTS'/' ','SYMB 99.'/' ','END')
   31   FORMAT(1X,'ACTUAL VOLTAGE VS LENGTH'/' ','LENGTH'/' ','VOLTAGE-
     LVOLTS'/' ','SYMB 99.'/' ','END')
   35   FORMAT(1X,'GAS TEMPERATURE VS LENGTH'/' ','LENGTH'/' ','TEMPERATURE
     L'/' ','SYMB 99.'/' ','END')
  100   CALL RESET
        STOP
        END


) Q
```

```
      COMPILER DOUBLE PRECISION
      COMPILER NOSTACK
      FUNCTION DA (B,C,D,P)
      COMMON A1,A2,A3,A4,A5,A6,A7,TAIR,TFEED,RQRD,YO,
     LPN,X,REX,REL,RECIP,A9,A10,PL,A12

C DA EVALUATES THE SECOND DERIVATIVE OF SOLID TEMPERATURE

      TEMP=B*TFEED
      TGAS=C*TFEED

C VOLT IS THE REVERSIBLE(NERNST) VOLTAGE
C CONC IS A FUNCTION THAT CALCULATES THE LOGARITHMIC COMPONENT OF THE VOLTAGE
C RES IS AN OHMIC TERM WHICH APPEARS IN THE DERIVATIVE EVALUATION
C CURRT IS RELATED TO THE LOCAL RATE OF HEAT GENERATION

C THE ARGUMENTS OF DA ARE SOLID TEMPERATURE,GAS TEMPERATURE,CONVERSION &
C CURRENT DISTRIBUTION COEFFICIENT

      VOLT=-5.181E-06*DELG(TEMP)+A1*B*CONC(D)
      RES=(PN+1.)*REL+REX
      CURRT=A3*PN*VOLT/(RES*((A2/A5)*DEXP(A4/B)+X*P))
      TM=.5*(TEMP+TAIR)
      CPAIR=(.79*CIN2(TM)+.21*CIO2(TM))*(4.1868/(TM-298.15))
      CAP=CPAIR*A6
      ZZ=(CURRT/DELH(298.15))*4.1868*(CICO2(TEMP)-CICO(TGAS)-.5*CIO2(TAIR))
      PP=A9*CPAIR*VOLT*(B-TAIR/TFEED)/(RES*(X*P+(A2/A5)*DEXP(A4/B)))
      DA=-CURRT*(1.-VOLT/(-DELH(298.15)*5.181E-06*(1.+(A2/A5)*(DEXP(A4/B))/
     L(X*P))))+CAP*(B-TAIR/TFEED)+A10*(B-C)-ZZ-PP
      RETURN
      END


)
```

```
        COMPILER DOUBLE PRECISION
        COMPILER NOSTACK

CFUNCTION DB EVALUATES THE 1st DERIVATIVE OF TEMPERATURE

        FUNCTION DB(A)
        DB=A
        RETURN
        END

)
```

```
      COMPILER DOUBLE PRECISION
      COMPILER NOSTACK
      FUNCTION DC(B,C,D,P)
      COMMON A1,A2,A3,A4,A5,A6,A7,TAIR,TFEED,RQRD,YO,PN,X,REX,REL,
     LRECIP,A9,A10,PL,A12

C DC EVALUATES THE FIRST DERIVATIVE OF GAS TEMPERATURE

      TEMP=B*TFEED
      TGAS=C*TFEED


C VOLT IS THE REVERSIBLE (NERNST) VOLTAGE
C CONC IS A FUNCTION THAT CALCULATES THE LOGARITHMIC VOLTAGE COMPONENT
C RES IS AN OHMIC TERM GROUPING ELECTRODE & EXTERNAL LOADS
C CPFUEL IS THE FUEL STREAM MOLAR HEAT CAPACITY(JOULE/MOLEK)

      VOLT=-5.181E-06*DELG(TEMP)+A1*B*CONC(D)
      RES=(PN+1.)*REL+REX
      CPFUEL=(4.1868/(TGAS-298.15))*((1.-YO)*CIN2(TGAS)+YO*D*CICO2(TGAS)+
     LYO*(1.-D)*CICO(TGAS))
      CONST=CPFUEL*RQRD*1.66666/PL
      CP=(CICO2(TEMP)-CICO(TGAS))/TFEED
      DC=(A12/CONST)*(B-C)+2.1693264E-03*PN*VOLT*RECIP/(CONST*PL*RES*(X*P
     L(A2/A5)*DEXP(A4/B)))*CP

      RETURN
      END

)
```

```
      COMPILER DOUBLE PRECISION
      COMPILER NOSTACK
      FUNCTION DD(B,D,P)
      COMMON A1,A2,A3,A4,A5,A6,A7,TAIR,TFEED,RQRD,YO,PN,X,
     LREX,REL,RECIP,A9,A10,PL,A12

C DD COMPUTES THE FIRST DERIVATIVE OF CONVERSION
C PARAMETERS OF DD ARE  TEMPERATURE,CONVERSION & CURRENT DISTRIBUTION
C COEFFICIENT

C VOLT IS THE REVERSIBLE (NERNST) VOLTAGE
C CONC IS A FUNCTION THAT EVALUATES THE LOGARITHMIC COMPONENT OF THE VOLTAGE
C RES IS A RESISTANCE TERM

      TEMPS=B*TFEED
      VOLT=-5.181E-06*DELG(TEMPS)+A1*B*CONC(D)
      RES=(PN+1.)*REL+REX
      DD=RECIP*3.108808E-04*(1./(RQRD*YO))*PN*VOLT/(RES*(P*X+(A2/A5)*DEXP(A4
     L/B)))
      RETURN
      END

)
```

```
C CONC CALCULATES THE LOGARITHMIC TERM IN THE REVERSIBLE VOLTAGE
C EXPRESSION

        COMPILER DOUBLE PRECISION
        COMPILER NOSTACK
        FUNCTION CONC(W)
        IF((W.GT.0.0).OR.(W.LT.1.0))GO TO 701
      WRITE(20,82)W
        STOP
 701    CONC=DLOG(0.4582*(1.-W)/W)
  82   FORMAT('1','MEANINGLESS CONVERSION CALLED FROM PROGRAM'/' ','CONV
     LERSION=',G11.4)
        RETURN
        END

)
```

```
C DELTAG CALCULATES THE MOLAR GIBBS FREE ENERGY CHANGE (PER MOLE OF CO)
C AS A FUNCTION OF TEMPERATURE(JOULE/MOLE)

      COMPILER DOUBLE PRECISION
      COMPILER NOSTACK
      FUNCTION DELG(Z)
      DELG=4.1868*(8.75E04/Z+23.25*Z-0.2*Z*DLOG(Z)-3.1E-04*(Z**2)-68310.38)
      RETURN
      END

)
```

```
C DELTAH CALCULATES THE MOLAR ENTHALPY CHANGE (PER MOLE OF CO)
C AS A FUNCTION OF TEMPERATURE(JOULE/MOLE)

      COMPILER DOUBLE PRECISION
      COMPILER NOSTACK
      FUNCTION DELH(Z)
      DELH=4.1868*(1.75E05/Z+0.2*Z+3.1E-04*(Z**2)-68310.38)
      RETURN
      END

)
```

```
C CICO COMPUTES THE INTEGRAL OF CO MOLAR HEAT CAPACITY
C BETWEEN 298K & ANY GIVEN TEMPERATURE(UNITS FOR MOLAR
C HEAT CAPACITY ARE CAL/MOLE*K)

      COMPILER DOUBLE PRECISION
      COMPILER NOSTACK
      FUNCTION CICO(Z)
      CICO=6.79*Z+4.9E-04*(Z**2)+0.11E 05/Z-2104.89
      RETURN
      END

)
```

```
C CICO2 COMPUTES THE INTEGRAL OF THE MOLAR CO2 HEAT CAPACITY
C BETWEEN 298K & ANY GIVEN TEMPERATURE(UNITS FOR CP ARE CAL/MOLE*K)

        COMPILER DOUBLE PRECISION
        COMPILER NOSTACK
        FUNCTION CICO2(Z)
        CICO2=10.57*Z+1.05E-03*(Z**2)+2.06E 05/Z-3935.711
        RETURN
        END

)
```

```
C CIO2 CALCULATES THE INTEGRAL OF O2 MOLAR SPECIFIC HEAT
C BETWEEN 298K & ANY GIVEN TEMPERATURE(UNITS FOR SP.HT. ARE
C CAL/MOLE*K)

      COMPILER DOUBLE PRECISION
      COMPILER NOSTACK
      FUNCTION CIO2(Z)
      CIO2=7.16*Z+5.0E-04*(Z**2)+0.4E 05/Z-2313.36
      RETURN
      END

)
```

```
C CIN2 CALCULATES THE INTEGRAL OF N2 MOLAR HEAT CAPACITY
C BETWEEN 298K & ANY GIVEN TEMPERATURE(UNITS FOR SP.HT. ARE
C CAL/MOLE*K)

        COMPILER DOUBLE PRECISION
        COMPILER NOSTACK
        FUNCTION CIN2(Z)
        CIN2=6.83*Z+4.5E-04*(Z**2)+0.12E 05/Z-2116.615
        RETURN
        END

)
```

SYMBOLS

a activity

A area

chemical specie A

Ael electrode area

Aex area associated with heat interactions per unit element in a stacked cell

[A] molar concentration of specie A

b electrode film thickness

B limiting Sherwood number for fully developed laminar flow with constant surface composition in equation (2.2.53).

chemical specie B

Bi Biot number

C surface roughness factor (equation (2.2.53))

chemical specie C

C' proportionality constant for potential flow free stream velocity in equation I-3 ($time^{-1}$)

$\hat{C}p$ temperature averaged heat capacity at constant pressure (molar unless G appears as a subscript)

d electrolyte thickness (cm)

D(K) current distribution coefficient for Kth element along a monolith channel

D' fuel feed tube restriction orifice (mm)

D diffusion coefficient (cm^2/sec)

e electron

E actual voltage produced by fuel cell

E* molar activation energy for electrolyte resistance

E_{rev} reversible voltage

E_{TN} thermoneutral voltage

E° voltage corresponding to Gibbs free energy change at unit activity

$E^{\circ}_{\circ}$ voltage corresponding to Gibbs free energy change at unit activity and reference temperature

f useful area ratio for a monolith channel

F volumetric flow rate

$\mathcal{F}$ Faraday's constant (96500 coulombs/g-equivalent)

ΔG° standard (unit activity) molar free energy change

ΔH° standard (unit activity) molar enthalpy change

H_{Ko} pure component K molar enthalpy @ T_o

h solid-gas heat transfer coefficient for channel flow in monolith reactor

I current (Ampères)

i current density (Ampères/cm^2)

total current per channel in section 2.2.3 (Ampères)

i_o exchange current density (Ampères/cm^2)

K equilibrium constant

kg' mass transfer coefficient (cm^2/S)

k thermal conductivity

ℓ channel side in monolith cell (cm)

ℓ' distance along a flat plate measured from stagnation point

L channel length in monolith cell (cm)

m number of elements in a monolith channel (reciprocal of integration step)

M molecular weight

n electrons transferred per each occurence of elementary reaction

$\dot{N}$ molar flux (moles/sec)

Nu Nusselt number

p partial pressure (atm)

Pe Peclet number for mass transfer

Pe_H Peclet number for heat transfer

Pe' interfacial Peclet number for heat transfer

Pr Prandtl number

P power output

$\dot{Q}$ rate of effective heat generation

Re Reynolds number

Re_ℓ, Reynolds number for stagnation flow (Appendix I)

r solid electrolyte resistivity (ohm-cm)

catalyst pore diameter in Appendix I

r_{el} electrode resistivity (ohm-cm)

r* preexponential factor in electrolyte resistivity (ohm-cm)

R gas-law constant

Rel electrode resistance (ohm)

Rex external load (ohm)

R_H hydraulic radius = flow area/perimeter

Ri electrolyte resistance (ohm)

R_i° preexponential factor in electrolyte resistance (ohm)

ΔS° standard molar entropy change

s cell spacing in stack (mm)

S electrolyte area measured transversely to anion flow (cm^2)

Sc Schmidt number

Sh Sherwood number

T absolute temperature

t electrode film effective thickness in a monolith channel (cm)

t' fuel feed tube-to-electrode distance (mm)

ΔV ohmic loss corresponding to current flow along a monlith channel (volts)

<u> mean gas velocity in monlith channel

U overall heat transfer coefficient for heat losses

W stoichiometric mass consumption of oxygen per mole of fuel

x conversion

X number of fuel channels in parallel per battery

y mole fraction

Y coordinate along monlith channel

number of air transverse channels per fuel channel

Z number of batteries in series per monolith

z air feed ratio = actual/stoichiometric air feed

Subscripts

b bulk-phase

c ambient

f fuel

g gas phase

G per unit mass

i inlet conditions

j air inlet conditions

K designates Kth element along a fuel channel

designates Knudsen diffusivity (Appendix I)

o reference temperature or pressure

m average between inlet and outlet conditions

p products

s solid

Greek symbols

α empirically determined factor in equation II-1

β ratio of mass transfer to ohmic limited rates

δ monolith wall thickness

tortuosity factor (Appendix I)

ε arbitrarily small number

η efficiency for chemical to electrochemical energy conversion

ρ density

θ dimensionless temperature

ψ scaling factor

ν kinematic viscosity

ϕ polarization in section 1-1 (volts)

REFERENCES

1. R.D. Farr, M.S. Thesis, Massachusetts Institute of Technology (1979)
2. R.D. Farr and C.G. Vayenas, J. Electrochem. Soc. 127 (7), 1478 (1980)
3. C. Teague, M.S. Thesis, Massachusetts Institute of Technology (1981)
4. J. O'M. Bockris and A.K.N. Reddy, "Modern Electrochemistry," Vol. 2., Ch. 8,9,11, Plenum Press , New York (1970)
5. C. Van Heerden, Ind. Eng. Chem., 45, 1242, (1953)
6. C. Van Heerden, Chem. Eng. Sci., 8, 133, (1958)
7. R. Aris, N.R. Amundson, Chem. Eng. Sci., 7, 121, 132 148, (1958)
8. O. Biolus, N.R. Amundson, AIChE J., 1, 513, (1955)
9. R.A. Schmitz, in Hulburt, ed., Chemical Reaction Engineering Reviews, Adv. Chem. Series, 148, 156 (1974)
10. G.P. Sakellaropoulos, G.A. Francis, J. Electrochem. Soc., 126 (11), 1928 (1979)
11. E.F. Sverdrup, C.J. Warde, R.L. Eback, Energy Conversion, 13, 129, (1973)
12. O. Adlhart, in D.M. Considine (ed.), "Energy Technology Handbook", ch 4, McGraw-Hill (1977)
13. E.C. Subbarao (ed.), "Solid Electrolytes and their applications" Plenum Press, New York (1980)
14. O. Levenspiel, "Chemical Reaction Engineering", 2nd ed., ch. 9, John Wiley and Sons (1972)
15. T.H. Etsell and S.N. Flengas, J. Electrochem. Soc., 118, (12), 1890 (1971)

16. D.H. Archer, L. Elikan and L. Zahradnik, in B.S. Baker, ed., "Hydrocarbon Fuel Cell Technology", Academic Press, New York (1965)

17. R.H. Perry and C.H. Chilton, "Chemical Engineer's Handbook", 5th ed., p. 3.137-3.144, McGraw-Hill (1973)

18. C.N. Satterfield, "Heterogeneous Catalysis in Practice", 1st ed., Ch 4, pp 94-95, ch 8, p. 226, McGraw-Hill (1980)

19. R.H. Heck, J. Wei, J.R. Katzer, "Mathematical Modeling of Monolithic Catlaysts", AIChE J., 22(3), 477,(1976)

20. L.H. Hegedus, "Temperature excursions in catalytic monoliths", AIChE J., 21(5), 849, (1975)

21. V. Hlavacek and J. Votruba, in L. Lapidus and N.R. Amundson (ed.), "Chemical Reactor Theory-a review", ch. 6, "Steady state operation of fixed bed reactors and monolithic structures", Prentice-Hall (1977)

22. R.H. Perry and C.H. Chilton,(ed.), "Chemical Engineer's Handbook", 5th ed., pp. 5.47-5.48, McGraw-Hill (1973)

23. E.F. Sverdrup, D.H. Archer, J.J. Alles and A.D. Glasser, in B.S. Baker, ed., "Hydrocarbon Fuel Cell Technology", Academic Press, New York (1965)

24. R.K. Shah and A.L. London, "Laminar Flow Forced Convection Heat Transfer and Flow Friction in Straight and Curved Ducts ... A Summary of Analytical Solutions", Technical Report N75, Department of Mechanical Engineering, Stanford University, Stanford, California (1971)

25. W.M. Rohsenow and J.P. Hartnett (ed.), "Handbook of Heat Transfer", ch. 19, p. 1948, McGraw-Hill (1973)

26. L.L. Hegedus, "Effects of Channel Geometry on the Performance of Catalytic Monoliths", Reprints of the Petroleum Chemistry Division, ACS, 18 (4), 487 (1973) (Symposium on Catalytic Approaches to Environmental Control, Chicago, Aug. 26-31, 1973)

27. R.B. Bird, W.E. Stewart and E.N. Lightfoot, "Transport Phenomena", ch. 16, pp. 510-511, John Wiley and Sons (1960)

28. W.M. Kays and M.E. Crawford, "Convective Heat and Mass Transfer", 2nd edition, McGraw-Hill (1980)

29. H. Schlichting, "Boundary Layer Theory", 7th edition, pp. 95-99, McGraw-Hill (1979)